ENDOPLASMIC RETICULUM ASSOCIATED DEGRADATION (ERAD) IN THE LIVER

A Dissertation

presented to the Graduate School of Cornell University

as per requirements for the degree of

Doctor of Philosophy

by
Asmita Bhattacharya
August 2019

To my paternal grandfather Dadu – my first friend and beginning to my world.

To my maternal grandmother Mamma – the philosopher and brightest star in my sky.

ENDOPLASMIC RETICULUM ASSOCIATED DEGRADATION (ERAD) IN THE LIVER

Asmita Bhattacharya, Ph.D. 2019

Recent literature has revolutionized our view on the patho-physiological importance and the underlying molecular mechanism of endoplasmic reticulum (ER)-associated degradation (ERAD) in health and disease. Aside from being a downstream element of ER stress response or the unfolded protein response (UPR), ERAD also plays a direct and vital role in health and disease, in a substrate-specific and largely UPR-independent manner. The Sel1L-Hrd1 complex is the most conserved branch of mammalian endoplasmic reticulum (ER)-associated degradation (ERAD) machinery. Here, we have focused on the role of ERAD in the liver in the context of energy metabolism, bile homeostasis and cancer pathogenesis. In a recent publication, we reported the discovery of a novel mechanism underlying ERAD-mediated regulation of *Fgf21* expression during growth and fasting-feeding. Mice with liver-specific deletion of Sel1L exhibit growth retardation with markedly elevated circulating Fgf21, leading to massive alterations in growth and systemic metabolic profile. Mechanistically, we show that the Sel1L-Hrd1 ERAD complex controls *Fgf21* transcription by regulating the ubiquitination and turnover (and thus nuclear abundance) of ER-resident transcription factor Crebh. This study not only establishes the importance of hepatic Sel1L-Hrd1 ERAD in the regulation of systemic energy metabolism, but also reveals a novel hepatic "ERAD-Crebh-Fgf21" axis directly linking ER protein turnover to gene transcription and systemic metabolic regulation. In another study, our data revealed the importance of ERAD in the regulation of bile metabolism, where a deficiency in hepatic ERAD causes significantly impaired secretion of bile acids, cholesterol and phosphatidylcholine into bile, leading to hypercholanemia and extreme sensitivity to dietary bile acid challenge. This occurs due to defective maturation of exporter proteins associated with bile production, owing to faulty ERAD of these proteins. Finally, in a parallel study, we identify and characterize a novel and significant relationship between hepatic ERAD and liver cancer pathogenesis via the Wnt signalling pathway. Here we demonstrate that Sel1L-Hrd1 ERAD in the liver functions to triage the secreted protein Wnt5A during its maturation in the ER. In the absence of ERAD, Wnt5A aggregates and allows unrestrained proliferation of hepatocytes, thereby markedly increasing the propensity to liver cancer development. Taken together, we propose the new concept of "constitutive" or "basal" ERAD and its significance in managing cellular and organismal function, and define novel paradigms underlying ERAD function in both quality and quantity control of proteins synthesized in the ER, and nuclear gene transcription.

BIOGRAPHICAL SKETCH

NAME: Asmita Bhattacharya	**DISSERTATION ADVISOR:**
CONTACT: ab2365@cornell.edu, asmita@umich.edu	Dr. Robert Weiss, Professor of Molecular Biology & Genetics, Cornell University Dr. Ling Qi, Professor of Molecular & Integrative Physiology, University of Michigan

EDUCATION/TRAINING

Institution and Location	Degree/ Position	Start date	End date	Field of Study
Indian Institute of Technology, Kanpur	B.Tech.	7/2008	5/2012	Biological Sciences and Biotechnology
Weill Cornell Medical College, New York	Research technician	9/2012	5/2013	Gastroenterology
Cornell University, Ithaca	Ph.D.	8/2013	8/2019	Molecular Biology and Genetics

PERSONAL STATEMENT

Having been always filled with an ardent desire to understand how simple entities associate to function as the complex organism throbbing with life, I found myself exploring various realms of biological research since an early age. During my undergraduate years, I worked in the limb development laboratory of Dr. Amitabha Bandyopadhyay, and did a short internship in the Weinberg laboratory on cancer genetics at the Whitehead Institute, M.I.T. Thereafter, I worked as a research technician in the colon cancer laboratory of Dr. Steven Lipkin at Weill Cornell Medical College. These experiences taught me key molecular and cell biology techniques and gave me the first thrills of performing cutting-edge research. These stints trained me mentally and physically for graduate study and made me realize where my scientific passion truly lies.

In Cornell, after two rotations investigating BMP signaling with Dr. Jun Liu, and asymmetric vascular patterning with Dr. Natasza Kurpios, I found my niche in the laboratory of Dr. Ling Qi – a leading group in the field of physiological ER homeostasis. Here I am investigating how perturbations in the cellular quality control machinery known as Endoplasmic Reticulum Associated Degradation (ERAD) affect liver function with emphasis on systemic metabolism and disease pathogenesis. The enthusiasm of the PI, the warm nurturing environment of the lab members, along with many mouse models generated by this lab that ably simulate disease conditions, are providing me with a plethora of opportunities to groom myself as a successful researcher. *Following my Ph.D., I wish to complete post-doctoral studies while teaching in parallel, and eventually set up my own research lab while teaching biology to students*.

RESEARCH POSITIONS

7/2014–present Dept. of Genetics Genomics and Development, **Cornell University**
Dept. of Molecular and Integrative Physiology, **University of Michigan**
Advisor: **Dr. Ling Qi** *Position*: Ph.D. candidate
Project: ER Associated Degradation in liver metabolism and disease

2/2014–5/2014	Dept. of Genetics Genomics and Development, **Cornell University** *Advisor*: **Dr. Natasza Kurpios** *Position*: Rotating graduate student Project: Investigating asymmetric vascular development in embryonic dorsal mesentery during gut looping
10/2013–12/2013	Dept. of Genetics Genomics and Development, **Cornell University** *Advisor*: **Dr. Jun Liu** *Position*: Rotating graduate student Project: Determine how UNC-40/neogenin function promotes BMP signaling in *C. elegans*
9/2012–4/2013	Dept. of Gastroenterology, **Weill Cornell Medical College** *Advisor*: **Dr. Steven M. Lipkin** *Position*: Research technician Project1: Engineering recellularized organotypic human colon an ex-vivo model to study cancer driver genes Project2: Investigating the effects of the drug Erlotinib on colorectal cancer
5/2011–7/2011	Whitehead Institute, **Massachusetts Institute of Technology** *Advisors*: **Drs. Robert Weinberg & Julia Rastelli** *Position*: Intern Project: Investigating the increased size of cancer cells in context of the IGF-AKT pathway
5/2010–10/2010, 12/2011–5/2012	Department of Biological Sciences & Bioengineering, **Indian Institute of Technology Kanpur** *Advisor*: **Dr. Amitabha Bandyopadhyay** *Position*: Undergraduate Project: Knockdown studies of several uncharacterized molecules involved in limb development in chick embryo
5/2009–7/2009	Dept. of Biological Sciences, **Indian Institute of Science Education and Research Kolkata** *Advisor*: **Dr. Srimonti Sarkar** *Position*: Intern Project: Characterization of putative sec61 alpha gene in *Giardia lamblia*

TEACHING ASSISTANT POSITIONS

9/2014–12/2014	Laboratory in Biochemistry and Molecular Biology, Cornell University
1/2015–4/2015	Nutrient Metabolism, Cornell University

ACADEMIC HONORS AND FELLOWSHIPS	YEAR
University of Michigan Summer Diabetes Symposium Best Oral Presentation Award	2018
ASBMB Graduate/Postdoctoral Travel Award	2018
American Heart Association (AHA) Predoctoral Fellowship	2016
Indian School Certificate (ISC) examination (12th std.): Marks secured = 93%	2008
Kishore Vaigyanik Protsahan Yojana (KVPY) Fellowship	2006
Indian Certificate of Secondary Examination (ICSE) (10th std.): Marks secured = 96%	2006
Cleared state levels of National Astronomy Olympiad, National Science Olympiad	2005

JOURNAL PUBLICATIONS

1) Bhattacharya A, Qi L. **New perspectives on ERAD in health and disease: from organism to cell**. *Invited review for* ***Journal of Cell Science***. To be submitted.

2) Bhattacharya A, Kakiyama G, Takei H, Nittono H, Qi L. **Hepatic Sel1L-Hrd1 ERAD regulates bile homeostasis via bile exporter proteins.** Manuscript *in preparation*.

3) Bhattacharya A, Thomas D, Chen L, Qi L. **Sel1L-Hrd1 ERAD suppresses liver cancer via the Wnt signaling pathway.** Manuscript *in preparation*.

4) Bhattacharya A, Sun S, Wang H, Liu M, Long Q, Yin L, Kersten S, Zhang K, Qi L. **Hepatic Sel1L-Hrd1 ER-Associated Degradation (ERAD) manages FGF21 levels and systemic metabolism via CREBH.** ***EMBO Journal***. 2018 Nov 15;37(22). *F1000 Faculty recommended*.

5) Oteng AB, Bhattacharya A, Brodesser S, Qi L, Tan NS, Kersten S. **Feeding Angptl4-/- mice trans-fat promotes foam cell formation in mesenteric lymph nodes without leading to ascites**. ***Journal of Lipid Research***. 2017 Jun;58(6):1100-1113.

6) Chen H, Wei Z, Sun J, Bhattacharya A, Miller P, Savage D, Serda R, Curley S, Chen S, Shen X, Lipkin S, Copeland N, Jenkins N, Shuler M. **Engineering Organotypic Human Colon through Recellularization: An ex vivo Model for Studying Cancer Driver genes**. ***Nature Biotechnology****.* 2016 Aug;34(8):845-51.

7) Kim H*, Bhattacharya A*, Qi L. **Endoplasmic reticulum quality control in cancer: Friend or foe**. ***Seminars in Cancer Biology***. 2015 Aug; 33:25-33. *, equal contribution.

8) Gillen DL, Meyskens FL, Morgan T, Zell J, Carroll R, Benya R, Chen WP, Bhattacharya A, Wong V, Chung J, Gonzalez R, Rodriguez L, Szabo E, Lipkin S. **A Phase IIa Randomized, Double-Blind Trial of Erlotinib in Inhibiting EGF Receptor Signaling in Aberrant Crypt Foci of the Colon**. ***Cancer Prevention Research***. 2015 Mar; 8(3):222-30.

CONFERENCE PRESENTATIONS

1) Bhattacharya A, Qi L. **Hepatic Sel1L-Hrd1 ERAD regulates bile homeostasis via transporter quality control**. ***University of Michigan Center for Gastrointestinal Research Annual Winter Retreat***. *Poster*. 2019 Feb.

2) Bhattacharya A, Zhang K, Qi L. **Hepatic ERAD manages FGF21 levels and systemic metabolism via CREBH**. ***University of Michigan Summer Diabetes Symposium***. *Oral presentation and poster*. *Best oral presentation awardee*. 2018 Aug.

3) Bhattacharya A, Zhang K, Qi L. **Hepatic ER-Associated Degradation manages FGF21 level and metabolism via CREBH turnover**. ***Michigan Medicine Annual Internal Medicine Research Symposium***. *Poster*. 2018 May.

4) Bhattacharya A, Zhang K, Qi L. **Hepatic ER-Associated Degradation manages FGF21 levels and metabolism via CREBH**. ***American Society for Biochemistry and Molecular Biology Annual Meeting***. *Poster*. *Travel awardee*. 2018 Apr.

5) Bhattacharya A, Zhang K, Qi L. **Hepatic ERAD manages FGF21 levels and metabolism via CREBH**. ***University of Michigan Center for Gastrointestinal Research Annual Winter Retreat***. *Poster*. 2018 Feb.

6) Bhattacharya A, Kersten S, Qi L. **Hepatic ERAD Regulates Overall Metabolic Profile via FGF21 Action**. ***Michigan Diabetes Research Center Annual Symposium****. Poster*. 2017 Mar.

TABLE OF CONTENTS

ABSTRACT ii

BIOGRAPHICAL SKETCH iii

TABLE OF CONTENTS vi

ACKNOWLEDGEMENTS 1

CHAPTER 1 NEW PERSPECTIVES ON ERAD IN HEALTH AND DISEASE: FROM ORGANISM TO CELL

1.0 TITLE 2
1.1 ABSTRACT 3
1.2 INTRODUCTION 3
1.3 CONSTITUTIVE VS. INDUCIBLE ERAD 4
1.4 QUALITY VS. QUANTITY CONTROL BY ERAD 6
1.5 ERAD IN REGULATING GENE TRANSCRIPTION 8
1.6 ERAD IN DISEASE AND DISEASE MUTANTS 9
1.7 CONCLUSIONS 10
1.8 OUTSTANDING QUESTIONS 10
1.9 REFERENCES 11
1.10 BOXES 18
1.11 TABLES 18
1.12 FIGURE 21

CHAPTER 2 HEPATIC SEL1L-HRD1 ER-ASSOCIATED DEGRADATION (ERAD) MANAGES FGF21 LEVELS AND SYSTEMIC METABOLISM VIA CREBH

2.0 TITLE 22
2.1 ABSTRACT 23
2.2 INTRODUCTION 23
2.3 RESULTS 25
2.4 DISCUSSION 33
2.5 METHODS 35
2.6 ACKNOWLEDGEMENTS 41
2.7 AUTHOR CONTRIBUTION 42
2.8 FIGURE LEGENDS 42
2.9 REFERENCES 46
2.10 FIGURES 51

CHAPTER 3 HEPATIC SEL1L-HRD1 ERAD REGULATES BILE HOMEOSTASIS VIA BILE EXPORTER PROTEINS
3.0 TITLE 68
3.1 ABSTRACT 69
3.2 INTRODUCTION 69
3.3 RESULTS 71
3.4 DISCUSSION 76
3.5 METHODS 78
3.6 ACKNOWLEDGEMENTS 81
3.7 AUTHOR CONTRIBUTION 81
3.8 FIGURE LEGENDS 81
3.9 REFERENCES 83
3.10 FIGURES 88

CHAPTER 4 ENDOPLASMIC RETICULUM QUALITY CONTROL IN CANCER: FRIEND OR FOE
4.0 TITLE 97
4.1 ABSTRACT 98
4.2 INTRODUCTION 98
4.3 THE IRE1α SIGNALING PATHWAY 99
4.4 THE ROLE OF IRE1α-XBP1S SIGNALING PATHWAY IN CANCER 100
4.5 ERAD 103
4.6 THE ROLE OF SEL1L-HRD1 ERAD IN CANCER 104
4.7 THERAPEUTICS 106
4.8 CONCLUSIONS 108
4.9 PERSPECTIVES 108
4.10 ACKNOWLEDGEMENTS 109
4.11 FIGURE LEGENDS 109
4.12 REFERENCES 110
4.13 FIGURES 118
4.14 TABLES 121

CHAPTER 5 SEL1L-HRD1 ERAD SUPPRESSES LIVER CANCER VIA THE WNT SIGNALING PATHWAY
5.0 TITLE 123
5.1 ABSTRACT 124
5.2 INTRODUCTION 124
5.3 RESULTS 126
5.4 DISCUSSION 129
5.5 METHODS 130
5.6 ACKNOWLEDGEMENTS 134
5.7 AUTHOR CONTRIBUTION 134
5.8 FIGURE LEGENDS 134
5.9 REFERENCES 136
5.10 FIGURES 140

CHAPTER 6 SEL1L-HRD1 ERAD IN THE LIVER: A PERSPECTIVE
6.0 SUMMARY 148

ACKNOWLEDGEMENTS

It is an absolutely undeniable fact that I owe every good part of my existence and achievements to my family. It would be presumptuous of me to try to thank my parents who happen to be the most interesting, charismatic and adorable people I have ever had the good fortune to meet. My father has always harbored the admirable ability to consistently be my closest friend and role model in life, giving meaning and purpose to my existence at every step. My mother keeps surprising me by being an unsolvable conundrum with her tenacity, ambition and benevolence to all around her. My brother always remains my most faithful partner-in-crime and never fails to fill my world with laughter and light with his sunny innocence and witty observations. Together, my family has always been an inimitable cocktail of love, support and encouragement, without whom I am nothing but wisps of air on this planet. I would also like to thank my large extended family for showering me with unconditional, unfettered love for my entire life. A special thank you goes to my youngest paternal aunt, a genius chemist in her day, for being my inspiration to study biochemistry. I have also been extremely lucky to have been supported through various difficult patches of my studies by my loyal friends – Esha, Jishnu and Ashim.

I would like to devote my sincerest gratitude to my mentor, Dr. Ling Qi for being a powerful force of reform in my life for the past five years. With his sharp guidance, scientific exuberance and go-getter spirit, he has instilled in my naïve young personality a sense of direction, the motivation to incessantly pursue one's dreams, and the courage to never be deterred by adversities that may crop up along the way. In addition, I would like to ardently thank my committee members Dr. Robert Weiss, Dr. Kenneth Simpson and Dr. Natasza Kurpios for their valuable support and scientific acumen without which this journey would not have been possible. I would also like to thank my colorful colleagues in the lab for their insightful critiques and discussions on my work. A very special token of gratitude goes to Guojun, Hyang and Jason – three highly intriguing postdocs in the lab, for providing me with technical advice and more importantly, emotional support by way of lending an ear to my problems and cheering me up with jokes and teasing comments whenever the going got tough. Finally, I would like to thank my mice for literally carrying the lion's share of the scientific progress for all my projects, and never ceasing to surprise me at every corner. I deeply cherish all the beautiful personal and professional relationships I have experienced during my graduate study and sincerely hope to maintain them for years to come.

CHAPTER 1

New perspectives on ERAD in health and disease: from organism to cell

Asmita Bhattacharya[1,2] and Ling Qi[1,3] *

[1] Department of Molecular and Integrative Physiology, University of Michigan Medical School, Ann Arbor, MI 48105, USA;
[2] Graduate Program of Genetics, Genomics and Development, Cornell University, Ithaca, NY 14853, USA;
[3] Division of Metabolism, Endocrinology & Diabetes, Department of Internal Medicine, University of Michigan Medical School, Ann Arbor, MI 48105, USA;

*** Correspondence:** lingq@med.umich.edu

Invited review for ***Journal of Cell Science*** (to be submitted)

1.1 ABSTRACT

Recent literature has revolutionized our view on the vital importance of endoplasmic reticulum (ER)-associated degradation (ERAD) in health and disease. ERAD is no longer merely a downstream element of ER stress or the unfolded protein response (UPR), but rather plays a direct and profound role in normal physiology and disease pathogenesis, in a largely substrate-specific manner, ranging from water balance, food intake, gut homeostasis, immune cell development and function, to systemic energy metabolism. In this review, we propose the new concept of “constitutive” or “basal” ERAD where it ensures constant turnover of substrate proteins under physiological conditions, thereby optimizing their functions at cellular and organismal levels. Furthermore, we define paradigms of “quality” vs. “quantity” control of ERAD substrates, and highlight how ERAD modulates nuclear gene transcription.

1.2 INTRODUCTION

Secreted proteins such as hormones and growth factors, and transmembrane receptors critically regulate nearly all aspects of life including food intake, water balance, growth, metabolism and immunity. The endoplasmic reticulum (ER) is a specialized cellular compartment where the folding and maturation of most of these proteins take place (1, 2). Aberrations in these complex thermodynamic folding processes can disrupt cellular homeostasis and lead to debilitating diseases such as cystic fibrosis, alpha-antitrypsin deficiency, diabetes, and etc (3). ER-associated degradation (ERAD) is a highly conserved, major regulatory system that guards against such events, thereby maintaining proteostasis within the cell (4, 5). Despite being well-characterized at biochemical levels which have been reviewed extensively (6-8), how ERAD functions on a systemic, physiological scale remained unknown until recently. This review will focus on the emerging roles of ERAD in health and disease, without which, our understanding of pathogenesis of a large number of diseases remains incomplete.

The Sel1L-Hrd1 protein complex – the focus of this review – forms the most conserved and best-characterized ERAD system in mammals. The ERAD process begins with substrate protein selection based on glycosylation tags, mannose trimming status and/or conformational change, and is aided by chaperones such as Grp78, Edem and Os9 (6, 9, 10). The second step is retro-translocation of the substrate into the cytosol through the polytopic dislocon unit formed by the RING-domain-containing E3 ligase Hrd1, where Hrd1 forms a ubiquitin-gated channel activated by auto-ubiquitination (11-13). The adaptor protein Sel1L is indispensable for Hrd1 stability and function (14-16). Subsequently, substrates are

ubiquitinated by Hrd1 (17), and targeted for proteasomal degradation by the ATPase p97 and other ubiquitin-modifying enzymes (18, 19). Other E3 ligases such as Gp78, March6, Rma1 and Trim13 may work either in parallel or together with Hrd1; however, these systems remain poorly characterized (20-24) and will not be discussed here.

Deletion of any key component of Sel1L-Hrd1 ERAD such as Sel1L, Hrd1 and p97 results in embryonic lethality in mice (25-27), underscoring the physiological significance of ERAD in development. To circumvent the lethality issues, various cell- and tissue-specific knockouts of specific ERAD genes have been generated using the Cre/loxP system. These studies have linked ERAD to a plethora of physiological conditions, often in a substrate-specific manner (28). These findings have allowed us to map out the stipulations necessary for the identification of a bona fide ERAD substrate protein (Box 1), and changed our view on the physiological and pathological importance of ERAD. In this review, we highlight the emerging importance of ERAD in physiology and disease pathogenesis, and propose several new concepts and paradigms risen from recent animal studies: constitutive or basal vs. inducible ERAD, quality vs. quantity control by ERAD, and ERAD-mediated regulation of gene transcription (Figure 1).

1.3 CONSTITUTIVE VS. INDUCIBLE ERAD

Accumulation of misfolded proteins triggers ER stress or UPR, which in turn induces the expression of genes encoding ER chaperones and ERAD, as a means to relieve the protein load within the cell (29, 30). This UPR-centric view supposedly occurs via Ire1α- or Atf6-mediated transcriptional control of ERAD gene expression, and is largely based on reports using chemical agents such as DTT, tunicamycin or thapsigargin that cause massive ER stress (31, 32). Whether or not this scenario applies *in vivo* under physiological conditions remains to be determined.

Various studies using animal models suggest that Sel1L-Hrd1 ERAD plays a critical role constitutively within the cell. Indeed, ERAD is constitutively expressed and active in mammalian cells. This basal or constitutive ERAD is indispensable for the maintenance of ER homeostasis by maintaining optimal levels of substrate proteins, misfolded or not, and ensuring ER homeostasis within the cell.

Recent publications by Fang and our groups independently showed that Sel1L-Hrd1 ERAD is constitutively active in the liver under basal conditions (with very mild, if any, UPR), and increases in expression with age or feeding (33, 34). This ERAD function is instrumental in

regulating the abundance of its substrate protein Crebh, an ER-resident transcription factor that moves to the nucleus following proteolytic cleavage at the Golgi (35). One of the Crebh target genes is Fgf21, a powerful hepatokine, that controls systemic energy metabolism in the body (33, 34). In the absence of this constitutive hepatic ERAD, mice exhibit growth retardation and significantly reduced systemic energy homeostasis – largely owing to highly elevated levels of Crebh, leading to increased Fgf21 gene transcription.

Other examples of constitutive ERAD are described in the Sel1L-Hrd1-mediated degradation of the UPR sensor protein Ire1α (36) and the pre-B cell receptor protein (pre-BCR) (37). Sun et al. (36) demonstrates that Ire1α is an endogenous substrate of Sel1L-Hrd1 ERAD. The degradation of Ire1α by Sel1L-Hrd1 (with the help of the ER chaperones Os9 and Grp78) occurs constitutively to restrain Ire1α activity under physiological conditions and protecting the intestines from inflammatory disease (36, 38). Similarly, Ji et al. (37) showed that in developing B cells, ERAD constitutively functions to control the abundance of pre-B cell receptor (pre-BCR), thereby regulating pre-BCR signaling and allowing smooth transition from large to small pre-B cell stage.

In neurons expressing the antidiuretic hormone arginine-vasopressin (Avp), Sel1L-Hrd1 ERAD constitutively acts to manage systemic water levels by clearing misfolded proAvp proteins from the ER (39). Sel1L deletion in AVP neurons under basal conditions causes diabetes insipidus with low urine osmolality. proAVP contains 16 cysteines with 8 disulfide bonds and is likely misfolding prone. Indeed, many mutations, causing the retention of nascent proAVP proteins in the ER, have been identified in humans with diabetes insipidus (40-44). Changes in serum hyperosmolality, caused due to water deprivation or salt overload, can alter the expression of Hrd1 in Avp-neurons (39). Similarly, in the hypothalamic arcuate nucleus, ERAD functions at a basal level, fluctuating with the body's feeding cycle, to oversee the maturation of pro-opiomelanocortin (Pomc), a metabolic prohormone that promotes satiety post-feeding and controls food intake (45). Sel1L deletion in POMC neurons under basal conditions causes hyperphagia and early-onset obesity (45).

Hence, we propose that constitutive or basal ERAD, i.e. UPR-independent ERAD function, plays a critical role *in vivo* under physiological condition. The constitutive or basal ERAD actively clears ER proteins, controls their abundance and thus fine-tunes the levels of metabolic proteins and signaling pathways within the cell. We propose that this process exerts a key homeostatic control of basic physiologic processes such as feeding, water intake, systemic energy homeostasis and cellular development.

In other words, we propose that ERAD exerts UPR-independent functions *in vivo*. To further this point, we compare phenotypes of animal models deficient in each pathway to assess the relative contribution and importance of UPR and ERAD in governing key physiological processes in the body (Table 1). Interestingly, UPR- and ERAD-deficient mice models exhibited distinct set of phenotypes in most if not all cases, suggesting that they exert separate effects in vivo. Additionally, in several instances, ERAD-deficient models showcased more severe phenotype than corresponding UPR-deficient models, suggesting that constitutive ERAD may be playing a more pertinent role than UPR in the context of normal physiology.

1.4 QUALITY VS. QUANTITY CONTROL BY ERAD

Classically ERAD has largely been associated with quality control, i.e. the clearance of misfolded proteins in the ER. Recent work using neuron-specific Sel1L-knockout mice and cells delineated how Sel1L-Hrd1 ERAD is responsible for the quality control of the prohormone maturation process in neuroendocrine cells. Using Avp-neuron-specific Sel1L-knockout mice, Shi et al. (39) showed that the precursor of arginine-vasopressin (proAvp) is an endogenous substrate of Sel1L-Hrd1 ERAD. In Sel1L-deficient Avp-neurons, misfolded proAvp along with its natively folded counterpart accumulate together in a dominant negative manner to form disulfide-bonded aggregates, aided by Pdi. Avp being an antidiuretic hormone regulating systemic water homeostasis, this aggregation and ER-retention of proAvp in the absence of Sel1L leads to a loss of function effect causing profound polyuria and polydipsia (i.e. diabetes insipidus) in these mice.

Similarly, using Pomc-neuron-specific Sel1L-knockout mice, Kim et al. (45) showed that pro-opiomelanocortin (Pomc) is another endogenous substrate of Sel1L-Hrd1 ERAD. In the absence of Sel1L, aberrantly-folded Pomc molecules accumulate and abrogate the maturation of their properly folded counterparts by engaging them in aggregate formation in a dominant negative manner. This resultant loss of function effect of Pomc (a precursor for metabolically active neuropeptides) leads to hyperphagia and early onset obesity. Interestingly, neither of these mouse models show any overt signs of neuronal death, inflammation or ER stress (39, 45).

In Schwann cells, deletion of another ERAD dislocon protein Derlin2 leads to ER retention of misfolded myelin protein zero (P0), leading to defective myelin morphology and function, and increased propensity to Charcot-Marie-Tooth 1B (CMT1B) neuropathy (46). Moreover, another recent study showed that depleting Sel1L from pancreatic β cells leads to the

accumulation of misfolded proinsulin aggregates in the ER, causing impaired glucose-stimulated insulin secretion and hyperglycemia in mice (47).

In addition to this quality control function, ERAD may also work at a quantity control capacity where it is responsible for the turnover of properly folded or not-misfolded proteins, thereby optimizing associated downstream processes. In the absence of ERAD, these proteins accumulate, and ultimately lead to their gain-of-function phenotypes. Although quantity control by ERAD had been proposed in the past (48, 49), *in vivo* evidence remained limited.

Recent studies by Fang and our group (33, 34) showed, using proteomic and biochemical approaches in the liver, that Sel1L-Hrd1 ERAD is able to recruit and ubiquitinate Crebh for proteasomal degradation. In the absence of Sel1L or Hrd1, Crebh accumulates in the ERAD-deficient hepatocytes in the ER as well as the nucleus (following proteolytic cleavage at the Golgi), where it induces the expression of Fgf21. Consequently, these mice phenocopy Fgf21 gain-of-function mouse models, with growth retardation, reduced female fertility, lower serum lipid levels, increased insulin sensitivity and adipose tissue browning, and resistance to diet-induced obesity. Similarly, in the intestine, Sel1L-Hrd1 ERAD functions to regulate the quantity of the UPR sensor protein Ire1α. Deletion of either Sel1L or Hrd1 leads to the accumulation of Ire1α protein and mild activation of Ire1α (36).

In the immune system, Sel1L-Hrd1 ERAD is critical for the proper maturation and function of developing B lymphocytes (37). In the immature stage, Sel1L-Hrd1 mediated ubiquitination and turnover of the pre-BCR complex is critical for the developing B cell to transition from large to small pre-B stage (37, 50). In the absence of ERAD, pre-BCR complex continually accumulates and migrates to the B cell surface, leading to excessive signaling and developmental blockade at the large pre-B stage. On the other hand, in mature B cells, another study showed that Hrd1-mediated turnover of the cell death receptor Cd95/Fas maintains an optimal low level of activation-induced cell death, thereby protecting B cells from rapidly undergoing Fas-mediated apoptosis (51).

ERAD has also been reported to be responsible for the turnover of non-ER proteins in specific cell types. In dendritic cells, Hrd1 degrades the B lymphocyte-induced maturation protein-1 (Blimp1), a known transcriptional repressor of MHC-II, thereby priming $Cd4^+$ T cells (and not $Cd8^+$ T cells) for activation – a mechanism that is critical in the pathogenesis of myelin oligodendrocyte glycoprotein (MOG) induced experimental autoimmune encephalomyelitis (EAE) (52).

In adipocytes, Fujita et al. (53) showed that Hrd1-mediated ERAD downregulates the amount of Pgc1β, thereby regulating mitochondrial biogenesis and lipid oxidation pathways. In *ob/ob* and *db/db* mice adipose tissues, higher levels of Hrd1 are correlated with lower Pgc1β levels, which is responsible for the obesity development in these animal models. Moreover, Sha et al. (54) demonstrated that adipocyte-specific Sel1L-knockout mice exhibit postprandial hypertriglyceridemia and are resistance to diet-induced obesity owing to the faulty maturation and subsequent aggregation of the lipoprotein lipase (Lpl) protein in the ER.

Another recent work reported that the newly identified Hrd1-Aida ERAD complex ubiquitinates and degrades key triglyceride synthesis enzymes – Gpat3, Mogat2 and Dgat2 – in enterocytes, thereby protecting the mice from obesity and postprandial hypertriglyceridemia (55). In the liver, a recent study showed that Hrd1 is responsible for degrading other metabolic enzymes, namely Entpd5, Cpt2, Rmnd1 and Hsd17b4 (56). In addition, Hrd1 has been known to degrade the hepatic nuclear transcription factor Nrf2, which effectively attenuates downstream anti-oxidant signaling pathways (57). However, it is unclear how Hrd1 recognizes and targets nuclear and mitochondria/peroxisome-residing proteins for proteasomal degradation.

In summary, while ERAD function has previously largely been associated with the triage of misfolded proteins in the ER, i.e. quality control (e.g. prohormones), several recent studies now demonstrate in a physiological setting that ERAD also works as a quantity control mechanism to regulate the abundance of key metabolic proteins (e.g. Crebh, Ire1α, pre-BCR). Unlike quality control which safeguards the maturation process in the ER, quantity control by ERAD restrains substrate function and fine-tunes associated downstream processes to optimal levels, thereby playing a critical role in normal physiology and disease pathogenesis in the body (Table 2).

1.5 ERAD IN REGULATING GENE TRANSCRIPTION

A direct communication from the ER membrane to gene transcription at the nucleus has been documented in cases of UPR activation, whereby sensor proteins on the ER membrane (Ire1α, Perk, Atf6) activate downstream processes (Xbp1 splicing, eIF2α phosphorylation, Atf6 cleavage) that affect gene transcriptional events within the nucleus in an effort to restore cellular proteostasis (30). Whether or not ERAD exerts similar control over nuclear transcription remained unknown until recently.

Excitingly, recent studies have demonstrated a complex, intimate relationship between ERAD and nuclear gene transcription via regulating the abundance of ER-membrane proteins or nuclear transcription factors. This design represents a previously underappreciated regulatory cascade linking ER protein turnover to nuclear gene transcription, and regulating key physiological processes in the body.

In the liver, Sel1L-Hrd1 regulates the transcription of Fgf21 gene via degradation of an ER-resident transcription factor Crebh. In the absence of Sel1L-Hrd1, Crebh protein accumulates, gets cleaved at the Golgi and translocates to the nucleus to trigger the expression of many target genes including Fgf21 (33, 34). These studies present a novel "ERAD-Crebh-Fgf21" axis directly linking ERAD to gene transcription and systemic energy metabolism. In addition, Sel1L-Hrd1 ERAD has been established to regulate the turnover of the UPR sensor protein Ire1α, which is responsible for the production of a key UPR transcription factor Xbp1s (36). This ERAD-UPR interaction is required for the control of ER capacity and function.

In addition, Hrd1 may be able to directly target and degrade nuclear transcription factors such as B lymphocyte-induced maturation protein-1 (Blimp1) – a transcriptional repressor of MHC-II gene in dendritic cells (52), Nrf2 – regulator of anti-oxidant pathways in the liver (57), and Pgc1β that regulates lipolysis and mitochondrial dynamics in the adipose tissue (53). However, the underlying molecular mechanism as to how the ERAD complex recognizes nuclear substrates and whether these processes are Sel1L dependent remains unclear.

Collectively, these studies reveal an exciting regulatory system spanning from protein degradation at the ER membrane to gene transcription in the nucleus. More such examples will likely emerge from future investigations.

1.6 ERAD in DISEASE AND DISEASE MUTANTS

Recent progress in ERAD has provided key insights into the pathogenicity of human disease-causing mutations. Two recent papers revealed that ERAD plays a vital role in the clearance of misfolded prohormones – to prevent the dominant negative effects of misfolded proteins (39, 45). These studies help us extrapolate their findings to disease associated mutants since the pathogenic effect of these mutants is due to the inability of ERAD to efficiently triage them. These mutants can evade ERAD, form aggregates, and in the case of dominant negative mutants, interfere with their wildtype counterparts. These new revelations, and the implication that insufficient ERAD may be associated with disease

mutations, unlock great therapeutic potential targeting ERAD-mediated turnover of disease mutants.

LS-101 and LS-102 are two classes of Hrd1 inhibitors that have been identified to suppress the progression of rheumatoid arthritis – a disease in which Hrd1 expression is found to be highly elevated (58). Additionally, selective inhibition of Hrd1 by LS-102 has been shown to increase Pgc1β levels in white adipose tissues, leading to reduced fat accumulation and increased mitochondrial numbers in mouse models (53), further underscoring the therapeutic importance of this regulatory axis in obesity treatment. Finally, Sel1L being indispensable for Hrd1 stability and ERAD function, chemicals or small molecules targeting the interaction between Sel1L and Hrd1 may also have significant therapeutic implications.

1.7 CONCLUSIONS

Recent characterizations of ERAD-deficient animal models demonstrate that ERAD can function at a “constitutive” or “basal” capacity to maintain optimal levels of substrate proteins within the cell – a process that is critical for maintaining physiological homeostasis. Additionally, ERAD activity can perform both “quality control” of misfolded proteins (e.g. proAvp, Pomc) and “quantity control” of folded proteins (e.g. Crebh, preBCR, Ire1α), ensuring proper abundance of substrate proteins and maintaining desired levels of downstream processes. Finally, ERAD is capable of integrating extracellular cues to regulate gene transcription in the nucleus via turnover of ER-resident transcription factors. Taken together, ERAD has become a crucial determinant of normal physiology and acts as a sentinel against disease pathogenesis in the body. Future explorations into physiological ERAD are hence truly an inescapable need of the hour.

1.8 OUTSTANDING QUESTIONS

There is a need in the field now to focus on the gaps that exist in the characterization of ERAD capacity and function, specifically in a (patho)physiological context. Some outstanding questions that need addressing in ERAD biology start with identification of a reliable tool/marker to directly detect ERAD activity levels, especially in a physiological setting, akin to tools available for measurement for UPR activity (Ire1α and Perk phosphorylation, Xbp1 splicing) (Box 2) and autophagic flux (Lc3 lipidation, p62 degradation).

An important question arising now is – what dictates a protein’s susceptibility to ERAD? Ongoing research has been looking for ERAD-responsive signature motifs in structure (e.g.

disulfide bond, transmembrane domain, glycosylation), function (e.g. hormone, ligand, receptor), and/or subcellular localization (e.g. secreted, ER-resident, nuclear). This brings to mind the question whether the ERAD recognition process is relatively stochastic, largely driven by local stoichiometric concentrations, or do specific chaperones (e.g. Os9, Grp78) intervene to make this a deterministic choice. Furthermore, while several recent studies (33, 34, 39, 45) using mouse models have demonstrated that changes in the physiological states of the body (e.g. fasting-feeding, water deprivation, growth) induces ERAD gene expression in specific tissues (Pomc neurons, Avp neurons, liver), an open area of research is to identify transcription factors and/or post-translational modifications responsible for this. Is it possible to translate this regulation to therapeutic drugs aimed at tuning ERAD function in the cell?

One key issue with ERAD is the popular belief that ERAD deficiency is always associated with massive ER stress and cell death. However, that does not appear to hold true under physiological settings (34, 45). Instead, specific substrates for ERAD likely contribute collectively to the phenotypes exhibited by ERAD-deficient animal models. While the erstwhile belief was that disease-causing, misfolding-prone proteins exert their pathogenicity by triggering ER stress and activating UPR, recent work suggest that these disease mutants primarily aim to circumvent ERAD-mediated quantity/quality control, often leading to the abrogation of function of properly folded “bystander” proteins along the way (39, 45). Further emphasis is needed to explore the emerging interplay between these mutant proteins and ERAD function in the context of disease pathogenesis in the body.

Another area that warrants investigation is the inevitable cross-talk among the three key quality control systems within the cell – ERAD, UPR and autophagy – in terms of complementation, redundancy as well as competition, especially in the contexts of substrate choice, cellular resource allocation, and disease development. Animal models bearing tissue-specific deficiencies of ERAD, UPR and autophagy, singly and in combinations with each other, are necessary to tease apart this challenging but critical question.

1.9 REFERENCES

1. Hegde RS, Lingappa VR. Regulation of protein biogenesis at the endoplasmic reticulum membrane. Trends Cell Biol. 1999;9(4):132-7. PubMed PMID: 10203789.
2. Hegde RS, Lingappa VR. Membrane protein biogenesis: regulated complexity at the endoplasmic reticulum. Cell. 1997;91(5):575-82. PubMed PMID: 9393851.
3. Braakman I, Bulleid NJ. Protein folding and modification in the mammalian endoplasmic reticulum. Annual review of biochemistry. 2011;80:71-99. doi: 10.1146/annurev-biochem-062209-093836. PubMed PMID: 21495850.

4. Guerriero CJ, Brodsky JL. The delicate balance between secreted protein folding and endoplasmic reticulum-associated degradation in human physiology. Physiol Rev. 2012;92(2):537-76. Epub 2012/04/27. doi: 10.1152/physrev.00027.2011. PubMed PMID: 22535891.
5. Aridor M, Balch WE. Integration of endoplasmic reticulum signaling in health and disease. Nat Med. 1999;5(7):745-51. doi: 10.1038/10466. PubMed PMID: 10395318.
6. Olzmann JA, Kopito RR, Christianson JC. The Mammalian Endoplasmic Reticulum-Associated Degradation System. Cold Spring Harbor perspectives in biology. 2013;5(9). Epub 2012/12/13. doi: 10.1101/cshperspect.a013185. PubMed PMID: 23232094.
7. Christianson JC, Ye Y. Cleaning up in the endoplasmic reticulum: ubiquitin in charge. Nat Struct Mol Biol. 2014;21(4):325-35. doi: 10.1038/nsmb.2793. PubMed PMID: 24699081.
8. Merulla J, Fasana E, Solda T, Molinari M. Specificity and regulation of the endoplasmic reticulum-associated degradation machinery. Traffic. 2013;14(7):767-77. doi: 10.1111/tra.12068. PubMed PMID: 23521725.
9. Christianson JC, Shaler TA, Tyler RE, Kopito RR. OS-9 and GRP94 deliver mutant alpha1-antitrypsin to the Hrd1-SEL1L ubiquitin ligase complex for ERAD. Nature cell biology. 2008;10(3):272-82. doi: 10.1038/ncb1689. PubMed PMID: 18264092; PMCID: 2757077.
10. van der Goot AT, Pearce MMP, Leto DE, Shaler TA, Kopito RR. Redundant and Antagonistic Roles of XTP3B and OS9 in Decoding Glycan and Non-glycan Degrons in ER-Associated Degradation. Molecular cell. 2018;70(3):516-30 e6. doi: 10.1016/j.molcel.2018.03.026. PubMed PMID: 29706535; PMCID: PMC5935522.
11. Baldridge RD, Rapoport TA. Autoubiquitination of the Hrd1 Ligase Triggers Protein Retrotranslocation in ERAD. Cell. 2016;166(2):394-407. doi: 10.1016/j.cell.2016.05.048. PubMed PMID: 27321670; PMCID: PMC4946995.
12. Carvalho P, Stanley AM, Rapoport TA. Retrotranslocation of a misfolded luminal ER protein by the ubiquitin-ligase Hrd1p. Cell. 2010;143(4):579-91. doi: 10.1016/j.cell.2010.10.028. PubMed PMID: 21074049; PMCID: PMC3026631.
13. Christianson JC, Olzmann JA, Shaler TA, Sowa ME, Bennett EJ, Richter CM, Tyler RE, Greenblatt EJ, Harper JW, Kopito RR. Defining human ERAD networks through an integrative mapping strategy. Nature cell biology. 2012;14(1):93-105. Epub 2011/11/29. doi: 10.1038/ncb2383. PubMed PMID: 22119785; PMCID: 3250479.
14. Mueller B, Klemm EJ, Spooner E, Claessen JH, Ploegh HL. SEL1L nucleates a protein complex required for dislocation of misfolded glycoproteins. Proc Natl Acad Sci U S A. 2008;105(34):12325-30. doi: 10.1073/pnas.0805371105. PubMed PMID: 18711132; PMCID: 2527910.
15. Mueller B, Lilley BN, Ploegh HL. SEL1L, the homologue of yeast Hrd3p, is involved in protein dislocation from the mammalian ER. The Journal of cell biology. 2006;175(2):261-70. Epub 2006/10/18. doi: jcb.200605196 [pii]
10.1083/jcb.200605196. PubMed PMID: 17043138.
16. Sun S, Shi G, Han X, Francisco AB, Ji Y, Mendonca N, Liu X, Locasale JW, Simpson KW, Duhamel GE, Kersten S, Yates JR, 3rd, Long Q, Qi L. Sel1L is indispensable for mammalian endoplasmic reticulum-associated degradation, endoplasmic reticulum homeostasis, and survival. Proc Natl Acad Sci U S A. 2014;111(5):E582-91. doi: 10.1073/pnas.1318114111. PubMed PMID: 24453213; PMCID: 3918815.
17. Kikkert M, Doolman R, Dai M, Avner R, Hassink G, van Voorden S, Thanedar S, Roitelman J, Chau V, Wiertz E. Human HRD1 is an E3 ubiquitin ligase involved in degradation of proteins from the endoplasmic reticulum. J Biol Chem. 2004;279(5):3525-34. doi: 10.1074/jbc.M307453200. PubMed PMID: 14593114.
18. Meyer H, Bug M, Bremer S. Emerging functions of the VCP/p97 AAA-ATPase in the ubiquitin system. Nature cell biology. 2012;14(2):117-23. doi: 10.1038/ncb2407. PubMed PMID: 22298039.
19. Ernst R, Mueller B, Ploegh HL, Schlieker C. The otubain YOD1 is a deubiquitinating enzyme that associates with p97 to facilitate protein dislocation from the ER. Molecular cell. 2009;36(1):28-38. doi: 10.1016/j.molcel.2009.09.016. PubMed PMID: 19818707; PMCID: PMC2774717.

20. Fang S, Ferrone M, Yang C, Jensen JP, Tiwari S, Weissman AM. The tumor autocrine motility factor receptor, gp78, is a ubiquitin protein ligase implicated in degradation from the endoplasmic reticulum. Proc Natl Acad Sci U S A. 2001;98(25):14422-7. doi: 10.1073/pnas.251401598. PubMed PMID: 11724934; PMCID: PMC64697.
21. Hassink G, Kikkert M, van Voorden S, Lee SJ, Spaapen R, van Laar T, Coleman CS, Bartee E, Fruh K, Chau V, Wiertz E. TEB4 is a C4HC3 RING finger-containing ubiquitin ligase of the endoplasmic reticulum. Biochem J. 2005;388(Pt 2):647-55. doi: 10.1042/BJ20041241. PubMed PMID: 15673284; PMCID: PMC1138973.
22. Younger JM, Chen L, Ren HY, Rosser MF, Turnbull EL, Fan CY, Patterson C, Cyr DM. Sequential quality-control checkpoints triage misfolded cystic fibrosis transmembrane conductance regulator. Cell. 2006;126(3):571-82. doi: 10.1016/j.cell.2006.06.041. PubMed PMID: 16901789.
23. Altier C, Garcia-Caballero A, Simms B, You H, Chen L, Walcher J, Tedford HW, Hermosilla T, Zamponi GW. The Cavbeta subunit prevents RFP2-mediated ubiquitination and proteasomal degradation of L-type channels. Nat Neurosci. 2011;14(2):173-80. doi: 10.1038/nn.2712. PubMed PMID: 21186355.
24. Zhang T, Xu Y, Liu Y, Ye Y. gp78 functions downstream of Hrd1 to promote degradation of misfolded proteins of the endoplasmic reticulum. Molecular biology of the cell. 2015;26(24):4438-50. doi: 10.1091/mbc.E15-06-0354. PubMed PMID: 26424800; PMCID: PMC4666138.
25. Francisco AB, Singh R, Li S, Vani AK, Yang L, Munroe RJ, Diaferia G, Cardano M, Biunno I, Qi L, Schimenti JC, Long Q. Deficiency of suppressor enhancer Lin12 1 like (SEL1L) in mice leads to systemic endoplasmic reticulum stress and embryonic lethality. J Biol Chem. 2010;285(18):13694-703. doi: 10.1074/jbc.M109.085340. PubMed PMID: 20197277; PMCID: PMC2859532.
26. Dougan SK, Hu CC, Paquet ME, Greenblatt MB, Kim J, Lilley BN, Watson N, Ploegh HL. Derlin-2-deficient mice reveal an essential role for protein dislocation in chondrocytes. Molecular and cellular biology. 2011;31(6):1145-59. doi: 10.1128/MCB.00967-10. PubMed PMID: 21220515; PMCID: PMC3067910.
27. Muller JM, Deinhardt K, Rosewell I, Warren G, Shima DT. Targeted deletion of p97 (VCP/CDC48) in mouse results in early embryonic lethality. Biochem Biophys Res Commun. 2007;354(2):459-65. doi: 10.1016/j.bbrc.2006.12.206. PubMed PMID: 17239345.
28. Qi L, Tsai B, Arvan P. New Insights into the Physiological Role of Endoplasmic Reticulum-Associated Degradation. Trends Cell Biol. 2017;27(6):430-40. doi: 10.1016/j.tcb.2016.12.002. PubMed PMID: 28131647; PMCID: PMC5440201.
29. Ron D, Walter P. Signal integration in the endoplasmic reticulum unfolded protein response. Nature reviews Molecular cell biology. 2007;8(7):519-29. doi: 10.1038/nrm2199. PubMed PMID: 17565364.
30. Walter P, Ron D. The unfolded protein response: from stress pathway to homeostatic regulation. Science (New York, NY). 2011;334(6059):1081-6. doi: 10.1126/science.1209038. PubMed PMID: 22116877.
31. Hampton RY. ER stress response: getting the UPR hand on misfolded proteins. Curr Biol. 2000;10(14):R518-21. PubMed PMID: 10898996.
32. Zhang K, Wang S, Malhotra J, Hassler JR, Back SH, Wang G, Chang L, Xu W, Miao H, Leonardi R, Chen YE, Jackowski S, Kaufman RJ. The unfolded protein response transducer IRE1alpha prevents ER stress-induced hepatic steatosis. Embo J. 2011;30(7):1357-75. Epub 2011/03/17. doi: emboj201152 [pii] 10.1038/emboj.2011.52. PubMed PMID: 21407177; PMCID: 3094110.
33. Wei J, Chen L, Li F, Yuan Y, Wang Y, Xia W, Zhang Y, Xu Y, Yang Z, Gao B, Jin C, Melo-Cardenas J, Green RM, Pan H, Wang J, He F, Zhang K, Fang D. HRD1-ERAD controls production of the hepatokine FGF21 through CREBH polyubiquitination. The EMBO journal. 2018;37(22). doi: 10.15252/embj.201898942. PubMed PMID: 30389664; PMCID: PMC6236336.
34. Bhattacharya A, Sun S, Wang H, Liu M, Long Q, Yin L, Kersten S, Zhang K, Qi L. Hepatic Sel1L-Hrd1 ER-associated degradation (ERAD) manages FGF21 levels and

systemic metabolism via CREBH. The EMBO journal. 2018;37(22). doi: 10.15252/embj.201899277. PubMed PMID: 30389665; PMCID: PMC6236331.
35. Zhang K, Shen X, Wu J, Sakaki K, Saunders T, Rutkowski DT, Back SH, Kaufman RJ. Endoplasmic reticulum stress activates cleavage of CREBH to induce a systemic inflammatory response. Cell. 2006;124(3):587-99. doi: 10.1016/j.cell.2005.11.040. PubMed PMID: 16469704.
36. Sun S, Shi G, Sha H, Ji Y, Han X, Shu X, Ma H, Inoue T, Gao B, Kim H, Bu P, Guber RD, Shen X, Lee AH, Iwawaki T, Paton AW, Paton JC, Fang D, Tsai B, Yates Iii JR, Wu H, Kersten S, Long Q, Duhamel GE, Simpson KW, Qi L. IRE1alpha is an endogenous substrate of endoplasmic-reticulum-associated degradation. Nature cell biology. 2015;17(12):1546-55. doi: 10.1038/ncb3266. PubMed PMID: 26551274; PMCID: PMC4670240.
37. Ji Y, Kim H, Yang L, Sha H, Roman CA, Long Q, Qi L. The Sel1L-Hrd1 Endoplasmic Reticulum-Associated Degradation Complex Manages a Key Checkpoint in B Cell Development. Cell Rep. 2016;16(10):2630-40. doi: 10.1016/j.celrep.2016.08.003. PubMed PMID: 27568564; PMCID: PMC5014582.
38. Sun S, Lourie R, Cohen SB, Ji Y, Goodrich JK, Poole AC, Ley RE, Denkers EY, McGuckin MA, Long Q, Duhamel GE, Simpson KW, Qi L. Epithelial Sel1L is required for the maintenance of intestinal homeostasis. Molecular biology of the cell. 2016;27(3):483-90. doi: 10.1091/mbc.E15-10-0724. PubMed PMID: 26631554; PMCID: PMC4751599.
39. Shi G, Somlo DRM, Kim GH, Prescianotto-Baschong C, Sun S, Beuret N, Long Q, Rutishauser J, Arvan P, Spiess M, Qi L. ER-associated degradation is required for vasopressin prohormone processing and systemic water homeostasis. J Clin Invest. 2017;127(10):3897-912. doi: 10.1172/JCI94771. PubMed PMID: 28920920; PMCID: PMC5617659.
40. Birk J, Friberg MA, Prescianotto-Baschong C, Spiess M, Rutishauser J. Dominant pro-vasopressin mutants that cause diabetes insipidus form disulfide-linked fibrillar aggregates in the endoplasmic reticulum. Journal of cell science. 2009;122(Pt 21):3994-4002. doi: 10.1242/jcs.051136. PubMed PMID: 19825939.
41. Phillips JA, 3rd. Dominant-negative diabetes insipidus and other endocrinopathies. J Clin Invest. 2003;112(11):1641-3. doi: 10.1172/JCI20441. PubMed PMID: 14660740; PMCID: PMC281655.
42. Ito M, Yu RN, Jameson JL. Mutant vasopressin precursors that cause autosomal dominant neurohypophyseal diabetes insipidus retain dimerization and impair the secretion of wild-type proteins. J Biol Chem. 1999;274(13):9029-37. doi: 10.1074/jbc.274.13.9029. PubMed PMID: 10085151.
43. Ito M, Jameson JL, Ito M. Molecular basis of autosomal dominant neurohypophyseal diabetes insipidus. Cellular toxicity caused by the accumulation of mutant vasopressin precursors within the endoplasmic reticulum. J Clin Invest. 1997;99(8):1897-905. doi: 10.1172/JCI119357. PubMed PMID: 9109434; PMCID: PMC508014.
44. Rittig S, Robertson GL, Siggaard C, Kovacs L, Gregersen N, Nyborg J, Pedersen EB. Identification of 13 new mutations in the vasopressin-neurophysin II gene in 17 kindreds with familial autosomal dominant neurohypophyseal diabetes insipidus. Am J Hum Genet. 1996;58(1):107-17. PubMed PMID: 8554046; PMCID: PMC1914959.
45. Kim GH, Shi G, Somlo DR, Haataja L, Song S, Long Q, Nillni EA, Low MJ, Arvan P, Myers MG, Jr., Qi L. Hypothalamic ER-associated degradation regulates POMC maturation, feeding, and age-associated obesity. J Clin Invest. 2018;128(3):1125-40. doi: 10.1172/JCI96420. PubMed PMID: 29457782; PMCID: PMC5824855.
46. Volpi VG, Ferri C, Fregno I, Del Carro U, Bianchi F, Scapin C, Pettinato E, Solda T, Feltri ML, Molinari M, Wrabetz L, D'Antonio M. Schwann cells ER-associated degradation contributes to myelin maintenance in adult nerves and limits demyelination in CMT1B mice. PLoS genetics. 2019;15(4):e1008069. doi: 10.1371/journal.pgen.1008069. PubMed PMID: 30995221; PMCID: PMC6488099.
47. Hu Y, Gao Y, Zhang M, Deng KY, Singh R, Tian Q, Gong Y, Pan Z, Liu Q, Boisclair YR, Long Q. Endoplasmic Reticulum-Associated Degradation (ERAD) Has a Critical Role in

Supporting Glucose-Stimulated Insulin Secretion in Pancreatic beta-Cells. Diabetes. 2019;68(4):733-46. doi: 10.2337/db18-0624. PubMed PMID: 30626610.
48. Hegde RS, Ploegh HL. Quality and quantity control at the endoplasmic reticulum. Curr Opin Cell Biol. 2010;22(4):437-46. doi: 10.1016/j.ceb.2010.05.005. PubMed PMID: 20570125; PMCID: PMC2929805.
49. Johnson BM, DeBose-Boyd RA. Underlying mechanisms for sterol-induced ubiquitination and ER-associated degradation of HMG CoA reductase. Semin Cell Dev Biol. 2018;81:121-8. doi: 10.1016/j.semcdb.2017.10.019. PubMed PMID: 29107682; PMCID: PMC6341991.
50. Yang Y, Kong S, Zhang Y, Melo-Cardenas J, Gao B, Zhang Y, Zhang DD, Zhang B, Song J, Thorp E, Zhang K, Zhang J, Fang D. The endoplasmic reticulum-resident E3 ubiquitin ligase Hrd1 controls a critical checkpoint in B cell development in mice. J Biol Chem. 2018;293(33):12934-44. doi: 10.1074/jbc.RA117.001267. PubMed PMID: 29907570; PMCID: PMC6102136.
51. Kong S, Yang Y, Xu Y, Wang Y, Zhang Y, Melo-Cardenas J, Xu X, Gao B, Thorp EB, Zhang DD, Zhang B, Song J, Zhang K, Zhang J, Zhang J, Li H, Fang D. Endoplasmic reticulum-resident E3 ubiquitin ligase Hrd1 controls B-cell immunity through degradation of the death receptor CD95/Fas. Proc Natl Acad Sci U S A. 2016;113(37):10394-9. doi: 10.1073/pnas.1606742113. PubMed PMID: 27573825; PMCID: PMC5027446.
52. Yang H, Qiu Q, Gao B, Kong S, Lin Z, Fang D. Hrd1-mediated BLIMP-1 ubiquitination promotes dendritic cell MHCII expression for CD4 T cell priming during inflammation. The Journal of experimental medicine. 2014;211(12):2467-79. doi: 10.1084/jem.20140283. PubMed PMID: 25366967; PMCID: PMC4235642.
53. Fujita H, Yagishita N, Aratani S, Saito-Fujita T, Morota S, Yamano Y, Hansson MJ, Inazu M, Kokuba H, Sudo K, Sato E, Kawahara K, Nakajima F, Hasegawa D, Higuchi I, Sato T, Araya N, Usui C, Nishioka K, Nakatani Y, Maruyama I, Usui M, Hara N, Uchino H, Elmer E, Nishioka K, Nakajima T. The E3 ligase synoviolin controls body weight and mitochondrial biogenesis through negative regulation of PGC-1beta. The EMBO journal. 2015;34(8):1042-55. doi: 10.15252/embj.201489897. PubMed PMID: 25698262; PMCID: PMC4406651.
54. Sha H, Sun S, Francisco AB, Ehrhardt N, Xue Z, Liu L, Lawrence P, Mattijssen F, Guber RD, Panhwar MS, Brenna JT, Shi H, Xue B, Kersten S, Bensadoun A, Peterfy M, Long Q, Qi L. The ER-associated degradation adaptor protein Sel1L regulates LPL secretion and lipid metabolism. Cell metabolism. 2014;20(3):458-70. doi: 10.1016/j.cmet.2014.06.015. PubMed PMID: 25066055; PMCID: 4156539.
55. Luo H, Jiang M, Lian G, Liu Q, Shi M, Li TY, Song L, Ye J, He Y, Yao L, Zhang C, Lin ZZ, Zhang CS, Zhao TJ, Jia WP, Li P, Lin SY, Lin SC. AIDA Selectively Mediates Downregulation of Fat Synthesis Enzymes by ERAD to Retard Intestinal Fat Absorption and Prevent Obesity. Cell metabolism. 2018;27(4):843-53 e6. doi: 10.1016/j.cmet.2018.02.021. PubMed PMID: 29617643.
56. Wei J, Yuan Y, Chen L, Xu Y, Zhang Y, Wang Y, Yang Y, Peek CB, Diebold L, Yang Y, Gao B, Jin C, Melo-Cardenas J, Chandel NS, Zhang DD, Pan H, Zhang K, Wang J, He F, Fang D. ER-associated ubiquitin ligase HRD1 programs liver metabolism by targeting multiple metabolic enzymes. Nat Commun. 2018;9(1):3659. doi: 10.1038/s41467-018-06091-7. PubMed PMID: 30201971; PMCID: PMC6131148.
57. Wu T, Zhao F, Gao B, Tan C, Yagishita N, Nakajima T, Wong PK, Chapman E, Fang D, Zhang DD. Hrd1 suppresses Nrf2-mediated cellular protection during liver cirrhosis. Genes & development. 2014;28(7):708-22. doi: 10.1101/gad.238246.114. PubMed PMID: 24636985; PMCID: PMC4015486.
58. Yagishita N, Aratani S, Leach C, Amano T, Yamano Y, Nakatani K, Nishioka K, Nakajima T. RING-finger type E3 ubiquitin ligase inhibitors as novel candidates for the treatment of rheumatoid arthritis. Int J Mol Med. 2012;30(6):1281-6. doi: 10.3892/ijmm.2012.1129. PubMed PMID: 22992760; PMCID: PMC4042867.
59. Yang L, Xue Z, He Y, Sun S, Chen H, Qi L. A Phos-tag-based approach reveals the extent of physiological endoplasmic reticulum stress. PLoS One. 2010;5(7):e11621. doi: 10.1371/journal.pone.0011621. PubMed PMID: 20661282; PMCID: PMC2905412.

60. Sha H, He Y, Chen H, Wang C, Zenno A, Shi H, Yang X, Zhang X, Qi L. The IRE1alpha-XBP1 pathway of the unfolded protein response is required for adipogenesis. Cell metabolism. 2009;9(6):556-64. doi: 10.1016/j.cmet.2009.04.009. PubMed PMID: 19490910; PMCID: PMC2963107.
61. Yao T, Deng Z, Gao Y, Sun J, Kong X, Huang Y, He Z, Xu Y, Chang Y, Yu KJ, Findley BG, Berglund ED, Wang RT, Guo H, Chen H, Li X, Kaufman RJ, Yan J, Liu T, Williams KW. Ire1alpha in Pomc Neurons Is Required for Thermogenesis and Glycemia. Diabetes. 2017;66(3):663-73. doi: 10.2337/db16-0533. PubMed PMID: 28028078; PMCID: PMC5319716.
62. Xiao Y, Xia T, Yu J, Deng Y, Liu H, Liu B, Chen S, Liu Y, Guo F. Knockout of inositol-requiring enzyme 1alpha in pro-opiomelanocortin neurons decreases fat mass via increasing energy expenditure. Open Biol. 2016;6(8). doi: 10.1098/rsob.160131. PubMed PMID: 27558934; PMCID: PMC5008012.
63. Shao M, Shan B, Liu Y, Deng Y, Yan C, Wu Y, Mao T, Qiu Y, Zhou Y, Jiang S, Jia W, Li J, Li J, Rui L, Yang L, Liu Y. Hepatic IRE1alpha regulates fasting-induced metabolic adaptive programs through the XBP1s-PPARalpha axis signalling. Nat Commun. 2014;5:3528. doi: 10.1038/ncomms4528. PubMed PMID: 24670948.
64. Jiang S, Yan C, Fang QC, Shao ML, Zhang YL, Liu Y, Deng YP, Shan B, Liu JQ, Li HT, Yang L, Zhou J, Dai Z, Liu Y, Jia WP. Fibroblast growth factor 21 is regulated by the IRE1alpha-XBP1 branch of the unfolded protein response and counteracts endoplasmic reticulum stress-induced hepatic steatosis. J Biol Chem. 2014;289(43):29751-65. doi: 10.1074/jbc.M114.565960. PubMed PMID: 25170079; PMCID: PMC4207989.
65. Wang JM, Qiu Y, Yang Z, Kim H, Qian Q, Sun Q, Zhang C, Yin L, Fang D, Back SH, Kaufman RJ, Yang L, Zhang K. IRE1alpha prevents hepatic steatosis by processing and promoting the degradation of select microRNAs. Sci Signal. 2018;11(530). doi: 10.1126/scisignal.aao4617. PubMed PMID: 29764990; PMCID: PMC6075656.
66. Niederreiter L, Fritz TM, Adolph TE, Krismer AM, Offner FA, Tschurtschenthaler M, Flak MB, Hosomi S, Tomczak MF, Kaneider NC, Sarcevic E, Kempster SL, Raine T, Esser D, Rosenstiel P, Kohno K, Iwawaki T, Tilg H, Blumberg RS, Kaser A. ER stress transcription factor Xbp1 suppresses intestinal tumorigenesis and directs intestinal stem cells. The Journal of experimental medicine. 2013;210(10):2041-56. doi: 10.1084/jem.20122341. PubMed PMID: 24043762; PMCID: PMC3782039.
67. Kaser A, Lee AH, Franke A, Glickman JN, Zeissig S, Tilg H, Nieuwenhuis EE, Higgins DE, Schreiber S, Glimcher LH, Blumberg RS. XBP1 links ER stress to intestinal inflammation and confers genetic risk for human inflammatory bowel disease. Cell. 2008;134(5):743-56. doi: 10.1016/j.cell.2008.07.021. PubMed PMID: 18775308; PMCID: PMC2586148.
68. Deng Y, Wang ZV, Gordillo R, Zhu Y, Ali A, Zhang C, Wang X, Shao M, Zhang Z, Iyengar P, Gupta RK, Horton JD, Hill JA, Scherer PE. Adipocyte Xbp1s overexpression drives uridine production and reduces obesity. Mol Metab. 2018;11:1-17. doi: 10.1016/j.molmet.2018.02.013. PubMed PMID: 29551634; PMCID: PMC6001360.
69. Sha H, Yang L, Liu M, Xia S, Liu Y, Liu F, Kersten S, Qi L. Adipocyte spliced form of X-box-binding protein 1 promotes adiponectin multimerization and systemic glucose homeostasis. Diabetes. 2014;63(3):867-79. doi: 10.2337/db13-1067. PubMed PMID: 24241534; PMCID: PMC3931404.
70. Benhamron S, Hadar R, Iwawaky T, So JS, Lee AH, Tirosh B. Regulated IRE1-dependent decay participates in curtailing immunoglobulin secretion from plasma cells. Eur J Immunol. 2014;44(3):867-76. doi: 10.1002/eji.201343953. PubMed PMID: 24242955.
71. Goldfinger M, Laviad EL, Hadar R, Shmuel M, Dagan A, Park H, Merrill AH, Jr., Ringel I, Futerman AH, Tirosh B. De novo ceramide synthesis is required for N-linked glycosylation in plasma cells. J Immunol. 2009;182(11):7038-47. doi: 10.4049/jimmunol.0802990. PubMed PMID: 19454701.
72. Medel B, Costoya C, Fernandez D, Pereda C, Lladser A, Sauma D, Pacheco R, Iwawaki T, Salazar-Onfray F, Osorio F. IRE1alpha Activation in Bone Marrow-Derived Dendritic Cells Modulates Innate Recognition of Melanoma Cells and Favors CD8(+) T Cell

Priming. Front Immunol. 2018;9:3050. doi: 10.3389/fimmu.2018.03050. PubMed PMID: 30687308; PMCID: PMC6338037.
73. Tsuchiya Y, Saito M, Kadokura H, Miyazaki JI, Tashiro F, Imagawa Y, Iwawaki T, Kohno K. IRE1-XBP1 pathway regulates oxidative proinsulin folding in pancreatic beta cells. The Journal of cell biology. 2018;217(4):1287-301. doi: 10.1083/jcb.201707143. PubMed PMID: 29507125; PMCID: PMC5881499.
74. Xu T, Yang L, Yan C, Wang X, Huang P, Zhao F, Zhao L, Zhang M, Jia W, Wang X, Liu Y. The IRE1alpha-XBP1 pathway regulates metabolic stress-induced compensatory proliferation of pancreatic beta-cells. Cell research. 2014;24(9):1137-40. doi: 10.1038/cr.2014.55. PubMed PMID: 24797433; PMCID: PMC4152740.
75. Zhang W, Feng D, Li Y, Iida K, McGrath B, Cavener DR. PERK EIF2AK3 control of pancreatic beta cell differentiation and proliferation is required for postnatal glucose homeostasis. Cell metabolism. 2006;4(6):491-7. doi: 10.1016/j.cmet.2006.11.002. PubMed PMID: 17141632.
76. Iida K, Li Y, McGrath BC, Frank A, Cavener DR. PERK eIF2 alpha kinase is required to regulate the viability of the exocrine pancreas in mice. BMC Cell Biol. 2007;8:38. doi: 10.1186/1471-2121-8-38. PubMed PMID: 17727724; PMCID: PMC2072952.
77. Zhang P, McGrath B, Li S, Frank A, Zambito F, Reinert J, Gannon M, Ma K, McNaughton K, Cavener DR. The PERK eukaryotic initiation factor 2 alpha kinase is required for the development of the skeletal system, postnatal growth, and the function and viability of the pancreas. Molecular and cellular biology. 2002;22(11):3864-74. doi: 10.1128/mcb.22.11.3864-3874.2002. PubMed PMID: 11997520; PMCID: PMC133833.
78. Sun S, Shi G, Sha H, Ji Y, Han X, Shu X, Ma H, Inoue T, Gao B, Kim H, Bu P, Guber RD, Shen X, Lee AH, Iwawaki T, Paton AW, Paton JC, Fang D, Tsai B, Yates JR, 3rd, Wu H, Kersten S, Long Q, Duhamel GE, Simpson KW, Qi L. IRE1alpha is an endogenous substrate of endoplasmic-reticulum-associated degradation. Nature cell biology. 2015;17(12):1546-55. doi: 10.1038/ncb3266. PubMed PMID: 26551274; PMCID: PMC4670240.

1.10 BOXES

Box 1. How to identify a *bona fide* endogenous ERAD substrate.

Hallmarks (necessary):

1. Stabilization of substrate protein (elongation of half-life) in the absence of ERAD
2. Significant increase in substrate protein levels in the absence of ERAD
3. No significant upregulation of substrate mRNA levels
4. E3 ligase-dependent poly-ubiquitination of substrate protein

Auxiliary (optional):

5. Interaction with core ERAD components (E3 ligase, adaptor protein)
6. High-molecular-weight complex formation or aggregation of substrate protein in the absence of ERAD

Box 2. Tools to accurately quantitate changes in ER homeostasis

I. Phosphorylation of the UPR sensors Ire1α and Perk is required to accurately assess the status of ER stress **(59)**.

II. Downstream effectors of Ire1α and Perk: *Xbp1* mRNA splicing and phosphorylation of eIF2α in total eIF2α protein level **(60)**.

III. Expression of downstream target genes may be measured, but cannot be used by themselves to assess ER stress level under patho-physiological condition.

Reliable antibodies for Western Blotting:

(i) Ire1α, Cell Signaling #3294

(ii) Xbp1s, Cell Signaling #83418

(iii) Perk, Cell Signaling #3192

(iv) Phospho-eIF2α, Cell Signaling #3597

(v) eIF2α-total, Cell Signaling #9722

1.11 TABLES

Table 1. ERAD- versus UPR-deficient animal models.

Cell type	*In vivo loss of ERAD*	*In vivo loss of UPR*
Pomc neuron	Tg(Pomc-Cre); Sel1L-flox/flox. Early-onset obesity under normal chow diet, hyperphagia. (45)	Tg(Pomc-Cre); Ire1-flox/flox. Obesity after 3-month high-fat diet, hyperphagia. (61); resistance to high-fat diet-induced obesity, adipose tissue browning. (62)
Hepatocyte	Tg(Alb-Cre); Sel1L/Hrd1-flox/flox. High serum Fgf21 levels, decreased growth, activity and female fertility, increased insulin sensitivity and fat browning. (33, 34)	Tg(Alb-Cre); Ire1-flox/flox. Lower serum Fgf21 levels, impaired β-oxidation and ketogenesis, chemical- or diet-induced hepatic steatosis. (32, 63-65)
Enterocyte	Tg(Villin-Cre); Sel1L-flox/flox. Paneth cell defect, spontaneous enteritis, inflammation-associated dysbiosis, susceptibility to experimental colitis. (36, 38)	Tg(Villin-Cre); Xbp1-flox/flox. Paneth cell defect, spontaneous enteritis, hyper-proliferative stem cells, susceptibility to colitis and intestinal tumors. (66, 67)
Adipocyte	Tg(Adipoq-Cre); Sel1L-flox/flox. Resistance to diet-induced obesity, postprandial hypertriglyceridemia. (53, 54)	rTA(Adipoq); Tre-Xbp1s, Tg(Adipoq-Cre); Xbp1-flox/flox. Regulation of UMP pathway, lipolysis, obesity (68). Tg-Xbp1s. Improved glucose homeostasis, adiponectin maturation/assembly (69).
B cell	Cd19-Cre; Sel1L/Hrd1-flox/flox. Blocked development of large pre-B cells, reduced mature plasma cells; increased activation-induced B-cell death (AICD). (37, 50, 51)	Cd19-Cre; Xbp1/Ire1-flox/flox. Normal B cell development, reduced secretory function of plasma cells. (70, 71)
Dendritic cell	Cd11c-Cre; Hrd1-flox/flox. Impaired CD4+T cell priming, resistance to experimental autoimmune encephalomyelitis (EAE) by myelin oligodendrocyte glycoprotein (52).	Cd11c-Cre; Ire1-flox/flox. Impaired CD8+T cell proliferation/priming to melanoma-associated antigen. (72)
Pancreatic β cell	Tg(Ins2-Cre); Sel1L-flox/flox. Blunted glucose-stimulated insulin secretion, chronic hyperglycemia, glucose intolerance, diabetes mellitus. (47)	Tg(Ins2-Cre); Ire1-flox/flox. Impaired insulin production, chronic hyperglycemia, glucose intolerance, diabetes mellitus. (15, 73-75)
Whole pancreas	Tg(Cre-Ertm); Sel1L-flox/flox. Profound pancreatic atrophy, exocrine pancreatic insufficiency/atrophy, apoptosis (16)	Ela-Ert2-Cre/Ngn3-Cre/Pdx1-Cre; Perk-flox/flox: exocrine/endocrine/pancreas. Diabetes mellitus, β cell death, exocrine pancreatic atrophy (75-77).

Table 2. Endogenous ERAD substrates vis-à-vis localization and pathology.

Substrate	*ERAD complex*	*Subcellular localization*	*Cell type*	*Pathology*
Pre-BCR	Sel1L, Hrd1	Plasma membrane, ER membrane	B cell	Developmental block in transition from large to small pre-B cells (37, 50)
Fas	Hrd1		B cell	Activation-induced B-cell death (AICD), reduced mature B cells (51)
Protein0	Derlin2		Schwann cell	Impaired myelin homeostasis, Charcot-Marie-Tooth 1B neuropathy (46)
Crebh	Sel1L, Hrd1	ER membrane, Nucleus	Hepatocyte	Highly elevated Fgf21 levels, altered growth and metabolism (33, 34)
Ire1α	Sel1L, Hrd1	ER membrane	Ubiquitous	Spontaneous ileitis, susceptibility to experimental colitis, dysbiosis (78)
Mogat2	Aida, Hrd1		Enterocyte	Increased fatty acid re-esterification and lipid absorption in intestine, postprandial hypertriglyceridemia, severe obesity in the absence of increased adipogenesis (55)
Dgat2	Aida, Hrd1		Enterocyte	
Gpat3	Aida, Hrd1		Enterocyte	
Pro-Avp	Sel1L, Hrd1	ER	Avp neuron	Central diabetes insipidus, polydipsia, polyuria (39)
Pomc	Sel1L, Hrd1		Pomc neuron	Hyperphagia, hyperleptinemia, age-associated obesity (45)
Nrf2	Hrd1	Nucleus	Hepatocyte	Suppression of anti-oxidation pathway, liver cirrhosis (57)
Pgc1β	Hrd1		White adipocyte	Altered mitochondrial dynamics, weight gain and obesity (53)
Blimp1	Hrd1		Dendritic cell	Myelin oligodendrocyte glycoprotein-induced experimental autoimmune encephalomyelitis (52)
Hsd17b4	Hrd1	Peroxisome	Hepatocyte	Over activation of Ampk/Akt, insulin sensitivity, resistance to diet-induced obesity, fatty liver disease (Entpd5 aids in ATP hydrolysis, Cpt2, Rmnd1 in lipid/protein translocation, Hsd17b4 in fatty acid oxidation) (56)
Entpd5	Hrd1	ER lumen	Hepatocyte	
Cpt2	Hrd1	Mitochondrial inner membrane	Hepatocyte	
Rmnd1	Hrd1	Mitochondria	Hepatocyte	

1.12 FIGURE

Figure 1. A bird's eye view of ERAD: from biochemistry to physiology.

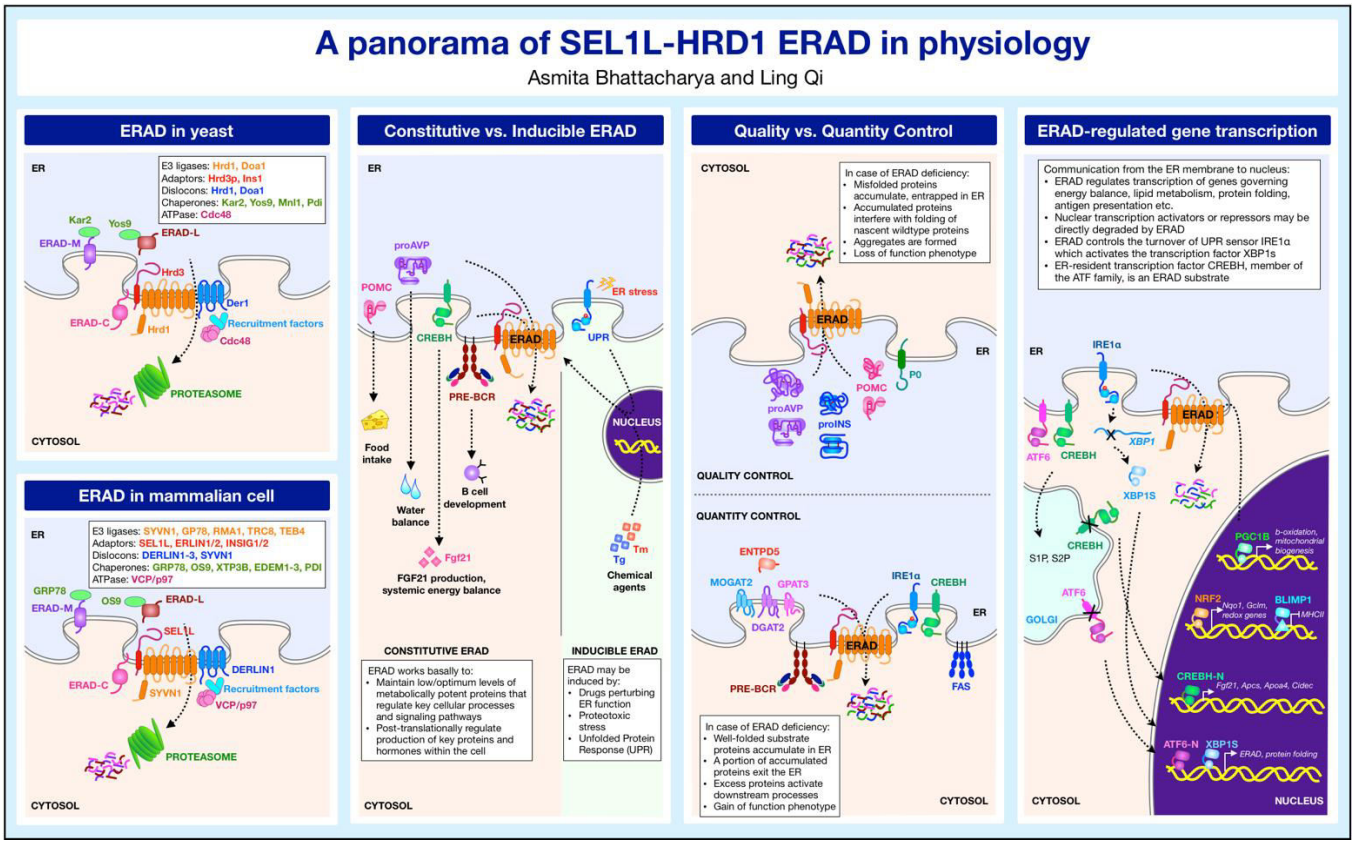

CHAPTER 2

Hepatic Sel1L-Hrd1 ER-Associated Degradation (ERAD) manages FGF21 levels and systemic metabolism via CREBH

Asmita Bhattacharya[1,2,8], Shengyi Sun[3], Heting Wang[4], Ming Liu[4,8], Qiaoming Long[5]*, Lei Yin[1,8], Sander Kersten[6], Kezhong Zhang[7], Ling Qi[1,8]*

[1] Department of Molecular and Integrative Physiology, University of Michigan Medical School, Ann Arbor, MI 48105, USA;
[2] Graduate Program of Genetics, Genomics and Development, Cornell University, Ithaca, NY 14853, USA;
[3] Department of Pharmacology, University of Texas Southwestern Medical Center, Dallas, TX 75390, USA
[4] Department of Endocrinology and Metabolism, Tianjin Medical University General Hospital, Tianjin 300052, China;
[5] Cam-Su Mouse Genomic Resource Center, Soochow University, Suzhou, Jiangsu 215123, China;
[6] Nutrition Metabolism and Genomics group, Wageningen University, Wageningen, The Netherlands;
[7] Center for Molecular Medicine and Genetics, Department of Immunology and Microbiology, Wayne State University School of Medicine, Detroit, MI 48201, USA;
[8] Division of Metabolism, Endocrinology & Diabetes, Department of Internal Medicine, University of Michigan Medical School, Ann Arbor, MI 48105, USA;

*** Correspondence:**
Ling Qi: lingq@med.umich.edu; Qiaoming Long: qmlong@suda.edu.cn

This chapter has recently been published as an article in **EMBO Journal** in 2018.

2.1 ABSTRACT

Fibroblast growth factor 21 (Fgf21) is a liver-derived, fasting-induced hormone with broad effects on growth, nutrient metabolism and insulin sensitivity. Here, we report the discovery of a novel mechanism regulating *Fgf21* expression under growth and fasting-feeding. The Sel1L-Hrd1 complex is the most conserved branch of mammalian endoplasmic reticulum (ER)-associated degradation (ERAD) machinery. Mice with liver-specific deletion of Sel1L exhibit growth retardation with markedly elevated circulating Fgf21, reaching levels close to those in Fgf21 transgenic mice or pharmacological models. Mechanistically, we show that the Sel1L-Hrd1 ERAD complex controls *Fgf21* transcription by regulating the ubiquitination and turnover (and thus nuclear abundance) of ER-resident transcription factor Crebh, while having no effect on the other well-known Fgf21 transcription factor Pparα. Our data reveal a physiologically-regulated, inverse correlation between Sel1L-Hrd1 ERAD and Crebh-Fgf21 levels under fasting-feeding and growth. This study not only establishes the importance of Sel1L-Hrd1 ERAD in the liver in the regulation of systemic energy metabolism, but also reveals a novel hepatic "ERAD-Crebh-Fgf21" axis directly linking ER protein turnover to gene transcription and systemic metabolic regulation.

2.2 INTRODUCTION

The liver regulates growth and systemic energy homeostasis through inter-organ communication via the secretion of growth factors, hormones and peptides. The "starvation hormone" Fgf21 is predominantly secreted from the liver, activating energy-saving pathways that reduce activity, growth and anabolic reactions, while increasing insulin sensitivity, lipolysis and adipose tissue browning (1-3). Recent reports have shown the therapeutic potential of Fgf21 in a variety of human disease conditions such as diabetes, obesity and cardiovascular disorders (4, 5). Expression of *Fgf21* is primarily known to be induced in response to metabolic cues such as fasting by a synergistic interaction between the nuclear receptor peroxisome proliferator-activated receptor α (Pparα) and the recently identified ER-resident transcription factor cAMP-responsive element-binding protein 3-like protein 3, hepatocyte-specific (Creb3l3 or Crebh) (6-10). Unlike Pparα, Crebh encodes an ER membrane-anchored transcription factor, which requires regulated intramembrane proteolysis at the Golgi to generate the Crebh N-terminal fragment (Crebh-N) (11-13). Subsequently, Crebh-N goes to the nucleus and is believed to recruit and form a complex with Pparα, which induces transcriptional activation of the *Fgf21* gene (9, 14). While it is well known that *Fgf21* expression is induced by the nuclear

receptor Pparα during fasting, how *Fgf21* expression is regulated and the importance of CREBH under physiological contexts remains to be established.

In this study, we identified a surprising link between Fgf21 gene transcription and a principal ER quality control machinery, known as ER-associated degradation (ERAD). ERAD is responsible for recognizing and retro-translocating protein substrates, misfolded or not, from the ER for cytosolic proteasomal degradation (15, 16). The most conserved ERAD system in mammals is the Sel1L-Hrd1 protein complex: Hrd1 being the E3 ubiquitin ligase, and Sel1L being its essential cofactor. Studies from yeast and mammalian systems have suggested that the single-spanning ER transmembrane protein Sel1L is required for the stability of Hrd1 as well as substrate recruitment and selection (17-20). Germline deletion of *Sel1L* or *Hrd1* in mice leads to embryonic lethality (21, 22) and acute deletion of either gene in adult mice leads to premature death (18, 23).

Subsequent characterization of cell type-specific Sel1L- (18, 24-28) and Hrd1- (23, 29-32) knockout mouse models, including gene deletion in adipocytes, immune cells, enterocytes and various neurons, has revealed the significance of Sel1L-Hrd1 ERAD in a cell type- and substrate- specific manner in vivo (16). For example, mice with Sel1L deficiency in adipocytes exhibit lipodystrophy and postprandial hyperlipidemia due to the ER retention of lipoprotein lipase (LPL) (24). Further, mice with Sel1L ablation in arginine-vasopressin (AVP) neurons progressively develop polyuria and polydipsia — characteristics of diabetes insipidus, due to a maturation defect of AVP precursor, proAVP, in the ER (28). Similarly, mice with Sel1L ablation in proopiomelanocortin (POMC) neurons develop hyperphagia and obesity even under low-fat chow diet due to ER retention of POMC prohormone (33).

In the characterization of hepatocyte-specific Sel1L-deficient mice, we discovered that the Sel1L-Hrd1 ERAD complex plays a key role in regulating *Fgf21* transcription and growth in a Crebh-dependent manner. ER-resident Crebh is an unstable protein with a half-life of about 1 hour, and is targeted for proteasomal degradation by the Sel1L-Hrd1 ERAD complex. In the absence of Sel1L, Crebh accumulates intracellularly, leading to a marked elevation of *Fgf21* gene transcription in the liver and circulating Fgf21 levels. Our data further show that physiological effect of hepatic Sel1L-Hrd1 ERAD is indeed mediated, at least partially, through the CREBH-FGF21 axis. Pointing to the physiological significance of Sel1L-Hrd1 ERAD, we further showed that hepatic Sel1L-Hrd1 protein complex represses the expression of the Crebh-

Fgf21 axis during growth and fasting-feeding. Thus, this study identifies the Sel1L-Hrd1 ERAD complex as a key repressor of *Fgf21* transcription in the liver.

2.3 RESULTS

Expression of Sel1L-Hrd1 ERAD in the liver is responsive to physiological signals

As the liver plays a vital role in nutrient metabolism, we speculate that the levels of Sel1L-Hrd1 ERAD in the liver may fluctuate in response to metabolic signals during growth and fasting-feeding. Indeed, protein levels of hepatic Sel1L and Hrd1 were steadily elevated during growth from 3 to 24 weeks of age (Figure 1A) and were significantly higher during feeding than after an overnight fast (Figure 1B). mRNA level of Hrd1, but not Sel1L, was also elevated during growth and feeding (Appendix Figure S1A-B).

Growth retardation of *Sel1L*^{Alb} mice

To explore the role of hepatic Sel1L-Hrd1 ERAD in vivo, we generated liver-specific Sel1L knockout mice (*Sel1L*^{Alb}) by crossing *Sel1L*$^{f/f}$ with the hepatocyte-specific driver mouse line expressing Cre recombinase under the albumin promoter (Appendix Figure S1C). Sel1L was specifically deleted in the liver (Figure 1C), but not in other tissues such as small intestine (Appendix Figure S1D-F). The protein level of the E3 ligase Hrd1 was significantly reduced by 50% in the absence of Sel1L while its mRNA level was increased by 2.5-fold (Figure 1C and Appendix Figure S1G). On the other hand, protein levels of the previously published Sel1L-Hrd1 ERAD substrate Ire1α and Os9 (24, 25) were increased by 5-10 fold in the *Sel1L*^{Alb} liver (Figure 1C), while their mRNA levels were only modestly upregulated (Appendix Figure S1G).

Interestingly, both male and female *Sel1L*^{Alb} mice showed significant growth retardation post weaning compared to their WT littermates on regular chow diet (Figure 1D). This growth retardation was due to shorter stature as demonstrated by body length measurements (Figure 1E-F), while ratios of organ to body weights for the liver and kidneys were unaffected (Figure 1G). Daily food intake was comparable (Figure 1H) between the two genotypes. Female *Sel1L*^{Alb} mice at 2-4 months of age had reduced estrous cycle, which normally lasted 4-5 days in *Sel1L*$^{f/f}$ littermates (Figure 1I) and hence were largely infertile, but not the males.

Histological examination of the *Sel1L*^{Alb} livers revealed no obvious abnormalities (Figure 1J), and there was no increase in cell death as measured by TUNEL staining (Figure EV1A) and

Caspase-3 cleavage (Figure 1K), nor inflammation as measured by the expression of various inflammatory genes (Figure EV1B). ER stress was only moderately increased in the Sel1L-deficient hepatocytes, as measured by Ire1α phosphorylation and *Xbp1* mRNA splicing in the livers of 9-week-old *Sel1L*^{Alb} mice (Figure EV1C-D) as well as in *Sel1L*^{Alb} primary hepatocytes (Figure EV1E). Morphologically, the ER in *Sel1L*^{Alb} hepatocytes was dilated (Figure 1L). These observations are in line with our previous reports in several cell types such as adipocytes and enterocytes that Sel1L deficiency in vivo is associated with a mild adaptive UPR, and uncoupled from inflammation and cell death (16, 18, 24-26). Taken together, these data demonstrate that Sel1L deficiency in the liver leads to growth retardation without overt inflammation or cell death.

Elevated Fgf21 levels in the absence of Sel1L

To explore how deletion of Sel1L in the liver has such a profound effect on growth, we performed transcriptomics analysis of the livers from *Sel1L*^{Alb} mice and their control littermates at 9-weeks of age. A total of 169 genes were significantly upregulated while 129 genes were significantly downregulated ($p < 0.05$, black dots represent fold change >2) in *Sel1L*^{Alb} livers (Figure 2A). Gene set enrichment analysis confirmed significant upregulation of "protein processing in the ER", in keeping with the notion that Sel1L deficiency triggers cellular adaptation in hepatocytes. Additionally, various key metabolic pathways, including "insulin sensitivity", "PI3K-Akt pathways", "steroid hormone synthesis" and more, were significantly affected in *Sel1L*^{Alb} livers (Appendix Figure S2A).

Interestingly, *Fgf21*, a fasting-induced hormone, was one of the top hits among the most highly upregulated genes in *Sel1L*^{Alb} mice (Figure 2A). Quantitative PCR (qPCR) and Western blot analyses showed a 13- and 4-fold increase of *Fgf21* mRNA and protein levels, respectively, in the *Sel1L*^{Alb} livers (Figure 2B-C). Strikingly, serum levels of Fgf21 were elevated by over 20-fold in *Sel1L*^{Alb} mice, reaching to ~10 ng/ml vs. ~0.5 ng/ml in WT littermates (Figure 2D). As a control, *Fgf21* expression in brown and white adipose was not changed (Appendix Figure S2B).

To exclude potential developmental defects associated with chronic *Sel1L* deletion, we performed acute Sel1L deletion in the following two experiments. First, we cultured primary hepatocytes from a tamoxifen-inducible Sel1L-floxed mouse model (*Sel1L*^{ERCre}) and found that *Fgf21* expression was significantly increased upon the addition of tamoxifen (Figure 2E). Second, we injected 8-week-old *Sel1L*$^{f/f}$ mice once i.v. with adeno-associated virus serotype 8 (AAV8)-expressing Cre recombinase (or control GFP). Acute injection of AAV8-Cre abolished

Sel1L protein level specifically in the liver, not in white adipose tissue (Figure 2F) 2-3 weeks' post injection. Similar to the chronic *Sel1L*^{Alb} model, acute *Sel1L* deletion led to an 8-fold increase of hepatic *Fgf21* mRNA, and a profound 14-fold elevation of circulating Fgf21 levels (Figure 2G). Hence, these data firmly establish the key role of hepatic Sel1L-Hrd1 ERAD in regulating Fgf21 levels in both chronic and acute Sel1L-deficient models.

We next performed an unbiased comparison of genome-wide expression analyses of genes that were altered in *Sel1L*^{Alb} livers to genome-wide expression analysis of genes altered in Fgf21-overexpressing transgenic mouse livers (*Fgf21 Tg*; GEO dataset series GSE39313). Indeed, the two datasets showed a large overlap among the top 15 upregulated or downregulated hepatic genes (Figure 2H and Appendix Figure S2C). This analysis further revealed a positive correlation between the genes altered in both datasets, as evident from the polarization of the scatter plot towards the top-right and bottom-left quadrants (Figure 2I). Several examples of shared genes are highlighted in red (up-regulated) and blue (down-regulated) while those unique to each dataset, i.e. close to either axis, are marked in green (Figure 2I). Therefore, Sel1L deficiency in the liver results in elevated *Fgf21* expression and circulating Fgf21.

Systemic metabolism changes of *Sel1L*^{Alb} mice are in part mediated by Fgf21

To further establish the causal link between elevated Fgf21 levels and Sel1L-deficiency-associated systemic changes, we injected *Sel1L*^{Alb} mice with AAV8 encoding shRNA against *Fgf21* or control luciferase (*luc*). As a result of this knockdown, both the hepatic mRNA and circulating levels of Fgf21 in these mice were reduced by around 60% (Figure 2J-K) while having no effect on the Sel1L-Hrd1 protein levels in the liver (Appendix Figure S3A). Interestingly, this knockdown partially reversed the growth retardation (Figure 2L) and rescued the reduced female fertility (Appendix Figure S3B) of the *Sel1L*^{Alb} mice.

To provide further evidence for the Sel1L-Fgf21 link, we next asked whether *Sel1L*^{Alb} mice phenocopy Fgf21 gain-of-function models. Fgf21 has many metabolic effects aimed at promoting organismal adaptation to starvation (2, 34). Importantly, similar to our *Sel1L*^{Alb} mice, Fgf21 transgenic mice also exhibited growth retardation, which was partially mediated by Stat5-dependent signaling pathways (1, 35-37). Indeed, in line with Fgf21 gain-of-function models, Stat5 phosphorylation was markedly decreased in *Sel1L*^{Alb} livers (Figure 3A) with diminished expression of various growth-related, p-Stat5-associated genes such as *Growth hormone receptor (Ghr), Insulin-like growth factor-1 (Igf1), Acid labile subunit (Als), Na*$^{+}$*-taurocholate*

cotransporting polypeptide (Ntcp), and Organic anion transporter family member-1 (Oatp1) (Figure 3B). Moreover, in line with the suppressive effect of Fgf21 on hepatic lipogenesis (38, 39), many genes involved in hepatic lipid synthesis and transport, including *Sterol regulatory element-binding protein-1c (Srebp1c), 3-Hydroxy-3-methylglutaryl-CoA reductase (Hmgcr), Acetyl-CoA carboxylase-1/2 (Acc1/2), Low density lipoprotein receptor (Ldlr), ATP binding cassette subfamily G member-5/8 (Abcg5/8),* and *ATP binding cassette subfamily A member-1 (Abca1)* were significantly downregulated in *Sel1L*^{Alb} livers compared to those of their WT littermates (Figure EV2A).

In mice, Fgf21 is known to induce torpor, a hibernation-like energy-conserving, low-activity physical state (6, 40). Indeed, *Sel1L*^{Alb} mice exhibited lower ambulatory activity compared to that of WT littermates (Figure 3C). Moreover, similar to Fgf21 gain-of-function mouse models (6, 35, 37), *Sel1L*^{Alb} mice exhibited reduced blood glucose levels (Figure 3D), lower serum insulin levels (Figure 3E) with comparable serum glucagon levels (Figure EV2B), and significantly decreased serum triglyceride and cholesterol levels (Figure 3F-G) compared to wildtype littermates. Additionally, *Sel1L*^{Alb} mice exhibited improved insulin sensitivity, but comparable glucose tolerance (Figure EV2C-D). This improved insulin sensitivity phenotype was also partially reversed upon AAV-mediated Fgf21 knockdown (Figure EV2E) in *Sel1L*^{Alb} mice.

Fgf21 is known to affect white adipose tissue browning (2, 3, 8, 37, 41). Histological assessment of inguinal white adipose tissue depots from *Sel1L*^{Alb} mice revealed smaller lipid droplets (Figure 3H), which was confirmed by immunostaining for the lipid droplet marker perilipin (Appendix Figure S4A-B). Indeed, in the inguinal white adipose tissues of *Sel1L*^{Alb} mice, expression levels of genes associated with browning such as *Uncoupling protein-1 (Ucp1)*, and *Iodothyronine deiodinase-2 (Dio2)* were significantly elevated by ~20- and ~10-fold, respectively (Figure 3I). Protein levels of Ucp1 were tripled in inguinal white adipose tissues of *Sel1L*^{Alb} mice (Figure 3J).

Fgf21 is also considered as an anti-obesity hormone owing to its ability to confer resistance to diet-induced weight gain (35). In keeping with this, *Sel1L*^{Alb} mice exhibited significantly reduced weight gain (Figure 3K) upon being fed a 60% high-fat diet, along with significantly reduced fat depots (Figure 3L and Appendix Figure S4C) and improved insulin sensitivity (Appendix Figure S4D), overall suggestive of an ameliorated response to diet-induced obesity. Therefore, we conclude that the metabolic phenotypes of *Sel1L*^{Alb} mice are in part mediated through Fgf21.

Crebh, not Pparα, accumulates intracellularly in the absence of Sel1L

We next explored how Sel1L or Sel1L-Hrd1 ERAD is linked to *Fgf21* in the liver. *Fgf21* expression is transcriptionally controlled synergistically by nuclear receptor Pparα and Crebh. The schematic model depicting the intracellular trafficking of Crebh from ER to Golgi, proteolytic cleavage at Golgi and nuclear entry is shown in Figure EV3A. Additionally, Fgf21 expression may also be regulated via transcription factors such as Xbp1s in response to ER stress (42-46); however, the physiological significance of these regulators remains to be established.

Excitingly, Crebh protein levels were significantly elevated (> 20-fold) in the livers of *Sel1L*^{Alb} mice at 9-weeks of age (Figure 4A and quantitated in Figure 4C). By contrast, the protein levels of Pparα and Xbp1s were unchanged (Figure 4B and quantitated in Figure 4C). Importantly, this Crebh protein accumulation was due to a post-transcriptional mechanism as the mRNA levels of *Crebh* were not affected by Sel1L deficiency (Figure 4D). Moreover, the nuclear, active form of Crebh (Crebh-N) was also significantly upregulated by ~8 fold in *Sel1L*^{Alb} livers (Figure 4B and quantitated in Figure 4C). Similar induction of Crebh protein was observed in the livers of adult mice with acute deletion of Sel1L (Figure 4E).

Q-PCR analysis further confirmed that, in addition to *Fgf21*, several other known Crebh target genes, such as *Amyloid P component, serum (Apcs), Apolipoprotein-A4 (Apoa4),* and *Cell death inducing DFFA like effector c (Cidec)* (11, 41, 47, 48), were also significantly upregulated in *Sel1L*^{Alb} livers (Figure EV3B). In contrast, canonical Pparα targets such as *Acyl-CoA synthetase long-chain family member 1 (Acsl1), Carnitine palmitoyltransferase 1A (Cpt1a), Acyl-CoA oxidase 1, (Acox1)* and *Microsomal triglyceride transfer protein (Mttp)* were significantly downregulated in *Sel1L*^{Alb} livers (Figure EV3C).

As *Fgf21* expression is reportedly induced by ER stress (49-51), we next compared the effect of Sel1L-Hrd1 ERAD deficiency to pharmacological UPR activation on Crebh accumulation and *Fgf21* expression. First, the Crebh protein accumulation in *Sel1L*^{Alb} livers was much higher than that in the livers of wildtype mice challenged with the potent pharmacological ER stress inducer tunicamycin (Figure 4F). Additionally, the transcriptional induction of *Fgf21* in *Sel1L*^{Alb} livers or primary hepatocytes was much more pronounced compared to that in tunicamycin-challenged WT liver or in thapsigargin-treated WT primary hepatocytes (Figure EV3D-E), in spite of much higher ER stress observed in the latter (Figure EV1C-E). We conclude that hepatic Sel1L-Hrd1

ERAD regulates *Fgf21* induction through a mechanism involving Crebh, but independently of Pparα- or ER stress.

Like the other recently characterized Sel1L-Hrd1 ERAD substrate Ire1α (25), the accumulated Crebh protein in Sel1L-deficient hepatocytes remained soluble in mild detergent NP40 (Figure 4G), suggesting that Crebh does not form insoluble aggregates in the absence of Sel1L-Hrd1 ERAD. Moreover, confocal immunostaining of Crebh further demonstrated the intracellular accumulation of Crebh protein including in the nucleus of *Sel1L*^{Alb} hepatocytes when compared to WT livers (Figure 4H and zoomed-out images shown in Figure EV3F). Chromatin immunoprecipitation (ChIP) of Crebh revealed increased binding of Crebh onto the proximal promoter of the *Fgf21* gene in *Sel1L*^{Alb} liver versus WT liver (Figure 4I).

Finally, to demonstrate a similar mechanism in human hepatocytes, we knocked out Sel1L via the CRISPR/Cas9 system in the human hepatoma cell line Hep3B. Acute deletion of Sel1L significantly increased CREBH protein level and *Fgf21* gene expression (Figure 4J-K). Taken together, we conclude that Sel1L deficiency in the liver leads to intracellular and nuclear accumulation of Crebh in both mice and humans.

ER-resident Crebh is an endogenous Sel1L-Hrd1 ERAD substrate

A marked accumulation of Crebh protein in Sel1L-deficient cells prompted us to test the hypothesis that Crebh is a bona fide endogenous Sel1L-Hrd1 ERAD substrate in the liver. In keeping with our hypothesis, a previous study showed that Crebh is degraded by proteasomes (52), but the nature and significance of this degradation event remains unknown. Indeed, Crebh protein was unstable with a half-life of about 45 minutes in Crebh-transfected HEK293T cells treated with the translation inhibitor cycloheximide (Figure 5A). Crebh protein became greatly stabilized with half-lives of over 4 hours in *SEL1L-/-* and *HRD1-/-* cells (Figure 5A and Figure EV4A).

As Crebh is cleaved in the Golgi to generate N-terminal fragment Crebh-N, we next generate cleavage-defective-Crebh by mutating its S1P and S2P cleavage sites (11). Indeed, similar to wildtype Crebh, non-cleavable Crebh mutant was unstable and became stabilized in the absence of Sel1L and Hrd1 (Figure EV4B). Moreover, unlike Crebh, steady-state protein levels and half-life of Crebh-N protein were not affected by Hrd1 deficiency (Figure EV4C-D). Hence,

these data point to the specificity of the Sel1L-Hrd1 ERAD effect towards ER-resident Crebh, not cleaved the Crebh-N fragment.

To further examine the contribution of proteasomes versus lysosomes in the clearance of Crebh protein, we treated Crebh-transfected cells with proteasome inhibitor bortezomib (BTZ) or lysosomal inhibitor chloroquine (CHQ) in the presence of cycloheximide (CHX). BTZ, but not CHQ, stabilized Crebh protein (Figure 5B). Moreover, the effect of BTZ on Crebh protein was dampened in HRD1-deficient cells (Figure 5C), further supporting the notion that degradation of Crebh is largely mediated by the Sel1L-Hrd1 ERAD complex.

Crebh interacted strongly with both Hrd1 and Sel1L under regular native immunoprecipitation conditions (Figure EV4E-F and Lane 2, Figure 5D). Additionally, following lysate denaturing prior to immunoprecipitation, robust ubiquitination of Crebh protein was detected and blocked upon expression of catalytically inactive Hrd1 C2A mutant (top panel Lanes 1-3, Figure 5D). In contrast, Crebh-N did not interact strongly with, nor was ubiquitinated by, Hrd1 (Lanes 4-5, Figure 5D). Together, these data demonstrate that Crebh is targeted for proteasomal degradation by Sel1L-Hrd1 ERAD, requiring the activity of Hrd1 E3 ligase.

Sel1L-Hrd1 ERAD deficiency does not affect the ER-to-Golgi trafficking of Crebh

Although ER stress was previously reported to be required for the ER exit of Crebh (11), a recent study suggested that may not be the case, but rather Crebh constitutively migrates to the Golgi (47). Does Sel1L-Hrd1 ERAD affect ER-to-Golgi trafficking of Crebh? As Crebh undergoes N-linked glycosylation in the ER, a step required for its ER exit to Golgi (52, 53), we next tested the endoglycosidase-H (endoH) sensitivity of Crebh protein to distinguish ER- versus Golgi-resident Crebh. Interestingly, despite having elevated total protein level at the basal state, Sel1L-deficient liver exhibited a similar percent of endoH resistant to sensitive Crebh protein to that in WT liver (Lanes 3 vs. 4, Figure 5E). Indeed, at the steady state, nearly 50% of CREBH were endoH resistant, i.e. at the Golgi, regardless of ERAD status, suggesting that a large portion of CREBH constitutively exits the ER. As a control, Sel1L as an ER-resident protein was completely endoH sensitive (Lanes 1 vs. 3, Figure 5E). Hence, our data suggest that Sel1L-Hrd1 ERAD does not regulate the trafficking of Crebh from the ER to Golgi.

Crebh links hepatic Sel1L-Hrd1 ERAD to Fgf21 and systemic metabolic regulation

To demonstrate whether Crebh indeed links Sel1L-Hrd1 ERAD to Fgf21 and systemic metabolic regulation, we deleted Crebh in the livers of *Sel1L*^{Alb} mice by i.v. injecting GFP-encoding AAV8 expressing shRNA against *Crebh* (*shCrebh*) or control luciferase (*shLuc*). Five weeks after AAV injection, GFP-positive livers were observed in all cohorts (Figure EV5A). *shCrebh* injection resulted in a ~60% reduction of Crebh protein and mRNA levels in *Sel1L*^{Alb} livers (Figure 6A-B), and in conjunction, both mRNA and circulating levels of Fgf21 in *Sel1L*^{Alb} mice were reduced by ~75% (Figure 6B-C). Importantly, the ER stress response markers such as *Xbp1* mRNA splicing and Ire1a/Perk pathway activation was not affected by Crebh knockdown in *shCrebh*-injected *Sel1L*^{Alb} livers compared to the *shLuc*-injected *Sel1L*^{Alb} livers (Figure EV5B-D), further underscoring that the effect of Sel1L-Hrd1 ERAD on Fgf21 is largely uncoupled from ER stress.

Upon Crebh deletion, the expression levels of p-Stat5-depdendent, growth-associated genes were also elevated in *Sel1L*^{Alb} mice compared to those receiving *shLuc* (Figure 6D). Indeed, *Sel1L*^{Alb} mice with Crebh deletion showed better weight gain than *Sel1L*^{Alb} mice injected with *shLuc* control (Figure 6E and Figure EV5E). Moreover, deletion of Crebh in *Sel1L*^{Alb} mice also partially reversed the insulin sensitivity of *Sel1L*^{Alb} mice (Figure 6F). Lastly, Crebh knockdown markedly reduced the Ucp1 expression in white adipose tissue that was observed in *Sel1L*^{Alb} mice (Figure 6G-H). Hence, hepatic Sel1L-Hrd1 ERAD regulates growth and systemic metabolism, at least in part, via the suppression of the "Crebh-Fgf21" axis.

Sel1L-Hrd1 ERAD suppresses "Crebh-Fgf21" axis under multiple physiological contexts

The above results pointed to Sel1L-Hrd1 ERAD as a key regulator of the "Crebh-Fgf21" axis with significant impact on systemic metabolism. We next asked whether there is a correlation between Sel1L-Hrd1 ERAD and Crebh-Fgf21 under two physiological settings – fasting-feeding and growth.

During feeding, hepatic Sel1L and Hrd1 levels were markedly higher than during fasting (Figure 1B and Lanes 3 vs. 4, Figure 7A), while protein levels of Crebh and Crebh-N exhibited the opposite trend (Lanes 3 vs. 4 and 1 vs. 2, Figure 7A). Indeed, there was negative correlation between Sel1L-Hrd1 proteins and Crebh protein/*Fgf21* mRNA levels under fasting-feeding (Figure 7B). Furthermore, Crebh protein level was highly elevated and remained largely constant during fasting-feeding in Sel1L-deficient liver (Lanes 7-8 vs. 3-4, Figure 7A and quantitated in Figure 7C), suggesting that Sel1L-Hrd1 ERAD is largely responsible for the

decline of Crebh protein level in the fed state. Consequently, the circulating levels of Fgf21 were also greatly elevated in both fasted and fed states of Sel1L-deficient mice (Figure 7D).

During growth, hepatic Sel1L and Hrd1 proteins also steadily increased with age from 3 to 24 weeks (Figure 1A and Lanes 4-6, Figure 7E), while protein levels of both Crebh and Crebh-N steadily decreased (Lanes 1-6, Figure 7E). There was a negative correlation between Sel1L-Hrd1 proteins and Crebh protein/*Fgf21* mRNA levels in WT mice during growth (Figure 7F). Importantly, in the *Sel1L*^{Alb} mice, the decline of hepatic Crebh protein were markedly blunted by the Sel1L deficiency (Lanes 7-12 vs. 1-6, Figure 7E and quantitated in Figure 7G). This results in highly elevated circulating Fgf21 levels over the different ages of the *Sel1L*^{Alb} mice, unlike the gradual decline with age in WT mice (Figure 7H).

Therefore, these data not only demonstrate an inverse association between hepatic Sel1L-Hrd1 ERAD and Crebh protein levels under various physiological setting, but also establish Sel1L-Hrd1 ERAD as a key repressor of the "Crebh-Fgf21" axis during growth and fasting-feeding.

2.4 DISCUSSION

The liver controls overall energy metabolism and regulates a wide range of key processes in the body, including growth and fasting-feeding cycle (54). The hepatokine Fgf21 is a key metabolic endocrine hormone involved in inter-organ crosstalk and is considered as a potent therapeutic agent for the treatment of obesity and obesity-associated diabetes (55). This study reports Sel1L-Hrd1 ERAD as a key physiological repressor of Fgf21 gene transcription in the nucleus under various metabolic states in the body. Indeed, our data reveal a common mechanism by which diverse physiological contexts such as fasting-feeding and growth integrate at the level of Sel1L-Hrd1 ERAD via the control of Crebh protein abundance on the ER membrane to regulate *Fgf21* gene transcription (Figure 8). This metabolic tuning of Fgf21 levels by Sel1L-Hrd1 ERAD plays a key role in setting the normal growth and physiological paradigm in the body, as evident from the strong metabolic phenotypes of *Sel1L*^{Alb} mice.

Our study reveals that growth and feeding can both increase the expression of the Sel1L-Hrd1 ERAD protein complex in the ER, which in turn negatively regulates the protein level of Crebh and Fgf21 gene transcription. ER-resident Crebh protein is unstable and its abundance is tightly controlled by the Sel1L-Hrd1 protein complex. Indeed, Crebh or Fgf21 deletion in Sel1L-

deficient mice significantly reverses or attenuates some growth and metabolic phenotypes of the hepatic Sel1L-deficient mice, suggesting that hepatic Sel1L-Hrd1 ERAD effect is at least partially mediated through the "Crebh-Fgf21" axis. The impact of Sel1L-Hrd1 ERAD deficiency on Crebh and *Fgf21* induction is profound, as demonstrated by the dramatic elevation of serum Fgf21 levels (~10 ng/ml), nearly reaching those in models of transgenic Fgf21-overexpression or pharmacological administration (~10-25 ng/ml). Therefore, systemic energy homeostasis and *Fgf21* expression, both in the liver and circulation, is tightly linked to the activity of hepatic Sel1L-Hrd1 ERAD, the expression of which, in turn, may be responsive to the metabolic state of the body. For example, specific hormones and metabolites (such as insulin, glucagon, leptin, corticosterone, glucose, fatty acids etc.) associated with fasting-feeding and/or growth may be involved in the transcriptional regulation of Sel1L and/or Hrd1. In this regard, further investigation will be needed to dissect the molecular pathways that link physiological cues to hepatic ERAD gene expression.

An outstanding question remains as to which transcription factor – Crebh or Pparα – is the more pertinent regulator of *Fgf21* expression in the liver in response to physiological cues. A recent study showed that Crebh is required for transcriptional activation of *Fgf21* by Pparα by forming the Crebh-Pparα complex and also by regulating the expression of *Pparα* (9). Our study demonstrates a profound effect of Sel1L-Hrd1 ERAD on *Fgf21* gene transcription via Crebh, but not Pparα, during growth and fasting-feeding. Although our study does not exclude the importance of Pparα in *Fgf21* transcription, it reveals another layer of regulation of *Fgf21* expression during fasting-feeding and growth, centered at the level of ER membrane.

ERAD is often considered to be responsible for clearing "misfolded" proteins from the ER, and hence ERAD deficiency is mostly known to cause the accumulation of misfolded proteins and thereby trigger ER stress. Indeed, one recurrent question associated with ERAD-deficient models is whether the presumptive induction of ER stress in ERAD deficiency is the true cause of observed phenotypes. Our data show that the effect of ER stress on Crebh and *Fgf21* expression pales when compared to that of Sel1L-Hrd1 ERAD deficiency in the liver or hepatocytes. Moreover, our data showed that Sel1L deficiency only triggers very moderate ER stress response, likely due to cellular adaptation as shown in other cell types (28, 33). Hence, while modest but tonic ER stress may contribute somewhat to the overall phenotype of the Sel1L-deficient mice, the marked elevation of Fgf21 is likely a direct result of Crebh stabilization and accumulation in the absence of Sel1L-Hrd1 ERAD. Indeed, a recent study reported that ER

stress is dispensable for Crebh activation in the liver (47). Providing further support to our model, none of the previous hepatic UPR mouse models showed metabolic phenotypes similar to our hepatocyte-specific Sel1L-Hrd1 ERAD-deficient system or to the Fgf21 gain-of-function mouse models (56-61). For example, genetic ablation of the UPR sensor Ire1α alters lipid metabolism and ketogenic programs in the liver (56, 61). Silencing a major Ire1α effector *X-box Binding Protein-1 (Xbp1)* in the liver leads to marked disequilibrium in lipid homeostasis and impaired recovery from pharmacologically induced ER stress (57). Thus, we believe that mammalian Sel1L-Hrd1 ERAD in the liver plays an intimate and critical role in growth and fasting-feeding by directly regulating the activity of the "Crebh-Fgf21" axis. Additionally, liver specific deletion of *Autophagy related-7 (Atg7)* appears to lead to improved energy metabolism in the body owing to mitochondrial defect-associated Fgf21 production (50). While we did not find any mitochondrial structural defects in our Sel1L-deficient livers, further investigation will be done to assess the relative importance and potential crosstalk between these two, distinct cellular quality control pathways in modulating Fgf21 expression under physiological contexts.

Overall, this study delineates a novel role of Sel1L-Hrd1 ERAD in the liver, and importantly, establishes Sel1L-Hrd1 ERAD-mediated Crebh degradation as an important regulatory mechanism underlying *Fgf21* transcription regulation. This novel "ERAD-Crebh-Fgf21" cascade from the ER to the nucleus (Figure 8) represents another beautiful example of the regulation of cellular, and in this case, systemic response by Sel1L-Hrd1 ERAD and may provide with multiple components that could be utilized for therapeutic intervention in diseases associated with growth defects, lipid disequilibrium and insulin resistance.

2.5 METHODS

Mice. The *Sel1L*$^{f/f}$ mice (18) were crossed with mice expressing Albumin-promoter-driven Cre on the C57BL/6J background (JAX 003574, B6.Cg-Tg(Alb-Cre)21Mgn/J) to generate hepatocyte-specific Sel1L deficient mice (*Sel1L*^{Alb}) and its WT littermates *Sel1L*$^{f/f}$. Due to the infertility of *Sel1L*^{Alb} female mice, only male *Sel1L*^{Alb} mice were used for breeding. Mice were fed a low-fat diet (13% fat, 57% carbohydrate, and 30% protein, LabDiet 5LOD) or a high-fat diet (60% fat, 20% carbohydrate, and 20% protein) where indicated. Comprehensive Lab Animal Monitoring System (CLAMS, Columbus Instruments) was used with 1 day acclimatization period followed by 1 day measurement for metabolic cage analyses studies. Mice were housed on a regular 12-hour light/dark cycle and regulated temperature (22°C). All animal procedures were

done in accordance with the IACUC at Cornell University (2007-0051) and University of Michigan Medical School (PRO00006888). Mice were routinely fasted in the morning for 5-6 hours before sacrifice except as whenever stated (e.g. longer fasting or ad libitum). Mice were fasted for 6 hours before ITT and 16 hours overnight before GTT experiments. Cervical dislocation was used for euthanasia and tissues were immediately either fixed or frozen in liquid nitrogen upon collection. Vaginal smears were examined on a daily basis for estrus cycle analysis.

Serum metabolite analysis. Multiplex analysis was carried out with appropriate standards and blanks for serum insulin and glucagon measurement. Serum triglycerides (TG) and cholesterol (CHOL) was measured by IDEXX Laboratories. Blood glucose was measured via the TrueTest Glucometer. Serum levels of Fgf21 was measured by ELISA analyses as per the protocol provided by the mouse Fgf21 ELISA kit (R&D Systems MF2100).

Western blot analysis. Protein extraction from cell and tissue lysates and Western blotting following SDS-PAGE separation (and phos-tag gel for p-Ire1α) were performed as previously described (62-64). The quantification of signals was done using BioRad ImageLab software and protein levels among samples were normalized to Hsp90, β-Actin or α-tubulin as loading controls. The commercially available antibodies used are as follows: Flag (1:500 for staining, 1:5000 for Western blot; Sigma F1804); HA (1:3,000; Sigma H9658); Myc (1:1000; Sigma); Ucp1 (1:10,000; Sigma U6382); Hsp90 (1:4,000; Santa Cruz sc-7947); α-Tubulin (1:2,000; Santa Cruz sc-5286); Lamin (1:1000; Santa Cruz sc-6215); Xbp1 (1:1000; Santa Cruz sc-7160); BiP (1:1,000; Santa Cruz sc-1051); KDEL (1:500; Abcam ab50601); Sel1L (1:2,000; Abcam ab78298); Os9 (1:5,000; Abcam ab109510); β-Actin (1:10,000, Abcam ab20272); Crebh (1:1000 for Western, 1:100 for immunostaining; Kerafast EWS101); Fgf21 (1:1000; R&D AF3057); Pparα (1:500; Millipore MAB3890); Perilipin (1:200; Cell Signaling 9349); phospho-Stat5 (1:1000; Cell Signaling 9359); Stat5 (1:1000; Cell Signaling #94205); Ire1α (1:2,000; Cell Signaling 3294); Perk (1:1,000; Cell Signaling 3192); p-eIf2α (1:1,000; Cell Signaling 9721); eIF2α (1:2,000; Cell Signaling 9722); caspase-3 (1:1,000; Cell Signaling 9665); cleaved-caspase-3 (1:1,000; Cell Signaling 9661). Hrd1 antibody (1:300) was kindly provided by Dr. Richard Wojcikiewicz (SUNY Upstate Medical University); H2a antibody (1:5,000) was kindly provided by Dr. Yihong Ye (NIDDK). Secondary antibodies for Western blot were goat anti-rabbit IgG-HRP and goat anti-mouse IgG-HRP (1:5,000; BioRad), and donkey anti-goat IgG-HRP (1:5000; Jackson ImmunoResearch). Secondary antibodies for immunostaining were anti-

mouse IgG Cy3 and FITC; anti-rabbit IgG Alexa Fluor 488, Alexa Fluor 594, Alexa Fluor 647; and anti-goat IgG Alexa Fluor 594, Alexa Fluor 680 (all 1:500; Jackson ImmunoResearch).

Immunoprecipitation. Cells/tissue were lysed in a buffer containing 150 mM NaCl, 50 mM Tris-HCl pH 7.5, 1 mM EDTA, 1% NP-40, protease inhibitors and phosphatase inhibitors, and 10 mM N-ethylmaleimide. A total of 2-6 mg protein lysates was incubated with antibody coated agarose beads overnight with gentle rocking at 4°C. Immuno-complexes were washed in a buffer containing 137 mM NaCl, 20 mM Tris-HCl pH 7.5, 2 mM EDTA and 10% glycerol and eluted by boiling at 95°C for 5 mins in SDS sample buffer. For "denaturing" immunoprecipitation conditions in Figure 5D, lysis was first carried out in 200 µl of above stated buffer with 5 mM DTT and 1% SDS, and denatured for 10 min at 95°C before diluting 1:5 with lysis buffer and continuing with antibody incubation.

Detergent solubility analysis. Frozen liver tissue was weighed and homogenized as previously described in NP40 lysis buffer. The lysate volume was then normalized by tissue weight and protein concentration via Bradford assay. The lysate was then centrifuged for 10 minutes at 12,000g and the supernatant collected was the NP40-Soluble fraction after addition of 5X SDS-containing sample buffer and heating at 65°C for 15 minutes. The pellet obtained was re-suspended in 1X SDS sample buffer with a volume normalized to its corresponding soluble fraction, and boiled at 95°C for 30 minutes to form the NP40-Insoluble/Pellet fraction.

Nuclear fractionation. Nuclear fractionation of the liver was performed as previously described (64).

RNA extraction, RT and qPCR. Total RNA was extracted from liver tissues and cells using Trizol and BCP phase separation reagent, and RNA quality was measured via OD. RT–PCR for Xbp1 splicing was performed as previously described (64). qPCR analysis was carried out using Taq polymerase, oilgo-dT primer, SYBR-Green based master mix and Applied Biosystems qPCR machine. All PCR data were normalized to the ribosomal *L32* gene expression level. qPCR primer sequences are: *Sel1L* F: TGGGTTTTCTCTCTCTCCTCTG, R: CCTTTGTTCCGGTTACTTCTTG; *Hrd1* F: AGCTACTTCAGTGAACCCCACT, R: CTCCTCTACAATGCCCACTGAC; *Os9* F: GCTGGCTGACTGATGAGGAT, R: CGGTAGTTGCTCTCCAGCTC; *Ire1α* F: CTGTGGTCAAGATGGACTGG, R: GAAGCGGGAAGTGAAGTAGC; *BiP* F: TGTGGTACCCACCAAGAAGTC, R:

TTCAGCTGTCACTCGGAGAAT; *Chop* F: TATCTCATCCCCAGGAAACG, R: GGGCACTGACCACTCTGTTT; *Fgf21* F: CTGGGGGTCTACCAAGCATA, R: CACCCAGGATTTGAATGACC; *Ghr* F: AGCCTCGATTCACAAGTGTCG, R: GATGACCAATTCTTGCAGCTTG; *Igf1* F: GCTCTTCAGTTCGTGTGTGGAC, R: TTGGGCTGTCAGTGTGGCGC; *Als* F: AACCTCAGGAATAACTCCTTGC, R: CACCGGCTGGCAGTCATCTCCC; *Oatp1* F: CCTCAGCTGTACAATGATTGCC, R: TTTTGGTTCAATGCAGGGTTG; *Ntcp* F: GAAGTCCAAAAGGCCACACTATGT, R: ACAGCCACAGAGAGGGAGAAAG; *Abcg5* F: TCAATGAGTTTTACGGCCTGAA, R: GCACATCGGGTGATTTAGCA; *Abcg8* F: TGCCCACCTTCCACATGTC, R: ATGAAGCCGGCAGTAAGGTAGA; *Ldlr* F: AGGCTGTGGGCTCCATAGG, R: TGCGGTCCAGGGTCATCT; *Hmgcr* F: CTTGTGGAATGCCTTGTGATTG, R: AGCCGAAGCAGCACATGAT; *Srebp1c* F: GGAGCCATGGATTGCACATT, R: CCTGTCTCACCCCCAGCATA; *Abca1* F: GCTTGTTGGCCTCAGTTAAGG, R: GTAGCTCAGGCGTACAGAGAT; *Crebh* F: CAGCTCAAGAAAGCAGGAAG, R: AGCTGCTCCAGAAGAGACAA; *Ppara* F: GCGTACGGCAATGGCTTTAT, R: GAACGGCTTCCTCAGGTTCTT; *Ucp1* F: CCAGTGGATGTGGTAAAAACAA, R: TCAAAGCACACAAACATGATGA; *Dio2* F: CAGTGTGGTGCACGTCTCCAATC, R: TGAACCAAAGTTGACCACCAG; *Cidea* F: TGCTCTTCTGTATCGCCCAGT, R: GCCGTGTTAAGGAATCTGCTG; *Apcs* F: ACAGTCCGTGGTATGGAAGA, R: TGGGGCTTTCACAGTGTATT; *Apoa4* F: CCAGCTAAGCAACAATGCCA, R: TGGAAGAGGGTACTGAGCTGC; *Cidec* F: ATGGACTACGCCATGAAGTCT, R: CGGTGCTAACACGACAGGG; *Acc1* F: ATGGGCGGAATGGTCTCTTTC, R: TGGGGACCTTGTCTTCATCAT; *Acc2* F: CACCATCCGTGAAAACATCA, R: AGCAGCTGAGCCACCTGTAT; *Xbp1* F: ACACGCTTGGGAATGGACAC, R: CCATGGGAAGATGTTCTGGG; *Acsl1*: F: AACGATGTACGATGGCTTCC, R: CATATGGCTGGTTTGGCTTT; *Acox1*: F: GATGTGACCCTTGGCTCTGT, R: AGAGATTCGGCCTCTCTGTG; *Cpt1a* F: ATGACGGCTATGGTGTTTCC, R: GGCTTGTCTCAAGTGCTTCC; *Mttp*: F: TACCCGTTCTTGGTCTGCAT, R: TCTGGCTGAGGTGGGAATAC.

Primary hepatocyte culture. Mice (6-8 weeks of age) were euthanized with isoflurane inhalation, and the liver was perfused first with warm calcium/magnesium-free HBSS containing 25 mM HEPES, EDTA, 1% penicillin-streptomycin, and then with warm calcium/magnesium-free HBSS containing 25 mM HEPES, 2 mM CaCl2, 1% penicillin-streptomycin and 0.75 mg/ml

collagenase (Sigma-Aldrich C8051). After removal and mechanical dispersion of the swollen, digested liver, cells were suspended in ice-cold plating medium (DMEM with 2% Sodium pyruvate, 2% penicillin-streptomycin, 10% heat-inactivated FBS, 1 μM dexamethasone and 0.1 μM insulin) and passed through a 70 μm cell strainer. The cells were then pelleted by centrifugation for 3 min at 60g at 11°C and re-suspended buffered Percoll before pelleting by centrifugation for 4 min at 800×g at 11°C. The final cells were washed thrice in plating medium (centrifugation for 3 min at 60×g at 11°C), viability-checked (via trypan blue exclusion as >80%), and plated on 6-well plates. Once the cells attached well (2-4 hours after plating), the plating medium was replaced with culture medium (DMEM containing 2% Sodium pyruvate, 2% penicillin-streptomycin, 0.2% BSA, 0.1uM dexamethasone and 1nM insulin). Before treatment with nutrients/hormones, the cells were kept in starvation media (no serum/growth factors/hormones) for 4 hours.

Chromatin Immunoprecipitation. Chromatin IP from liver tissue was carried out as per the protocol previously described (65) using 1:250-500 dilution of the Crebh antibody, regular Protein A agarose beads (Invitrogen) instead of magnetic beads, and phenol-chloroform-based DNA extraction in place of columns. The final precipitated DNA was amplified via qPCR using following primers: *Fgf21* promoter (positions -8 to -125 relative to transcribed region) F: ATCCCCAGCTGAGAAGACAC, R: GCCCTTTTCATTCAGACCCC; end of *Fgf21* coding sequence (positions +1214 to +1439 relative to transcribed region) F: AAGGCTCTACCATGCTCAGG, R: CGTCTGCCTCAGAAGGACTC.

Immunostaining and histology. For H&E staining, tissues upon dissection were directly placed in 10% neutral buffered formalin, stored at 4°C, and processed by the Michigan Histology Core for paraffin embedding, section cutting and H&E staining on a fee-for-service basis. For other in vivo staining, livers on anesthetized mice were perfused first with PBS and then with 4% paraformaldehyde for fixation. After further overnight fixation, the tissues were dehydrated overnight in 15% sucrose solution and then frozen in Tissue-Tek O.C.T. Compound. 5 μm sections were cut using a cryotome for further staining. During immunocytochemistry, cells were cultured on poly-L-lysine coated coverslips and were fixed in 4% formalin for 10 mins. For paraffin embedded sections, boiling in 1mM EDTA for 25 minutes was done for antigen retrieval. For cryo-sections and cells, permeabilization was carried out in 0.3% Triton X-100 and 0.3% Glycine for 10 min at room temperature. Thereafter, the sections/cells and incubated in blocking solution (1% donkey serum, 0.03% TritonX-100 in PBS) for 40-60 minutes at room

temperature, and then incubated with primary antibodies for 24-72 hours, as needed at 4°C in humidified chambers. Thereafter, they were washed thrice with PBST (0.03% TritonX-100 in PBS) and incubated with secondary antibodies for 2 hours at room temperature. Counterstaining and mounting were performed using hard-set mounting medium containing DAPI (Vector H-1200). Fluorescent samples were imaged with Nikon A1 Confocal Microscope at the University of Michigan Imaging Core using identical imaging parameters within each experiment. H&E stained samples were scanned using Aperio Scanscope (Leica Biosystems). Images were processed using ImageJ plugin (FIJI).

TUNEL assay. Paraffin embedded liver sections were subjected to TUNEL assay as per manufacturer's protocol using the In-Situ Cell Death detection kit (Roche, 11684795910). Images were obtained by Zeiss LSM710 Confocal Microscope at the Cornell University Biotechnology Resource Center Imaging Facility.

Transmission Electron Microscopy (TEM). The livers of anesthetized mice were perfused via the hepatic portal vein first with Sorenson's buffer to wash out the blood and then with 2.5% glutaraldehyde and 4% paraformaldehyde in 0.1M Na-cacodylate buffer as fixative. The liver was then cut into tiny pieces (about 1-2mm cubes) and soaked overnight in the same fixative. Thereafter, the samples were submitted to the University of Michigan Histology and Imaging Core for washing, embedding, sectioning and imaging via TEM.

Cell lines and transfection. Cells lines were cultured in DMEM (Corning, NY) containing 1% penicillin/streptomycin, 1% sodium pyruvate and heat inactivated 10% FBS (GIBCO). Cells were transfected within 16-22 hours after plating with Lipofectamine 2000 and harvested around 24 hours after. Human hepatoma Hep3B cells were used to generate CRISPR knockouts of SEL1L via lentiviral packaging system with guide sequences ACTGCAGGCAGAGTAGTTGC and GACATCAGATGAGTCAGTAA. *HRD1-/-* HEK293T cells were previously described (28), and *Sel1L-/-* and *Hrd1-/-* N2a cells were previously described (33).

Plasmids. All Crebh plasmid constructs (Crebh, Crebh-N) were generated as described (11). The pAAV8-D(+)-U6-siRNA-CMV-GFP vector was purchased from Addgene. Myc-tagged WT and mutant (C2A) Hrd1 constructs were kindly provided by Dr. Yihong Ye (NIDDK). pcDNA3-HA-Ub was a kind gift from Dr. Hideki Nishitoh (University of Miyazaki, Japan). Sequences used for mutagenesis to generate cleavage defective Crebh (mutating to Alanines the

RNNNRNL of the S1P cleavage site to ANNNANA and the LP of the S2P cleavage site to AA) is as follows, with the new Alanines underlined:
CCTCATCATCGCCGCCTCCATCAGCCCTTTTGGCCCCAACAAAACCGAGAGCCCTGGGGA
CTTTGCGCCTGTAGCAGTGTTCTCCGCAACTGCGCACAACGATG.

AAV-mediated gene delivery. siRNA sequences against mouse *Fgf21* (GGGATTCAACACAGGAGAAAC) encoding siRNA, *Crebh* (TCGAGAAAAAAGACATAGCGGCTGGAAAGATCTCTTGAATCTTTCCAGCCGCTATGTCA) encoding the hairpin shRNA, and control luciferase (GTTGCGCGGAGGAGTTGTG) were cloned into pAAV8-D(+)-U6-siRNA-CMV-GFP vector via BamHI and EcoRI restriction sites. AAV was generated from these plasmids at the Harvard Children's Hospital Virus Core (Boston, MA) on a fee-for-service basis. AAV8 was injected once into 5-8-wk old mice via the tail vein at the dose of 5-10 x 10^{11} viral genome copies/mouse. Blood was collected via a small nick in the tail for subsequent ELISA analysis of circulating Fgf21 levels after 2 or more weeks' post injection.

Microarray analysis. Liver tissues were snap-frozen in liquid nitrogen. RNA was extracted as described above followed by DNaseI (New England Biolabs) digestion. RNA quality and concentration were measured using an Agilent 2100 bioanalyser. Microarray analysis was carried out as previously described (66) and will be deposited into a public database upon acceptance of the manuscript.

Statistical Analysis. All results have been expressed as mean ± SEM unless otherwise stated. Comparisons between groups are done by paired two-tailed Student's t test or 2-way ANOVA as needed. All experiments have been repeated at least twice or thrice, and performed with multiple independent biological samples from which representative data have been shown.

2.6 ACKNOWLEDGEMENTS

We thank Drs. Richard Wojcikiewicz and Yihong Ye for reagents, and Drs. Gerald Duhammel, Jiandie Lin, Peter Arvan, Robert Weiss, Kenneth Simpson, and Natasza Kurpios for insightful discussions and comments; the Histology and Vision Research Core Facilities at University of Michigan Medical School for their assistance and other members of Qi/Arvan laboratories for comments and technical assistance. This work is supported by NIH R01DK099593 (L.Y.),

R01DK090313 (K.Z), R01GM113188, R01DK105393, University of Michigan Protein Folding Diseases Initiative, and American Diabetes Association (ADA) 1-12-CD-04 (L.Q.). A.B. is supported by AHA Predoctoral Fellowship grant #16PRE29750001. L.Q. is the recipient of the Junior Faculty and Career Development Awards from American Diabetes Association (ADA).

2.7 AUTHOR CONTRIBUTION

A.B. designed and performed most experiments; S.S. designed and performed experiments with human hepatocytes; H.W. and M.L. provided technical assistant; Q.L. provided reagents; S.K. performed microarray analyses; L.Y. and K.Z. provided reagents and discussion; A.B. and L.Q. wrote the manuscript; everybody commented on and approved the manuscript.

2.8 FIGURE LEGENDS

Figure 1. Liver-specific Sel1L deficiency in mice (*Sel1L*^{Alb}) causes growth retardation. (A) Western blot analysis and quantitation of Sel1L-Hrd1 ERAD proteins in the livers of WT mice at 3, 9 and 24 weeks of age (n=3-6 per group, 2 independent repeats). (B) Western blot analysis and quantitation of Sel1L-Hrd1 ERAD proteins in the livers of 10-week-old WT mice under fasted (overnight) or ad libitum fed conditions (n=3-6 per group, 2 independent repeats). (C) Western blot analysis and quantitation of ERAD proteins in *Sel1L*$^{f/f}$ and *Sel1L*^{Alb} livers (n=4 per group, 3 independent repeats). (D) Growth curves of male (n=10 each) and female (n=7 each) mice. (E-F) Representative images (E) and nose-to-anus length (F) of male mice at 6 weeks of age (n=6-10 per group). (G) Organ-to-body-weight ratios of liver and kidney in 6-week-old male mice (n=6 per group, 3 independent repeats). (H) Daily food intake (g/d) normalized to gram of body weight (gbw) (n=3 per group, measured over 3 days). (I) Representative estrus cycle mapping in 2-4-month old females (n=6 per group). (J) H&E images of paraffin-embedded liver sections from 9-week-old mice (n=4 per group, 3 independent repeats). (K) Western blot analysis of cell death (cleaved and pro- Caspase-3) in livers of 9-week-old mice, with WT ileum as positive control (n=3 per group, 3 independent repeats). (L) Representative transmission electron microscope (TEM) images obtained from 9-week-old female mice livers (n=10-12 cells from one mouse each). N, nucleus; mito, mitochondria; ER, endoplasmic reticulum. Hsp90 and α-Tubulin, loading controls for Western blot analysis. Values, mean ± SEM; *, $p<0.05$; **, $p<0.01$; ***, $p<0.001$, n.s., non-significant by Student's t test.

Figure 2. Elevated *Fgf21* expression in the liver as well as circulating Fgf21 in the absence of Sel1L. (A) Volcano plot depicting transcriptomics data from the livers of 9-week-old *Sel1L*$^{f/f}$ and *Sel1L*^{Alb} mice (n=3 per group); dotted line marks p=0.05; black dots represent fold change>2. (B-C) qPCR (B) and Western blot (C) analyses of *Fgf21* expression in 9-week-old livers (n=3-6 per group, 3 independent repeats). (D) ELISA analysis of Fgf21 in serum from 8-9-week-old mice (n=6-7 per group). (E) Protein levels of Sel1L (left panel) and mRNA levels of Fgf21 (right panel) in primary mouse hepatocytes isolated from the tamoxifen-inducible Sel1L-knockout *Sel1L*^{ERCre} mice (2 independent repeats). (F-G) Acute loss-of-function model where 8-week-old *Sel1L*$^{f/f}$ mice were injected i.v. with either AAV8-Cre or control AAV8-GFP: (F) Western blot analysis of hepatic and control adipose Sel1L protein (n=3 per group); and (G)

qPCR analysis of hepatic *Fgf21* expression and ELISA analysis of serum Fgf21 (n=3 per group, 2 independent repeats). (H) Heatmaps of top 15 significantly upregulated and downregulated genes in *Fgf21 Tg* livers and their expression levels in *Sel1L*^{Alb} livers (n=3 per group). (I) Scatter plot depicting the logarithmic fold-change (FC) for 16,402 genes in *Sel1L*^{Alb} and *Fgf21 transgenic (Tg)* livers (n=3 per group); genes that are highly upregulated or downregulated in both datasets are marked in red and blue, respectively; genes that are upregulated unique to each data set (e.g. *Derl3* for Sel1L-Hrd1 ERAD-deficient liver) are marked in green. (J-L) Data from rescue experiments where 5-week-old *Sel1L*$^{f/f}$ and *Sel1L*^{Alb} mice were injected i.v. with AAV8-*shFgf21* or control AAV8-*shLuc*: (J-K) qPCR analysis of *Fgf21* mRNA (J) and ELISA analysis of Fgf21 in serum (K) 3 weeks after injection (n=4 per group). (L) Weight gain curve after injection (n=7 per group). Hsp90 and α-Tubulin, loading control for Western blot analysis. Ribosomal *L32*, loading control for qPCR analysis. Values, mean ± SEM; *, p<0.05; **, p<0.01; ***, p<0.001, n.s., non-significant by Student's t test (B-G) or 2-way ANOVA analysis (J-L).

Figure 3. *Sel1L*^{Alb} mice phenocopy Fgf21-gain-of-function mice. (A) Western blot analysis of p-Stat5 in livers of 9-week-old mice (n=3 per group, 3 independent repeats), with quantitation of the ratio of p- to total Stat5 shown below the blot. (B) qPCR analysis of p-Stat5-associated growth genes in the livers of 9-week-old mice (n=6 per group, 2 independent repeats). (C) Z ambulatory activity of 9-week-old male mice as measured over 24 hr (n=4 males per group). (D-G) Blood glucose (D), serum insulin (E), serum triglyceride (TG) (F), serum cholesterol (CHOL) (G) levels in 9-week-old mice after 6 hr fasting (n=6-10 per group). (H) H&E images of inguinal white adipose tissue (iWAT) from 8-week-old mice (n=3 per group, 2 independent repeats). (I) qPCR analysis of browning-related genes in iWAT (n=3-6 per group). (J) Western blot analysis of Ucp1 in iWAT of 8-week-old mice (n=3-4 per group, 3 independent repeats). (K) Weight gain curve of male mice after 60% high fat diet (HFD) starting at 5 weeks of age (n=4 per group, 2 independent repeats). (L) Adipose tissue weight normalized to body weight in male mice following 9 weeks of HFD feeding (n=4 per group). Hsp90, loading control for Western blot analysis. Ribosomal *L32*, loading control for qPCR analysis. Values, mean ± SEM; *, p<0.05; **, p<0.01; ***, p<0.001, n.s., non-significant by Student's t test or 2-way ANOVA, as needed.

Figure 4. Sel1L deficiency leads to the accumulation of Crebh in the liver. (A-C) Western blot analysis of Crebh, Crebh-N, Pparα and Xbp1s in whole cell lysates (A) and nuclear extracts (B) in WT and *Sel1L*^{Alb} livers (n=3 per group, 3 independent repeats) with quantitation shown in (C). (D) qPCR analysis of *Crebh*, *Ppara* and *Xbp1s* in WT and *Sel1L*^{Alb} livers (n=4-6 per group, 2 independent repeats). (E) Western blot analysis of Crebh in acute Sel1L loss of function model as described in Figure 2F-G (n=3 per group). (F) Western blot analysis of Crebh protein in 9-week-old mice (n=3 per group, 2 independent repeats). WT mice injected i.p. with tunicamycin (Tm, 1.5 μg/g body weight) for 72 hours were included as a control. (G) Western blot analysis of Crebh in the livers of 9-week-old mice after NP40-detergent fractionation into NP40 soluble (NP40S) and pellet (NP40P) (n=3 per group, 2 independent repeats). (H) Representative confocal images of Crebh in the liver cryosections of 8-week-old mice (zoomed out versions in Figure EV3F). Note that a fraction of hepatocytes is binucleated. (I) ChIP analysis of Crebh binding onto the *Fgf21* promoter in the livers of 9-week-old mice, normalized first to 5% input group and then to no-antibody ChIP samples (n=3 pooled per group, 2 independent repeats). (J-K) Western blot analysis of SEL1L, HRD1 and CREBH proteins (J) and qPCR analysis of *SEL1L*, *HRD1* and *FGF21* (K) in human Hep3B hepatocytes upon CRISPR deletion of SEL1L with two different guides. Hsp90, H2A, β-Actin and Lamin, loading controls for Western blot analysis. Ribosomal *L32*, loading control for qPCR analysis. Values, mean ± SEM; *, p<0.05; **, p<0.01; ***, p<0.001; n.s., non-significant by Student's t test.

Figure 5. Crebh is an Sel1L-Hrd1 ERAD substrate. (A) Western blot analysis of Crebh protein half-life in transfected WT and HRD1-/- HEK293T cells treated with cycloheximide (CHX) for indicated times. The decay of protein from one experiment is shown below. (B-C) Western blot analysis and quantitation of Crebh in Crebh-transfected *WT* (B) and *HRD1-/-* (C) HEK293T cells pre-treated with the proteasomal inhibitor bortezomib (BTZ) or lysosomal inhibitor chloroquine (CHQ) for 2 hours and then with CHX for additional 1 hour. (D) Western blot analysis of Crebh ubiquitination following immunoprecipitation (IP) of Crebh-Flag and Crebh-N-Flag in HEK293T cells transfected with indicated plasmids. Samples were boiled with SDS before IP for denaturing IP and not so for native IP. These cells were treated with proteasomal inhibitor BTZ for the last 6 hr prior to immunoprecipitation. (E) Western blot analysis of endoglycosidase H (endoH)-sensitivity of Crebh in the livers of 9-week-old mice (n=3 per group, 2 independent repeats). Hsp90, loading control for Western blot analysis. Values, mean ± SEM; *, p<0.05; **, p<0.01; ***, p<0.001; n.s., non-significant by 2-way ANOVA analysis.

Figure 6. Crebh links hepatic Sel1L-Hrd1 ERAD to Fgf21. 5-week-old *Sel1L*$^{f/f}$ and *Sel1L*^{Alb} mice were injected i.v. once with AAV8-*shCrebh* or control AAV8-*shLuc*: (A) Western blot analysis of hepatic Sel1L and Crebh 5 weeks post injection (n=3 mice each, 2 independent repeats). (B-C) qPCR analysis of *Crebh* and *Fgf21* mRNA (B) and ELISA analysis of circulating Fgf21 (C) 5 weeks post injection (n=3 per group, 2 independent repeats). (D) qPCR analysis of hepatic growth-associated genes 5 weeks after injection (n=6 per group). (E) Weight gain 6 weeks post injection (n=10 per group). (F) Insulin tolerance test (ITT) 5-weeks after injection (n=10 per group). (G-H) qPCR (G) and Western blot analysis (H) of Ucp1 levels in inguinal white adipose tissue (iWAT) 5 weeks post injection (n=3 per group, 2 independent repeats). Hsp90, loading control for Western blot analysis. Ribosomal *L32*, loading control for qPCR analysis. Values, mean ± SEM; *, p<0.05; **, p<0.01; ***, p<0.001; n.s., non-significant by 2-way ANOVA analysis (B-G) and Student's t test (A,H).

Figure 7. Sel1L-Hrd1 ERAD represses Crebh and Fgf21 under fasting-feeding and growth. Analysis of correlation between Sel1L-Hrd1 ERAD and Crebh-Fgf21 during fasting-feeding (A-D) and growth (E-H): (A) Western blot analysis of hepatic Sel1L-Hrd1 ERAD and Crebh of nuclear (Nuc) and cytosolic (Cyto) fractions from 10-week-old *Sel1L*$^{f/f}$ and *Sel1L*^{Alb} mice under overnight fasted or fed states. (B) Quantitation of levels of Sel1L/Hrd1/Crebh proteins and *Fgf21* mRNA in the livers of 10-week-old *Sel1L*$^{f/f}$ mice. (C) Quantitation of total Crebh (Crebh+Crebh-N) protein levels in the livers of 10-week-old *Sel1L*$^{f/f}$ and *Sel1L*^{Alb} mice. (D) Serum Fgf21 levels in 10-week-old *Sel1L*$^{f/f}$ and *Sel1L*^{Alb} mice. (E-H) Similar to A-D with the exception that these experiments were done with the livers from *Sel1L*$^{f/f}$ and *Sel1L*^{Alb} mice at 3, 9 and 24 weeks of age. Hsp90 and Lamin, loading controls for cytosolic and nuclear fractions. Values, mean ± SEM; *, p<0.05; **, p<0.01; ***, p<0.001, n.s., non-significant by two-way ANOVA analysis. n=3-4 per group, 2 independent repeats.

Figure 8. Model: Hepatic Sel1L-Hrd1 ERAD regulates systemic metabolism via modulation of the "Crebh-Fgf21" axis in physiological contexts. Model depicting how physiological signals such as growth and fasting-feeding are integrated at the ER membrane via the Sel1L-Hrd1 ERAD complex in liver to regulate CREBH protein turnover at the ER membrane, and *Fgf21* transcription and metabolic states in the body. New findings elucidated by this study are highlighted in red arrows.

Figure EV1. Lack of cell death, inflammation and overt ER stress in Sel1L-deficient hepatocytes. (A) TUNEL staining of paraffin-embedded livers of 9-week-old mice with quantitiation shown on the right (n=4 per group, 2 independent repeats). (B) qPCR analysis of inflammation associated hepatic gene expression in *Sel1L*$^{f/f}$ and *Sel1L*^{Alb} mice (n=4 per group, 3

independent repeats). (C) Western blot analysis of Sel1L and UPR proteins (Ire1α and BiP) in the livers of 9-week-old mice (n=3 per group, 3 independent repeats). +/- Gly, refers to proteins with or without glycosylation; and p/0 refers to phosphorylated or non-phosphorylated Ire1α. (D) RT-PCR analysis of *Xbp1* splicing in the livers of 9-week-old mice (n=3 per group, 3 independent repeats); u/s/t refers to unspliced/spliced/total *Xbp1*. (C-D) WT mice injected i.p. with tunicamycin (Tm, 1.5 μg/g body weight) for 72 hours were included as a control. (E) RT-PCR analysis of *Xbp1* splicing in primary mouse hepatocytes (n=2 per group, 2 independent repeats). WT primary hepatocytes treated with 200 nM thapsigargin (Tg) for 6 hours were included as a control. Quantitation of the percent of Xbp1s in total Xbp1 mRNA is shown below. Hsp90, loading control for Western blot analysis. Ribosomal *L32*, loading control for qPCR and RT-PCR analysis. Values, mean ± SEM; *, p<0.05; **, p<0.01; ***, p<0.001, n.s., not significant by Student's t test.

Figure EV2. Hepatic Sel1L-Hrd1 ERAD deficient mice have altered metabolism. (A) qPCR analysis of lipid synthesis and transport genes in 9-week-old mice (n=6 per group, 2 independent repeats). (B) Serum glucagon levels after 6 hr of fast in the morning (n=5-6 per group). (C-D) Insulin tolerance test (ITT) (C) and glucose tolerance test (GTT) (D) of 10-week-old male mice (n=6 per group). (E) Insulin tolerance test (ITT) 3 weeks after i.v. injection (n=5-6 per group) with AAV8-*shFgf21* or control AAV8-*shLuc*. Ribosomal *L32*, loading control for qPCR analysis. Values, mean ± SEM; *, p<0.05; **, p<0.01; ***, p<0.001, n.s., non-significant by Student's t test.

Figure EV3. Hepatic Sel1L regulates protein stability and activity of Crebh, not Pparα. (A) Schematic diagram showing the intracellular trafficking of ER-resident Crebh protein to the Golgi for proteolysis, leading to the generation of Crebh-N. Crebh-N subsequently translocates into the nucleus to activate gene transcription. (B-C) qPCR analysis of Crebh (B) and Pparα (C) target genes in WT and *Sel1L*^{Alb} livers of 9-week-old mice (n=4 per group, 2 independent repeats). (D) qPCR analysis of hepatic *Fgf21* expression in the livers of 9-week-old *Sel1L*$^{f/f}$ and *Sel1L*^{Alb} mice (n=3 per group, 2 independent repeats). WT mice injected i.p. with tunicamycin (Tm, 1.5 μg/g body weight) for 72 hr were included as a control. (E) qPCR analysis of *Fgf21* expression in primary hepatocytes (n=2 per group, 2 independent repeats). WT primary hepatocytes treated with 200 nM thapsigargin (Tg) for 6 hr are included as a control. (F) Representative immunostaining images (zoomed out from Figure 4H) from 8-week-old liver cryosections. Ribosomal *L32*, loading control for qPCR analysis. Values, mean ± SEM; *, p<0.05; **, p<0.01; ***, p<0.001, n.s., non-significant by Student's t test.

Figure EV4. Crebh, and not Crebh-N, is an ERAD substrate. (A-B) Western blot analysis of Crebh (A) and cleavage-defective-Crebh (B, Crebh*) half-life in transfected *WT, Sel1L-/-* and *Hrd1-/-* N2a cells treated with cycloheximide (CHX) for indicated times. The decay of Crebh proteins is shown below. (C) Representative immunostaining images of transfected Crebh-N-Flag protein 24-hr post transfection into *WT* and *HRD1-/-* HEK293T cells. (D) Western blot analysis and quantitation of Crebh-N protein decay in Crebh-N-Flag-transfected *WT* and *HRD1-/-* HEK293T cells with cycloheximide (CHX) treatment for the indicated times, with quantitiation shown below. (E-F) Co-immunoprecipitation analysis of Crebh with Hrd1 (E) and Sel1L (F) when co-expressed in HEK293T cells. All cell culture experiments were done in 2-3 independent repeats with cells passaged less than 3 times. Hsp90, loading control for Western blot analysis.

Figure EV5. Crebh deletion does not affect ER stress level in *Sel1L*^{Alb} liver. (A) Representative images of livers from *Sel1L*$^{f/f}$ and *Sel1L*^{Alb} mice (n=6 per group) post AAV-shRNA-GFP injection showing green (GFP positive) livers. (B-D) Western blot analysis (B),

qPCR analysis (C) and RT-PCR analysis of *Xbp1* mRNA splicing (D) of hepatic UPR markers in *Sel1L*$^{f/f}$ and *Sel1L*^{Alb} mice 5 weeks post one i.v. AAV8-*shCrebh* or control AAV8-*shLuc* injection (n=3 per group, 2 independent repeats). Quantitation of protein levels (B) and the percent of Xbp1s in total Xbp1 mRNA (D) is shown below. WT mice injected i.p. with tunicamycin (Tm, 1.5 μg/g body weight) for 72 hr were included as a control. (E) Weekly weight gain post i.v. injection (n=10 per group) with AAV8-*shFgf21* or control AAV8-*shLuc*. Hsp90, loading control for Western blot analysis. Ribosomal *L32*, loading control for qPCR analysis. Values, mean ± SEM; *, p<0.05; **, p<0.01; ***, p<0.001, n.s., non-significant by 2-way ANOVA analysis.

Appendix Figure S1. Generation of liver-specific Sel1L-Hrd1 ERAD deficient mouse model. (A) mRNA levels of ERAD genes (*Sel1L, Hrd1*) in the livers of WT mice at 3, 9 and 24 weeks of age (n=3-4 per group, 2 independent repeats). (B) mRNA levels of Sel1L-Hrd1 ERAD genes in the livers of 10-week-old WT mice under fasted (overnight) or fed conditions (n=3-4 per group, 2 independent repeats). (C) Schematic breeding plan for generation of liver-specific Sel1L-knockout mouse model. (D-F) Western blot analysis (D), quantitation (E) and qPCR analysis (F) of ERAD genes (*Hrd1, Sel1L, Ire1α, Os9*) in small intestines of *Sel1L*$^{f/f}$ and *Sel1L*^{Alb} mice (n=3 per group, 2 independent repeats). (G) qPCR analysis of ERAD genes (*Hrd1, Sel1L, Ire1α, Os9*) in the livers of 9-week-old *Sel1L*$^{f/f}$ and *Sel1L*^{Alb} mice (n=6 per group, 2 independent repeats). Values, mean ± SEM; *, p<0.05; **, p<0.01; ***, p<0.001, n.s., not significant by Student's t test.

Appendix Figure S2. Transcriptomics analysis of Sel1L-Hrd1 ERAD deficient liver. (A) KEGG pathway Gene Set Enrichment Analysis (GSEA) of differentially expressed hepatic genes of p<0.05 and fold change >1.9. (B) qPCR analysis of *Fgf21* in brown and inguinal white adipose tissues (BAT, iWAT) of 9-week-old mice (n=3 per group, 3 independent repeat). (C) Heatmaps of top 15 significantly upregulated and downregulated genes in *Sel1L*^{Alb} livers and their expression levels in *Fgf21 Tg* livers (n=3 per group). Ribosomal *L32*, loading control for qPCR and RT-PCR analysis. Values, mean ± SEM; *, p<0.05; **, p<0.01; ***, p<0.001, n.s., not significant by Student's t test.

Appendix Figure S3. Fgf21 knockdown partially reverses the phenotypes of *Sel1L*^{Alb} mice. (A-B) Data from the rescue experiments where 5-week-old *Sel1L*$^{f/f}$ and *Sel1L*^{Alb} mice were injected i.v. with AAV8-*shFgf21* or control AAV8-*shLuc*: (A) Western blot analysis of hepatic Sel1L and Hrd1, 3 weeks after injection (n=3 mice each). (B) Representative estrus cycles 3 weeks after injection (n=5-6 per group). Hsp90, loading control for Western blots. Values, mean ± SEM; *, p<0.05; **, p<0.01; ***, p<0.001, n.s., non-significant by 2-way ANOVA.

Appendix Figure S4. Hepatic ERAD deficient mice show resistance to diet induced weight gain. (A-B) Confocal immuno-stained images (A) and quantitation (B, 100 droplets per image) of perilipin in inguinal white adipose tissues (iWAT) of 8-week-old mice (n=3 per group, 2 independent repeats). (C) Representative images of adipose tissues in male mice (n=4 per group) depicting difference in color and amount of WAT after 9 weeks of HFD feeding. (D) Insulin tolerance test (ITT) after 6 weeks of HFD (n=3-4 per group). Values, mean ± SEM; *, p<0.05; **, p<0.01; ***, p<0.001, n.s., non-significant by Student's t test.

2.9 REFERENCES

1. Inagaki T, Lin VY, Goetz R, Mohammadi M, Mangelsdorf DJ, and Kliewer SA. Inhibition of growth hormone signaling by the fasting-induced hormone FGF21. *Cell Metab.* 2008;8(1):77-83.

2. BonDurant LD, Ameka M, Naber MC, Markan KR, Idiga SO, Acevedo MR, Walsh SA, Ornitz DM, and Potthoff MJ. FGF21 Regulates Metabolism Through Adipose-Dependent and -Independent Mechanisms. *Cell Metab.* 2017;25(4):935-44 e4.
3. Fisher FM, Kleiner S, Douris N, Fox EC, Mepani RJ, Verdeguer F, Wu J, Kharitonenkov A, Flier JS, Maratos-Flier E, et al. FGF21 regulates PGC-1alpha and browning of white adipose tissues in adaptive thermogenesis. *Genes & development.* 2012;26(3):271-81.
4. Kharitonenkov A, and Adams AC. Inventing new medicines: The FGF21 story. *Mol Metab.* 2014;3(3):221-9.
5. Zhao Y, Dunbar JD, and Kharitonenkov A. FGF21 as a therapeutic reagent. *Adv Exp Med Biol.* 2012;728(214-28.
6. Inagaki T, Dutchak P, Zhao G, Ding X, Gautron L, Parameswara V, Li Y, Goetz R, Mohammadi M, Esser V, et al. Endocrine regulation of the fasting response by PPARalpha-mediated induction of fibroblast growth factor 21. *Cell Metab.* 2007;5(6):415-25.
7. Badman MK, Pissios P, Kennedy AR, Koukos G, Flier JS, and Maratos-Flier E. Hepatic fibroblast growth factor 21 is regulated by PPARalpha and is a key mediator of hepatic lipid metabolism in ketotic states. *Cell Metab.* 2007;5(6):426-37.
8. Hondares E, Rosell M, Gonzalez FJ, Giralt M, Iglesias R, and Villarroya F. Hepatic FGF21 expression is induced at birth via PPARalpha in response to milk intake and contributes to thermogenic activation of neonatal brown fat. *Cell Metab.* 2010;11(3):206-12.
9. Kim H, Mendez R, Zheng Z, Chang L, Cai J, Zhang R, and Zhang K. Liver-enriched transcription factor CREBH interacts with peroxisome proliferator-activated receptor alpha to regulate metabolic hormone FGF21. *Endocrinology.* 2014;155(3):769-82.
10. Omori Y, Imai J, Watanabe M, Komatsu T, Suzuki Y, Kataoka K, Watanabe S, Tanigami A, and Sugano S. CREB-H: a novel mammalian transcription factor belonging to the CREB/ATF family and functioning via the box-B element with a liver-specific expression. *Nucleic Acids Res.* 2001;29(10):2154-62.
11. Zhang K, Shen X, Wu J, Sakaki K, Saunders T, Rutkowski DT, Back SH, and Kaufman RJ. Endoplasmic reticulum stress activates cleavage of CREBH to induce a systemic inflammatory response. *Cell.* 2006;124(3):587-99.
12. Zhang C, Wang G, Zheng Z, Maddipati KR, Zhang X, Dyson G, Williams P, Duncan SA, Kaufman RJ, and Zhang K. Endoplasmic reticulum-tethered transcription factor cAMP responsive element-binding protein, hepatocyte specific, regulates hepatic lipogenesis, fatty acid oxidation, and lipolysis upon metabolic stress in mice. *Hepatology (Baltimore, Md).* 2012;55(4):1070-82.
13. Vecchi C, Montosi G, Zhang K, Lamberti I, Duncan SA, Kaufman RJ, and Pietrangelo A. ER stress controls iron metabolism through induction of hepcidin. *Science.* 2009;325(5942):877-80.
14. Nakagawa Y, Satoh A, Yabe S, Furusawa M, Tokushige N, Tezuka H, Mikami M, Iwata W, Shingyouchi A, Matsuzaka T, et al. Hepatic CREB3L3 controls whole-body energy homeostasis and improves obesity and diabetes. *Endocrinology.* 2014;155(12):4706-19.
15. Guerriero CJ, and Brodsky JL. The delicate balance between secreted protein folding and endoplasmic reticulum-associated degradation in human physiology. *Physiol Rev.* 2012;92(2):537-76.
16. Qi L, Tsai B, and Arvan P. New Insights into the Physiological Role of Endoplasmic Reticulum-Associated Degradation. *Trends Cell Biol.* 2017;27(6):430-40.
17. Mueller B, Klemm EJ, Spooner E, Claessen JH, and Ploegh HL. SEL1L nucleates a protein complex required for dislocation of misfolded glycoproteins. *Proc Natl Acad Sci USA.* 2008;105(34):12325-30.

18. Sun S, Shi G, Han X, Francisco AB, Ji Y, Mendonca N, Liu X, Locasale JW, Simpson KW, Duhamel GE, et al. Sel1L is indispensable for mammalian endoplasmic reticulum-associated degradation, endoplasmic reticulum homeostasis, and survival. *Proc Natl Acad Sci U S A.* 2014;111(E582-91.
19. Mehnert M, Sommermeyer F, Berger M, Kumar Lakshmipathy S, Gauss R, Aebi M, Jarosch E, and Sommer T. The interplay of Hrd3 and the molecular chaperone system ensures efficient degradation of malfolded secretory proteins. *Mol Biol Cell.* 2015;26(2):185-94.
20. Vashistha N, Neal SE, Singh A, Carroll SM, and Hampton RY. Direct and essential function for Hrd3 in ER-associated degradation. *Proc Natl Acad Sci U S A.* 2016;113(21):5934-9.
21. Francisco AB, Singh R, Li S, Vani AK, Yang L, Munroe RJ, Diaferia G, Cardano M, Biunno I, Qi L, et al. Deficiency of suppressor enhancer lin12 1 like (SEL1L) in mice leads to systemic endoplasmic reticulum stress and embryonic lethality. *J Biol Chem.* 2010;285(18):13694-703.
22. Yagishita N, Ohneda K, Amano T, Yamasaki S, Sugiura A, Tsuchimochi K, Shin H, Kawahara K, Ohneda O, Ohta T, et al. Essential role of synoviolin in embryogenesis. *J Biol Chem.* 2005;280(9):7909-16.
23. Fujita H, Yagishita N, Aratani S, Saito-Fujita T, Morota S, Yamano Y, Hansson MJ, Inazu M, Kokuba H, Sudo K, et al. The E3 ligase synoviolin controls body weight and mitochondrial biogenesis through negative regulation of PGC-1beta. *EMBO J.* 2015;34(8):1042-55.
24. Sha H, Sun S, Francisco AB, Ehrhardt N, Xue Z, Liu L, Lawrence P, Mattijssen F, Guber RD, Panhwar MS, et al. The ER-associated degradation adaptor protein Sel1L regulates LPL secretion and lipid metabolism. *Cell Metab.* 2014;20(3):458-70.
25. Sun S, Shi G, Sha H, Ji Y, Han X, Shu X, Ma H, Inoue T, Gao B, Kim H, et al. IRE1a is an endogenous substrate of endoplasmic-reticulum-associated degradation. *Nat Cell Biol.* 2015;17(12):1546-55.
26. Sun S, Louri R, Cohen SB, Ji Y, Goodrich JK, Poole AC, Ley RE, Denkers EY, Mcguckin MA, Long Q, et al. Epithelial Sel1L is required for the maintenance of intestinal homeostasis. *Mol Biol Cell.* 2016;27(3):483-90.
27. Ji Y, Kim H, Yang L, Sha H, Roman CA, Long Q, and Qi L. The Sel1L-Hrd1 Endoplasmic Reticulum-Associated Degradation Complex Manages a Key Checkpoint in B Cell Development. *Cell reports.* 2016;16(10):2630-40.
28. Shi G, Somlo D, Kim GH, Prescianotto-Baschong C, Sun S, Beuret N, Long Q, Rutishauser J, Arvan P, Spiess M, et al. ER-associated degradation is required for vasopressin prohormone processing and systemic water homeostasis. *J Clin Invest.* 2017;127(10):3897-912.
29. Wu T, Zhao F, Gao B, Tan C, Yagishita N, Nakajima T, Wong PK, Chapman E, Fang D, and Zhang DD. Hrd1 suppresses Nrf2-mediated cellular protection during liver cirrhosis. *Genes Dev.* 2014;28(7):708-22.
30. Yang H, Qiu Q, Gao B, Kong S, Lin Z, and Fang D. Hrd1-mediated BLIMP-1 ubiquitination promotes dendritic cell MHCII expression for CD4 T cell priming during inflammation. *J Exp Med.* 2014;211(12):2467-79.
31. Kong S, Yang Y, Xu Y, Wang Y, Zhang Y, Melo-Cardenas J, Xu X, Gao B, Thorp EB, Zhang DD, et al. Endoplasmic reticulum-resident E3 ubiquitin ligase Hrd1 controls B-cell immunity through degradation of the death receptor CD95/Fas. *Proc Natl Acad Sci U S A.* 2016;113(37):10394-9.
32. Xu Y, Zhao F, Qiu Q, Chen K, Wei J, Kong Q, Gao B, Melo-Cardenas J, Zhang B, Zhang J, et al. The ER membrane-anchored ubiquitin ligase Hrd1 is a positive regulator of T-cell immunity. *Nature communications.* 2016;7(12073.

33. Kim GH, Shi G, Somlo DRM, Haataja L, Soon S, Long Q, Nillni EA, Low MJ, Arvan P, Myers MG, et al. Hypothalamic ER-associated degradation regulates POMC maturation, feeding and age-associated obesity. *J Clin Invest.* 2018;128(3):1125-40.
34. Potthoff MJ, Kliewer SA, and Mangelsdorf DJ. Endocrine fibroblast growth factors 15/19 and 21: from feast to famine. *Genes Dev.* 2012;26(4):312-24.
35. Kharitonenkov A, Shiyanova TL, Koester A, Ford AM, Micanovic R, Galbreath EJ, Sandusky GE, Hammond LJ, Moyers JS, Owens RA, et al. FGF-21 as a novel metabolic regulator. *J Clin Invest.* 2005;115(6):1627-35.
36. Zhang Y, Xie Y, Berglund ED, Coate KC, He TT, Katafuchi T, Xiao G, Potthoff MJ, Wei W, Wan Y, et al. The starvation hormone, fibroblast growth factor-21, extends lifespan in mice. *Elife.* 2012;1(e00065.
37. Owen BM, Ding X, Morgan DA, Coate KC, Bookout AL, Rahmouni K, Kliewer SA, and Mangelsdorf DJ. FGF21 acts centrally to induce sympathetic nerve activity, energy expenditure, and weight loss. *Cell Metab.* 2014;20(4):670-7.
38. Chau MD, Gao J, Yang Q, Wu Z, and Gromada J. Fibroblast growth factor 21 regulates energy metabolism by activating the AMPK-SIRT1-PGC-1alpha pathway. *Proc Natl Acad Sci U S A.* 2010;107(28):12553-8.
39. Zhu S, Ma L, Wu Y, Ye X, Zhang T, Zhang Q, Rasoul LM, Liu Y, Guo M, Zhou B, et al. FGF21 treatment ameliorates alcoholic fatty liver through activation of AMPK-SIRT1 pathway. *Acta Biochim Biophys Sin (Shanghai).* 2014;46(12):1041-8.
40. Bookout AL, de Groot MH, Owen BM, Lee S, Gautron L, Lawrence HL, Ding X, Elmquist JK, Takahashi JS, Mangelsdorf DJ, et al. FGF21 regulates metabolism and circadian behavior by acting on the nervous system. *Nat Med.* 2013;19(9):1147-52.
41. Park JG, Xu X, Cho S, Hur KY, Lee MS, Kersten S, and Lee AH. CREBH-FGF21 axis improves hepatic steatosis by suppressing adipose tissue lipolysis. *Sci Rep.* 2016;6(27938.
42. De Sousa-Coelho AL, Relat J, Hondares E, Perez-Marti A, Ribas F, Villarroya F, Marrero PF, and Haro D. FGF21 mediates the lipid metabolism response to amino acid starvation. *Journal of lipid research.* 2013;54(7):1786-97.
43. De Sousa-Coelho AL, Marrero PF, and Haro D. Activating transcription factor 4-dependent induction of FGF21 during amino acid deprivation. *Biochem J.* 2012;443(1):165-71.
44. Kim KH, Kim SH, Min YK, Yang HM, Lee JB, and Lee MS. Acute exercise induces FGF21 expression in mice and in healthy humans. *PLoS One.* 2013;8(5):e63517.
45. Laeger T, Henagan TM, Albarado DC, Redman LM, Bray GA, Noland RC, Munzberg H, Hutson SM, Gettys TW, Schwartz MW, et al. FGF21 is an endocrine signal of protein restriction. *J Clin Invest.* 2014;124(9):3913-22.
46. Wan XS, Lu XH, Xiao YC, Lin Y, Zhu H, Ding T, Yang Y, Huang Y, Zhang Y, Liu YL, et al. ATF4- and CHOP-dependent induction of FGF21 through endoplasmic reticulum stress. *Biomed Res Int.* 2014;2014(807874.
47. Xu X, Park JG, So JS, Hur KY, and Lee AH. Transcriptional regulation of apolipoprotein A-IV by the transcription factor CREBH. *Journal of lipid research.* 2014;55(5):850-9.
48. Park JG, Xu X, Cho S, and Lee AH. Loss of Transcription Factor CREBH Accelerates Diet-Induced Atherosclerosis in Ldlr-/- Mice. *Arterioscler Thromb Vasc Biol.* 2016;36(9):1772-81.
49. Jiang S, Yan C, Fang QC, Shao ML, Zhang YL, Liu Y, Deng YP, Shan B, Liu JQ, Li HT, et al. Fibroblast growth factor 21 is regulated by the IRE1alpha-XBP1 branch of the unfolded protein response and counteracts endoplasmic reticulum stress-induced hepatic steatosis. *J Biol Chem.* 2014;289(43):29751-65.

50. Kim KH, Jeong YT, Oh H, Kim SH, Cho JM, Kim YN, Kim SS, Kim DH, Hur KY, Kim HK, et al. Autophagy deficiency leads to protection from obesity and insulin resistance by inducing Fgf21 as a mitokine. *Nat Med.* 2013;19(1):83-92.
51. Schaap FG, Kremer AE, Lamers WH, Jansen PL, and Gaemers IC. Fibroblast growth factor 21 is induced by endoplasmic reticulum stress. *Biochimie.* 2013;95(4):692-9.
52. Bailey D, Barreca C, and O'Hare P. Trafficking of the bZIP transmembrane transcription factor CREB-H into alternate pathways of ERAD and stress-regulated intramembrane proteolysis. *Traffic.* 2007;8(12):1796-814.
53. Chan CP, Mak TY, Chin KT, Ng IO, and Jin DY. N-linked glycosylation is required for optimal proteolytic activation of membrane-bound transcription factor CREB-H. *J Cell Sci.* 2010;123(Pt 9):1438-48.
54. Lajtha A, Latzkovits L, and Toth J. Comparison of turnover rates of proteins of the brain, liver and kidney in mouse in vivo following long term labeling. *Biochim Biophys Acta.* 1976;425(4):511-20.
55. Fisher FM, and Maratos-Flier E. Understanding the Physiology of FGF21. *Annu Rev Physiol.* 2016;78(223-41.
56. Zhang K, Wang S, Malhotra J, Hassler JR, Back SH, Wang G, Chang L, Xu W, Miao H, Leonardi R, et al. The unfolded protein response transducer IRE1alpha prevents ER stress-induced hepatic steatosis. *The EMBO journal.* 2011;30(7):1357-75.
57. Olivares S, and Henkel AS. Hepatic Xbp1 Gene Deletion Promotes Endoplasmic Reticulum Stress-induced Liver Injury and Apoptosis. *J Biol Chem.* 2015;290(50):30142-51.
58. Lee AH, Scapa EF, Cohen DE, and Glimcher LH. Regulation of hepatic lipogenesis by the transcription factor XBP1. *Science.* 2008;320(5882):1492-6.
59. Hur KY, So JS, Ruda V, Frank-Kamenetsky M, Fitzgerald K, Koteliansky V, Iwawaki T, Glimcher LH, and Lee AH. IRE1alpha activation protects mice against acetaminophen-induced hepatotoxicity. *J Exp Med.* 2012;209(2):307-18.
60. Jurczak MJ, Lee AH, Jornayvaz FR, Lee HY, Birkenfeld AL, Guigni BA, Kahn M, Samuel VT, Glimcher LH, and Shulman GI. Dissociation of inositol-requiring enzyme (IRE1alpha)-mediated c-Jun N-terminal kinase activation from hepatic insulin resistance in conditional X-box-binding protein-1 (XBP1) knock-out mice. *J Biol Chem.* 2012;287(4):2558-67.
61. So JS, Hur KY, Tarrio M, Ruda V, Frank-Kamenetsky M, Fitzgerald K, Koteliansky V, Lichtman AH, Iwawaki T, Glimcher LH, et al. Silencing of lipid metabolism genes through IRE1alpha-mediated mRNA decay lowers plasma lipids in mice. *Cell metabolism.* 2012;16(4):487-99.
62. Yang L, Xue Z, He Y, Sun S, Chen H, and Qi L. A Phos-tag-based method reveals the extent of physiological endoplasmic reticulum stress. *PLos ONE.* 2010;5(7):e11621.
63. Qi L, Yang L, and Chen H. Detecting and quantitating physiological endoplasmic reticulum stress. *Meth Enzymol.* 2011;490(137-46.
64. Sha H, He Y, Chen H, Wang C, Zenno A, Shi H, Yang X, Zhang X, and Qi L. The IRE1alpha-XBP1 pathway of the unfolded protein response is required for adipogenesis. *Cell Metab.* 2009;9(6):556-64.
65. Murgatroyd C, Hoffmann A, and Spengler D. In vivo ChIP for the analysis of microdissected tissue samples. *Methods Mol Biol.* 2012;809(135-48.
66. Sun S, Xia S, Ji Y, Kersten S, and Qi L. The ATP-P2X7 Signaling Axis Is Dispensable for Obesity-Associated Inflammasome Activation in Adipose Tissue. *Diabetes.* 2012;61(6):1471-8.

2.10 FIGURES

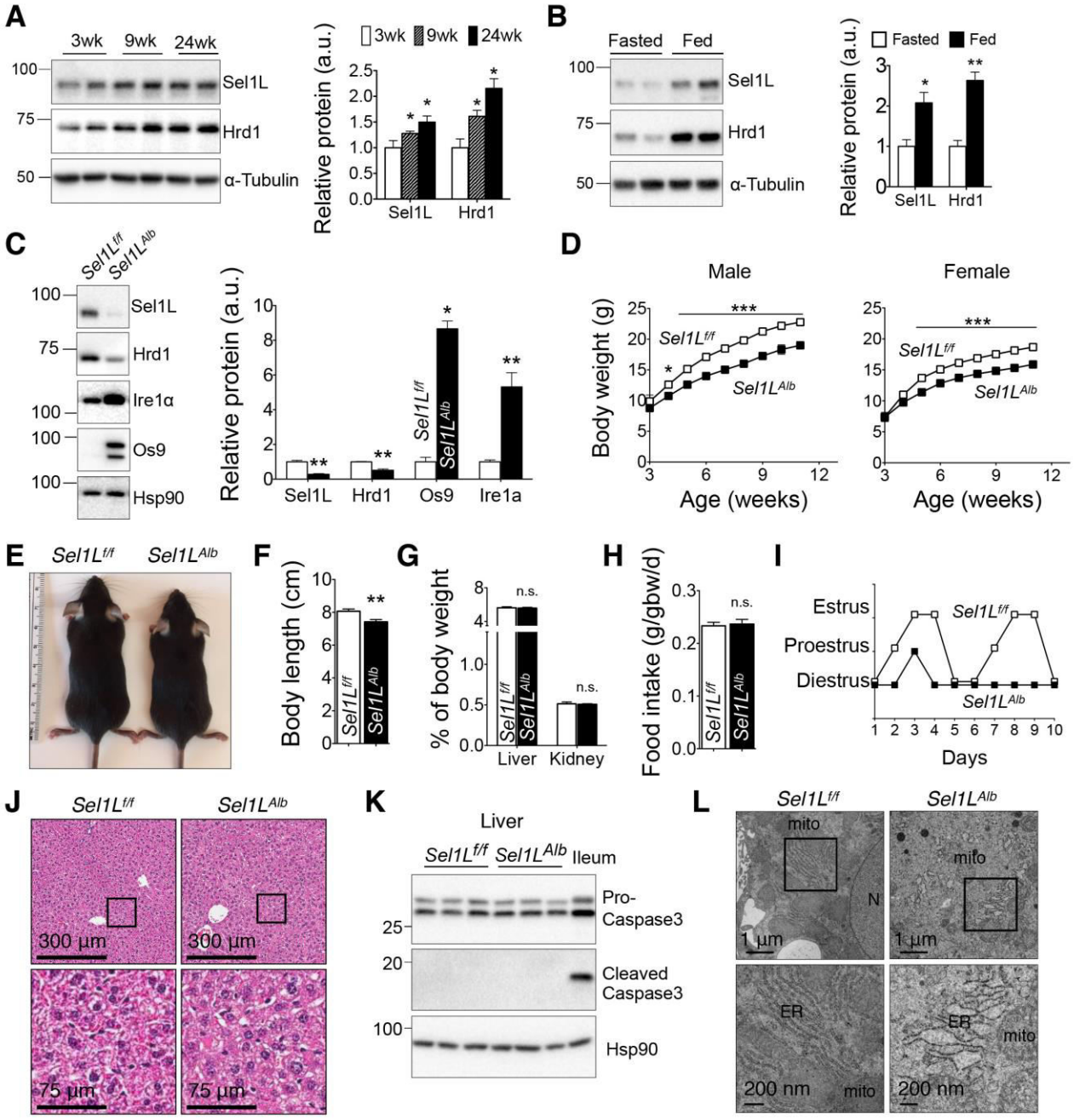

Figure 1. Liver-specific Sel1L deficiency in mice (*Sel1L^{Alb}*) causes growth retardation.

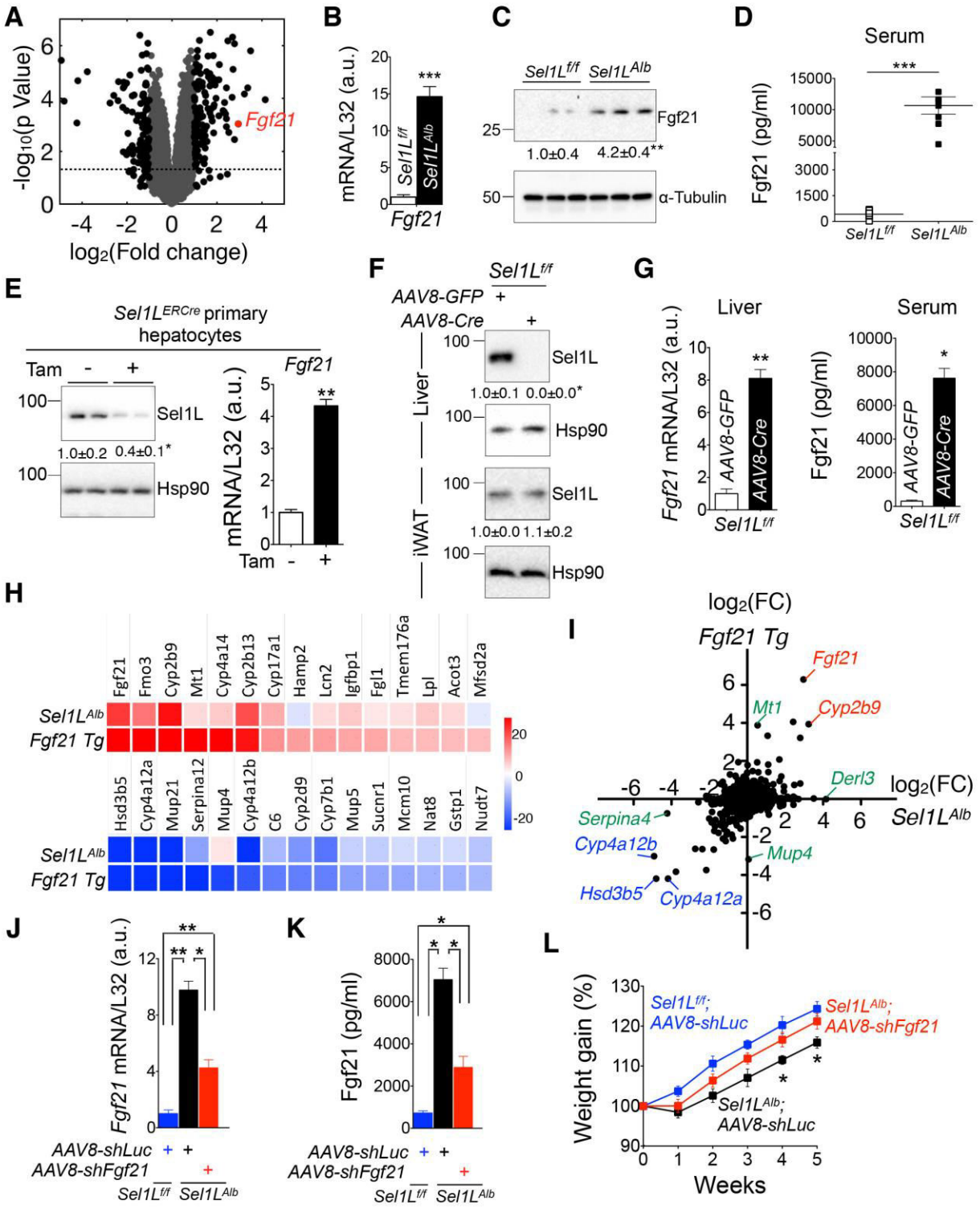

Figure 2. Elevated *Fgf21* expression in the liver as well as circulating Fgf21 in the absence of Sel1L.

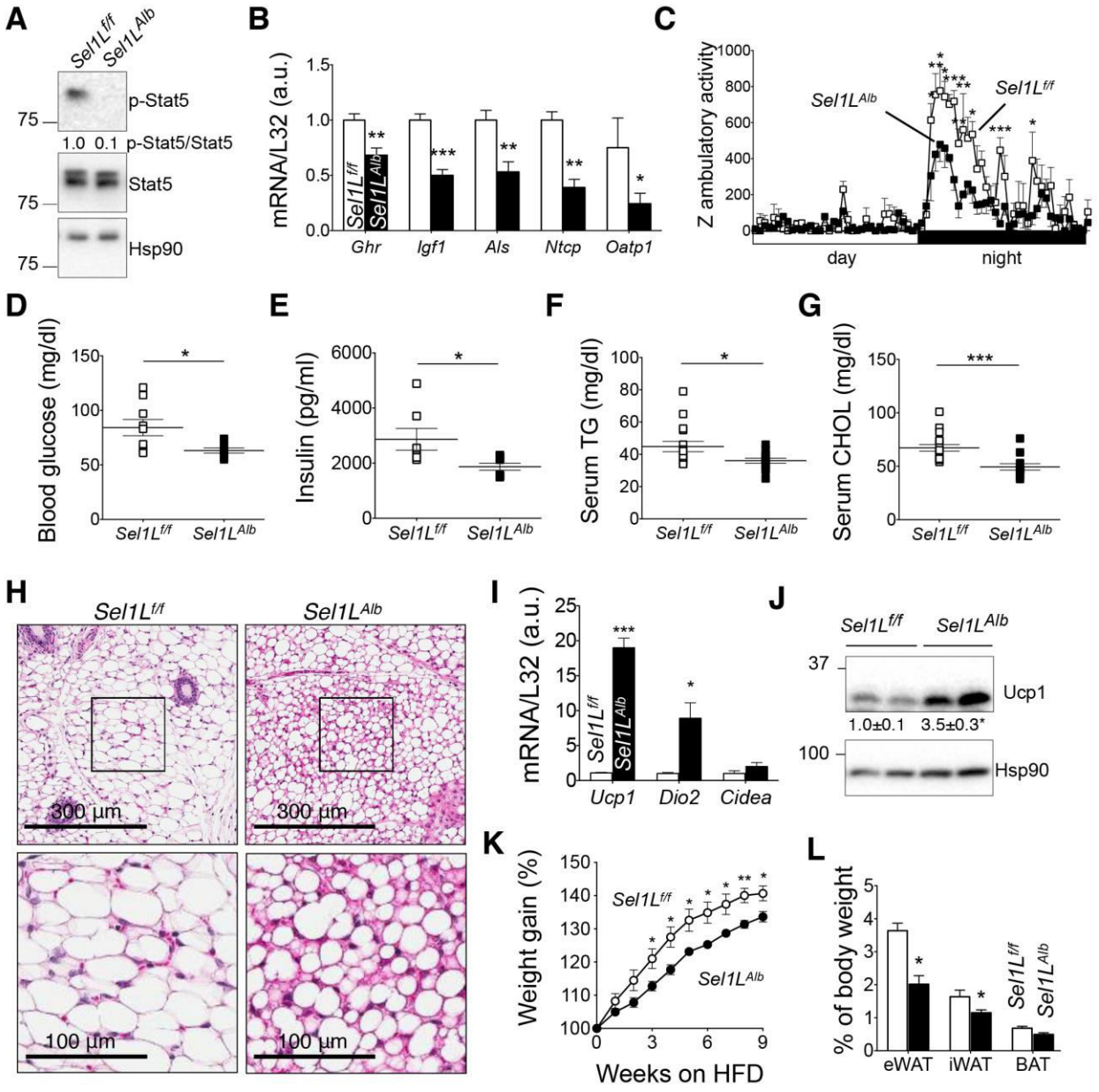

Figure 3. *Sel1L^{Alb}* mice phenocopy Fgf21-gain-of-function mice.

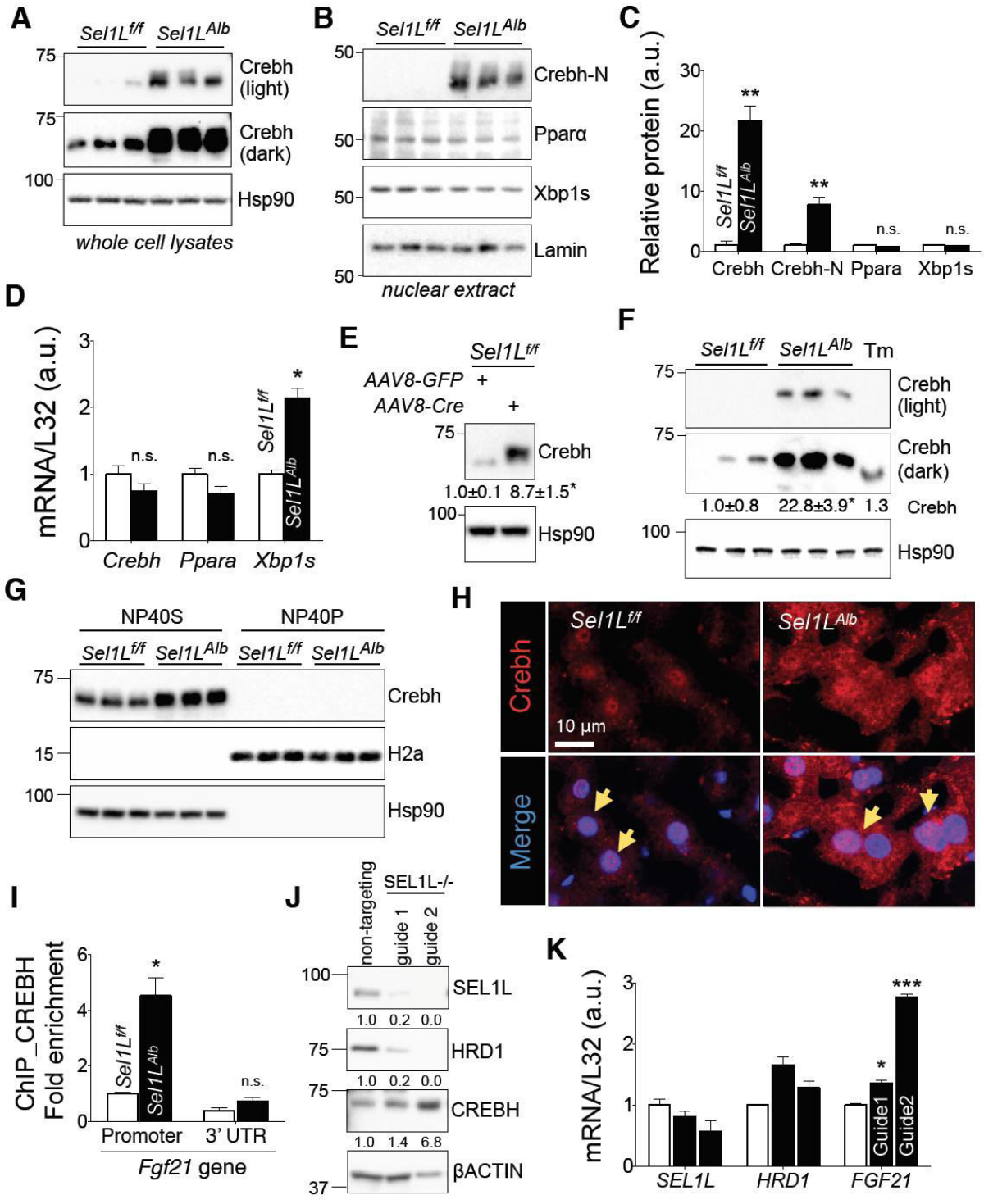

Figure 4. Sel1L deficiency leads to the accumulation of Crebh in the liver.

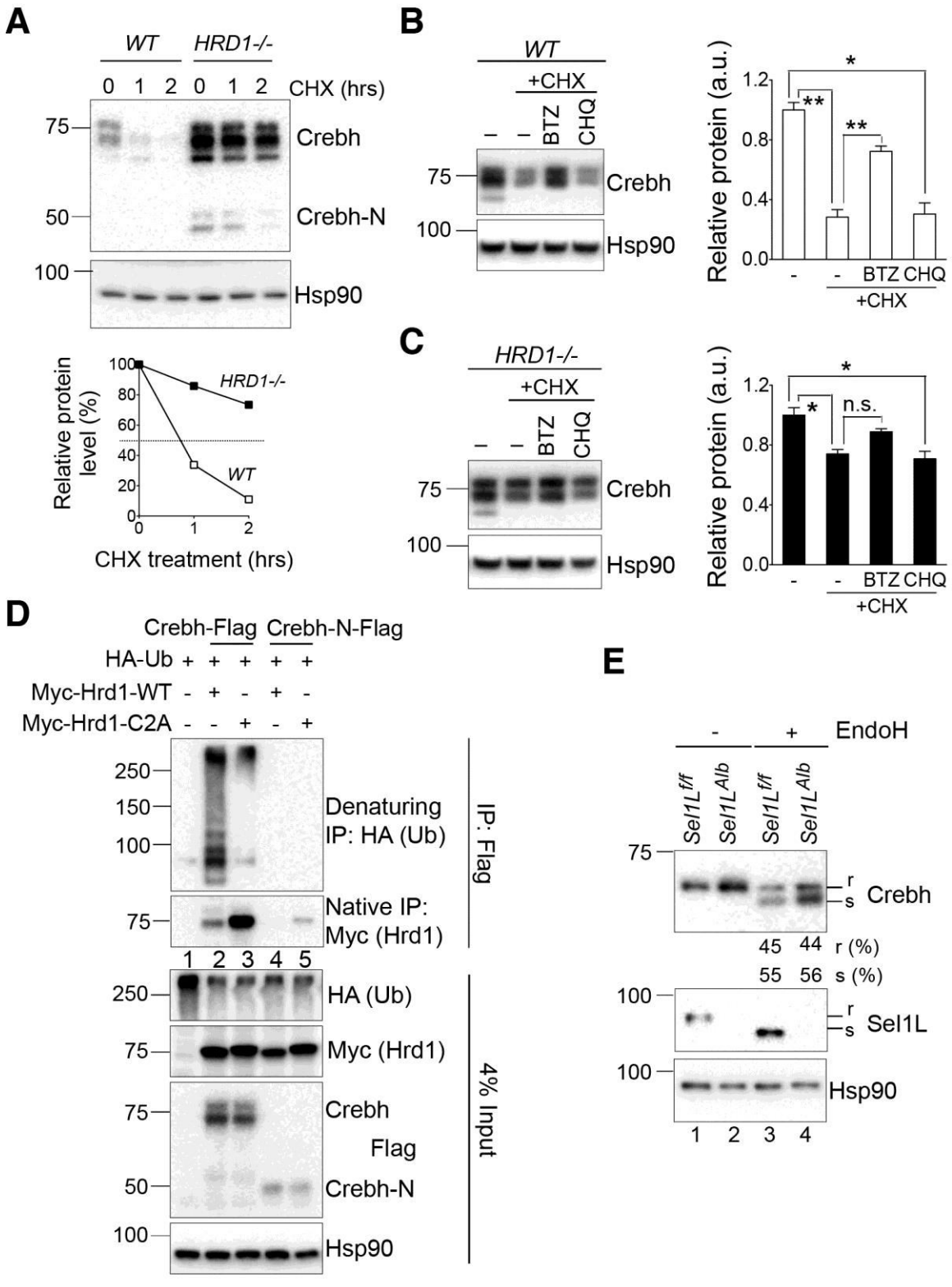

Figure 5. Crebh is an Sel1L-Hrd1 ERAD substrate.

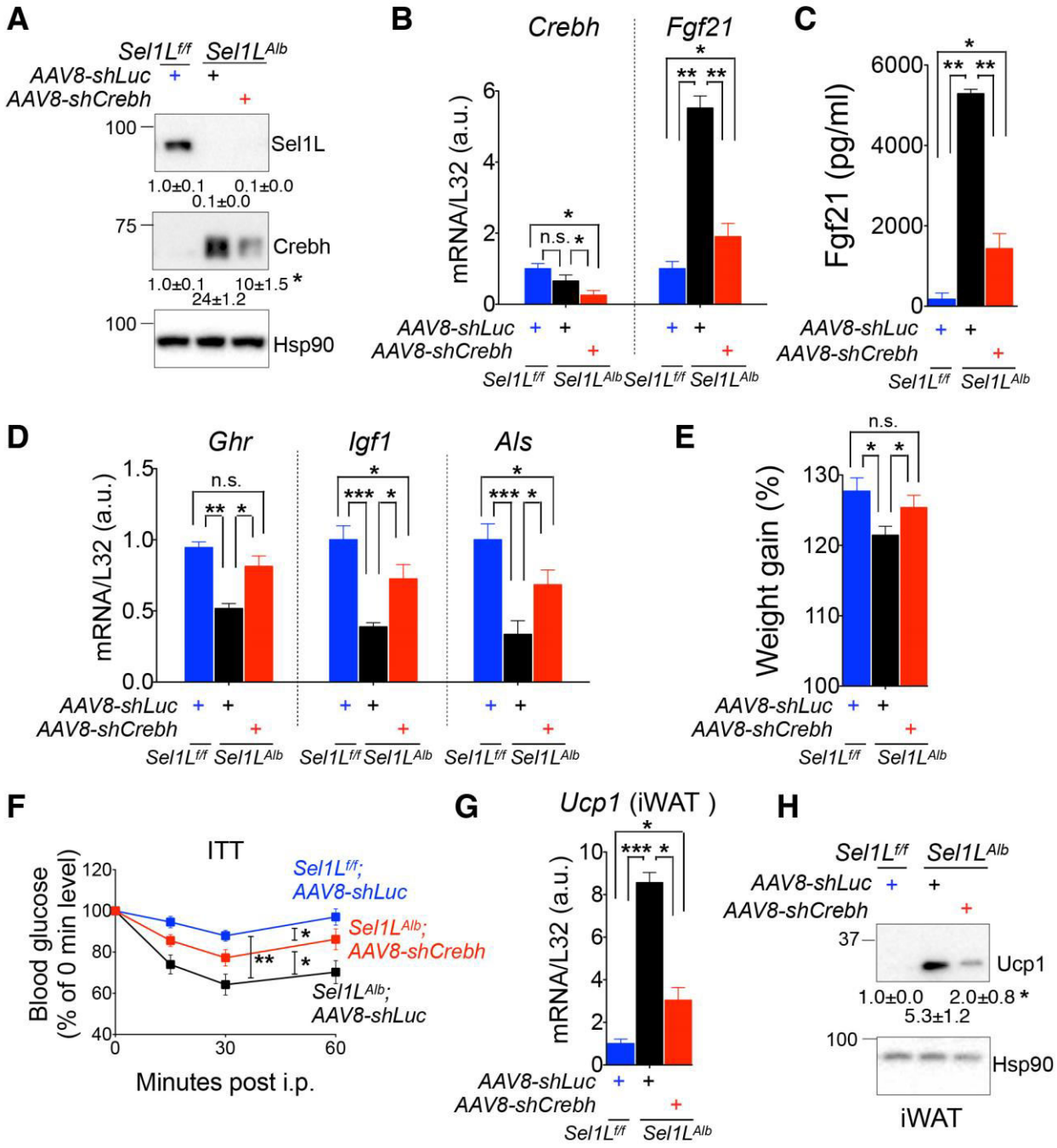

Figure 6. Crebh links hepatic Sel1L-Hrd1 ERAD to Fgf21.

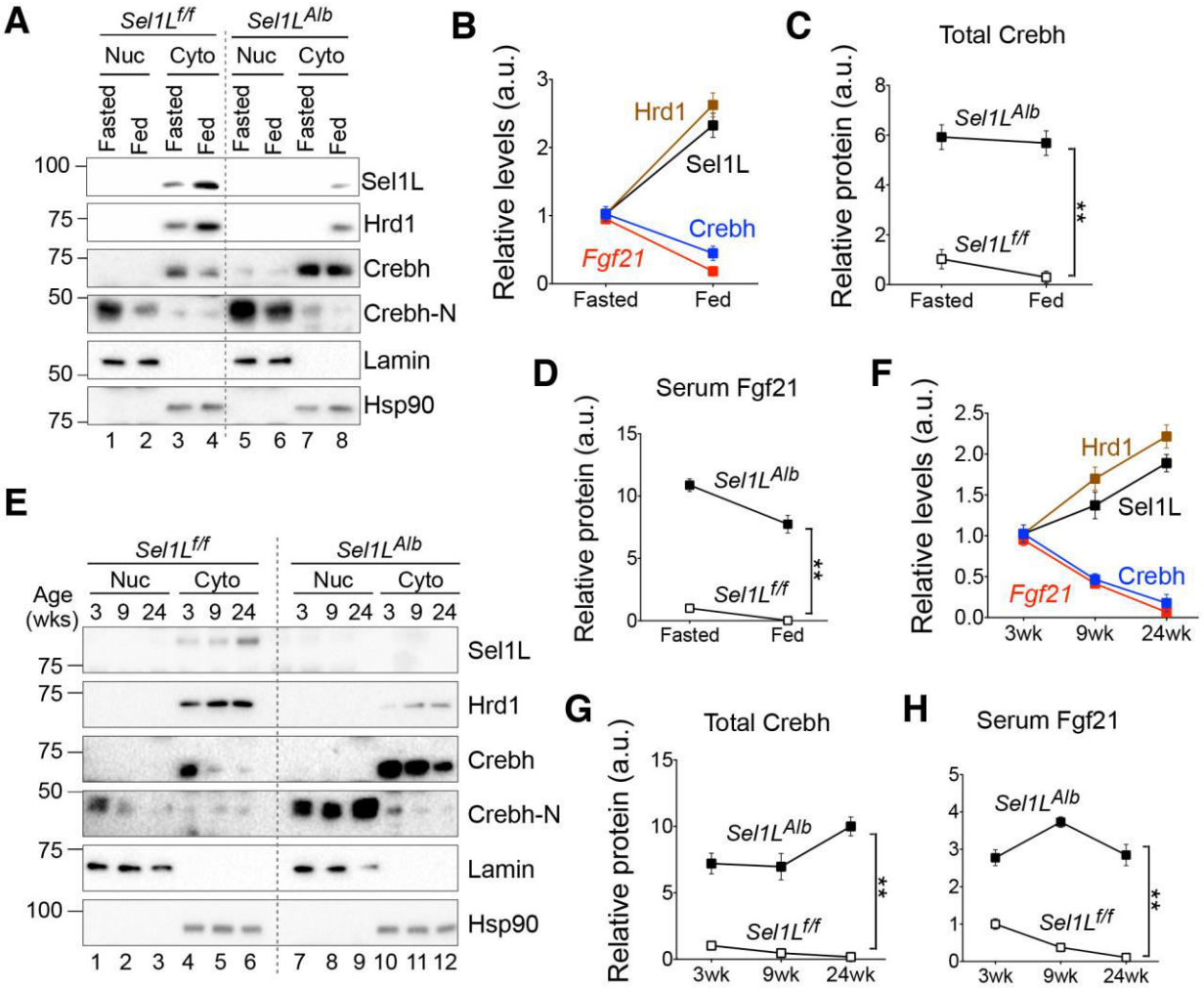

Figure 7. Sel1L-Hrd1 ERAD represses Crebh and Fgf21 under fasting-feeding and growth.

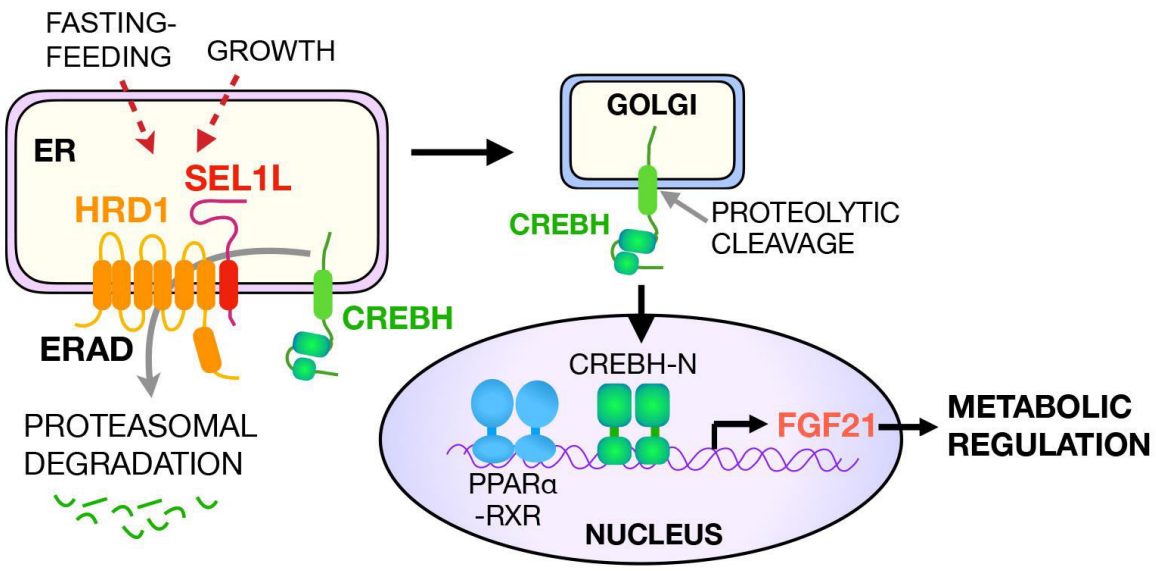

Figure 8. Model: Hepatic Sel1L-Hrd1 ERAD regulates systemic metabolism via modulation of the "Crebh-Fgf21" axis in physiological contexts.

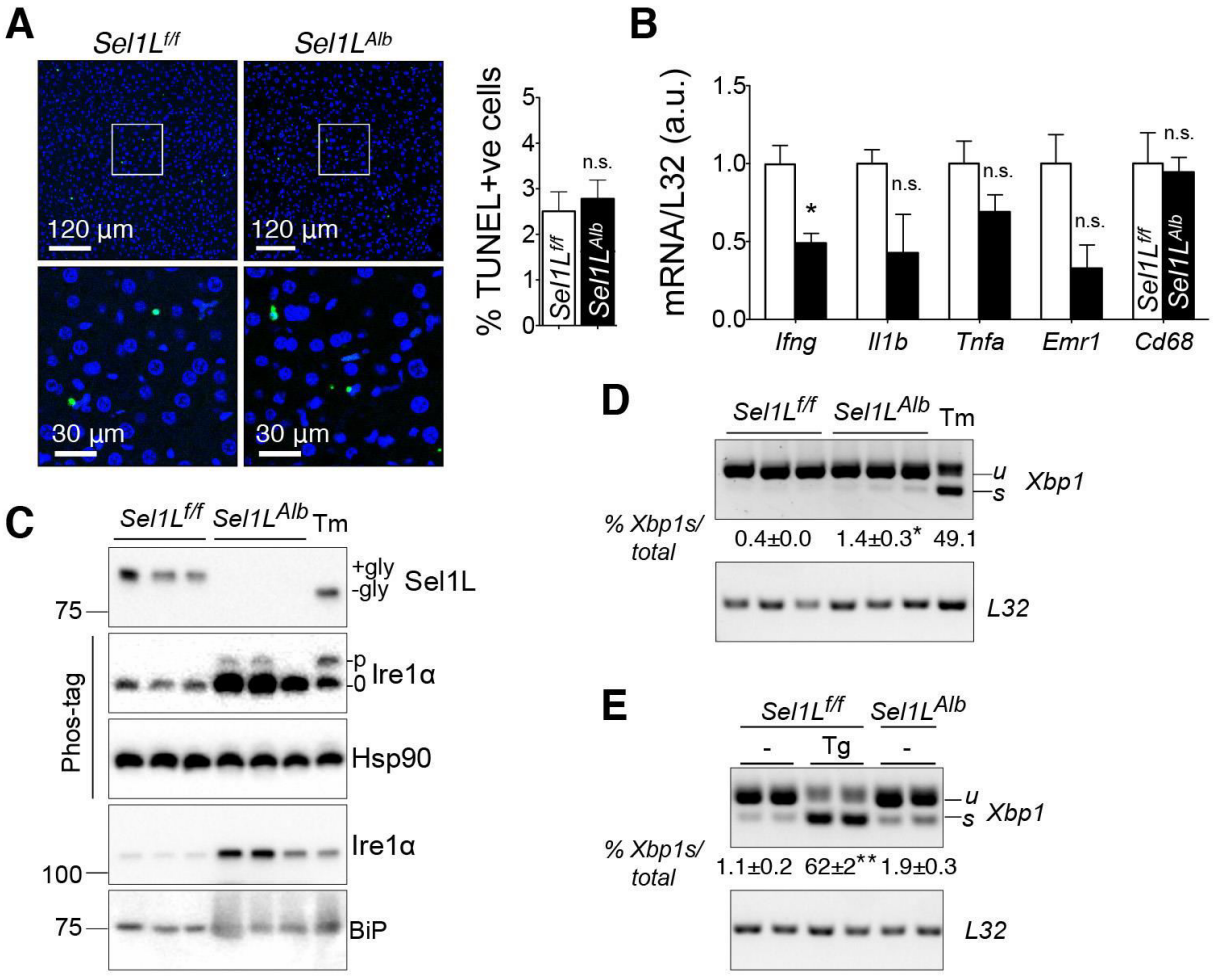

Figure EV1. Lack of cell death, inflammation and overt ER stress in Sel1L-deficient hepatocytes.

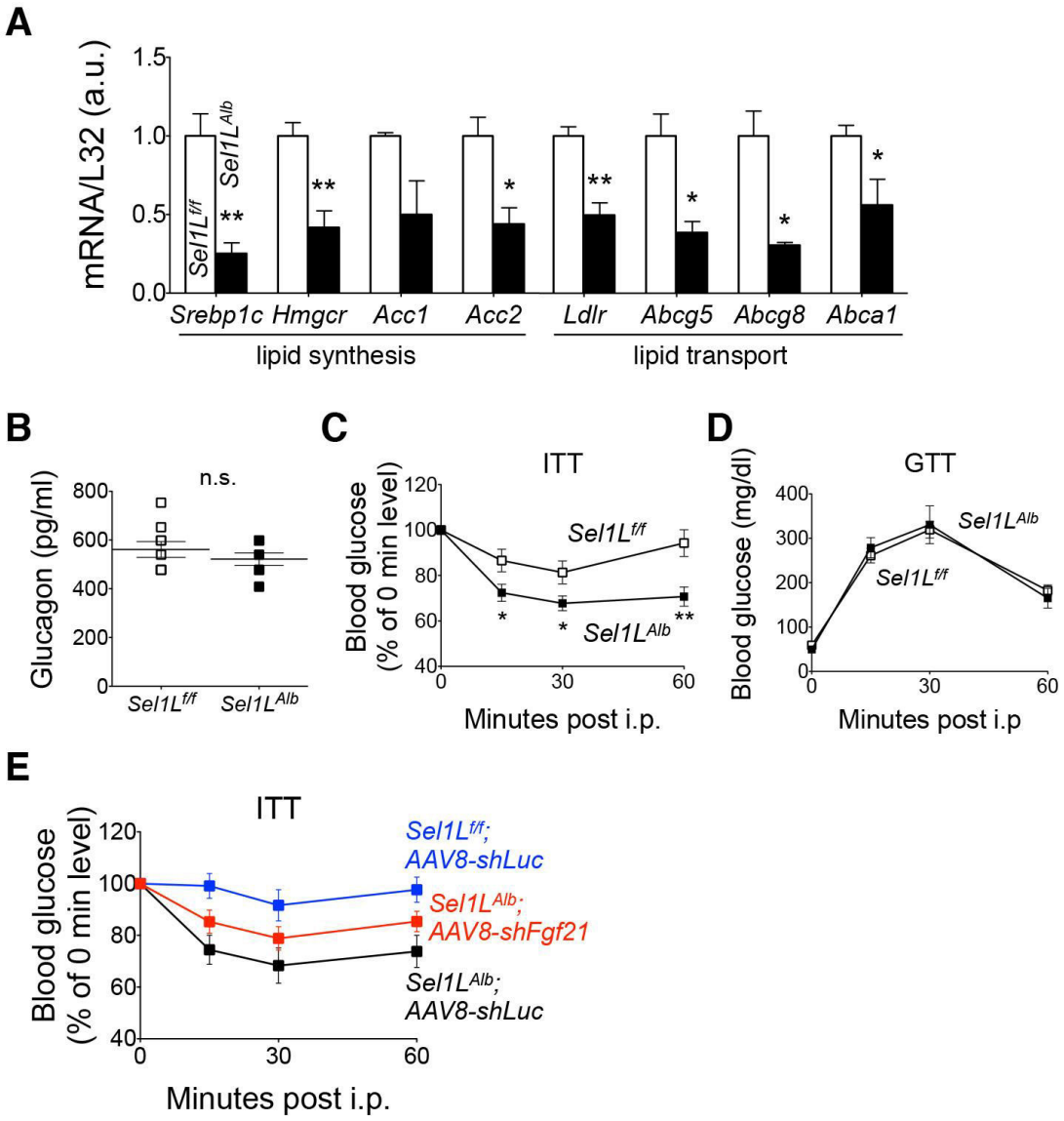

Figure EV2. Hepatic Sel1L-Hrd1 ERAD deficient mice have altered metabolism.

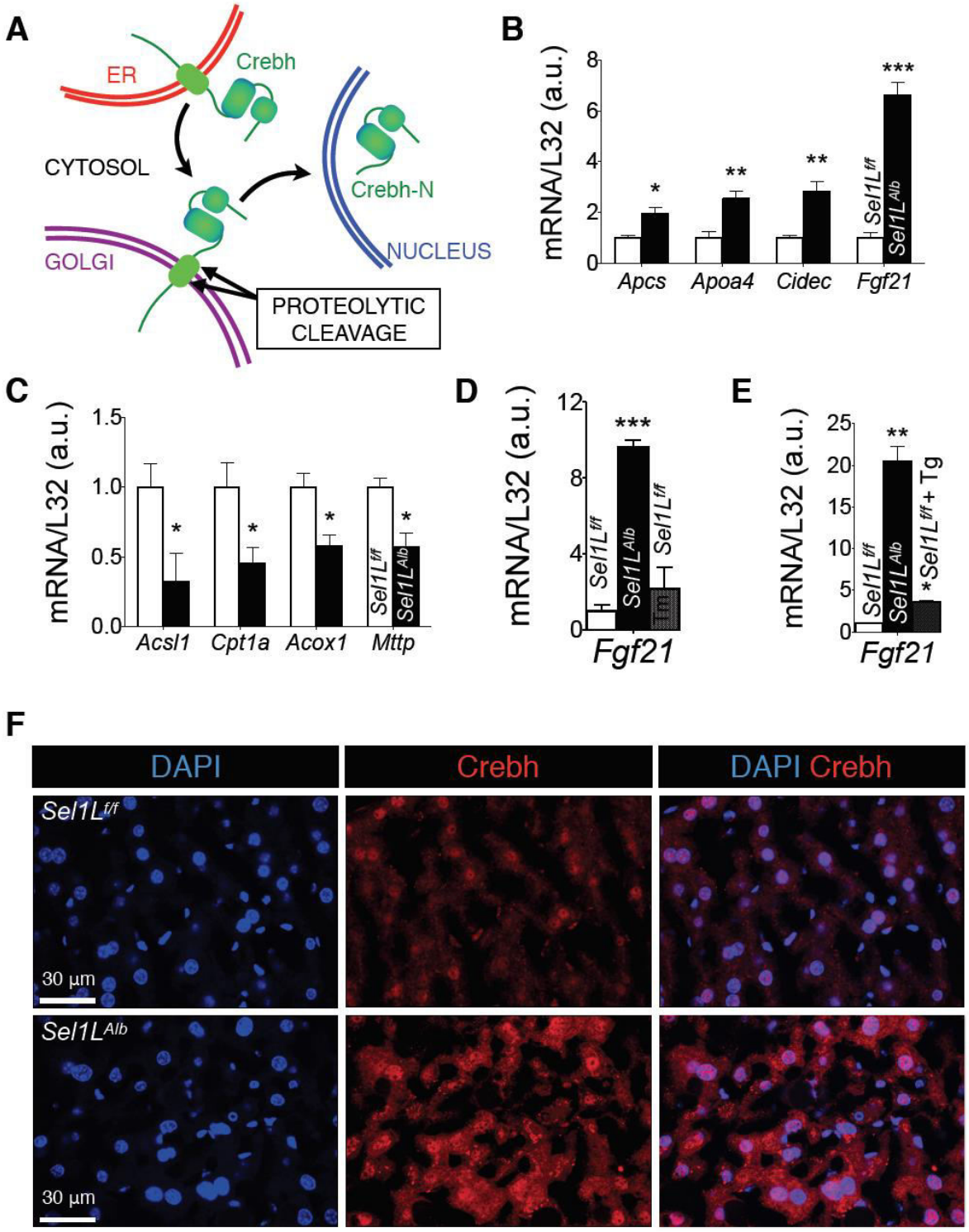

Figure EV3. Hepatic Sel1L regulates protein stability and activity of Crebh, not Pparα.

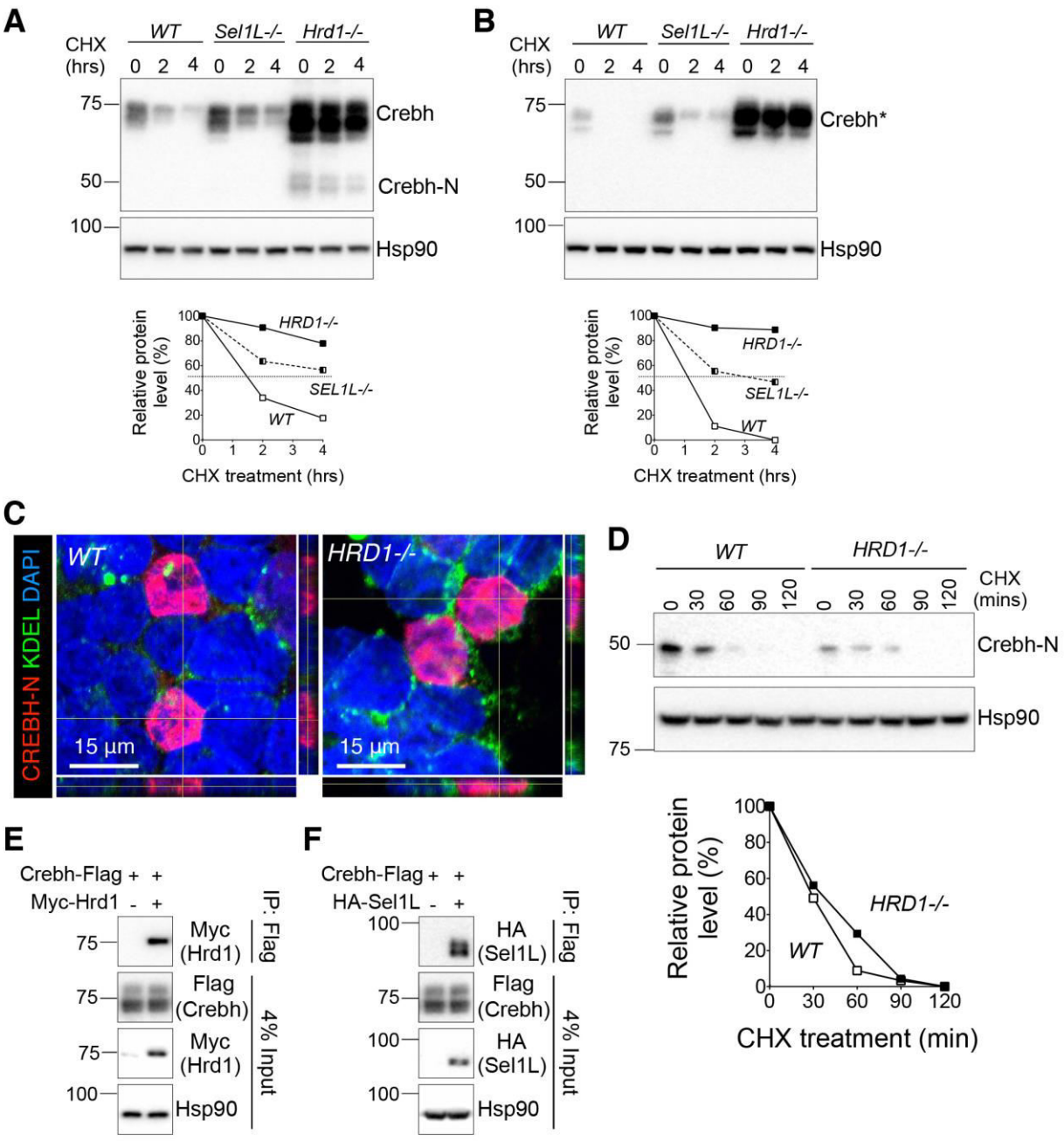

Figure EV4. Crebh, and not Crebh-N, is an ERAD substrate.

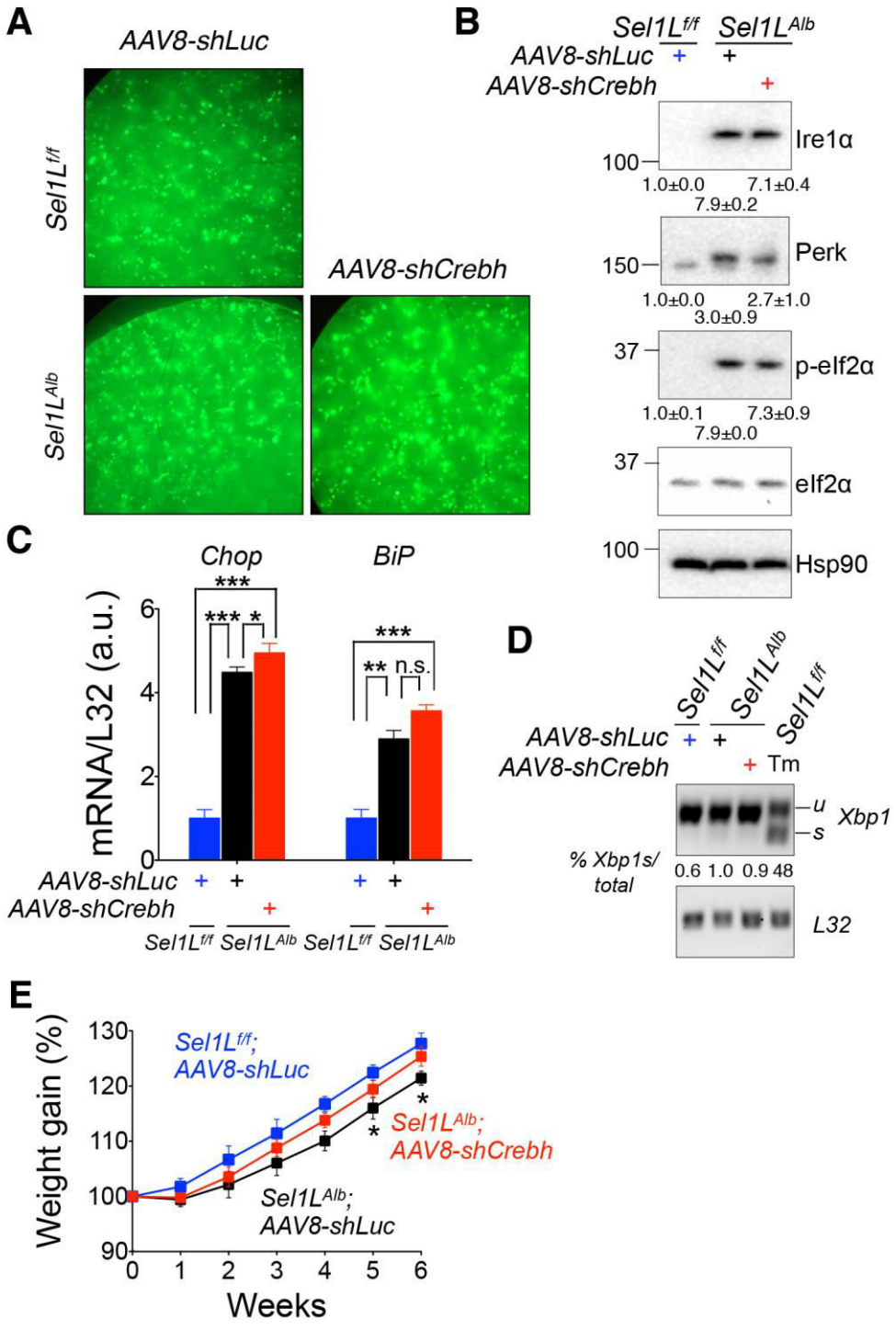

Figure EV5. Crebh deletion does not affect ER stress level in *Sel1L*^{Alb} liver.

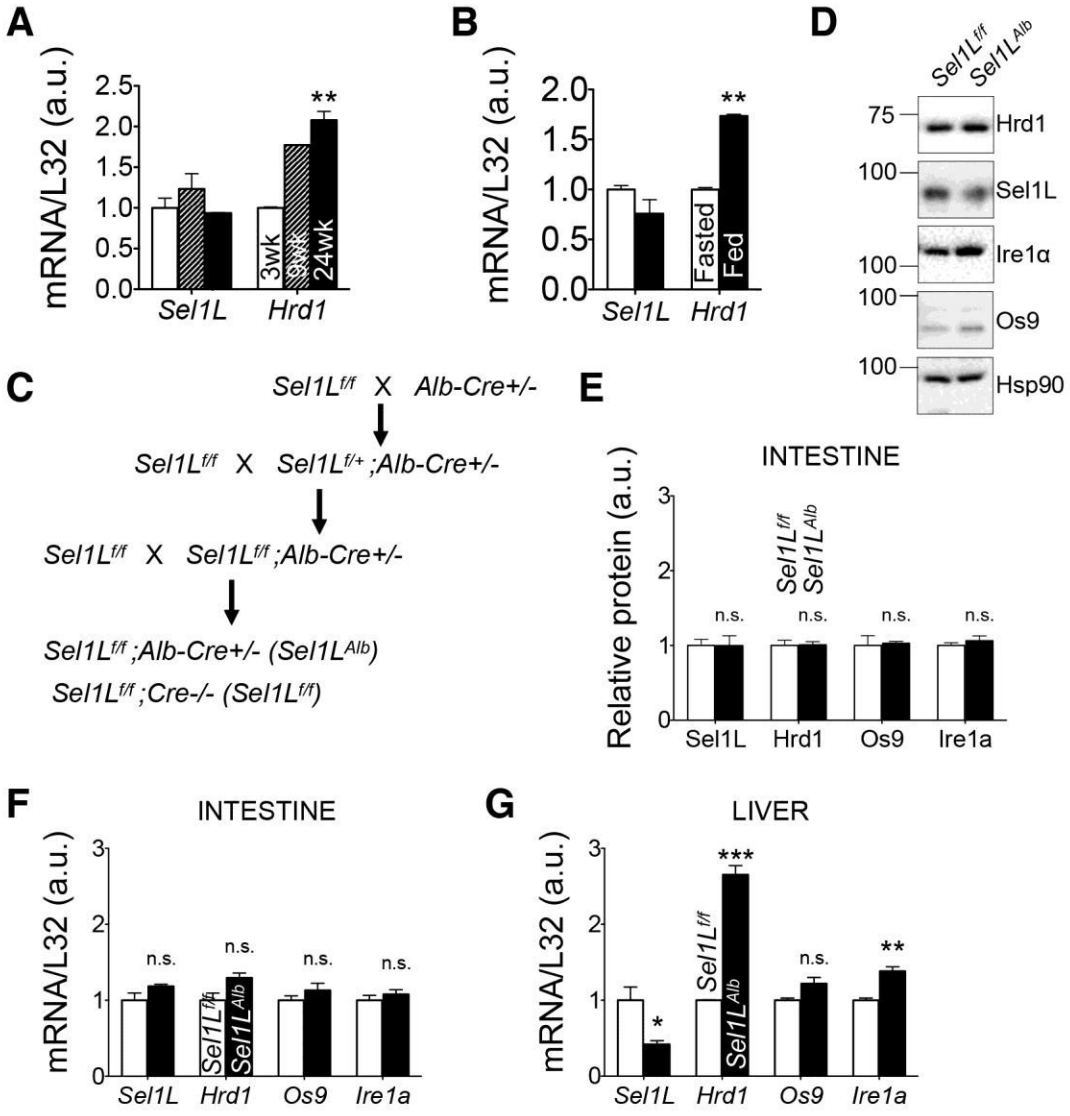

Appendix Figure S1. Generation of liver-specific Sel1L-Hrd1 ERAD deficient mouse model.

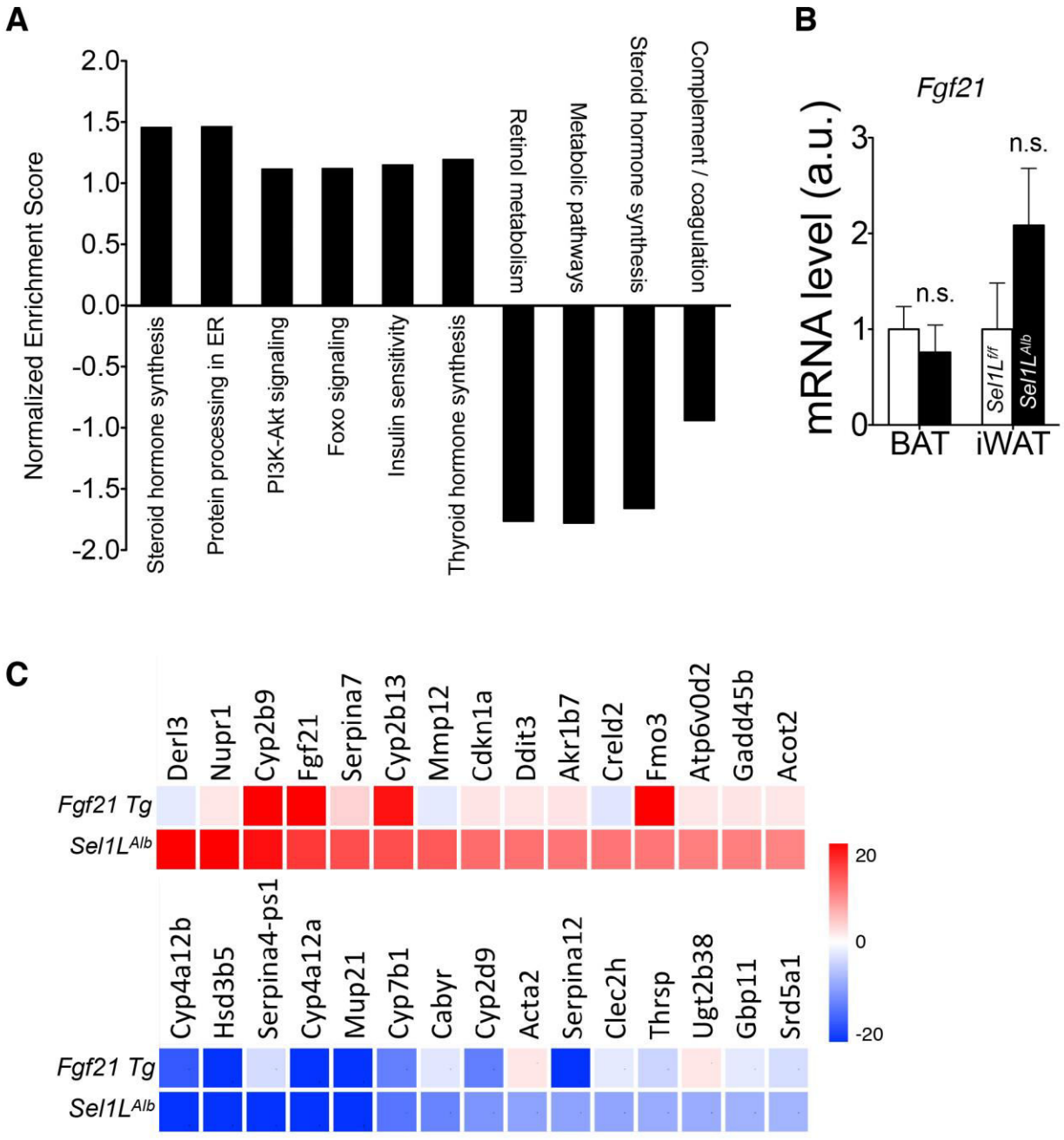

Appendix Figure S2. Transcriptomics analysis of Sel1L-Hrd1 ERAD deficient liver.

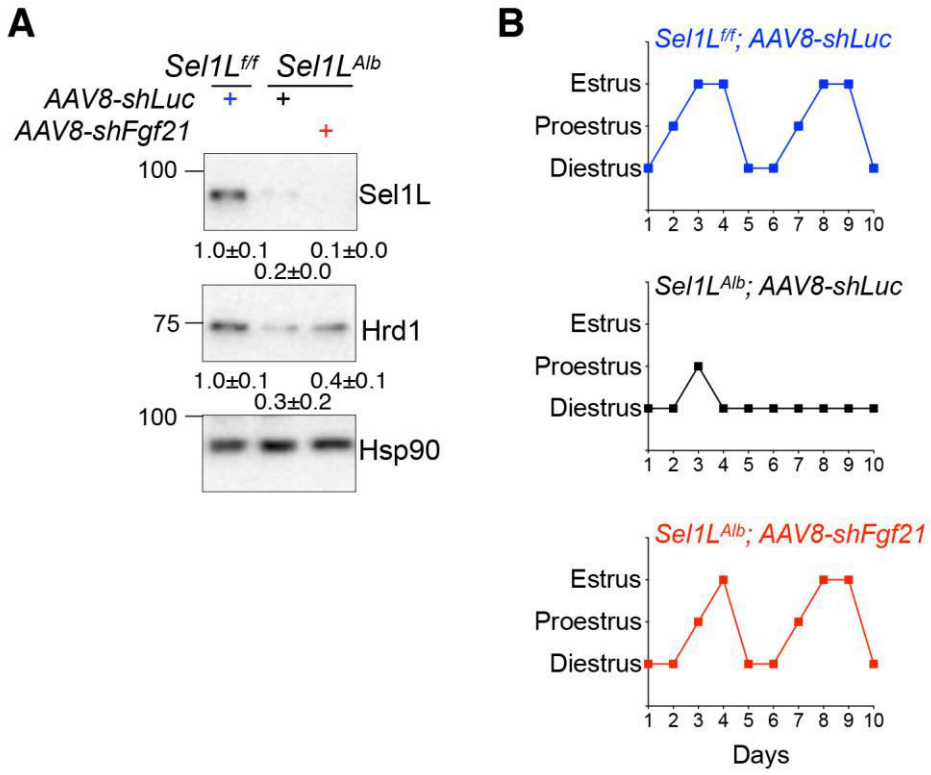

Appendix Figure S3. Fgf21 knockdown partially reverses the phenotypes of *Sel1L*^{Alb} mice.

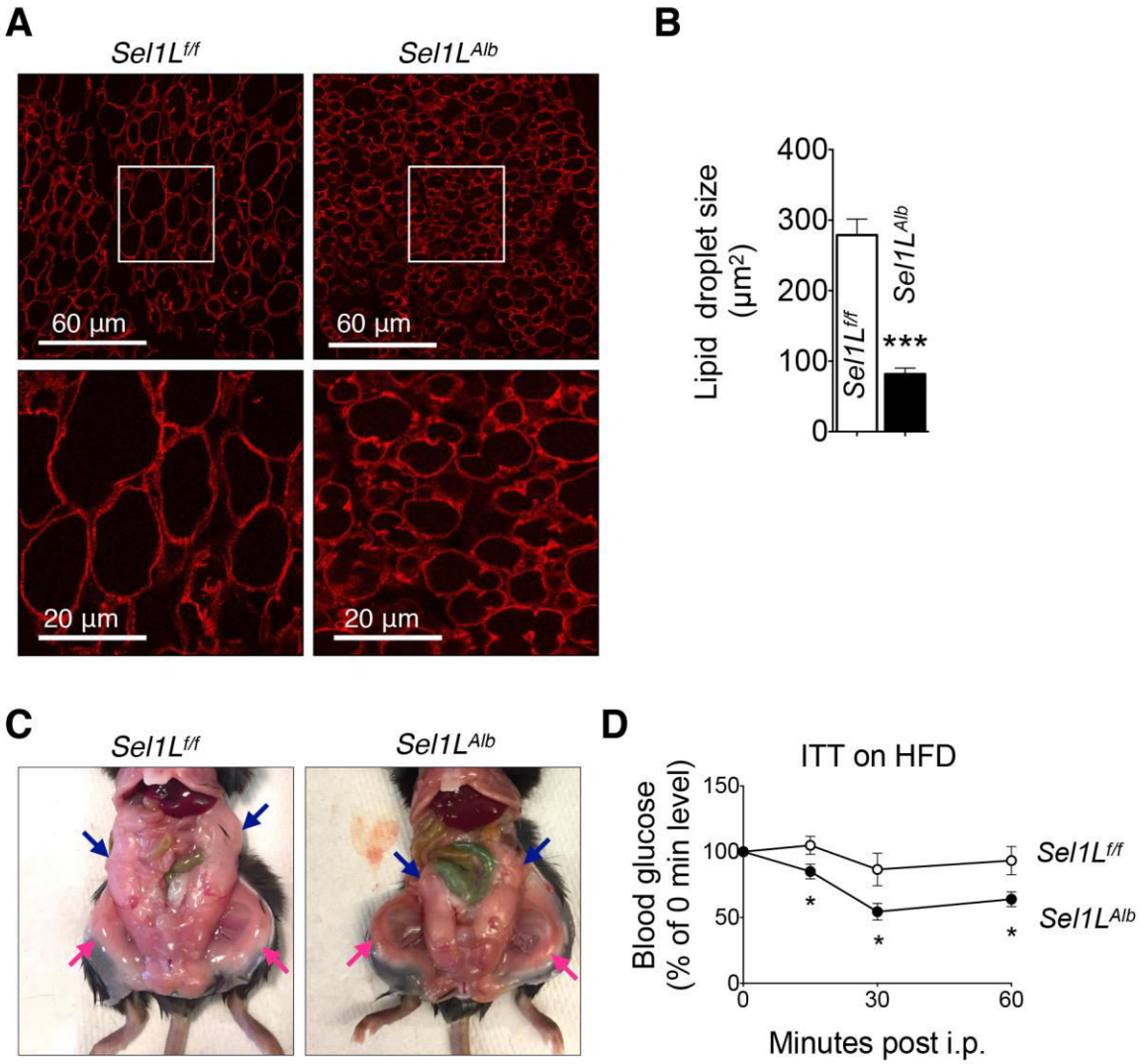

Appendix Figure S4. Hepatic ERAD deficient mice show resistance to diet induced weight gain.

CHAPTER 3

Hepatic Sel1L-Hrd1 ERAD regulates bile homeostasis via bile exporter proteins

Asmita Bhattacharya[1,2], Genta Kakiyama[3], Hajime Takei[4], Hiroshi Nittono[4], Ling Qi[1,5] *

[1] Department of Molecular and Integrative Physiology, University of Michigan Medical School, Ann Arbor, MI 48105, USA;
[2] Graduate Program of Genetics, Genomics and Development, Cornell University, Ithaca, NY 14853, USA;
[3] Division of Gastroenterology, Hepatology and Nutrition, Virginia Commonwealth University and McGuire VA Medical Center, Richmond, VA;
[4] Junshin Clinic Bile Acid Institute, Haramachi, Meguro-ku, Tokyo, Japan;
[5] Division of Metabolism, Endocrinology & Diabetes, Department of Internal Medicine, University of Michigan Medical School, Ann Arbor, MI 48105, USA;

*** Correspondence:** lingq@med.umich.edu

This chapter is in preparation for journal submission.

3.1 ABSTRACT

The liver is the central organ critically regulating the balance of metabolically potent yet toxic bile acids in the body. Here, we describe how hepatic Sel1L-Hrd1 mediated endoplasmic reticulum (ER)-associated degradation (ERAD), the principal protein quality control system in the mammalian cell, manages bile homeostasis in the body. Mice harboring *Sel1L* deficiency in the liver develop intrahepatic cholestasis, with significant overload of bile acids in hepatocytes and blood. These livers exhibit prominent hepatocyte ballooning, inflammation and liver dysfunction. Strikingly, these mice are hypersensitive to dietary bile acid challenge, which results in further accruing of liver damage and steatosis. Proteomics analysis revealed significant accumulation of Abcb11/Bsep, the primary bile acid exporter, and Abcb4/Mdr2, the floppase secreting bile-stabilizing phosphatidylcholine, in Sel1L-deficient hepatocytes, while the transcript levels of these genes remained unaffected. Mechanistically, we show that Sel1L-Hrd1 ERAD directly controls the maturation of these complex transporter proteins in the ER, thereby ensuring their proper function and bile equilibrium in the body.

3.2 INTRODUCTION

Bile is a potent fluid synthesized daily by the vertebrate liver, stored in the gallbladder (for most animal species), and secreted into the intestines postprandially. Bile is primarily composed of bile acids/salts, cholesterol and lecithin (phosphatidylcholine), along with pigments such as bilirubin and biliverdin, and mucus (1). Bile acids are special detergent-like molecules synthesized in the liver from cholesterol via a process that adds ionic moieties on one face of the planar steroid structure to give the molecule an amphipathic character (one face hydrophilic, the other face hydrophobic) (2, 3). These bile acids often exist in the form of salts, conjugated to amino acids (e.g. glycine, taurine), thus increasing their polar nature and making them more efficient surfactants for lipid digestion. This also limits their ability to diffuse across lipid membranes, thereby protecting cells from caustic side-effects. The polar lecithin and amphipathic bile acid/salt molecules are necessary to solubilize the nonpolar cholesterol molecules in bile by binding together in the form of mixed micelles. Bile micelles serve two primary functions – the absorptive micelle emulsifies and solubilizes dietary fats and cholesterol, and the excretory micelle works to eliminate waste such as bilirubin, heavy metals etc.

Owing to this functional yet toxic nature of bile components, the synthesis, export/import, and 20-fold recycling of bile acids are tightly regulated by the master transcription factor and nuclear

receptor Fxr, for which bile acids themselves serve as ligands (4-6). Fxr functions to (i) inhibit *Cyp7a1*, rate limiting enzyme for bile acid synthesis (7), (ii) upregulate transcription of exporters to pump out intracellular bile acids and lecithin into bile (8-10), and (iii) downregulate transcription of importers that take up bile acids from the enterohepatic recycling of bile acids (11, 12), thereby maintaining a low, safe intrahepatic concentration of bile acids via negative feedback regulation. Mutations in these transporter proteins have been associated with various imbalances of bile metabolism and debilitating diseases such as Progressive Familial Intrahepatic Cholestasis or PFIC – type I (mutant *Atp8b1*, flippase importing phospholipids to balance out the export of lecithin from the cell) (13-15), type II (mutant *Abcb11*, primary bile acid exporter) (16-18), type III (mutant *Abcb4*, floppase exporting lecithin into bile) (19-21), Dubin-Johnson syndrome (mutant *Abcc2*, primary bilirubin exporter) (22-24), hypercholanemia (elevated serum bile acids), pruritus (itching), gallstone disease (25, 26), and cancers of the liver or intestine (27-29). These multi-transmembrane domain-containing transporter proteins are hence subject to tight quality control during their folding in the endoplasmic reticulum (ER).

Endoplasmic Reticulum Associated Degradation (ERAD) is a major protein folding quality control system that functions to recognize and retro-translocate substrate proteins, often misfolded, from the ER to cytosol for proteasomal degradation (30, 31). The Sel1L-Hrd1 complex is the most highly studied and conserved ERAD system in mammalian cells, where Hrd1 serves as the E3 ubiquitin ligase, and Sel1L as the adaptor protein essential for the stability and function of Hrd1 (32-35), and the global deletion of either of these two genes leading to embryonic lethality (36, 37). We and others have previously shown using several different tissue-specific ERAD-knockout mouse models that Sel1L-Hrd1 ERAD functions to maintain quality and quantity control for prohormone maturation and transmembrane-domain-containing protein folding in the ER (31). Most of these ERAD-deficient mouse models were associated with metabolic disorders arising out of impaired clearance of specific substrate proteins, such as – central diabetes insipidus owing to pro-arginine-vasopressin (proAVP) misfolding in *Sel1L*-deficient AVP-neurons (38), hyperphagia and obesity owing to pro-opiomelanocortin (POMC) dysfunction in *Sel1L*-deficient POMC-neurons (39), and spontaneous ileitis owing to inositol-requiring enzyme-1a (Ire1α) accumulation in *Sel1L*-deficient enterocytes (40). Recently, we and others independently characterized *Sel1L*- and *Hrd1*-specific liver-knockout mouse models, both of which showed these mice to have massively altered growth and metabolic profiles owing to highly elevated Fgf21 hormone levels produced as a result of

accumulation and over-activation of the hepatic ERAD substrate – ER-resident transcription factor cAMP-responsive element-binding protein, hepatocyte specific (Crebh) (41, 42).

Here, we delineate yet another novel role played by hepatic Sel1L-Hrd1 mediated ERAD in bile metabolism. In this study, we have described how liver-specific *Sel1L*-knockout mice exhibit elevated levels of serum bile acids, along with intrahepatic cholestasis and associated liver damage accruing with age. Upon further amplification of the bile homeostasis defect in these mice with the help of dietary bile acid challenge, we found that these mice develop severe hypercholanemia, along with significant secretion defect of bile acids, cholesterol and lecithin. This in turn leads to cholesterol crystal precipitation, profound liver damage and increased propensity to steatosis and gallstone disease. Mechanistically, we show that faulty ERAD-mediated quality control of bile transporter proteins is the basis for this phenotype, thereby discovering a unique role played by hepatic Sel1L-mediated ERAD in regulating bile homeostasis in the body.

3.3 RESULTS

Expression profile of bile associated genes is altered in *Sel1L^{Alb}* livers

The liver being a central figure in regulating bile homeostasis in the body, we examined gene expression profiles in the *Sel1L$^{f/f}$* and *Sel1L^{Alb}* livers as obtained from the microarray analysis performed earlier on these tissues, deposited as GSE118658 (41). Interestingly, we found that several genes associated with bile synthesis (e.g. *Cyp7b1, Cyp46a1, Cyp39a1, Cyp2c70, Slc27a2, Slc27a5, Amacr*), export (*Abcc4, Abcc6, Abcg2, Abcg5, Abcg8*) and import (*Slc10a1, Slc22a12, Slc22a7, Slco1a1, Slco1b2*) were significantly altered, mostly downregulated, in *Sel1L^{Alb}* livers as compared to their WT counterparts (Figure 1A). This pattern warranted further investigation into the state of bile homeostasis in these mice.

Sel1L^{Alb} mice exhibit intrahepatic cholestasis

To comprehensively assess the bile balance in *Sel1L$^{f/f}$* and *Sel1L^{Alb}* mice, we measured total bile acid and cholesterol levels in serum, liver, bile and intestines of adult (3 months old) mice of both genders. Strikingly, even under basal state, *Sel1L^{Alb}* mice showed significantly higher circulating levels of serum bile acids (Figure 1B), with majority of these mice reaching hypercholanemic levels, i.e. serum bile acids higher than 20μM. Furthermore, these mice had significantly higher levels of intrahepatic bile acids or cholestasis (Figure 1C) while having

significantly lower levels of bile acids in bile (Figure 1D), when measured after 6 hours of fasting during the day. This suggested that there may be a significant defect in bile export from the hepatocyte into the bile canaliculus. The intestinal bile acid pool in these mice remained unaffected (Supplementary Figure 1A).

As described earlier (41), *Sel1L*^{Alb} mice showed a significant yet mild decrease in serum cholesterol levels compared to their WT littermates (Figure 1E). Interestingly, while their intrahepatic cholesterol levels remained unchanged (Figure 1F), *Sel1L*^{Alb} mice showed significantly lower levels of biliary cholesterol (Figure 1G), suggestive of a potential cholesterol secretion defect into bile as well. Again, the intestinal cholesterol pool in these cohorts remained unaffected (Supplementary Figure 1B).

Next, we aimed to assess if these secretion defects in bile acids and cholesterol had any effect on the cholesterol solubility potential of bile. Upon measurement of lecithin (phosphatidylcholine) content in bile, we found it to be slightly yet significantly reduced in *Sel1L*^{Alb} mice (Figure 1H). However, we noted no specific patterns in the individual species of bile acids in the serum, liver or bile (Supplementary Figures 1C-E) of these mice. Furthermore, the overall hydrophobicity index of biliary bile acids, calculated as described previously (43), was similar between these two groups (Figure 1J), suggesting that the bile acid and lecithin secretion defect observed in this mouse model was an overall phenomenon, and did not affect any particular species of bile acids specifically.

Sel1L^{Alb} mice develop progressive liver damage

As bile acid imbalances are often associated with cellular toxicity and hepatocyte injury, especially in cases of intrahepatic cholestasis, we measured serum parameters reflecting liver damage over time in *Sel1L*$^{f/f}$ and *Sel1L*^{Alb} mice. Interestingly, serum levels of alanine aminotransferase (ALT), aspartate amino transferase (AST) and alkaline phosphatase (ALP) started out as significantly higher in young (1-month-old) *Sel1L*^{Alb} mice compared to their WT littermates (Figures 2A-C). At an older age (3-month-old), ALT and AST levels rose to even higher levels in *Sel1L*^{Alb} animals, while ALP levels decreased slightly, but not as sharply as in *Sel1L*$^{f/f}$ control animals. This trend signified that *Sel1L*^{Alb} livers accrued damage progressively over time. This was reflected upon histological examination of 3-month-old mice which showed a large number of lightly-stained, ballooned hepatocytes in *Sel1L*^{Alb} livers (Figure 2D). Ballooning of hepatocytes, commonly called ballooning degeneration, is a classic marker of

hepatocyte damage, hepatic toxicity and liver disease development (44-46). As these mice progressed to 6-month age, their livers showed marked increase in bile duct proliferation and inflammatory infiltration (Figure 2E). Cholestatic disease has long been associated hepatocyte and cholangiocyte damage, owing to the toxic effect of bile acids on cell membranes, almost always leading to bile duct hyperplasia and inflammation (47, 48). In keeping with this, immunofluorescent staining revealed a significant increase in F4/80-positive resident macrophages of *Sel1L*^{Alb} livers (Figure 2F), accompanied by an increase in CD11b-positive infiltrating macrophages (Figure 2G), overall suggesting an increased inflammatory tone in *Sel1L*^{Alb} livers compared to *Sel1L*$^{f/f}$ ones.

Sel1L^{Alb} mice are hypersensitive to dietary bile acid challenge

Bile acid supplementation in normal chow diet is often used as a standard model to exacerbate any potential bile-associated defects in mice. In order to amplify the aforementioned bile-related imbalances in these mice, we fed *Sel1L*$^{f/f}$ and *Sel1L*^{Alb} mice with normal chow diet supplemented with 0.5% cholic acid (a common primary bile acid species naturally synthesized in the body). In response to this dietary challenge, *Sel1L*^{Alb} mice rapidly and significantly lost body weight over the next 2 weeks while their *Sel1L*$^{f/f}$ littermates quickly recovered after 3-4 days (Figure 3A). Of note here, male *Sel1L*^{Alb} mice showed extreme sensitivity to this dietary challenge, losing body weight more sharply than females, becoming nearly morbid by 2 weeks on this diet (Supplementary Figures 2A-B). This sort of gender bias is a common, characteristic feature of bile associated disorders in mice (49, 50), although the mechanism behind it is still under investigation. Strikingly, *Sel1L*^{Alb} mice developed severe hypercholanemia after 2 weeks on the cholic acid diet, as evident from the greatly elevated level of serum bile acids (Figure 3B). Intrahepatic concentration of bile acids rose to similar levels (possibly saturation level) in *Sel1L*$^{f/f}$ and *Sel1L*^{Alb} mice (Figure 3C), whereas biliary concentration of bile acids consistently remained significantly lower in *Sel1L*^{Alb} mice (Figure 3D). This suggested that, in *Sel1L*^{Alb} mice, owing to severe bile acid export defect, bile acids first accumulate within the hepatocytes (normal chow diet), and then upon further dietary challenge (cholic acid diet), leak out into the perisinusoidal space of Disse, ultimately entering blood circulation in the body, leading to hypercholanemia. The intestinal pool of bile acids remained unaffected in both cohorts of mice under both diets (Supplementary Figure 2C).

Upon examination of cholesterol levels, we found that under cholic acid diet, serum cholesterol levels were comparable in *Sel1L*$^{f/f}$ and *Sel1L*^{Alb} mice (Figure 3E). Interestingly, after 2 weeks on

this diet, intrahepatic levels of cholesterol became significantly higher in *Sel1L*^{Alb} mice (Figure 3F), whereas biliary concentrations of cholesterol remained significantly lower (Figure 3G), depicting an acute defect in cholesterol secretion into bile. Again, intestinal cholesterol levels remained comparable between the two cohorts of mice under both diets (Supplementary Figure 2D). Additionally, upon measuring lecithin (phosphatidylcholine) content in bile, we found it to be again significantly lowered in *Sel1L*^{Alb} mice (Figure 3H). However, upon analysis of individual bile acids in serum, liver or bile of these mice, we found no significant patterns restricted to specific species (Supplementary Figures 2E-G). The overall hydrophobicity indices of bile were comparable between the two cohorts of mice (Figure 3I), albeit being expectedly higher in the cholic acid diet groups than under normal chow diet.

Sel1L^{Alb} livers accrue profound damage and steatosis upon prolonged cholic acid diet

Upon continuation of the cholic acid diet, some of the *Sel1L*^{Alb} mice recovered a part of their body weight loss (Supplementary Figure 3A), but developed severe hepatic steatosis after 3 months (Figure 4A). This was further confirmed via histological analysis and Oil Red O staining for lipid droplets where we found that *Sel1L*^{Alb} livers steadily worsened into fatty liver (steatosis) upon prolonged cholic acid diet feeding, compared to their *Sel1L*$^{f/f}$ littermates (Figure 4B). This *Sel1L*^{Alb} phenotype started out as microsteatosis and upon prolonged feeding, converted to a mixture of micro and macrosteatosis. While their overall liver to body weight ratios remained comparable (Supplementary Figure 3B), *Sel1L*^{Alb} mice registered with significantly higher gallbladder weights upon prolonged cholic acid feeding (Figure 4C). In keeping with this trend of profound liver disease, serum parameters of liver damage (ALT, ALP, AST) were also highly and significantly elevated in *Sel1L*^{Alb} mice, compared to *Sel1L*$^{f/f}$, upon being fed the cholic acid diet (Figures 4D-F). Furthermore, these livers showed increased incidences of ductular proliferation (Supplementary Figure 3C), yet another sign of increased bile duct damage and inflammation (47, 48).

Sel1L deficiency does not affect bile acid synthesis

In order to get to the molecular basis of the perturbed bile homeostasis observed in the *Sel1L*^{Alb} system, we next examined the genes primarily responsible for synthesis, export and import of bile acids, cholesterol and lecithin in the livers of *Sel1L*$^{f/f}$ and *Sel1L*^{Alb} mice. The expression levels of *Cyp7a1*, primary rate limiting enzyme in the bile acid synthesis pathway was comparable between the two cohorts of mice under normal chow diet, while being completely suppressed in the cholic acid diet fed mice, as is expected owing to Fxr-induced negative

feedback (51). The expression levels of another minor bile acid synthesis enzyme, *Cyp27a1*, was significantly reduced in *Sel1L*^{Alb} livers under normal conditions, while being comparable and lower under cholic acid diet (Figure 5A). Measurement of Cyp7a1 protein levels also showed a trend similar to that of its mRNA levels (Figure 5B). This suggested that under normal chow diet, although there was some decrease in *Cyp27a1* expression levels, overall bile acid synthesis remained comparable between *Sel1L*$^{f/f}$ and *Sel1L*^{Alb} livers, whereas upon cholic acid diet feeding, the bile acid overload led to complete suppression of further synthesis of bile acids in both cohorts of mice. This pattern was further confirmed by the measurement of 7α-hydroxy-4-cholesten-3-one (or C4, an intermediate of the bile acid synthesis pathway) levels in the serum of these mice (Figure 5C).

Sel1L^{Alb} livers show altered levels of bile-associated transporters

A chronic overload of bile acids within the hepatocyte can often lead to the increased expression of alternate bile acid exporters that pump bile acids out from within the cell into the perisinusoidal space of Disse around cells (which ultimately leak into blood circulation). Upon examination of these alternate bile acid exporters, we found that while mRNA level of *Mrp3/Abcc3* was slightly reduced in *Sel1L*^{Alb} livers, the expression levels of *Mrp4/Abcc4* was greatly elevated in these livers compared to those of their *Sel1L*$^{f/f}$ littermates (Supplementary Figure 4A). This trend is often seen in cases of intrahepatic cholestasis in mice (52). Next, we measured the expression levels of bile acid importer genes in these livers. Owing to the bile acid overload within the *Sel1L*^{Alb} hepatocytes, Fxr activation is expected to limit any further uptake of bile acids within the cells by downregulating bile acid importer genes. Indeed, we found that majority of the bile acid importers, *Ntcp/Slc10a1*, *Oatp1/Slc21a1/Slco1a1* and *Oatp4/Slc21a10/Slco1b2* were significantly downregulated in the *Sel1L*^{Alb} livers compared to *Sel1L*$^{f/f}$ livers, while *Oatp2/Slc21a5/Slco1a4* levels remained unaffected (Figure 5D).

Putting together the biliary secretion defect of bile acids, cholesterol and lecithin, we next examined the levels of bile-related exporter genes in *Sel1L*$^{f/f}$ and *Sel1L*^{Alb} livers under these diets. As ERAD deficiency often leads to accumulation of substrate proteins in the ER owing to faulty degradation, we performed a proteomics screen on all ER proteins in *Sel1L*$^{f/f}$ and *Sel1L*^{Alb} livers, in order to identify candidate ERAD substrates. Interestingly, we found that the protein levels of lecithin exporter Mdr2/Abcb4 and bile acid exporter Bsep/Abcb11 were significantly elevated in the *Sel1L*^{Alb} hepatic ER (Figure 5E). However, mRNA levels of *Bsep/Abcb11* (primary bile acid exporter), *Mrp2/Abcc2* (primary bilirubin exporter) and *Mdr2/Abcb4* (primary

lecithin exporter) were comparable between the two animal groups, suggesting that the protein level increase was non-transcriptional. Additionally, under the bile acid diet, *Bsep* and *Mdr2* mRNA levels were significantly downregulated in *Sel1L*^{Alb} livers (Figure 5F). This was especially intriguing because Fxr activation caused by intrahepatic bile acid overload in *Sel1L*^{Alb} livers is expected to increase the transcription of these genes with the motive of increasing bile secretion and reducing the intracellular bile acid load (53) – a pattern that is maintained for *Bsep* in *Sel1L*$^{f/f}$ livers as these mice go from normal chow to bile acid supplemented diet (Figure 5F). But surprisingly, this trend is not recapitulated in the *Sel1L*^{Alb} livers.

The significant yet non-transcriptional accumulation pattern was unique to Mdr2 and Bsep, and not observed for any other transporter proteins associated with bile metabolism in these livers (Figure 5E). Next, we validated these findings by directly measuring Bsep and Mdr2 protein levels, which were found to be indeed significantly elevated in *Sel1L*^{Alb} livers, as compared to *Sel1L*$^{f/f}$ livers (Figure 5G). Interestingly, the localization of these exporter proteins was at the plasma membrane for both genotypes (Figure 5H and Supplementary Figure 4C). In contrast, protein levels of Mrp2 and Oatp1 were not significantly altered between these cohorts (Figure 5G). Additionally, we measured expression levels of genes primarily responsible for synthesis, export and import of cholesterol in hepatocytes. In keeping with the cholesterol export defect phenotype, we found the expression levels of *Abcg5* and *Abcg8*, primary bile cholesterol exporters (54), to be significantly downregulated in *Sel1L*^{Alb} livers (Supplementary Figure 4B). Moreover, as described previously (41), expression levels of *Ldlr* (involved in receptor-mediated cholesterol endocytosis) and *Hmgcr* (rate limiting enzyme in cholesterol biosynthesis pathway) were also significantly reduced in these livers, compared to their *Sel1L*$^{f/f}$ counterparts.

3.4 DISCUSSION

Bile homeostasis maintenance is a dynamic process critical for proper functioning and health of various organ systems in the body. While on one hand, bile acids aid in the digestion of dietary fats, solubilize cholesterol, and even act as ligands for specific receptors regulating various metabolic pathways in the body, on the other hand, their amphipathic characters render them highly toxic metabolites needing careful optimization. Distortion in bile equilibrium has been widely associated with cholesterol gallstone disease (CGD) formed in supersaturated bile, cholangitis formed from inflamed bile ducts, and cholestasis which can progress into cirrhosis, jaundice and liver cancer. In 2016, a genome-wide association study (GWAS) done in bile had

identified *Sel1L* as a locus influencing the circulating serum levels of bile acids (55). From a more biochemical point of view, various independent groups have speculated ERAD to be the quality control machinery designated for the triage of several bile associated transporter proteins, especially Abcb11/Bsep (30, 31, 56). This is the first in vivo model showcasing the intimate relationship that exists between Sel1L-mediated ERAD and bile metabolism in the liver via transporter quality control.

This study brings to light a new role played by Sel1L-Hrd1 ERAD in managing a unique facet of mammalian physiology. An absence of Sel1L-mediated ERAD in the liver leads to a significant secretion defect from hepatocytes into bile, which causes an overload of toxic bile acids within the hepatocytes, that finally leak out to rapidly increase the circulating levels of bile acids in the serum. This phenomenon leads to progressive liver injury and renders these mice hypersensitive to any further imbalances of bile homeostasis, ultimately causing profound liver damage, and predisposing these mice to steatosis and cholestatic disease. Mechanistically, we observe that, in the absence of ERAD, bile exporter proteins accumulate in a non-transcriptional manner in the hepatic ER, suggesting that Sel1L-Hrd1 exert their influence on bile metabolism in the body via the quality control of their substrates – bile transporter proteins.

Inferring from the non-transcriptional accumulation of Abcb11 and Abcb4 proteins in *Sel1L*^{Alb} livers, we hypothesize that these multi-transmembrane proteins may be substrates for Sel1L-Hrd1 ERAD. In order to test this idea, in future studies, we will express plasmid constructs carrying Abcb11 and Abcb4 genes in *WT* and *HRD1-/-* HEK293T cells, and check for ubiquitination and interaction with core ERAD components (Sel1L, Hrd1). Further characterization would include testing to see if there is protein stabilization in the absence of ERAD with the help of protein translation shut off assay, and dependency on ER chaperones such as Grp78. Furthermore, human patients harboring mutations in Abcb11 and Abcb4 are often associated with different forms of cholestatic liver disease (19, 56, 57), with characteristics often matching the phenotypes exhibited by *Sel1L*^{Alb} mice. Several of these mutants are associated with intracellular accumulation, ER entrapment and/or impaired function. As continuation of this study, we would like to explore the dependency of these disease mutants on Sel1L-Hrd1 by assessing their stability, localization and degradation with and without ERAD. Overall, with the help of physiological and biochemical analyses, this study establishes the critical role played by hepatic Sel1L-Hrd1 ERAD in mediating bile acid, lecithin and cholesterol export from hepatocytes to bile canaliculi, thereby overseeing bile homeostasis in the body.

3.5 METHODS

Mice. Liver-specific *Sel1L*-knockout mice (*Sel1L*^{Alb}) and WT littermates (*Sel1L*$^{f/f}$) were generated by crossing *Sel1L*$^{f/f}$ mice with C57BL/6J mice expressing Cre driven by the Albumin-promoter (JAX 003574, B6.Cg-Tg(Alb-Cre)21Mgn/J). These mice have been characterized previously (41). Due to the reduced fertility of *Sel1L*^{Alb} females, only *Sel1L*^{Alb} males were used for breeding. Mice were fed normal chow (20% protein, 13% fat, 67% carbohydrate, Harlan Teklad 2914) or normal chow supplemented with 0.5% cholic acid (19.3% protein, 10.5% fat, 70.2% carbohydrate, 0.5% cholic acid, Harlan Teklad .08766) as indicated. All mice procedures were done in compliance with IACUC at Cornell University (2007-0051) and at University of Michigan (PRO00008989). Mice were generally fasted for 5-6 hours in the morning before sacrifice except when stated. Isoflurane anesthesia followed by major organ removal was used for euthanasia and tissues were fixed or frozen in liquid nitrogen immediately upon collection.

Metabolite analysis. Bile acids (BA) in serum, liver, bile and total intestine, as well as 7-α-hydroxy-4-cholesten-3-one (C4) in serum were analyzed by liquid chromatography-mass spectrometry (LC-MS). Total cholesterol (CHOL) levels in serum, liver, bile and total intestine were measured by high performance liquid chromatography. Total phosphatidylcholine (PC) was measured using a colorimetric kit from Abcam (ab83377). Serum levels of alanine aminotransferase (ALT), alkaline phosphatase (ALP) and aspartate aminotransferase (AST) were measured by IDEXX Laboratories.

Western blot analysis. Total protein was extracted from cells and tissues followed by SDS-PAGE and Western blotting as previously described (58, 59). For large membrane proteins, final samples were not boiled but heated at 70C for 5 mins instead, and 1% SDS was used in lysis buffer as needed. Signals were quantified using BioRad ImageLab software and total protein levels were normalized to loading controls. Primary antibodies used are as follows: F4/80 (1:100 for staining, Biolegend 123109); Cd11b (1:100 for staining, BD Pharmingen 553310); Ki67 (1:200 for staining, Abcam ab16667); Hsp90 (1:4,000, Santa Cruz sc-7947); Abcb4 (1:200 for staining, 1:1000 for Western blot, Abcam ab24108); Bsep (1:100 for staining, 1:3000 for Western blot), Mrp2 (1:2000) and Ntcp (1:2000) were kind gifts from Dr. Bruno Stieger (University of Zurich); Oatp1 (1:1000) was a gift from Dr. Richard Kim (University of Western Ontario); and Cyp7a1 (1:1000) was gifted by Dr. David Russell (University of Texas

Southwestern). Secondary antibodies for Western blot were goat anti-rabbit IgG-HRP and goat anti-mouse IgG-HRP (1:5,000; BioRad). Secondary antibodies for immunostaining were anti-mouse IgG Alexa Fluor 594; anti-rabbit IgG Alexa Fluor 488; and anti-rat Alexa Fluor 680 (all 1:500; Jackson ImmunoResearch).

Proteomics analysis. Freshly isolated liver tissue was used to extract the ER fraction as the microsomal pellet after ultracentrifugation. The pellet was further purified by sucrose gradient fractionation. Bradford assay was used to measure protein concentration among samples. 75 µg of protein per sample was sent for mass spectrometric analysis using the Tandem Mass Tag technique.

RNA extraction, RT and qPCR. Total RNA was derived from tissues and cells using Trizol with BCP phase separation reagent. RNA quality was measured via a Nanodrop device. qPCR analysis was done using oligo-dT primer, Taq polymerase, SYBR-Green based master mix and the Applied Biosystems qPCR machine. All data were normalized to ribosomal *L32* expression level. qPCR primers are: *Cyp7a1* F: AGCAACTAAACAACCTGCCAGTACTA, R: GTCCGGATATTCAAGGATGCA; *Cyp27a1* F: GCCTCACCTATGGGATCTTCA, R: TCAAAGCCTGACGCAGATG; *Bsep* F: AAGCTACATCTGCCTTAGACACAGAA, R: CAATACAGGTCCGACCCTCTCT; *Mrp2* F: TCCAGGACCAAGAGATTTGC, R: TCTGTGAGTGCAAGAGACAGGT; *Mdr2* F: CTTGAGGCAGCGAGAAATG, R: GGTTGCTGATGCTGCCTAGT; *Mrp3* F: GATCGTCATTGATGGGCTCA, R: GCGCAGGTCGTGGAGG; *Mrp4* F: CATCAAGTCCAGGGAAAAGGTTG, R: GAGGGCCGAGATGAGGGAG; *Oatp4* F: GCATGGTGCTATTCTCTCCTGA, R: ATGCCACATCATGAAGCCCT; *Oatp2* F: TACATGTCAGCTTGCCTCGC, R: GCACACTCAGGACCCTTGTC; *Oatp1* F: CCTCAGCTGTACAATGATTGCC, R: TTTTGGTTCAATGCAGGGTTG; *Ntcp* F: GAAGTCCAAAAGGCCACACTATGT, R: ACAGCCACAGAGAGGGAGAAAG; *Abcg5* F: TCAATGAGTTTTACGGCCTGAA, R: GCACATCGGGTGATTTAGCA; *Abcg8* F: TGCCCACCTTCCACATGTC, R: ATGAAGCCGGCAGTAAGGTAGA; *Ldlr* F: AGGCTGTGGGCTCCATAGG, R: TGCGGTCCAGGGTCATCT; *Hmgcr* F: CTTGTGGAATGCCTTGTGATTG, R: AGCCGAAGCAGCACATGAT.

Immunostaining and histology. For staining, tissues upon dissection were directly fixed in 10% neutral buffered formalin and stored at 4°C. A portion of these were paraffin embedded, cut into

sections and stained with H&E on a fee-for-service basis by the Michigan Histology Core. The rest was dehydrated in 15% sucrose, embedded in OCT, cryosectioned and stained with Oil Red O for lipid droplet visualization. For other staining, mice livers were perfused first with warm PBS followed by 4% paraformaldehyde for fixation. After overnight fixing, these were dehydrated in 15% sucrose, embedded in OCT and cut into 5 μm sections. For immunocytochemistry, cells were cultured on coverslips and fixed in 4% formalin for 15 mins. For antigen retrieval, sections were either boiled in EDTA or citrate buffer for 20 minutes, or permeabilized for 10 mins in 0.3% TritonX/Glycine at room temperature. Thereafter, the sections/cells blocked in 1% donkey serum with 0.03% TritonX-100 for 1 hour at room temperature, and incubated with primary antibodies overnight at 4°C in humidified chambers. Next day, they were washed thrice in PBS containing 0.03% TritonX and incubated for 2 hours in secondary antibodies at room temperature. For immunohistochemistry, peroxide quenching was done before antigen retrieval and signal was amplified and detected using the avidin-biotin kit along with DAB substrate kit. Counterstaining and mounting were done using either the hard-set medium containing DAPI (Vector H-1200) or Permount, as applicable. Fluorescent images were taken with Nikon A1 Confocal Microscope with the University of Michigan Imaging Core. Imaging parameters were kept identical within each experiment, and all quantification was done using ImageJ plugin (FIJI). DAB and H&E stained samples were imaged using Aperio Scanscope (Leica Biosystems).

Cell lines and transfection. HEK293T cells (ATCC) were cultured in DMEM (Corning, NY) with heat inactivated 10% FBS (GIBCO), 1% penicillin/streptomycin and 1% sodium pyruvate. CRISPR was used to generate Hrd1-/- HEK293T cells as published previously (40). Transfection was done within 20-24 hours of plating using Lipofectamine 2000 and harvested within the next 24 hours.

Plasmids. All plasmid constructs for Abcb4 were kindly gifted by Dr. Kenneth Linton (Queen Mary University of London), and all plasmid constructs for Bsep were kindly gifted by Dr. James Boyer (Yale University).

Statistical Analysis. All results are expressed as mean ± SEM unless specifically stated. Comparisons between groups have been done either by paired two-tailed Student's t test or by 2-way ANOVA as required. All experiments were repeated at least thrice, and performed with independent, multiple biological samples out of which representative data are shown here.

3.6 ACKNOWLEDGEMENTS

We would like to thank Drs. Richard Wojcikiewicz, Yihong Ye, Kenneth Linton, Bruno Stieger, Richard Kim, David Russell and James Boyer for reagents, and Drs. Peter Arvan, Kenneth Simpson, Robert Weiss and Natasza Kurpios for insightful comments; Dr. Venkatesh Basrur and Proteomics Core at University of Michigan for helping with proteomics analysis; the Histology and Vision Research Cores at University of Michigan for assistance; and other members of Qi/Arvan laboratories for comments and discussion. This work is supported by R01GM113188, R01DK105393 and University of Michigan Protein Folding Diseases Initiative (L.Q.). A.B. has been supported by the AHA Predoctoral Fellowship #16PRE29750001.

3.7 AUTHOR CONTRIBUTION

A.B. designed and performed most experiments; G.K., H.T. and H.N. performed all bile acid and cholesterol analysis using HPLC and LCMS; A.B. and L.Q. wrote the manuscript.

3.8 FIGURE LEGENDS

Figure 1. ***Sel1L^{Alb}*** **mice exhibit intrahepatic cholestasis and impaired biliary cholesterol secretion**. (A) Heat map of genes associated with bile synthesis, export and import in 9-week-old *Sel1L^{Alb}* livers, logarithm of fold change over *Sel1L$^{f/f}$* livers depicted here (n=3 per group). (B-H) Serum total bile acids/salts (B), intrahepatic total bile acids/salts (C), biliary total bile acids/salts (D), serum total cholesterol (E), intrahepatic total cholesterol (F), biliary total cholesterol (G), and biliary lecithin (H) levels in 12-week-old mice after 6 hr fasting (n=5-8 per group). (I-J) Cholesterol saturation index of bile (I), and hydrophobicity index of bile (J) in 12-week-old mice after 6 hr fasting (n=5-8 per group). Values, mean ± SEM; *, $p<0.05$; **, $p<0.01$; ***, $p<0.001$ by Student's t test.

Figure 2. ***Sel1L^{Alb}*** **mice develop progressive liver damage and inflammation with age**. (A-C) Serum alanine aminotransferase (ALT) (A), serum aspartate aminotransferase (AST) (B), and serum alkaline phosphatase (ALP) levels in 1-month and 3-month-old mice after 6 hr fasting (n=5-8 per group). (D-E) H&E stained images of paraffin-embedded liver sections obtained from 3-month and 6-month-old mice after 6 hr fasting (n=5-8 per group). (F-G) Representative confocal images depicting F4/80-positive resident macrophages (F), and CD11b-positive infiltrating macrophages (G) in liver cryosections obtained from 3-month-old mice after 6 hr fasting (n=3-5 per group). Values, mean ± SEM; *, $p<0.05$; **, $p<0.01$; ***, $p<0.001$ by 2-way ANOVA.

Figure 3. **Bile metabolism in *Sel1L^{Alb}* mice is hypersensitive to dietary bile acid challenge**. (A) Body weight-gain curves obtained after putting 6-week-old *Sel1L$^{f/f}$* and *Sel1L^{Alb}* mice on

either normal chow diet (NCD) or 0.5% cholic acid supplemented diet (CAD) (n=8-10 per group). (B-H) Serum total bile acids/salts (B), intrahepatic total bile acids/salts (C), biliary total bile acids/salts (D), serum total cholesterol (E), intrahepatic total cholesterol (F), biliary total cholesterol (G), and biliary lecithin (H) levels in 8-week-old mice after 6 hr fasting following either NCD feeding or 2 weeks of CAD feeding (n=5-10 per group). (I-K) Cholesterol saturation index of bile (I), hydrophobicity index of bile (J), and microscopic images of cholesterol crystals within bile (K) obtained from 8-week-old mice after 6 hr fasting following either NCD feeding or 2 weeks of CAD feeding (n=4-8 per group). Values, mean ± SEM; *, p<0.05; **, p<0.01; ***, p<0.001 by Student's t test.

Figure 4. ***Sel1L^{Alb}*** **livers accrue profound damage and steatosis in response to dietary bile acid challenge**. (A) Representative images of liver and gallbladder obtained after putting 6-week-old mice on cholic acid diet (CAD) for 3 months (n=5 per group). (B) H&E stained images of paraffin-embedded liver sections (left), and Oil Red O stained images of OCT-embedded liver cryosections (right) obtained after putting 6-week-old mice on normal chow diet (NCD) for 2-weeks, or CAD for 2-weeks or 3-months (n=4-5 per group). (C-F) Gallbladder weights (C), serum alanine aminotransferase (ALT) (D), serum alkaline phosphatase (ALP) (E), and serum aspartate aminotransferase (AST) (F) levels obtained after putting 6-week-old mice on NCD for 2-weeks, or CAD for 2-weeks or 3-months (n=5-10 per group). Values, mean ± SEM; *, p<0.05; **, p<0.01; ***, p<0.001 by Student's t test.

Figure 5. ***Sel1L^{Alb}*** **livers show altered expression pattern for genes associated with bile metabolism**. (A-G) Data obtained after putting 8-week-old mice on either normal chow diet (NCD) or 0.5% cholic acid supplemented diet (CAD) for 2 weeks, followed by 6-hours fasting prior to dissection. (A) qPCR analysis and (B) Western blot analysis of genes associated with bile acid synthesis (n=3-5, 2 independent repeats). (C) Serum levels of 7-α-hydroxy-4-cholesten-3-one (C4) (n=4-8) obtained via LC/MS. qPCR analysis of genes associated with (D) bile acid import, and (F) primary bile acid/lecithin export (n=4-5, 2 independent repeats). (E) Tabular depiction of proteomics data obtained from TMT-LC/MS analysis of hepatic ER isolated from 3-months-old mice (n=3 per group). (G) Western blot analysis of bile-related transporter proteins in the livers of 3-month-old mice (n=3 per group, 3 independent repeats). (H) Representative confocal images depicting bile acid exporter Abcb11 and tight junction protein Zo1 in liver cryosections obtained from 3-month-old mice after 6-hr fasting (n=3-5 per group). *L32* and Hsp90, loading controls. Values, mean ± SEM; *, p<0.05; **, p<0.01; ***, p<0.001 by 2-way ANOVA (A-G) or by Student's t test (H-I).

Supplementary Figure 1. **Bile acid pool constituents under normal chow diet**. (A-B) Intestinal total bile acids/salts (A), and intestinal total cholesterol (B) levels in 12-week-old mice after 6 hr fasting (n=5-6 per group). (C-E) Individual bile acid/salt species as present in serum (C), liver (D), and bile (E) of 12-week-old mice after 6 hr fasting (n=5-8 per group). Values, mean ± SEM; *, p<0.05; **, p<0.01; ***, p<0.001 by Student's t test.

Supplementary Figure 2. **Bile acid pool constituents under cholic acid supplemented diet**. (A) Body weight-gain curves obtained from putting 6-week-old male and female *Sel1L$^{f/f}$* and *Sel1L^{Alb}* mice on 0.5% cholic acid supplemented diet (CAD) for 2 weeks (n=3-5 per group). (B-C) Intestinal total bile acids/salts (B), and intestinal total cholesterol (C) levels in 8-week-old mice after 6 hr fasting following either NCD feeding or 2 weeks of cholic acid diet (CAD) feeding (n=4-8 per group). (D-F) Individual bile acid/salt species as present in serum (D), liver (E), and bile (F) of 8-week-old mice after 6 hr fasting following either NCD feeding or 2 weeks of CAD feeding (n=4-8 per group). Values, mean ± SEM; *, p<0.05; **, p<0.01; ***, p<0.001 by 2-way ANOVA.

Supplementary Figure 3. **Liver damage upon prolonged cholic acid supplemented diet**. (A) Body weight-gain curves obtained after putting 6-week-old *Sel1L*$^{f/f}$ and *Sel1L*^{Alb} mice on 0.5% cholic acid supplemented diet (CAD) for 3 months (n=5 per group). (B) Liver-to-body-weight ratios obtained after putting 6-week-old mice on normal chow diet (NCD) for 2-weeks, or CAD for 2-weeks or 3-months (n=4-5 per group). (C) Ki67 stained images of paraffin-embedded liver sections obtained after putting 6-week-old mice on NCD for 2-weeks, or CAD for 2-weeks or 3-months (n=4-5 per group). Values, mean ± SEM; *, p<0.05; **, p<0.01; ***, p<0.001 by Student's t test.

Supplementary Figure 4. *Sel1L*^{Alb} livers show increased levels of bile exporter proteins. qPCR analysis of genes associated with (A) alternative bile acid export, and (B) cholesterol export, import and synthesis (n=4-5, 2 independent repeats). (C) Representative confocal images depicting bile acid (A) and lecithin (B) exporter proteins in liver cryosections obtained from 3-month-old mice after 6-hr fasting (n=3-5 per group). *L32*, loading control. Values, mean ± SEM; *, p<0.05; **, p<0.01; ***, p<0.001 by Student's t test.

3.9 REFERENCES

1. Boyer JL. Bile formation and secretion. Compr Physiol. 2013;3(3):1035-78. doi: 10.1002/cphy.c120027. PubMed PMID: 23897680; PMCID: PMC4091928.
2. Hofmann AF, Hagey LR. Bile acids: chemistry, pathochemistry, biology, pathobiology, and therapeutics. Cell Mol Life Sci. 2008;65(16):2461-83. doi: 10.1007/s00018-008-7568-6. PubMed PMID: 18488143.
3. Russell DW. The enzymes, regulation, and genetics of bile acid synthesis. Annual review of biochemistry. 2003;72:137-74. doi: 10.1146/annurev.biochem.72.121801.161712. PubMed PMID: 12543708.
4. Parks DJ, Blanchard SG, Bledsoe RK, Chandra G, Consler TG, Kliewer SA, Stimmel JB, Willson TM, Zavacki AM, Moore DD, Lehmann JM. Bile acids: natural ligands for an orphan nuclear receptor. Science (New York, NY). 1999;284(5418):1365-8. doi: 10.1126/science.284.5418.1365. PubMed PMID: 10334993.
5. Wang H, Chen J, Hollister K, Sowers LC, Forman BM. Endogenous bile acids are ligands for the nuclear receptor FXR/BAR. Molecular cell. 1999;3(5):543-53. PubMed PMID: 10360171.
6. Makishima M, Okamoto AY, Repa JJ, Tu H, Learned RM, Luk A, Hull MV, Lustig KD, Mangelsdorf DJ, Shan B. Identification of a nuclear receptor for bile acids. Science (New York, NY). 1999;284(5418):1362-5. doi: 10.1126/science.284.5418.1362. PubMed PMID: 10334992.
7. Lu TT, Makishima M, Repa JJ, Schoonjans K, Kerr TA, Auwerx J, Mangelsdorf DJ. Molecular basis for feedback regulation of bile acid synthesis by nuclear receptors. Molecular cell. 2000;6(3):507-15. PubMed PMID: 11030331.
8. Huang L, Zhao A, Lew JL, Zhang T, Hrywna Y, Thompson JR, de Pedro N, Royo I, Blevins RA, Pelaez F, Wright SD, Cui J. Farnesoid X receptor activates transcription of the phospholipid pump MDR3. J Biol Chem. 2003;278(51):51085-90. doi: 10.1074/jbc.M308321200. PubMed PMID: 14527955.
9. Ananthanarayanan M, Balasubramanian N, Makishima M, Mangelsdorf DJ, Suchy FJ. Human bile salt export pump promoter is transactivated by the farnesoid X receptor/bile acid receptor. J Biol Chem. 2001;276(31):28857-65. doi: 10.1074/jbc.M011610200. PubMed PMID: 11387316.

10. Liu Y, Binz J, Numerick MJ, Dennis S, Luo G, Desai B, MacKenzie KI, Mansfield TA, Kliewer SA, Goodwin B, Jones SA. Hepatoprotection by the farnesoid X receptor agonist GW4064 in rat models of intra- and extrahepatic cholestasis. J Clin Invest. 2003;112(11):1678-87. doi: 10.1172/JCI18945. PubMed PMID: 14623915; PMCID: PMC281645.
11. Denson LA, Sturm E, Echevarria W, Zimmerman TL, Makishima M, Mangelsdorf DJ, Karpen SJ. The orphan nuclear receptor, shp, mediates bile acid-induced inhibition of the rat bile acid transporter, ntcp. Gastroenterology. 2001;121(1):140-7. PubMed PMID: 11438503.
12. Simon FR, Fortune J, Iwahashi M, Qadri I, Sutherland E. Multihormonal regulation of hepatic sinusoidal Ntcp gene expression. Am J Physiol Gastrointest Liver Physiol. 2004;287(4):G782-94. doi: 10.1152/ajpgi.00379.2003. PubMed PMID: 15361361.
13. Bull LN, van Eijk MJ, Pawlikowska L, DeYoung JA, Juijn JA, Liao M, Klomp LW, Lomri N, Berger R, Scharschmidt BF, Knisely AS, Houwen RH, Freimer NB. A gene encoding a P-type ATPase mutated in two forms of hereditary cholestasis. Nat Genet. 1998;18(3):219-24. doi: 10.1038/ng0398-219. PubMed PMID: 9500542.
14. Ujhazy P, Ortiz D, Misra S, Li S, Moseley J, Jones H, Arias IM. Familial intrahepatic cholestasis 1: studies of localization and function. Hepatology (Baltimore, Md). 2001;34(4 Pt 1):768-75. doi: 10.1053/jhep.2001.27663. PubMed PMID: 11584374.
15. Paulusma CC, Groen A, Kunne C, Ho-Mok KS, Spijkerboer AL, Rudi de Waart D, Hoek FJ, Vreeling H, Hoeben KA, van Marle J, Pawlikowska L, Bull LN, Hofmann AF, Knisely AS, Oude Elferink RP. Atp8b1 deficiency in mice reduces resistance of the canalicular membrane to hydrophobic bile salts and impairs bile salt transport. Hepatology (Baltimore, Md). 2006;44(1):195-204. doi: 10.1002/hep.21212. PubMed PMID: 16799980.
16. Hu G, He P, Liu Z, Chen Q, Zheng B, Zhang Q. Diagnosis of ABCB11 gene mutations in children with intrahepatic cholestasis using high resolution melting analysis and direct sequencing. Mol Med Rep. 2014;10(3):1264-74. doi: 10.3892/mmr.2014.2349. PubMed PMID: 24969679; PMCID: PMC4121405.
17. Hayashi H, Takada T, Suzuki H, Akita H, Sugiyama Y. Two common PFIC2 mutations are associated with the impaired membrane trafficking of BSEP/ABCB11. Hepatology (Baltimore, Md). 2005;41(4):916-24. doi: 10.1002/hep.20627. PubMed PMID: 15791618.
18. Gerloff T, Stieger B, Hagenbuch B, Madon J, Landmann L, Roth J, Hofmann AF, Meier PJ. The sister of P-glycoprotein represents the canalicular bile salt export pump of mammalian liver. J Biol Chem. 1998;273(16):10046-50. PubMed PMID: 9545351.
19. Park HJ, Kim TH, Kim SW, Noh SH, Cho KJ, Choi C, Kwon EY, Choi YJ, Gee HY, Choi JH. Functional characterization of ABCB4 mutations found in progressive familial intrahepatic cholestasis type 3. Sci Rep. 2016;6:26872. doi: 10.1038/srep26872. PubMed PMID: 27256251; PMCID: PMC4891722.
20. Delaunay JL, Durand-Schneider AM, Delautier D, Rada A, Gautherot J, Jacquemin E, Ait-Slimane T, Maurice M. A missense mutation in ABCB4 gene involved in progressive familial intrahepatic cholestasis type 3 leads to a folding defect that can be rescued by low temperature. Hepatology (Baltimore, Md). 2009;49(4):1218-27. doi: 10.1002/hep.22775. PubMed PMID: 19185004.
21. Smit JJ, Schinkel AH, Oude Elferink RP, Groen AK, Wagenaar E, van Deemter L, Mol CA, Ottenhoff R, van der Lugt NM, van Roon MA, et al. Homozygous disruption of the murine mdr2 P-glycoprotein gene leads to a complete absence of phospholipid from bile and to liver disease. Cell. 1993;75(3):451-62. PubMed PMID: 8106172.
22. Keitel V, Nies AT, Brom M, Hummel-Eisenbeiss J, Spring H, Keppler D. A common Dubin-Johnson syndrome mutation impairs protein maturation and transport activity of MRP2 (ABCC2). Am J Physiol Gastrointest Liver Physiol. 2003;284(1):G165-74. doi: 10.1152/ajpgi.00362.2002. PubMed PMID: 12388192.

23. Dubin IN, Johnson FB. Chronic idiopathic jaundice with unidentified pigment in liver cells; a new clinicopathologic entity with a report of 12 cases. Medicine (Baltimore). 1954;33(3):155-97. doi: 10.1097/00005792-195409000-00001. PubMed PMID: 13193360.
24. Mayer R, Kartenbeck J, Buchler M, Jedlitschky G, Leier I, Keppler D. Expression of the MRP gene-encoded conjugate export pump in liver and its selective absence from the canalicular membrane in transport-deficient mutant hepatocytes. The Journal of cell biology. 1995;131(1):137-50. doi: 10.1083/jcb.131.1.137. PubMed PMID: 7559771; PMCID: PMC2120605.
25. Hay DW, Carey MC. Pathophysiology and pathogenesis of cholesterol gallstone formation. Semin Liver Dis. 1990;10(3):159-70. doi: 10.1055/s-2008-1040470. PubMed PMID: 2218580.
26. Hofmann AF. Pathogenesis of cholesterol gallstones. J Clin Gastroenterol. 1988;10 Suppl 2:S1-11. PubMed PMID: 3062078.
27. Knisely AS, Strautnieks SS, Meier Y, Stieger B, Byrne JA, Portmann BC, Bull LN, Pawlikowska L, Bilezikci B, Ozcay F, Laszlo A, Tiszlavicz L, Moore L, Raftos J, Arnell H, Fischler B, Nemeth A, Papadogiannakis N, Cielecka-Kuszyk J, Jankowska I, Pawlowska J, Melin-Aldana H, Emerick KM, Whitington PF, Mieli-Vergani G, Thompson RJ. Hepatocellular carcinoma in ten children under five years of age with bile salt export pump deficiency. Hepatology (Baltimore, Md). 2006;44(2):478-86. doi: 10.1002/hep.21287. PubMed PMID: 16871584.
28. Ikenaga N, Liu SB, Sverdlov DY, Yoshida S, Nasser I, Ke Q, Kang PM, Popov Y. A new Mdr2(-/-) mouse model of sclerosing cholangitis with rapid fibrosis progression, early-onset portal hypertension, and liver cancer. Am J Pathol. 2015;185(2):325-34. doi: 10.1016/j.ajpath.2014.10.013. PubMed PMID: 25478810.
29. Degirolamo C, Modica S, Palasciano G, Moschetta A. Bile acids and colon cancer: Solving the puzzle with nuclear receptors. Trends Mol Med. 2011;17(10):564-72. doi: 10.1016/j.molmed.2011.05.010. PubMed PMID: 21724466.
30. Guerriero CJ, Brodsky JL. The delicate balance between secreted protein folding and endoplasmic reticulum-associated degradation in human physiology. Physiological reviews. 2012;92(2):537-76. doi: 10.1152/physrev.00027.2011. PubMed PMID: 22535891; PMCID: PMC4162396.
31. Qi L, Tsai B, Arvan P. New Insights into the Physiological Role of Endoplasmic Reticulum-Associated Degradation. Trends Cell Biol. 2017;27(6):430-40. doi: 10.1016/j.tcb.2016.12.002. PubMed PMID: 28131647; PMCID: PMC5440201.
32. Mueller B, Klemm EJ, Spooner E, Claessen JH, Ploegh HL. SEL1L nucleates a protein complex required for dislocation of misfolded glycoproteins. Proc Natl Acad Sci USA. 2008;105(34):12325-30. doi: 10.1073/pnas.0805371105. PubMed PMID: 18711132.
33. Sun S, Shi G, Han X, Francisco AB, Ji Y, Mendonca N, Liu X, Locasale JW, Simpson KW, Duhamel GE, Kersten S, Yates JR, 3rd, Long Q, Qi L. Sel1L is indispensable for mammalian endoplasmic reticulum-associated degradation, endoplasmic reticulum homeostasis, and survival. Proc Natl Acad Sci U S A. 2014;111:E582-91. Epub 2014/01/24. doi: 10.1073/pnas.1318114111.
34. Mehnert M, Sommermeyer F, Berger M, Kumar Lakshmipathy S, Gauss R, Aebi M, Jarosch E, Sommer T. The interplay of Hrd3 and the molecular chaperone system ensures efficient degradation of malfolded secretory proteins. Mol Biol Cell. 2015;26(2):185-94. doi: 10.1091/mbc.E14-07-1202. PubMed PMID: 25428985; PMCID: PMC4294667.
35. Vashistha N, Neal SE, Singh A, Carroll SM, Hampton RY. Direct and essential function for Hrd3 in ER-associated degradation. Proc Natl Acad Sci U S A. 2016;113(21):5934-9. doi: 10.1073/pnas.1603079113. PubMed PMID: 27170191; PMCID: PMC4889393.
36. Francisco AB, Singh R, Li S, Vani AK, Yang L, Munroe RJ, Diaferia G, Cardano M, Biunno I, Qi L, Schimenti JC, Long Q. Deficiency of suppressor enhancer Lin12 1 like (SEL1L)

in mice leads to systemic endoplasmic reticulum stress and embryonic lethality. J Biol Chem. 2010;285(18):13694-703. doi: 10.1074/jbc.M109.085340. PubMed PMID: 20197277; PMCID: PMC2859532.
37. Yagishita N, Ohneda K, Amano T, Yamasaki S, Sugiura A, Tsuchimochi K, Shin H, Kawahara K, Ohneda O, Ohta T, Tanaka S, Yamamoto M, Maruyama I, Nishioka K, Fukamizu A, Nakajima T. Essential role of synoviolin in embryogenesis. J Biol Chem. 2005;280(9):7909-16. doi: 10.1074/jbc.M410863200. PubMed PMID: 15611074.
38. Shi G, Somlo D, Kim GH, Prescianotto-Baschong C, Sun S, Beuret N, Long Q, Rutishauser J, Arvan P, Spiess M, Qi L. ER-associated degradation is required for vasopressin prohormone processing and systemic water homeostasis. J Clin Invest. 2017;127(10):3897-912.
39. Kim GH, Shi G, Somlo D, Haataja L, Soon S, Long Q, Nillni EA, Low MJ, Arvan P, Myers MG, Qi L. Hypothalamic ER-associated degradation regulates POMC maturation, feeding and age-associated obesity. J Clin Invest. 2018;In press.
40. Sun S, Shi G, Sha H, Ji Y, Han X, Shu X, Ma H, Inoue T, Gao B, Kim H, Bu P, Guber RD, Shen X, Lee AH, Iwawaki T, Paton AW, Paton JC, Fang D, Tsai B, Yates Iii JR, Wu H, Kersten S, Long Q, Duhamel GE, Simpson KW, Qi L. IRE1alpha is an endogenous substrate of endoplasmic-reticulum-associated degradation. Nature cell biology. 2015;17(12):1546-55. doi: 10.1038/ncb3266. PubMed PMID: 26551274; PMCID: PMC4670240.
41. Bhattacharya A, Sun S, Wang H, Liu M, Long Q, Yin L, Kersten S, Zhang K, Qi L. Hepatic Sel1L-Hrd1 ER-associated degradation (ERAD) manages FGF21 levels and systemic metabolism via CREBH. The EMBO journal. 2018;37(22). doi: 10.15252/embj.201899277. PubMed PMID: 30389665; PMCID: PMC6236331.
42. Wei J, Chen L, Li F, Yuan Y, Wang Y, Xia W, Zhang Y, Xu Y, Yang Z, Gao B, Jin C, Melo-Cardenas J, Green RM, Pan H, Wang J, He F, Zhang K, Fang D. HRD1-ERAD controls production of the hepatokine FGF21 through CREBH polyubiquitination. The EMBO journal. 2018;37(22). doi: 10.15252/embj.201898942. PubMed PMID: 30389664; PMCID: PMC6236336.
43. Heuman DM. Quantitative estimation of the hydrophilic-hydrophobic balance of mixed bile salt solutions. Journal of lipid research. 1989;30(5):719-30. PubMed PMID: 2760545.
44. Guy CD, Suzuki A, Burchette JL, Brunt EM, Abdelmalek MF, Cardona D, McCall SJ, Unalp A, Belt P, Ferrell LD, Diehl AM, Nonalcoholic Steatohepatitis Clinical Research N. Costaining for keratins 8/18 plus ubiquitin improves detection of hepatocyte injury in nonalcoholic fatty liver disease. Hum Pathol. 2012;43(6):790-800. doi: 10.1016/j.humpath.2011.07.007. PubMed PMID: 22036053; PMCID: PMC3288773.
45. Caldwell S, Ikura Y, Dias D, Isomoto K, Yabu A, Moskaluk C, Pramoonjago P, Simmons W, Scruggs H, Rosenbaum N, Wilkinson T, Toms P, Argo CK, Al-Osaimi AM, Redick JA. Hepatocellular ballooning in NASH. J Hepatol. 2010;53(4):719-23. doi: 10.1016/j.jhep.2010.04.031. PubMed PMID: 20624660; PMCID: PMC2930100.
46. Zatloukal K, French SW, Stumptner C, Strnad P, Harada M, Toivola DM, Cadrin M, Omary MB. From Mallory to Mallory-Denk bodies: what, how and why? Exp Cell Res. 2007;313(10):2033-49. doi: 10.1016/j.yexcr.2007.04.024. PubMed PMID: 17531973.
47. Yokota S, Ono Y, Nakao T, Zhang P, Michalopoulos GK, Khan Z. Partial Bile Duct Ligation in the Mouse: A Controlled Model of Localized Obstructive Cholestasis. J Vis Exp. 2018(133). doi: 10.3791/56930. PubMed PMID: 29658929; PMCID: PMC5933264.
48. Mariotti V, Strazzabosco M, Fabris L, Calvisi DF. Animal models of biliary injury and altered bile acid metabolism. Biochim Biophys Acta Mol Basis Dis. 2018;1864(4 Pt B):1254-61. doi: 10.1016/j.bbadis.2017.06.027. PubMed PMID: 28709963; PMCID: PMC5764833.
49. Fu ZD, Csanaky IL, Klaassen CD. Gender-divergent profile of bile acid homeostasis during aging of mice. PLoS One. 2012;7(3):e32551. doi: 10.1371/journal.pone.0032551. PubMed PMID: 22403674; PMCID: PMC3293819.
50. Wang R, Lam P, Liu L, Forrest D, Yousef IM, Mignault D, Phillips MJ, Ling V. Severe cholestasis induced by cholic acid feeding in knockout mice of sister of P-glycoprotein.

Hepatology (Baltimore, Md). 2003;38(6):1489-99. doi: 10.1016/j.hep.2003.09.037. PubMed PMID: 14647060.
51. Chiang JY. Bile acids: regulation of synthesis. Journal of lipid research. 2009;50(10):1955-66. doi: 10.1194/jlr.R900010-JLR200. PubMed PMID: 19346330; PMCID: PMC2739756.
52. Wang R, Chen HL, Liu L, Sheps JA, Phillips MJ, Ling V. Compensatory role of P-glycoproteins in knockout mice lacking the bile salt export pump. Hepatology (Baltimore, Md). 2009;50(3):948-56. doi: 10.1002/hep.23089. PubMed PMID: 19650158.
53. Moschetta A, Bookout AL, Mangelsdorf DJ. Prevention of cholesterol gallstone disease by FXR agonists in a mouse model. Nat Med. 2004;10(12):1352-8. doi: 10.1038/nm1138. PubMed PMID: 15558057.
54. Yu L, Hammer RE, Li-Hawkins J, Von Bergmann K, Lutjohann D, Cohen JC, Hobbs HH. Disruption of Abcg5 and Abcg8 in mice reveals their crucial role in biliary cholesterol secretion. Proc Natl Acad Sci U S A. 2002;99(25):16237-42. doi: 10.1073/pnas.252582399. PubMed PMID: 12444248; PMCID: PMC138595.
55. Wu W, Patel A, Kyostila K, Lohi H, Mladkova N, Kiryluk K, Sun X, Lefkowitch JH, Worman HJ, Gharavi AG. Genome-wide association study in mice identifies loci affecting liver-related phenotypes including Sel1l influencing serum bile acids. Hepatology (Baltimore, Md). 2016;63(6):1943-56. doi: 10.1002/hep.28495. PubMed PMID: 26857093.
56. Wang L, Dong H, Soroka CJ, Wei N, Boyer JL, Hochstrasser M. Degradation of the bile salt export pump at endoplasmic reticulum in progressive familial intrahepatic cholestasis type II. Hepatology (Baltimore, Md). 2008;48(5):1558-69. doi: 10.1002/hep.22499. PubMed PMID: 18798335; PMCID: PMC2587109.
57. Andress EJ, Nicolaou M, McGeoghan F, Linton KJ. ABCB4 missense mutations D243A, K435T, G535D, I490T, R545C, and S978P significantly impair the lipid floppase and likely predispose to secondary pathologies in the human population. Cell Mol Life Sci. 2017;74(13):2513-24. doi: 10.1007/s00018-017-2472-6. PubMed PMID: 28220208; PMCID: PMC5487885.
58. Yang L, Xue Z, He Y, Sun S, Chen H, Qi L. A Phos-tag-based approach reveals the extent of physiological endoplasmic reticulum stress. PLoS One. 2010;5(7):e11621. doi: 10.1371/journal.pone.0011621. PubMed PMID: 20661282; PMCID: 2905412.
59. Sha H, He Y, Chen H, Wang C, Zenno A, Shi H, Yang X, Zhang X, Qi L. The IRE1alpha-XBP1 pathway of the unfolded protein response is required for adipogenesis. Cell metabolism. 2009;9(6):556-64. doi: 10.1016/j.cmet.2009.04.009. PubMed PMID: 19490910; PMCID: 2963107.

3.10 FIGURES

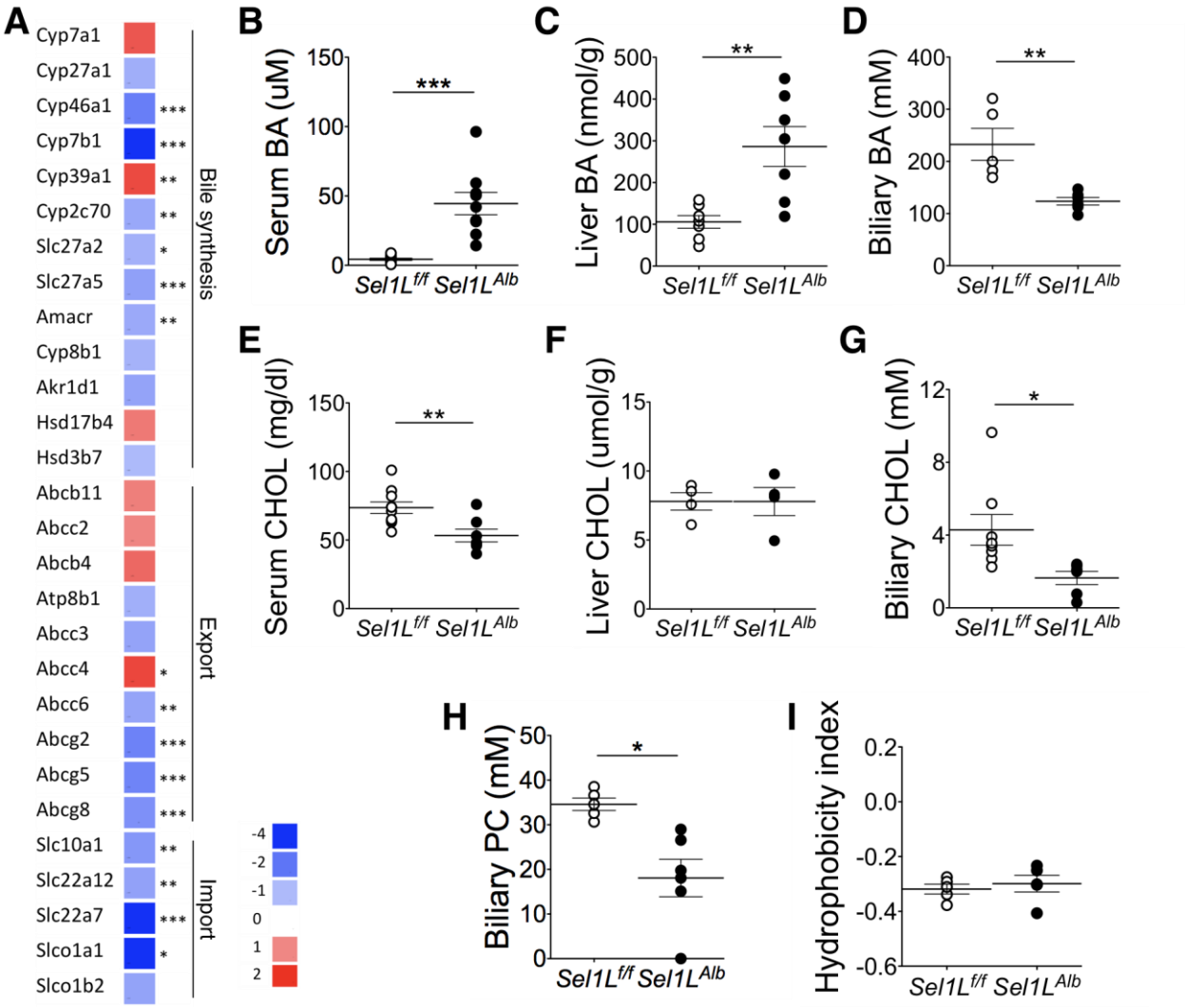

Figure 1. ***Sel1L*^{Alb} mice exhibit intrahepatic cholestasis and impaired biliary cholesterol secretion**.

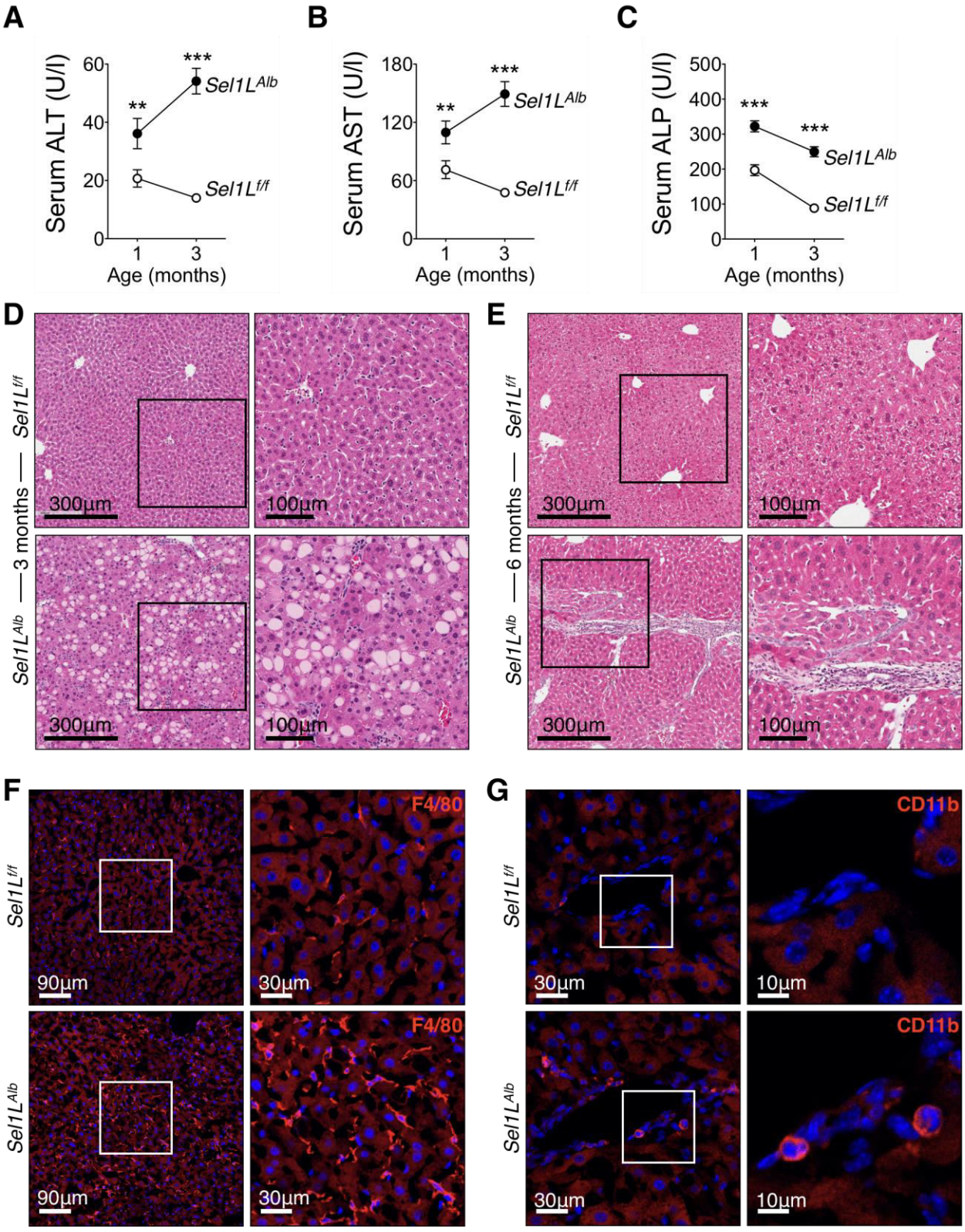

Figure 2. ***Sel1L^{Alb}*** **mice develop progressive liver damage and inflammation with age**.

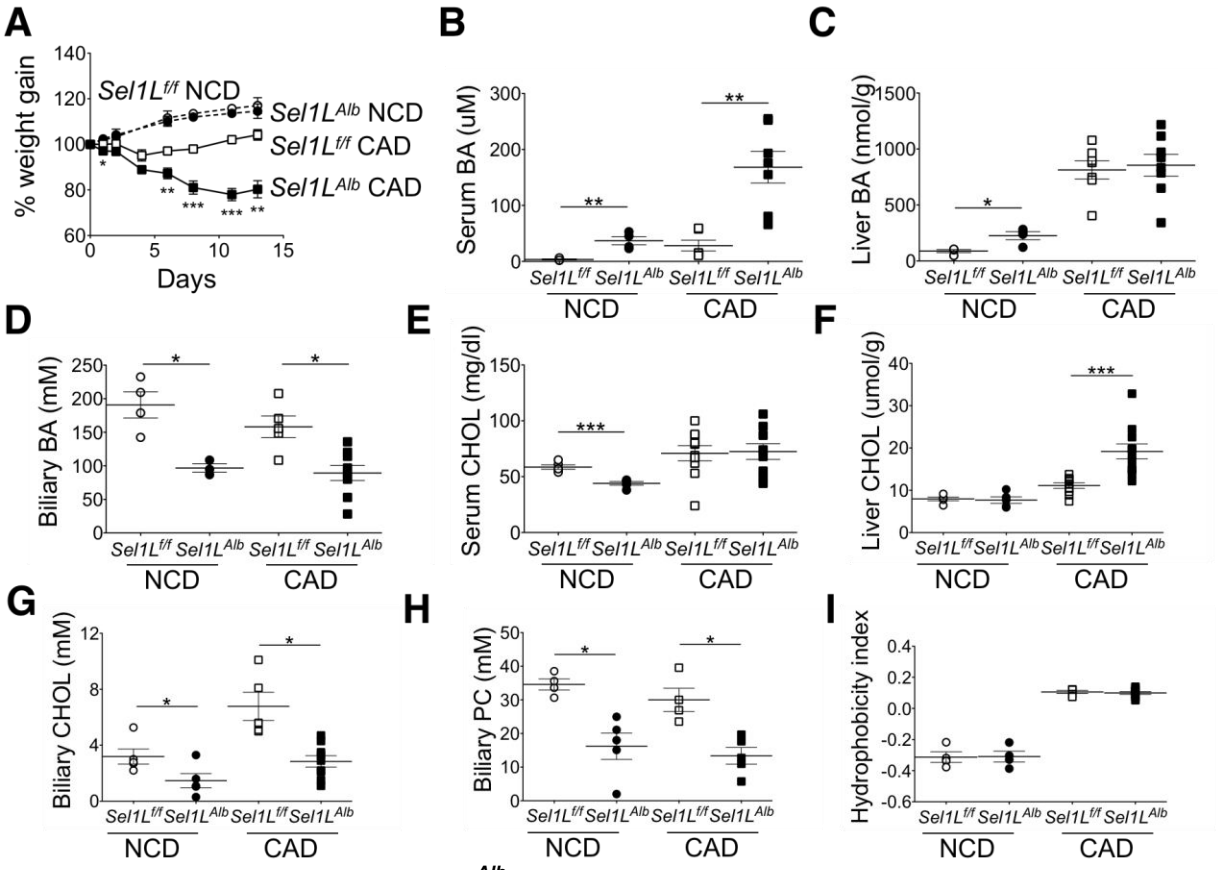

Figure 3. **Bile metabolism in *Sel1L^{Alb}* mice is hypersensitive to dietary bile acid challenge**.

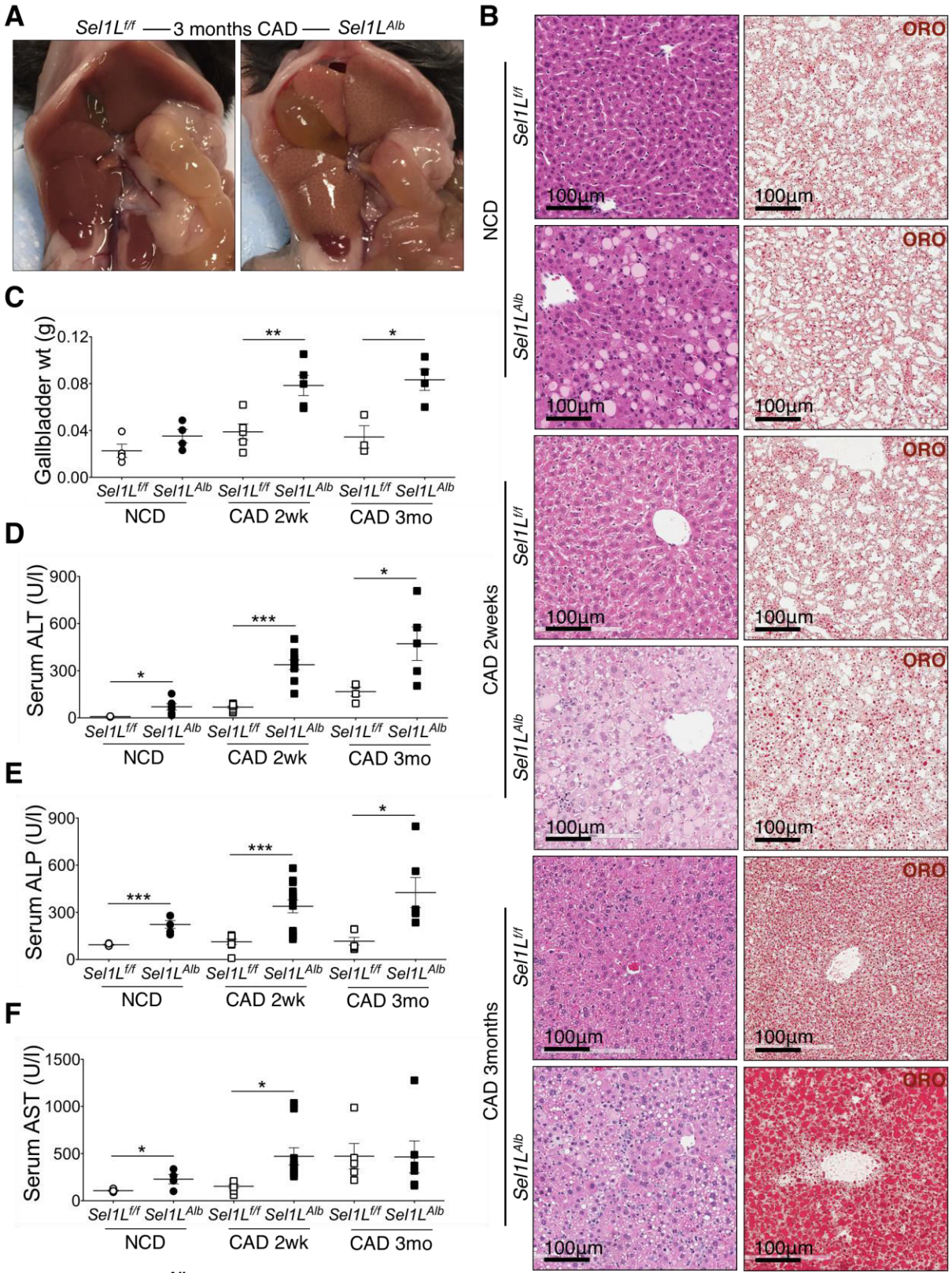

Figure 4. ***Sel1L^{Alb}*** **livers accrue profound damage and steatosis in response to dietary bile acid challenge**.

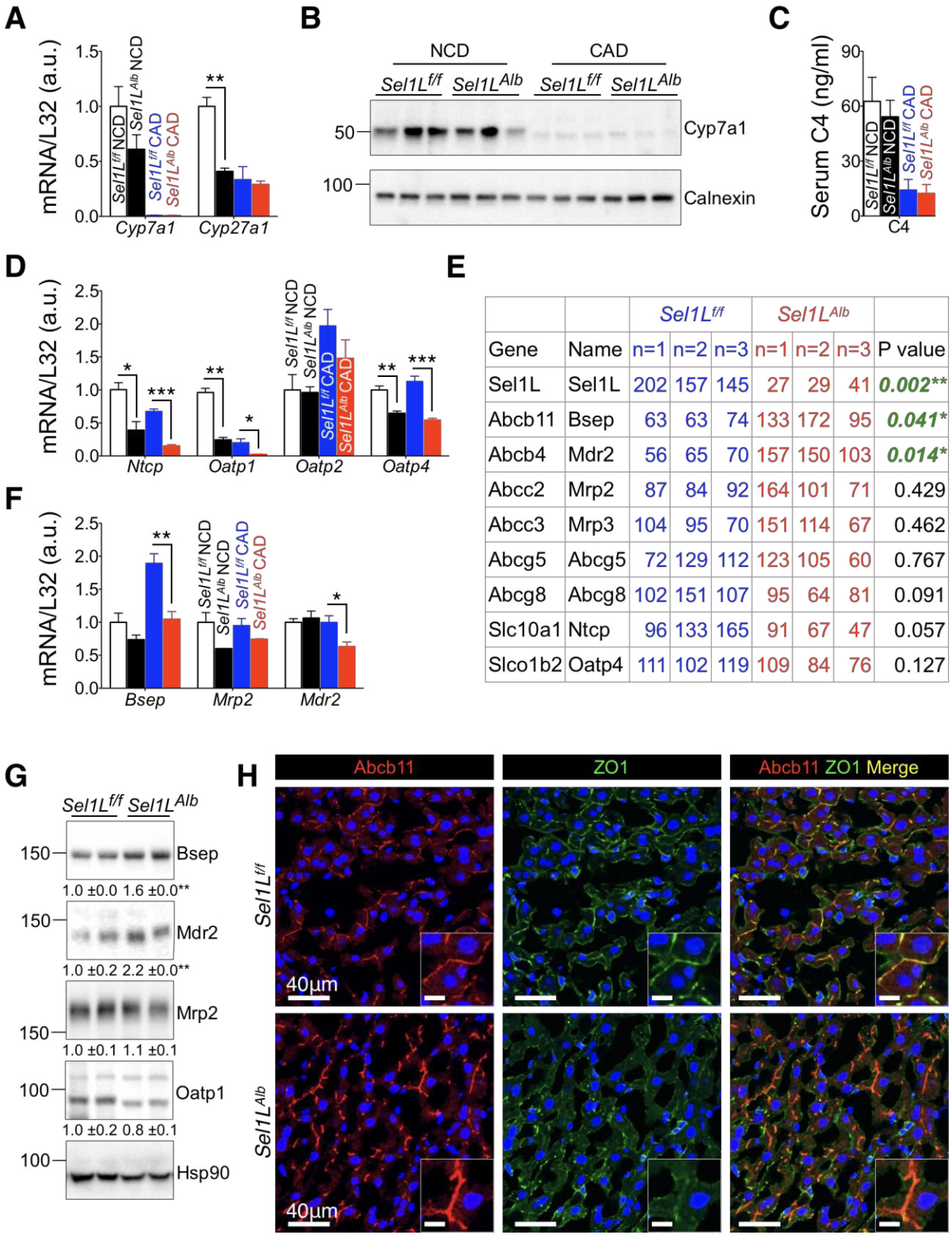

		Sel1L f/f			Sel1L Alb			
Gene	Name	n=1	n=2	n=3	n=1	n=2	n=3	P value
Sel1L	Sel1L	202	157	145	27	29	41	***0.002***
Abcb11	Bsep	63	63	74	133	172	95	***0.041***
Abcb4	Mdr2	56	65	70	157	150	103	***0.014***
Abcc2	Mrp2	87	84	92	164	101	71	0.429
Abcc3	Mrp3	104	95	70	151	114	67	0.462
Abcg5	Abcg5	72	129	112	123	105	60	0.767
Abcg8	Abcg8	102	151	107	95	64	81	0.091
Slc10a1	Ntcp	96	133	165	91	67	47	0.057
Slco1b2	Oatp4	111	102	119	109	84	76	0.127

Figure 5. ***Sel1L^{Alb}*** **livers show altered expression pattern for genes associated with bile metabolism**.

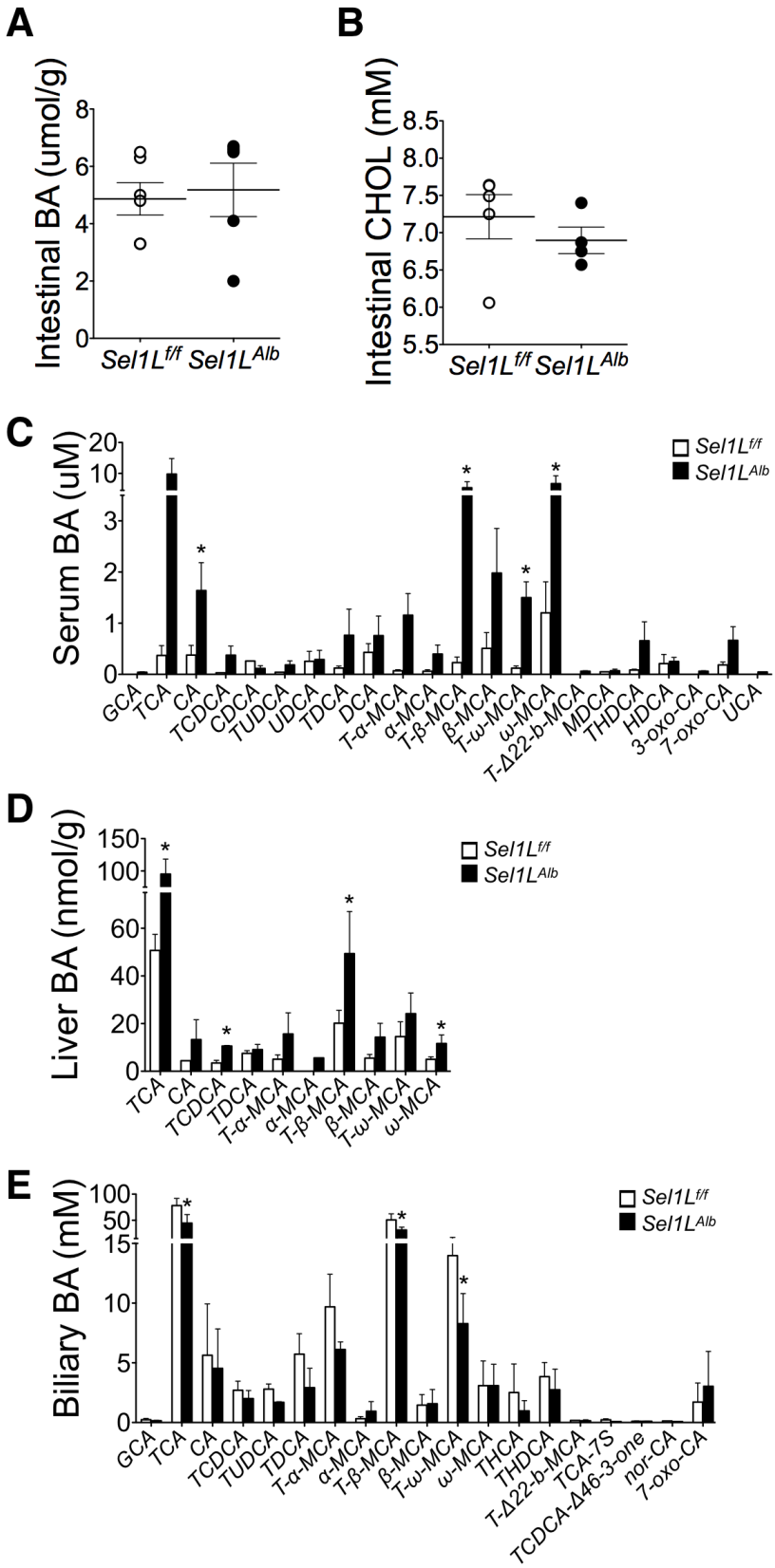

Supplementary Figure 1. **Bile acid pool constituents under normal chow diet**.

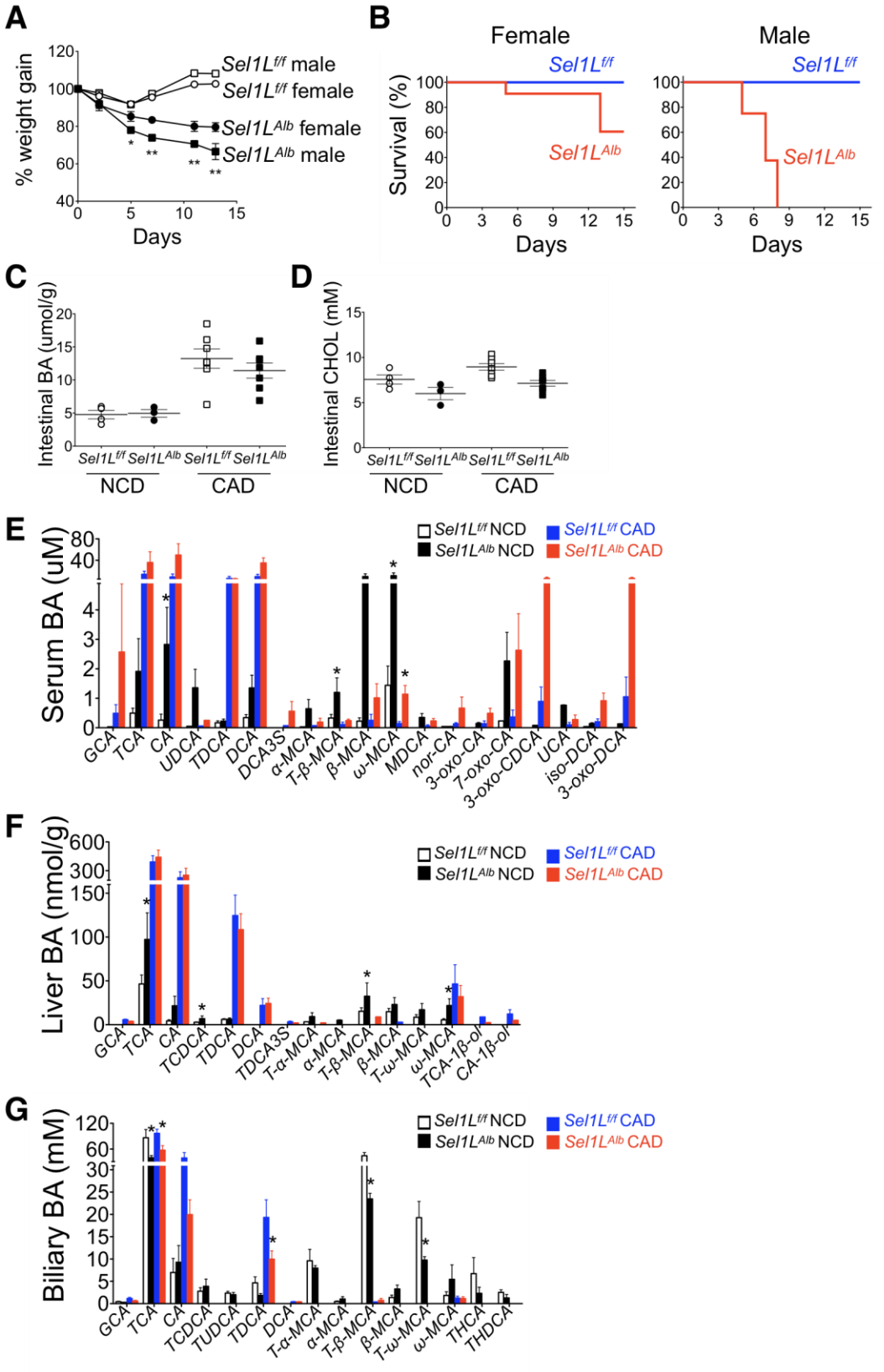

Supplementary Figure 2. Bile acid pool constituents under cholic acid supplemented diet.

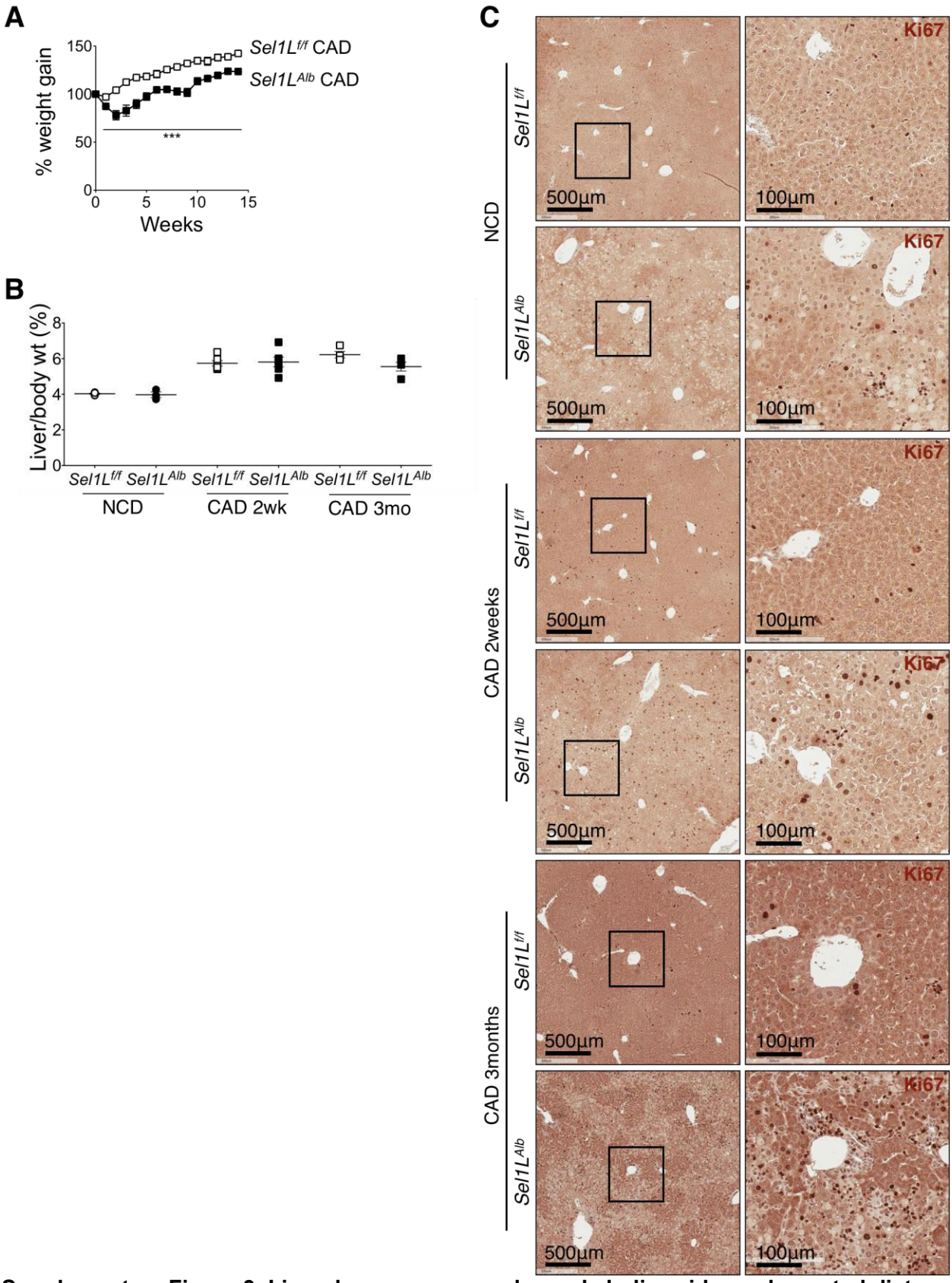

Supplementary Figure 3. **Liver damage upon prolonged cholic acid supplemented diet**.

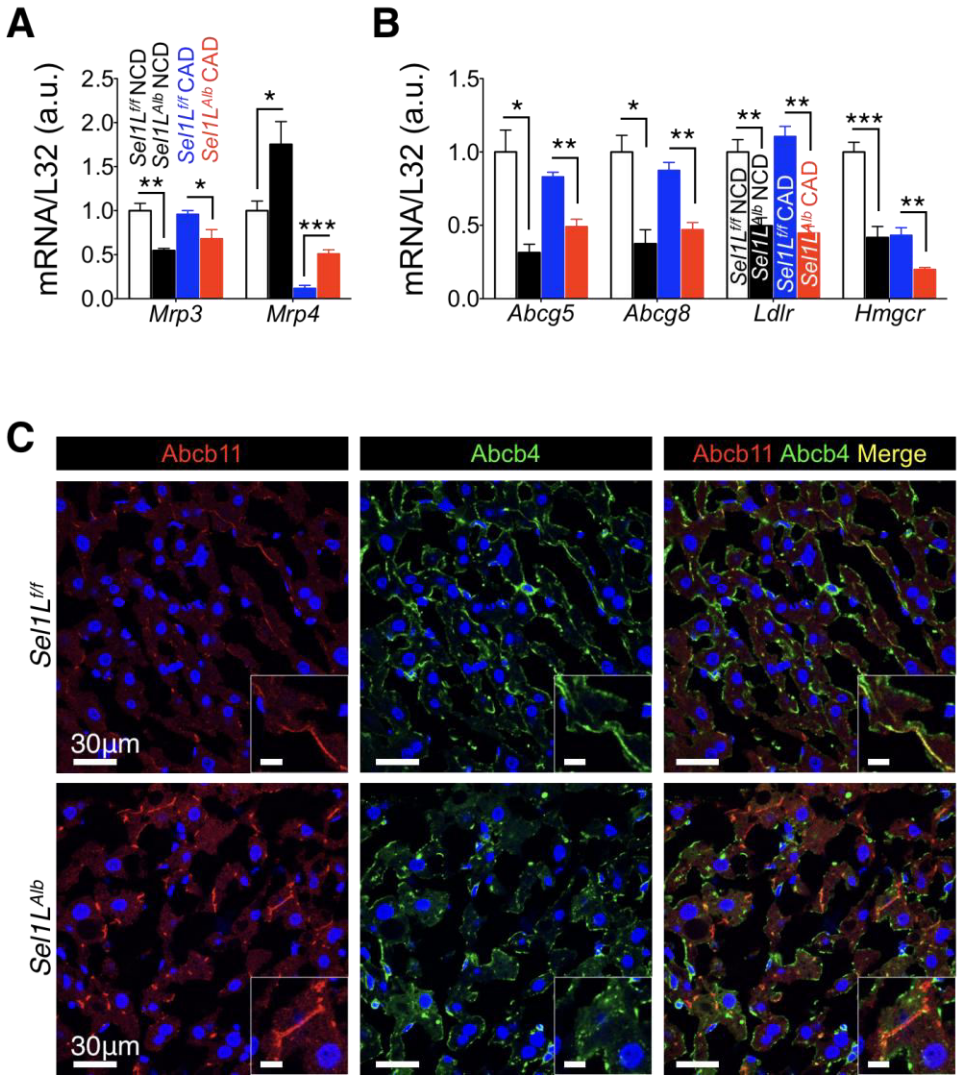

Supplementary Figure 4. *Sel1L^{Alb}* livers show increased levels of bile exporter proteins.

CHAPTER 4

Endoplasmic Reticulum Quality Control in Cancer: Friend or Foe

Hana Kim[1,3], Asmita Bhattacharya[2,3], Ling Qi[1,2] *

[1]Division of Nutritional Sciences, [2]Graduate Program in Genetics Genomics and Development, Cornell University, Ithaca, NY 14853

[3]These authors contributed equally

***CORRESPONDENCE:** lq35@cornell.edu

This chapter has been published as a review article in ***Seminars in Cancer Biology*** in 2015.

4.1 ABSTRACT

Quality control systems in the endoplasmic reticulum (ER) mediated by unfolded protein response (UPR) and endoplasmic reticulum associated degradation (ERAD) ensure cellular function and organismal survival. Recent studies have suggested that ER quality-control systems in cancer cells may serve as a double-edged sword that aids progression as well as prevention of tumor growth in a context-dependent manner. Here we review recent advances in our understanding of the complex relationship between ER proteostasis and cancer pathology, with a focus on the two most conserved ER quality-control mechanisms – the Ire1α-Xbp1 pathway of the UPR and Sel1L-Hrd1 complex of the ERAD.

4.2 INTRODUCTION

In eukaryotic cells, approximately one third of the total proteome is folded to maturity in the endoplasmic reticulum (ER) prior to transportation to various subcellular or extracellular compartments. A myriad of chaperones, folding enzymes and nascent proteins crowd the molecular environment of the ER lumen all the while maintaining a delicate homeostasis in its protein folding machinery. Various perturbations to this equilibrium, including both physiological and pathological stimuli, can lead to an accumulation of misfolded proteins inside the ER, subjecting the cell to a condition called “ER stress” and activating a series of adaptive mechanisms to alleviate the stress and restore ER homeostasis. These mechanisms consist of two major ER quality control machineries, including unfolded protein response (UPR) and ER-associated degradation (ERAD) (1-3).

Originally discovered as a response to nutrient depletion, autophagy is a cellular process involved in the lysosomal degradation of cellular components and in the maintenance of energy homeostasis through recycling of amino acids and nutrients (4). Several studies suggest that autophagy is activated as an adaptive mechanism in cells experiencing ER stress and may play a role in the maintenance of ER homeostasis in cancer (5, 6). However, as the role of autophagy goes beyond the ER (7), whether the effect of autophagy in cancer is related to its function in the ER remains to be established. Hence, as the role of autophagy in cancer has recently been extensively reviewed (8-10), it will not be the focus here.

Owing to a high proliferation rate, cancer cells often experience impaired ATP generation, hypoxia, hypoglycemia and specific mutations which may perturb ER homeostasis and trigger

the activation of UPR (2). Persistent ER stress often activates pathways that lead to cell death, effectively eliminating cells with a potential to go rogue. On the other hand, tumor cells may hijack the ER quality control machineries to provide survival signals required for neoplasm growth and eventually avoid cell death (11). Researchers have considered targeting various components of UPR and ERAD as potent therapeutic means to specifically modulate the survival of cancer cells (12). In this review, we will discuss the involvement of two most highly conserved branches of the ER quality control systems – the Ire1α signaling pathway of the UPR and the Sel1L-Hrd1 complex of the ERAD – in cancer pathogenesis.

4.3 THE IRE1α SIGNALING PATHWAY

Ire1 is a type-1 ER-resident membrane protein with bifunctional cytosolic kinase and endoribonuclease (RNase) domains (13, 14). In mammals, Ire1 exists in two isoforms, Ire1α (15) and Ire1β (16). Ire1α is ubiquitously expressed and global knockout of the gene results in early embryonic lethality (17, 18). In contrast, Ire1β expression is limited to the gastrointestinal epithelial cells (19) and has no RNase activity towards the classical Ire1α substrate X-box binding protein 1 (*Xbp1*) mRNA (20). While Ire1β knockout mice are viable, they are hypersensitive to experimental colitis (19), which may be in part due to reduced mucin biosynthesis (20).

Upon ER stress, Ire1α undergoes dimerization and/or oligomerization and trans-autophosphorylation, which triggers conformational change and activation of its RNase domain. Activated Ire1α splices 26 nucleotides from *Xbp1* mRNA, leading to translational frameshift and the generation of an active transcription factor Xbp1s. Subsequently, Xbp1s enters the nucleus, where it transactivates various target genes, including those involved in protein folding, ERAD, protein trafficking, and lipid biosynthesis (Figure 1) (21). Additionally, Ire1α has been shown to degrade a subset of mRNAs via a process called Regulated Ire1-Dependent Decay (RIDD) (Figure 1) (22-25). Moreover, Ire1α cleaves some premature microRNAs as a means of regulating apoptosis (26) as well as its own mRNA level (27, 28). The physiological significance of these extra-*Xbp1* activities of Ire1α in vivo remains poorly characterized.

Similar to Ire1α-deficient mice, global deletion of Xbp1 leads to embryonically lethal in mice (17, 18, 29). Using cell type-specific knockout mouse models, studies have demonstrated a critical role of Ire1α-Xbp1 pathway in secretory cells, most notably B cell-derived plasma cells and

pancreatic β cells. Mice with B cell-specific *Xbp1* deficiency show a profound defect in plasma cell production, along with decreased levels of antigen-specific immunoglobulin (30-32). Intriguingly, Ire1α deficiency in B cells affects not only plasma cell differentiation, but also early stage of B cell development (17). While VDJ rearrangement occurs normally in $Xbp1^{-/-}$ B cells (30), this event is severely defective in the pro-B cell stage of $Ire1\alpha^{-/-}$ B cells (17). The authors propose that the cytoplasmic domain of Ire1α may directly regulate transcriptional activation of genes involved in VDJ recombination such as *Rag1* (recombination-activating gene 1)*, Rag2* (recombination-activating gene 2)*,* and *TdT* (terminal deoxynucleotidyl transferase).

In vitro, Ire1α can be activated by glucose in a concentration-dependent manner (33) and hyperactivation of Ire1α by high glucose may lead to insulin mRNA degradation in pancreatic β cells (34). Intriguingly, β cell-specific deletion of *Xbp1* in mice results in islet atrophy and hyperglycemia associated with impaired β cell proliferation, insulin maturation and secretion at basal level (35). Moreover, deficiency of Xbp1 caused constitutive hyperactivation of Ire1α, leading to attenuation of *insulin* mRNA via RIDD. On the other hand, while Ire1α deficiency in β cells causes disruption in glucose homeostasis and impairs β cell proliferation under metabolic stress, it did not affect pancreatic structure or islet area (36). These differential phenotypes observed in β cell specific Ire1α- and Xbp1- null mice suggest that each component of this pathway may have its own unique function in cellular physiology. Alternatively, it points to a possible role of the unspliced form of Xbp1u, whose physiological role awaits further investigation. Taken together these studies highlight the indispensible role of the Ire1α-Xbp1 pathway in ER expansion and survival of highly secretory cell types.

4.4 THE ROLE OF IRE1α-XBP1S SIGNALING PATHWAY IN CANCER

Figure 2 depicts various possible molecular mechanisms underlying the role of Ire1α in cancer. The role of Ire1α in cancer is best illustrated and characterized in multiple myeloma (MM). MM is a malignant proliferation of plasma cells in the bone marrow and share phenotypical characteristics with long-lived plasma cells. Due to abundant synthesis of secretory proteins in the ER, MM cells are hypersensitive to the activation of UPR that aggravates as the disease advances (37). Thus, these cells require a large capacity of folding and disposal in the ER and are particularly sensitive to compounds targeting proteostasis. Ire1α activation can contribute to cancer progression in several pathways mediated by its substrate Xbp1s, which is highly

expressed in MM (38). Blocking of Ire1α RNase activity by Ire1 inhibitors such as STF-083010 or 4μ8C or similarly reducing Xbp1 expression by proteasome inhibitor or toyocamycin, an Xbp1 inhibitor, attenuates the growth of MM cells, via apoptosis (39-42). Conversely, forced expression of Xbp1s in B cells promotes multiple characteristics of myeloma pathogenesis with lytic bone lesions, plasmacytosis and increased monoclonal antibodies (43). More than 1,000 genes are upregulated in Xbp1s-transgenic myeloma cells compared to non-transgenic B cells, including CyclinD1, CyclinD2, Maf and Mafb, many of which are known to be involved in human MM pathogenesis. In clinical studies, human MM patients with high ratio of *Xbp1s* mRNA to *Xbp1u* mRNA have a significantly lower survival rate (38). Collectively, these studies suggest a potential causative role of Xbp1s in diseases pathogenesis in some MM patients and implicate Ire1α-Xbp1 axis as a potential therapeutic target in MM.

In addition to MM, the Ire1α-Xbp1 signaling pathway has been implicated in colon and breast cancers. As substantial evidence is lacking in most cases, we will discuss these studies in brief. Xbp1 has been implicated in colon carcinogenesis in a 2007 clinical study, where higher levels of total *Xbp1* mRNA and protein assessed via RT-PCR and immunohistochemistry, respectively, were found in colorectal polyps, colon carcinomas and colon cancer cell lines as compared to normal and stromal tissue (44). It should be pointed out that this study was limited by a small dataset of only 11 patients. In mice, loss of *Xbp1* in the intestinal epithelium leads to an increase in intestinal stem cell numbers in an Ire1α-dependent manner and Stat3-dependent hyper-proliferation of intestinal epithelial cells (45). Consequently, these *Xbp1* null mice are more susceptible to colitis-associated cancer as well as genetic-induced colorectal cancer associated with the mutation of adenomatous polyposis coli (Apc-min).

In addition to its role in ER maintenance, the Ire1α-Xbp1 signaling pathway may aid in the regulation of hypoxia in highly aggressive triple-negative breast cancer (TNBC) (46). In breast cancer cell lines and xenograft models, loss of *Xbp1* reduces tumor growth and metastasis due to impaired angiogenesis, independently of cell proliferation or apoptosis. ChIP-seq analysis coupled with co-IP experiments reveals that Xbp1s and Hif1α may function within the same transcriptional complex to regulate the expression of genes involved in survival and angiogenesis such as *Vegfa* (Vascular endothelial growth factor A), *Pdk1* (Phosphoinositide-dependent kinase 1), *Glut1* (Glucose transporter 1), *Ddit4* (DNA-damage-inducible transcript 4) via the recruitment of RNA polymerase II (46). In line with this notion, inhibition of Ire1α in gliomas reduces the expression of pro-angiogenic genes such as *Vegf-A, IL-6, IL-8 and IL-1β*,

while having an opposite effect on anti-angiogenic factors and matrix proteins such as *thrombospondin-1, decorin and osteonectin* (also known as *secreted protein acidic and rich in cysteine* or *Sparc*) (47, 48). Indeed, in tumors expressing a dominant negative Ire1α, where Ire1α transmembrane and luminal domains (aa 1–555) is fused upstream to full length Nck-1 (non-catalytic region of tyrosine kinase adaptor protein 1), there is a marked decrease in angiogenesis, tumor vascular density and growth (47, 49). Taken together, these studies point to a critical role of Ire1α in mediating hypoxia and angiogenesis in tumor growth and identify the Ire1α-Xbp1s signaling pathway as a candidate for therapeutic intervention in targeting the angiogenic switch in tumor development.

Ire1α may be involved in cancer pathogenesis via *Xbp1*-independent pathways as well (Figure 2). Various RIDD targets have recently been implicated in pathways promoting tumor growth and metastasis. Among them lies Sparc, a matrix-associated protein that retards cell-cycle progression, triggers changes in cell shape and induces synthesis of extracellular matrix, thereby promoting tumor cell invasiveness. (22, 50). Ire1α, via its RNase activity, leads to a downregulation of *Sparc* mRNA levels as shown in a rat glioma model. Expression of the same aforementioned dominant negative Ire1α transgene leads to an increase in tumor cell attachment and migration along with upregulation of Sparc and activation of its mediator RhoA, a cytoskeleton regulator protein (49, 51).

Glypican-3 (Gpc3) is an RIDD substrate as its mRNA is cleaved at the 3' UTR by Ire1α in an ER stress-independent manner (52). Gpc3 is a glycosylphosphatidylinositol (GPI)-anchored membrane protein that has been associated in diseases such as Wilms tumors and Simpson-Golabi-Behmel syndrome, and is highly overexpressed in hepatoblastoma and hepatocellular carcinoma (HCC) (53). Gpc3 stimulates canonical Wnt signaling by forming complexes with Wnts, thereby promoting aggressiveness, tumor growth and poor prognosis (54). In the $Gpc3^{high}$ HCC subgroups, the oncogenic microRNA, miR-1291, is particularly up-regulated (52). Intriguingly, miR-1291 downregulates Ire1α via destabilization of its mRNA by targeting a site in its 5' UTR region (52). This regulatory circuit whereby the oncomiR-1291 downregulates Ire1α leading to high levels of Gpc3 may promote tumor growth and invasiveness via stimulation of canonical Wnt signaling in liver cancer cells.

Finally, Ire1α has also been implicated in the pathogenesis of several cancers via mechanisms yet unknown. Studies conducted using glioblastoma, serous ovarian cancer and lung

adenocarcinoma models have demonstrated that mutations often accrue in Ire1α genomic loci (55). We recently analyzed the activities of some cancer-associated Ire1α mutants (P830L, S769F, L474R, and R635W) and found that a highly conserved proline residue at position 830 (Pro830) is crucial for maintaining Ire1α structural integrity (56). This residue seems to act as a structural linker with adjacent tyrosine (Tyr945) and tryptophan (Trp833) residues to link the kinase and RNase domains of Ire1α. The P830L mutation destabilizes Ire1α and renders both kinase and RNase domains of Ire1α inactive. Similarly, the Ser769Phe mutation abolishes Ire1α activation and signaling, although the mechanism remains unclear (56). It is possible that cancer cells may accrue these loss-of-function Ire1α mutations to attenuate the pro-apoptotic function of Ire1α as recently proposed (57). However, as whether or not Ire1α signaling exerts pro- and/or anti-apoptotic effects remains controversial (57, 58), further investigations are required to delineate physiological significance of Ire1α mutations in tumorigenesis.

4.5 ERAD

ERAD is responsible for the recognition, retrotranslocation and ubiquitination of misfolded proteins in the ER for proteasomal degradation in the cytosol (59). The ERAD system revolves around transmembrane ubiquitin E3 ligase proteins that connect together the substrate recognition machinery in the ER lumen and the ubiquitin-proteasome system in the cytosol. Failure to remove misfolded ER proteins may result in their accumulation and aggregation, which may account for the pathogenesis of various diseases such as cystic fibrosis, α1-antitrypsin deficiency and type-1 diabetes (60, 61)

There are two principle E3 ERAD complexes in yeast (Hrd1p and Doa10p), and at least half a dozen in metazoans, each of which recognizes a subset of misfolded proteins in the ER (59). Hrd1p forms a complex with Hrd3p in yeast (62, 63) and with Suppressor/Enhancer of Lin-12-like (Sel1L) in mammals (64, 65). As shown in Figure 1, Sel1L nucleates the Hrd1 ERAD complex by interacting with multiple ERAD components such as Hrd1, Derlin1/2, p97, Os9, and E2 enzyme Ubc6e (64-66). A recent proteomic analysis has implicated both Sel1L-dependent and -independent Hrd1-mediated degradation, which may be dictated by substrate topology or accessibility of specific E3 ligases (66).

Physiological importance of Sel1L and Hrd1 in vivo is recently emerging. Global deletion of *Sel1L* causes embryonic lethality in mice (67, 68). In the absence of *Sel1L*, the development of

embryonic pancreatic epithelial cell was blocked (69). Using inducible and adipocyte-specific *Sel1L* -deficient mouse and cell models, we recently demonstrated that *Sel1L* plays a critical role in the stabilization of Hrd1 protein in mammals (68, 70) and that the Sel1L –Hrd1 complex plays a critical role in mammalian ERAD, ER homeostasis and survival in vivo (68). Acute loss of *Sel1L* in adult mice causes premature lethality and severe pathologies of secretory tissues with striking abnormalities of the ER structure integrity, suggesting a crucial role of *Sel1L* in secretory cell types in particular. On the other hand, loss of *Sel1L* in adipocytes leads to resistance to diet-induced obesity and postprandial hypertriglyceridemia due to the ER retention of lipoprotein lipase (70). In addition, variants in the *Sel1L* gene have also been identified in humans with Alzheimer's diseases (71) and Sel1L mutations have been linked to early-onset cerebellar ataxia in canines (72), pointing to a possible role of Sel1L in maintaining homeostasis in neuronal/glial cells.

Global deletion of Hrd1, also known as Synoviolin (encoded by the gene *Syvn1*), also causes embryonic lethality in mice (73). Loss of Hrd1 in the liver upregulates the expression of *Nrf2* (Nuclear factor (erythroid-derived 2)-like 2) protein and its target genes *Nqo1* (NAD(P)H quinone oxidoreductase 1) and *Gclm* (glutamate-cysteine ligase, modifier subunit). This study demonstrated that Nrf2 is a substrate for Hrd1-mediated proteasomal degradation in the pathogenesis of liver cirrhosis. In this context, ER and oxidative stress response signaling pathways converge as ubiquitination of Nrf2 by Hrd1 results in downregulation of the Nrf2-mediated antioxidant response pathway (74). In dendritic cells (DC), Hrd1 seems to regulate the expression of MHC (major histocompatibility complex) class II via regulating the protein turnover of a key transcriptional repressor Blimp1 (B lymphocyte induced maturation protein 1) (75). Loss of *Hrd1* causes the accumulation of Blimp1, which represses gene transcription of MHC class II. Dendritic cell (DC)-specific *Hrd1* knockout mice exhibit splenomegaly with increased B cell numbers and defects in Cd4+ T cell priming in the autoimmune inflammatory response (75). How Hrd1 mediates the degradation of nuclear transcription factor and whether this function of Hrd1 is Sel1L dependent remain to be demonstrated.

4.6 THE ROLE OF SEL1L-HRD1 ERAD IN CANCER

While the role of ERAD in cancer remains largely unknown, Sel1L has been implicated in cancer pathogenesis. Ectopic Sel1L induction in pancreatic cancer cells leads to G1 phase cell cycle arrest via the induction of Pten – a phosphoinositide-3-phosphatase and well-known tumor

suppressor that normally inhibits cell proliferation, growth and motility. High levels of Sel1L in these cells also leads to reduction in invasiveness possibly via negative modulation of genes encoding matrix metalloproteinase inhibitors (76). Furthermore, a 2012 study discovered that the Sel1L SNP (rs12435998) shares a close association with the age at diagnosis of pancreatic ductal adenocarcinoma and the patient survival time with or without pancreaticoduodenectomy by analysis of DNA obtained from Caucasian (non-smoker) patients (77).

In the context of colorectal cancer, while basal Sel1L expression level in normal mucosa of the epithelial lining is low, it is elevated in adenoma and adenocarcinoma cells (78). Nonetheless, Sel1L expression pattern has so far been found to lack correlation with patient survival and the grade of colon cancer. In an investigation involving glioma stem cell lines and valproic acid (VPA), a histone deacetylase inhibitor, the same group reported that Sel1L downregulation in glioma stem cell lines leads to an impairment of neurosphere size and proliferative rate, while inducing differentiation towards a neuronal fate via Notch1 signaling (79). VPA, a promising therapeutic agent owing to its anti-cancer and minimally toxic properties, was found to upregulate the expression of Sel1L and other UPR genes in glioma stem cells. siRNA-mediated Sel1L knockdown in these cells negatively affects their self-renewal potential and exacerbates the cytotoxic effects of VPA. These data suggest that Sel1L may protect against VPA-mediated cytotoxicity via the maintenance of cancer stem cell properties (80). In addition, correlations between low Sel1L protein levels (detected by monoclonal antibody staining) and poor prognosis have been reported in breast carcinoma patients (81). In the context of esophageal cancers, while absent in normal cells, Sel1L is expressed in early neoplastic events and persists in later stages of esophageal cancer (82).

It should be noted that, as most of these studies implicating Sel1L in cancer pathogenesis are based on association studies, interpretation of their findings should proceed with caution. Many outstanding questions remain, for example, what is the mechanism by which Sel1L is involved in tumorigenesis? How do changes in Sel1L level in tumor cells affect ER homeostasis or specific ERAD substrates? How ER homeostasis affects tumorigenesis? Nonetheless, these studies are important because they have opened avenues for more definitive future investigations using animal models.

Another well-studied ERAD component is the lectin protein osteosarcoma amplified-9 (Os9) involved in the recognition and recruitment of misfolded glycoprotein or nonglycoproteins to the

ERAD complex (83, 84). Under hypoxic conditions, OS-9-mediated ubiquitination and subsequent degradation of Hif-1α, aided by an E3 ligase and tumor suppressor von Hippel–Lindau (Vhl), is instrumental in downregulating genes that promote cell survival, proliferation, invasion, angiogenesis and metastasis (85, 86). A recently identified gene Cim (Cancer Invasion or Metastasis-related) also known as Erlec1 (Endoplasmic Reticulum Lectin-1) has been found to sequester Os9 away from the Hif-1α complex in lung cancer cells, causing Hif-1α stabilization and accumulation thereby aiding tumor growth and metastasis (87). This study proposes Os9 to be an important link between hypoxia regulation and cancer progression. Intriguingly, we have recently shown that in the absence of Sel1L, Os9 accumulates and is stabilized (68, 70), suggesting that Os9 is a substrate of the Sel1L-Hrd1 ERAD complex. Thus, the Sel1L-Hrd1 ERAD complex, along with other ERAD components (such as Vhl) may exert its role in tumorigenesis via the regulation of either ER homeostasis in general or specific substrates such as Os9.

4.7 THERAPEUTICS

Maintaining ER proteostasis assumes high importance in cancer cells due to the increased pressure on protein folding owing to their enhanced metabolic needs, as is evident from the high basal level of expression of UPR markers in these cells. Consequently, developing interventions that aim to sensitize tumor cells to various anti-cancer agents by selectively inhibiting UPR has become a popular therapeutic strategy of late.

A recent endeavor that tested the efficacy of several Ire1α inhibitors (STF-083010, 3-Ethoxy-5,6-dibromosalicylaldehyde, 2-Hydroxy-1-naphthaldehyde, toyocamycin etc.) in a dosage and time-dependent manner on 14 pancreatic cancer cell lines observed growth retardation due to either cell cycle arrest or induced apoptosis as well as reduction in invasiveness demonstrated by soft agar assays and xenograft experiments (88). Irestatin is another Ire1α endonuclease activity inhibitor that has been seen to impair proliferation survival under starvation conditions of malignant myeloma cells (89). Interestingly, while there is considerable variability in cellular responses to these Ire1α inhibitors, synergistic effects have been observed when using various drug treatments in combination (89).

The use of oncolytic virus therapy (OVT) – viral induction of tumor cell lysis and recruitment of the immune system to the infected tissue – is quickly rising in popularity owing to its selectivity

in targeting malignancies based on the inherent abnormalities of cancer cells. A major drawback of this approach lies in the great variation in the response rates of these viruses on patients. In this context, a genome-wide RNAi screen recently identified various ER stress pathway components including Ire1α whose inhibition results in preconditioning of cancer cells to undergo apoptosis when challenged with rhabdoviral oncolysis. This sensitization to caspase-2-dependent cell death occurs via pro-apoptotic factors such as Mcl1 (myeloid cell leukemia 1), Raidd (RIP-Associated ICH1/CED3-Homologous Protein With Death Domain) and Pidd (p53-induced death domain) (90). This ‘‘one-two punch’’ tactic was validated using primary patient samples and can be useful in combating cancers that are otherwise individually resistant to UPR inhibition and oncolytic viruses.

Other means of sensitizing tumor cells towards proteotoxicity involve drugs that block proteasomal activity. Popular among these are the following – Bortezomib (BTZ) which leads to abrogation of NF-κB function and increases sensitivity to Tnfα-related and caspase-mediated apoptosis; Nelfinavir which blocks cellular proteasomal activity by virtue of its own protease property and elicits pro-apoptotic effects marked by amassing of polyubiquitinated proteins (91); Eeyarestatin I (EerI) which is an agent that targets p97 (ATPase functioning in the transportation of ubiquitinated proteins) as a means to blocking ERAD (92). Most of these therapeutic agents and their modes of action in combating cancer have been summarized in Table 2.

A 2003 study by Lee *et al.* (41) using MM cell line demonstrated Xbp1 to be an important therapeutic target in cancer as proteasome inhibition in MM cells suppresses Ire1α RNase activity and Xbp1s generation, resulting in an increased apoptotic cell death (41). However, despite recent advances in therapy with proteasome inhibitors (e.g. bortezomib, carfilzomib), MM remains incurable due to the resistance to most drugs (93). A recent study by Leung-Hagesteijn and colleagues demonstrated that silencing of Ire1α or Xbp1 in MM cell lines confers resistance to proteasome inhibitors (94). The loss of Xbp1 in MM results in attenuation of Ig production and a decline in ER stress and ERAD function, which reduces ER stress hypersensitivity in MM cells and accounts for the resistance to proteasomal inhibitors. Moreover, a subset of Xbp1s-negative MM cells lacks plasma cell features (94). These findings may explain the inability of proteasomeal inhibitors in treating MM patients, while underscoring the importance of targeting both the committed plasma cells and the progenitors in therapeutic treatment to overcome drug resistance.

4.8 CONCLUSIONS

When normal cells experience stress due to the accumulation of misfolded proteins inside the ER, a series of adaptive mechanisms are initiated, namely, UPR and ERAD. These pathways lead to global translational attenuation, the induction of specific signaling cascades and clearance of misfolded proteins in the ER aimed at restoring ER homeostasis in the cell. However, in the context of cancer cells, insults from hypoxia, nutrient deprivation, genetic mutations, and enhanced metabolic needs, can often lead to a gross accumulation of faulty proteins in the ER. Therefore, the survival of tumor cells may become especially dependent, relative to normal cells, on the adaptation to stressful conditions via UPR and ERAD. This can potentially serve as the Achilles heel of cancer cells and allow us to view UPR and ERAD components as lucrative therapeutic targets for cancer treatment. On the other hand, it is the same UPR activation that is wielded by the tumor cells in order to mount resistance to various anti-cancer drugs, thus becoming a double edged sword in tumor cell survival. Linking ER homeostasis to cancer progression may shed further light on the cell-intrinsic processes in tumor cells and allow us to potentially target them specifically over surrounding normal cells. However, most of the studies implicating various UPR and ERAD components in cancer pathogenesis are limited by their model system of study (cell culture based experiments) and small sample sizes (sampling of patient tissue). Hence our understanding of the mechanisms by which the ER quality control systems contribute to the function and survival of cancer cells still warrants further thoughtful investigations.

4.9 PERSPECTIVES

Although ER stress is thought to occur in many physiological and pathological conditions, what is lacking in most studies to date is the direct and accurate measurement of stress levels in the ER. Since cancer cells probably have an elevated protein turnover rate and are likely to accost this enhanced metabolic need by adaption via UPR and ERAD, it is quite possible that the basal levels of various components of ER chaperones are higher in tumor cells. Therefore, the induction or inhibition of these so-called “UPR markers” such as Grp78 and Chop may not serve as a reliable indicator of ER stress. Thus, although many studies have suggested various possible roles of ER stress and Ire1α signaling pathways in tumor progression, we still lack a deep and accurate understanding of exactly what the status of ER stress and the contribution of UPR pathways in cancer pathogenesis are. Hence we would like to emphasize the urgent need

to directly quantitate ER stress at the level of UPR sensors such as Ire1α and Perk activation. Using the phos-tag-based approach, one can directly measure and quantitate the extent of Ire1α phosphorylation (Fig. 3), which we have shown to correlate with the stress level in the ER. As this method is very sensitive and can detect mild ER stress under physiological and pathological conditions (56, 68, 70, 95-97), it promises to provide insights into several outstanding questions, including when and to what extent UPR and Ire1α are activated during tumorigenesis, how small molecules affect Ire1α signaling and ER homeostasis in tumors, and how perturbation of ER homeostasis affects the survival and death of cancer cells in humans.

4.10 ACKNOWLEDGEMENTS

The work in the Qi laboratory has been supported by NIH NIDDK R01DK082582, NIGMS R01GM113188, NIAAA R21AA020351, American Diabetes Association (ADA) 1-12-CD-04 and 7-08-JF-47, Juvenile Diabetes Research Foundation 47-2012-767 and 1-SRA-2014-251-Q-R, American Federation of Aging Research (RAG08061), Cornell University, HHMI International Student Research Fellowship and AHA Pre-doctoral Fellowship.

4.11 FIGURE LEGENDS

Figure 1. Schematic diagrams depicting the roles of Ire1α in UPR and Sel1L-Hrd1 in ERAD. Upon sensing ER stress, Ire1α undergoes dimerization or oligomerization, and trans-autophosphorylation, activating its cytosolic endonuclease activity. Subsequently, Ire1α alternatively splices *Xbp1* mRNA to generate Xbp1s which translocates into the nucleus and regulates different genes. Furthermore, activated Ire1α can selectively degrade particular mRNAs by a process called regulated Ire1-dependent decay (RIDD). Unlike Ire1α-Xbp1 pathway, physiological significance of other Ire1α pathways are not well established. (B) Misfolded proteins in the ER lumen are recognized, ubiquitinated and retrotranslocated by the Hrd1-Sel1L ERAD complex to the cytosol for proteasomal degradation. Bip and Os9 may be involved in the recognition of misfolded substrates.

Figure 2. The role of Ire1α-mediated signaling pathways in cancer pathogenesis. Ire1α can exert Xbp1s–dependent and –independent functions in cancer cells. In Xbp1s-dependent pathways, Ire1α activation can trigger plasma cell maturation and multiple myeloma cell survival; protection from colon cancer via maintenance of intestinal homeostasis; induction of transcription of angiogenic factors and other tumor promoting components in complex formation with Hif1α, as discovered in gliomas and breast cancer. Via RIDD, Ire1α downregulates Sparc mRNA thereby preventing RhoA-mediated increase in glioma invasiveness. In liver cancer, the oncogenic miR-1291 downregulates Ire1α, thereby allowing its otherwise RIDD substrate Glypican-3-to promote tumor growth and aggressiveness via canonical Wnt signaling.

Figure 3. Methods for quantitation of Ire1α activation and stress levels in the ER. (A and C) Immunoblots of Ire1α and Perk in HEK293T cells transfected with the indicated plasmids for 24 h. NHK, the unfolded form of a1-antitrypsin; p97-QQ, dominant negative form of p97-WT. ER-dsRed and Gfp, negative control plasmids. Hsp90, a position and loading control. (B and D) Quantitation of percent of phosphorylated Ire1α in total Ire1α protein in Phos-tag gels shown in A, C. Values are mean ± SEM *, P < 0.05 using unpaired two-tailed Student's t-test. This data is taken from (97).

4.12 REFERENCES

1. Ron D, Walter P. Signal integration in the endoplasmic reticulum unfolded protein response. Nature reviews Molecular cell biology. 2007;8(7):519-29. doi: 10.1038/nrm2199. PubMed PMID: 17565364.
2. Tsai YC, Weissman AM. The Unfolded Protein Response, Degradation from Endoplasmic Reticulum and Cancer. Genes & cancer. 2010;1(7):764-78. doi: 10.1177/1947601910383011. PubMed PMID: 21331300; PMCID: 3039444.
3. Hetz C, Chevet E, Harding HP. Targeting the unfolded protein response in disease. Nature reviews Drug discovery. 2013;12(9):703-19. doi: 10.1038/nrd3976. PubMed PMID: 23989796.
4. Ryter SW, Mizumura K, Choi AM. The impact of autophagy on cell death modalities. International journal of cell biology. 2014;2014:502676. doi: 10.1155/2014/502676. PubMed PMID: 24639873; PMCID: 3932252.
5. Ogata M, Hino S, Saito A, Morikawa K, Kondo S, Kanemoto S, Murakami T, Taniguchi M, Tanii I, Yoshinaga K, Shiosaka S, Hammarback JA, Urano F, Imaizumi K. Autophagy is activated for cell survival after endoplasmic reticulum stress. Molecular and cellular biology. 2006;26(24):9220-31. doi: 10.1128/MCB.01453-06. PubMed PMID: 17030611; PMCID: 1698520.
6. Kroemer G, Marino G, Levine B. Autophagy and the integrated stress response. Molecular cell. 2010;40(2):280-93. doi: 10.1016/j.molcel.2010.09.023. PubMed PMID: 20965422; PMCID: 3127250.
7. Levine B, Kroemer G. Autophagy in the pathogenesis of disease. Cell. 2008;132(1):27-42. Epub 2008/01/15. doi: 10.1016/j.cell.2007.12.018. PubMed PMID: 18191218; PMCID: 2696814.
8. Perez-Mancera PA, Young AR, Narita M. Inside and out: the activities of senescence in cancer. Nature reviews Cancer. 2014;14(8):547-58. doi: 10.1038/nrc3773. PubMed PMID: 25030953.
9. Nagelkerke A, Sweep FC, Geurts-Moespot A, Bussink J, Span PN. Therapeutic targeting of autophagy in cancer. Part I: Molecular pathways controlling autophagy. Seminars in cancer biology. 2014. doi: 10.1016/j.semcancer.2014.05.004. PubMed PMID: 24879905.
10. Gewirtz DA. The four faces of autophagy: implications for cancer therapy. Cancer research. 2014;74(3):647-51. doi: 10.1158/0008-5472.CAN-13-2966. PubMed PMID: 24459182.
11. Croft A, Tay KH, Boyd SC, Guo ST, Jiang CC, Lai F, Tseng HY, Jin L, Rizos H, Hersey P, Zhang XD. Oncogenic activation of MEK/ERK primes melanoma cells for adaptation to endoplasmic reticulum stress. The Journal of investigative dermatology. 2014;134(2):488-97. doi: 10.1038/jid.2013.325. PubMed PMID: 23921951.
12. Clarke HJ, Chambers JE, Liniker E, Marciniak SJ. Endoplasmic reticulum stress in malignancy. Cancer cell. 2014;25(5):563-73. doi: 10.1016/j.ccr.2014.03.015. PubMed PMID: 24823636.

13. Cox JS, Shamu CE, Walter P. Transcriptional induction of genes encoding endoplasmic reticulum resident proteins requires a transmembrane protein kinase. Cell. 1993;73(6):1197-206. PubMed PMID: 8513503.
14. Mori K, Ma W, Gething MJ, Sambrook J. A transmembrane protein with a cdc2+/CDC28-related kinase activity is required for signaling from the ER to the nucleus. Cell. 1993;74(4):743-56. PubMed PMID: 8358794.
15. Tirasophon W, Welihinda AA, Kaufman RJ. A stress response pathway from the endoplasmic reticulum to the nucleus requires a novel bifunctional protein kinase/endoribonuclease (Ire1p) in mammalian cells. Genes & development. 1998;12(12):1812-24. PubMed PMID: 9637683; PMCID: 316900.
16. Wang XZ, Harding HP, Zhang Y, Jolicoeur EM, Kuroda M, Ron D. Cloning of mammalian Ire1 reveals diversity in the ER stress responses. The EMBO journal. 1998;17(19):5708-17. doi: 10.1093/emboj/17.19.5708. PubMed PMID: 9755171; PMCID: 1170899.
17. Zhang K, Wong HN, Song B, Miller CN, Scheuner D, Kaufman RJ. The unfolded protein response sensor Ire1alpha is required at 2 distinct steps in B cell lymphopoiesis. J Clin Invest. 2005;115(2):268-81. doi: 10.1172/JCI21848. PubMed PMID: 15690081; PMCID: 546421.
18. Iwawaki T, Akai R, Yamanaka S, Kohno K. Function of Ire1 alpha in the placenta is essential for placental development and embryonic viability. Proc Natl Acad Sci U S A. 2009;106(39):16657-62. doi: 10.1073/pnas.0903775106. PubMed PMID: 19805353; PMCID: 2757843.
19. Bertolotti A, Wang X, Novoa I, Jungreis R, Schlessinger K, Cho JH, West AB, Ron D. Increased sensitivity to dextran sodium sulfate colitis in Ire1beta-deficient mice. J Clin Invest. 2001;107(5):585-93. doi: 10.1172/JCI11476. PubMed PMID: 11238559; PMCID: 199427.
20. Tsuru A, Fujimoto N, Takahashi S, Saito M, Nakamura D, Iwano M, Iwawaki T, Kadokura H, Ron D, Kohno K. Negative feedback by Ire1beta optimizes mucin production in goblet cells. Proc Natl Acad Sci U S A. 2013;110(8):2864-9. doi: 10.1073/pnas.1212484110. PubMed PMID: 23386727; PMCID: 3581977.
21. Sha H, He Y, Yang L, Qi L. Stressed out about obesity: Ire1alpha-Xbp1 in metabolic disorders. Trends in endocrinology and metabolism: TEM. 2011;22(9):374-81. doi: 10.1016/j.tem.2011.05.002. PubMed PMID: 21703863; PMCID: 3163776.
22. Hollien J, Lin JH, Li H, Stevens N, Walter P, Weissman JS. Regulated Ire1-dependent decay of messenger RNAs in mammalian cells. The Journal of cell biology. 2009;186(3):323-31. Epub 2009/08/05. doi: jcb.200903014 [pii]
10.1083/jcb.200903014. PubMed PMID: 19651891.
23. So JS, Hur KY, Tarrio M, Ruda V, Frank-Kamenetsky M, Fitzgerald K, Koteliansky V, Lichtman AH, Iwawaki T, Glimcher LH, Lee AH. Silencing of lipid metabolism genes through Ire1alpha-mediated mRNA decay lowers plasma lipids in mice. Cell metabolism. 2012;16(4):487-99. doi: 10.1016/j.cmet.2012.09.004. PubMed PMID: 23040070; PMCID: 3475419.
24. Sakaki K, Yoshina S, Shen X, Han J, DeSantis MR, Xiong M, Mitani S, Kaufman RJ. RNA surveillance is required for endoplasmic reticulum homeostasis. Proc Natl Acad Sci U S A. 2012;109(21):8079-84. doi: 10.1073/pnas.1110589109. PubMed PMID: 22562797; PMCID: 3361423.
25. Hollien J, Weissman JS. Decay of endoplasmic reticulum-localized mRNAs during the unfolded protein response. Science (New York, NY). 2006;313(5783):104-7. doi: 10.1126/science.1129631. PubMed PMID: 16825573.
26. Upton JP, Wang L, Han D, Wang ES, Huskey NE, Lim L, Truitt M, McManus MT, Ruggero D, Goga A, Papa FR, Oakes SA. Ire1alpha cleaves select microRNAs during ER stress to derepress translation of proapoptotic Caspase-2. Science (New York, NY).

2012;338(6108):818-22. Epub 2012/10/09. doi: 10.1126/science.1226191. PubMed PMID: 23042294.
27. Dai BH, Geng L, Wang Y, Sui CJ, Xie F, Shen RX, Shen WF, Yang JM. microRNA-199a-5p protects hepatocytes from bile acid-induced sustained endoplasmic reticulum stress. Cell death & disease. 2013;4:e604. doi: 10.1038/cddis.2013.134. PubMed PMID: 23598416; PMCID: 3668635.
28. Maurel M, Chevet E. Endoplasmic reticulum stress signaling: the microRNA connection. American journal of physiology Cell physiology. 2013;304(12):C1117-26. doi: 10.1152/ajpcell.00061.2013. PubMed PMID: 23515532.
29. Reimold AM, Etkin A, Clauss I, Perkins A, Friend DS, Zhang J, Horton HF, Scott A, Orkin SH, Byrne MC, Grusby MJ, Glimcher LH. An essential role in liver development for transcription factor XBP-1. Genes & development. 2000;14(2):152-7. PubMed PMID: 10652269; PMCID: 316338.
30. Reimold AM, Iwakoshi NN, Manis J, Vallabhajosyula P, Szomolanyi-Tsuda E, Gravallese EM, Friend D, Grusby MJ, Alt F, Glimcher LH. Plasma cell differentiation requires the transcription factor XBP-1. Nature. 2001;412(6844):300-7. doi: 10.1038/35085509. PubMed PMID: 11460154.
31. Shaffer AL, Shapiro-Shelef M, Iwakoshi NN, Lee AH, Qian SB, Zhao H, Yu X, Yang L, Tan BK, Rosenwald A, Hurt EM, Petroulakis E, Sonenberg N, Yewdell JW, Calame K, Glimcher LH, Staudt LM. Xbp1, downstream of Blimp-1, expands the secretory apparatus and other organelles, and increases protein synthesis in plasma cell differentiation. Immunity. 2004;21(1):81-93. doi: 10.1016/j.immuni.2004.06.010. PubMed PMID: 15345222.
32. Todd DJ, McHeyzer-Williams LJ, Kowal C, Lee AH, Volpe BT, Diamond B, McHeyzer-Williams MG, Glimcher LH. Xbp1 governs late events in plasma cell differentiation and is not required for antigen-specific memory B cell development. The Journal of experimental medicine. 2009;206(10):2151-9. doi: 10.1084/jem.20090738. PubMed PMID: 19752183; PMCID: 2757870.
33. Lipson KL, Fonseca SG, Ishigaki S, Nguyen LX, Foss E, Bortell R, Rossini AA, Urano F. Regulation of insulin biosynthesis in pancreatic beta cells by an endoplasmic reticulum-resident protein kinase Ire1. Cell metabolism. 2006;4(3):245-54. doi: 10.1016/j.cmet.2006.07.007. PubMed PMID: 16950141.
34. Lipson KL, Ghosh R, Urano F. The role of Ire1alpha in the degradation of insulin mRNA in pancreatic beta-cells. PLoS One. 2008;3(2):e1648. doi: 10.1371/journal.pone.0001648. PubMed PMID: 18286202; PMCID: 2241665.
35. Lee AH, Heidtman K, Hotamisligil GS, Glimcher LH. Dual and opposing roles of the unfolded protein response regulated by Ire1alpha and Xbp1 in proinsulin processing and insulin secretion. Proc Natl Acad Sci U S A. 2011;108(21):8885-90. doi: 10.1073/pnas.1105564108. PubMed PMID: 21555585; PMCID: 3102350.
36. Xu T, Yang L, Yan C, Wang X, Huang P, Zhao F, Zhao L, Zhang M, Jia W, Wang X, Liu Y. The Ire1alpha-Xbp1 pathway regulates metabolic stress-induced compensatory proliferation of pancreatic beta-cells. Cell research. 2014;24(9):1137-40. doi: 10.1038/cr.2014.55. PubMed PMID: 24797433; PMCID: 4152740.
37. Nakamura M, Gotoh T, Okuno Y, Tatetsu H, Sonoki T, Uneda S, Mori M, Mitsuya H, Hata H. Activation of the endoplasmic reticulum stress pathway is associated with survival of myeloma cells. Leukemia & lymphoma. 2006;47(3):531-9. doi: 10.1080/10428190500312196. PubMed PMID: 16396777.
38. Bagratuni T, Wu P, Gonzalez de Castro D, Davenport EL, Dickens NJ, Walker BA, Boyd K, Johnson DC, Gregory W, Morgan GJ, Davies FE. Xbp1s levels are implicated in the biology and outcome of myeloma mediating different clinical outcomes to thalidomide-based treatments. Blood. 2010;116(2):250-3. doi: 10.1182/blood-2010-01-263236. PubMed PMID: 20421453.

39. Papandreou I, Denko NC, Olson M, Van Melckebeke H, Lust S, Tam A, Solow-Cordero DE, Bouley DM, Offner F, Niwa M, Koong AC. Identification of an Ire1alpha endonuclease specific inhibitor with cytotoxic activity against human multiple myeloma. Blood. 2011;117(4):1311-4. doi: 10.1182/blood-2010-08-303099. PubMed PMID: 21081713; PMCID: 3056474.
40. Cross BC, Bond PJ, Sadowski PG, Jha BK, Zak J, Goodman JM, Silverman RH, Neubert TA, Baxendale IR, Ron D, Harding HP. The molecular basis for selective inhibition of unconventional mRNA splicing by an Ire1-binding small molecule. Proc Natl Acad Sci U S A. 2012;109(15):E869-78. doi: 10.1073/pnas.1115623109. PubMed PMID: 22315414; PMCID: 3326519.
41. Lee AH, Iwakoshi NN, Anderson KC, Glimcher LH. Proteasome inhibitors disrupt the unfolded protein response in myeloma cells. Proc Natl Acad Sci U S A. 2003;100(17):9946-51. doi: 10.1073/pnas.1334037100. PubMed PMID: 12902539; PMCID: 187896.
42. Ri M, Tashiro E, Oikawa D, Shinjo S, Tokuda M, Yokouchi Y, Narita T, Masaki A, Ito A, Ding J, Kusumoto S, Ishida T, Komatsu H, Shiotsu Y, Ueda R, Iwawaki T, Imoto M, Iida S. Identification of Toyocamycin, an agent cytotoxic for multiple myeloma cells, as a potent inhibitor of ER stress-induced Xbp1 mRNA splicing. Blood cancer journal. 2012;2(7):e79. doi: 10.1038/bcj.2012.26. PubMed PMID: 22852048; PMCID: 3408640.
43. Carrasco DR, Sukhdeo K, Protopopova M, Sinha R, Enos M, Carrasco DE, Zheng M, Mani M, Henderson J, Pinkus GS, Munshi N, Horner J, Ivanova EV, Protopopov A, Anderson KC, Tonon G, DePinho RA. The differentiation and stress response factor XBP-1 drives multiple myeloma pathogenesis. Cancer cell. 2007;11(4):349-60. doi: 10.1016/j.ccr.2007.02.015. PubMed PMID: 17418411; PMCID: 1885943.
44. Fujimoto T, Yoshimatsu K, Watanabe K, Yokomizo H, Otani T, Matsumoto A, Osawa G, Onda M, Ogawa K. Overexpression of human X-box binding protein 1 (XBP-1) in colorectal adenomas and adenocarcinomas. Anticancer research. 2007;27(1A):127-31. PubMed PMID: 17352224.
45. Niederreiter L, Fritz TM, Adolph TE, Krismer AM, Offner FA, Tschurtschenthaler M, Flak MB, Hosomi S, Tomczak MF, Kaneider NC, Sarcevic E, Kempster SL, Raine T, Esser D, Rosenstiel P, Kohno K, Iwawaki T, Tilg H, Blumberg RS, Kaser A. ER stress transcription factor Xbp1 suppresses intestinal tumorigenesis and directs intestinal stem cells. The Journal of experimental medicine. 2013;210(10):2041-56. doi: 10.1084/jem.20122341. PubMed PMID: 24043762; PMCID: PMC3782039.
46. Chen X, Iliopoulos D, Zhang Q, Tang Q, Greenblatt MB, Hatziapostolou M, Lim E, Tam WL, Ni M, Chen Y, Mai J, Shen H, Hu DZ, Adoro S, Hu B, Song M, Tan C, Landis MD, Ferrari M, Shin SJ, Brown M, Chang JC, Liu XS, Glimcher LH. Xbp1 promotes triple-negative breast cancer by controlling the Hif1alpha pathway. Nature. 2014;508(7494):103-7. doi: 10.1038/nature13119. PubMed PMID: 24670641; PMCID: 4105133.
47. Drogat B, Auguste P, Nguyen DT, Bouchecareilh M, Pineau R, Nalbantoglu J, Kaufman RJ, Chevet E, Bikfalvi A, Moenner M. Ire1 signaling is essential for ischemia-induced vascular endothelial growth factor-A expression and contributes to angiogenesis and tumor growth in vivo. Cancer research. 2007;67(14):6700-7. Epub 2007/07/20. doi: 67/14/6700 [pii] 10.1158/0008-5472.CAN-06-3235. PubMed PMID: 17638880.
48. Auf G, Jabouille A, Guerit S, Pineau R, Delugin M, Bouchecareilh M, Magnin N, Favereaux A, Maitre M, Gaiser T, von Deimling A, Czabanka M, Vajkoczy P, Chevet E, Bikfalvi A, Moenner M. Inositol-requiring enzyme 1alpha is a key regulator of angiogenesis and invasion in malignant glioma. Proc Natl Acad Sci U S A. 2010;107(35):15553-8. doi: 10.1073/pnas.0914072107. PubMed PMID: 20702765; PMCID: 2932600.
49. Nguyen DT, Kebache S, Fazel A, Wong HN, Jenna S, Emadali A, Lee EH, Bergeron JJ, Kaufman RJ, Larose L, Chevet E. Nck-dependent activation of extracellular signal-regulated kinase-1 and regulation of cell survival during endoplasmic reticulum stress. Molecular biology

of the cell. 2004;15(9):4248-60. doi: 10.1091/mbc.E03-11-0851. PubMed PMID: 15201339; PMCID: 515356.
50. Gaddam D, Stevens N, Hollien J. Comparison of mRNA localization and regulation during endoplasmic reticulum stress in Drosophila cells. Molecular biology of the cell. 2013;24(1):14-20. doi: 10.1091/mbc.E12-06-0491. PubMed PMID: 23135994; PMCID: 3530775.
51. Dejeans N, Pluquet O, Lhomond S, Grise F, Bouchecareilh M, Juin A, Meynard-Cadars M, Bidaud-Meynard A, Gentil C, Moreau V, Saltel F, Chevet E. Autocrine control of glioma cells adhesion and migration through Ire1alpha-mediated cleavage of Sparc mRNA. Journal of cell science. 2012;125(Pt 18):4278-87. doi: 10.1242/jcs.099291. PubMed PMID: 22718352.
52. Maurel M, Dejeans N, Taouji S, Chevet E, Grosset CF. MicroRNA-1291-mediated silencing of Ire1alpha enhances Glypican-3 expression. Rna. 2013;19(6):778-88. doi: 10.1261/rna.036483.112. PubMed PMID: 23598528; PMCID: 3683912.
53. Jakubovic BD, Jothy S. Glypican-3: from the mutations of Simpson-Golabi-Behmel genetic syndrome to a tumor marker for hepatocellular carcinoma. Experimental and molecular pathology. 2007;82(2):184-9. doi: 10.1016/j.yexmp.2006.10.010. PubMed PMID: 17258707.
54. Capurro MI, Xiang YY, Lobe C, Filmus J. Glypican-3 promotes the growth of hepatocellular carcinoma by stimulating canonical Wnt signaling. Cancer research. 2005;65(14):6245-54. doi: 10.1158/0008-5472.CAN-04-4244. PubMed PMID: 16024626.
55. Korennykh AV, Egea PF, Korostelev AA, Finer-Moore J, Zhang C, Shokat KM, Stroud RM, Walter P. The unfolded protein response signals through high-order assembly of Ire1. Nature. 2009;457(7230):687-93. doi: 10.1038/nature07661. PubMed PMID: 19079236; PMCID: 2846394.
56. Xue Z, He Y, Ye K, Gu Z, Mao Y, Qi L. A conserved structural determinant located at the interdomain region of mammalian inositol-requiring enzyme 1alpha. J Biol Chem. 2011;286(35):30859-66. Epub 2011/07/16. doi: 10.1074/jbc.M111.273714. PubMed PMID: 21757700; PMCID: 3162446.
57. Ghosh R, Wang L, Wang ES, Perera BG, Igbaria A, Morita S, Prado K, Thamsen M, Caswell D, Macias H, Weiberth KF, Gliedt MJ, Alavi MV, Hari SB, Mitra AK, Bhhatarai B, Schurer SC, Snapp EL, Gould DB, German MS, Backes BJ, Maly DJ, Oakes SA, Papa FR. Allosteric inhibition of the Ire1alpha RNase preserves cell viability and function during endoplasmic reticulum stress. Cell. 2014;158(3):534-48. doi: 10.1016/j.cell.2014.07.002. PubMed PMID: 25018104.
58. Lu M, Lawrence DA, Marsters S, Acosta-Alvear D, Kimmig P, Mendez AS, Paton AW, Paton JC, Walter P, Ashkenazi A. Cell death. Opposing unfolded-protein-response signals converge on death receptor 5 to control apoptosis. Science (New York, NY). 2014;345(6192):98-101. doi: 10.1126/science.1254312. PubMed PMID: 24994655.
59. Olzmann JA, Kopito RR, Christianson JC. The Mammalian Endoplasmic Reticulum-Associated Degradation System. Cold Spring Harbor perspectives in biology. 2013;5(9). Epub 2012/12/13. doi: 10.1101/cshperspect.a013185. PubMed PMID: 23232094.
60. Chiti F, Dobson CM. Protein misfolding, functional amyloid, and human disease. Annual review of biochemistry. 2006;75:333-66. doi: 10.1146/annurev.biochem.75.101304.123901. PubMed PMID: 16756495.
61. Guerriero CJ, Brodsky JL. The delicate balance between secreted protein folding and endoplasmic reticulum-associated degradation in human physiology. Physiological reviews. 2012;92(2):537-76. doi: 10.1152/physrev.00027.2011. PubMed PMID: 22535891; PMCID: 4162396.
62. Hampton RY, Gardner RG, Rine J. Role of 26S proteasome and HRD genes in the degradation of 3-hydroxy-3-methylglutaryl-CoA reductase, an integral endoplasmic reticulum membrane protein. Molecular biology of the cell. 1996;7(12):2029-44. Epub 1996/12/01. PubMed PMID: 8970163; PMCID: Pmc276048.

63. Gardner RG, Swarbrick GM, Bays NW, Cronin SR, Wilhovsky S, Seelig L, Kim C, Hampton RY. Endoplasmic reticulum degradation requires lumen to cytosol signaling. Transmembrane control of Hrd1p by Hrd3p. The Journal of cell biology. 2000;151(1):69-82. Epub 2000/10/06. PubMed PMID: 11018054; PMCID: 2189800.
64. Mueller B, Lilley BN, Ploegh HL. Sel1L, the homologue of yeast Hrd3p, is involved in protein dislocation from the mammalian ER. The Journal of cell biology. 2006;175(2):261-70. Epub 2006/10/18. doi: jcb.200605196 [pii]
10.1083/jcb.200605196. PubMed PMID: 17043138.
65. Mueller B, Klemm EJ, Spooner E, Claessen JH, Ploegh HL. Sel1L nucleates a protein complex required for dislocation of misfolded glycoproteins. Proc Natl Acad Sci U S A. 2008;105(34):12325-30. doi: 10.1073/pnas.0805371105. PubMed PMID: 18711132; PMCID: 2527910.
66. Christianson JC, Olzmann JA, Shaler TA, Sowa ME, Bennett EJ, Richter CM, Tyler RE, Greenblatt EJ, Harper JW, Kopito RR. Defining human ERAD networks through an integrative mapping strategy. Nature cell biology. 2012;14(1):93-105. Epub 2011/11/29. doi: 10.1038/ncb2383. PubMed PMID: 22119785; PMCID: 3250479.
67. Francisco AB, Singh R, Li S, Vani AK, Yang L, Munroe RJ, Diaferia G, Cardano M, Biunno I, Qi L, Schimenti JC, Long Q. Deficiency of suppressor enhancer Lin12 1 like (Sel1L) in mice leads to systemic endoplasmic reticulum stress and embryonic lethality. J Biol Chem. 2010;285(18):13694-703. doi: 10.1074/jbc.M109.085340. PubMed PMID: 20197277; PMCID: PMC2859532.
68. Sun S, Shi G, Han X, Francisco AB, Ji Y, Mendonca N, Liu X, Locasale JW, Simpson KW, Duhamel GE, Kersten S, Yates JR, 3rd, Long Q, Qi L. Sel1L is indispensable for mammalian endoplasmic reticulum-associated degradation, endoplasmic reticulum homeostasis, and survival. Proc Natl Acad Sci U S A. 2014;111(5):E582-91. doi: 10.1073/pnas.1318114111. PubMed PMID: 24453213; PMCID: 3918815.
69. Li S, Francisco AB, Munroe RJ, Schimenti JC, Long Q. Sel1L deficiency impairs growth and differentiation of pancreatic epithelial cells. BMC developmental biology. 2010;10:19. Epub 2010/02/23. doi: 10.1186/1471-213X-10-19. PubMed PMID: 20170518; PMCID: 2848149.
70. Sha H, Sun S, Francisco AB, Ehrhardt N, Xue Z, Liu L, Lawrence P, Mattijssen F, Guber RD, Panhwar MS, Brenna JT, Shi H, Xue B, Kersten S, Bensadoun A, Peterfy M, Long Q, Qi L. The ER-associated degradation adaptor protein Sel1L regulates LPL secretion and lipid metabolism. Cell metabolism. 2014;20(3):458-70. doi: 10.1016/j.cmet.2014.06.015. PubMed PMID: 25066055; PMCID: 4156539.
71. Saltini G, Dominici R, Lovati C, Cattaneo M, Michelini S, Malferrari G, Caprera A, Milanesi L, Finazzi D, Bertora P, Scarpini E, Galimberti D, Venturelli E, Musicco M, Adorni F, Mariani C, Biunno I. A novel polymorphism in Sel1L confers susceptibility to Alzheimer's disease. Neuroscience letters. 2006;398(1-2):53-8. doi: 10.1016/j.neulet.2005.12.038. PubMed PMID: 16412574.
72. Kyostila K, Cizinauskas S, Seppala EH, Suhonen E, Jeserevics J, Sukura A, Syrja P, Lohi H. A Sel1L mutation links a canine progressive early-onset cerebellar ataxia to the endoplasmic reticulum-associated protein degradation (ERAD) machinery. PLoS genetics. 2012;8(6):e1002759. doi: 10.1371/journal.pgen.1002759. PubMed PMID: 22719266; PMCID: 3375262.
73. Yagishita N, Ohneda K, Amano T, Yamasaki S, Sugiura A, Tsuchimochi K, Shin H, Kawahara K, Ohneda O, Ohta T, Tanaka S, Yamamoto M, Maruyama I, Nishioka K, Fukamizu A, Nakajima T. Essential role of synoviolin in embryogenesis. J Biol Chem. 2005;280(9):7909-16. doi: 10.1074/jbc.M410863200. PubMed PMID: 15611074.
74. Wu T, Zhao F, Gao B, Tan C, Yagishita N, Nakajima T, Wong PK, Chapman E, Fang D, Zhang DD. Hrd1 suppresses Nrf2-mediated cellular protection during liver cirrhosis. Genes &

development. 2014;28(7):708-22. doi: 10.1101/gad.238246.114. PubMed PMID: 24636985; PMCID: PMC4015486.
75. Yang H, Qiu Q, Gao B, Kong S, Lin Z, Fang D. Hrd1-mediated BLIMP-1 ubiquitination promotes dendritic cell MHCII expression for CD4 T cell priming during inflammation. The Journal of experimental medicine. 2014;211(12):2467-79. doi: 10.1084/jem.20140283. PubMed PMID: 25366967; PMCID: PMC4235642.
76. Cattaneo M, Fontanella E, Canton C, Delia D, Biunno I. Sel1L affects human pancreatic cancer cell cycle and invasiveness through modulation of Pten and genes related to cell-matrix interactions. Neoplasia. 2005;7(11):1030-8. PubMed PMID: 16331889; PMCID: 1502024.
77. Liu Q, Chen J, Mai B, Amos C, Killary AM, Sen S, Wei C, Frazier ML. A single-nucleotide polymorphism in tumor suppressor gene Sel1L as a predictive and prognostic marker for pancreatic ductal adenocarcinoma in Caucasians. Molecular carcinogenesis. 2012;51(5):433-8. doi: 10.1002/mc.20808. PubMed PMID: 21656579; PMCID: 3780592.
78. Ashktorab H, Green W, Finzi G, Sessa F, Nouraie M, Lee EL, Morgano A, Moschetta A, Cattaneo M, Mariani-Costantini R, Brim H, Biunno I. Sel1L, an UPR response protein, a potential marker of colonic cell transformation. Digestive diseases and sciences. 2012;57(4):905-12. doi: 10.1007/s10620-011-2026-y. PubMed PMID: 22350780; PMCID: 3345950.
79. Cardano M, Diaferia GR, Cattaneo M, Dessi SS, Long Q, Conti L, Deblasio P, Cattaneo E, Biunno I. mSEL-1L (Suppressor/enhancer Lin12-like) protein levels influence murine neural stem cell self-renewal and lineage commitment. The Journal of biological chemistry. 2011;286(21):18708-19. doi: 10.1074/jbc.M110.210740. PubMed PMID: 21454627; PMCID: 3099688.
80. Cattaneo M, Baronchelli S, Schiffer D, Mellai M, Caldera V, Saccani GJ, Dalpra L, Daga A, Orlandi R, DeBlasio P, Biunno I. Down-modulation of Sel1L, an unfolded protein response and endoplasmic reticulum-associated degradation protein, sensitizes glioma stem cells to the cytotoxic effect of valproic acid. J Biol Chem. 2014;289(5):2826-38. doi: 10.1074/jbc.M113.527754. PubMed PMID: 24311781; PMCID: 3908415.
81. Orlandi R, Cattaneo M, Troglio F, Casalini P, Ronchini C, Menard S, Biunno I. Sel1L expression decreases breast tumor cell aggressiveness in vivo and in vitro. Cancer research. 2002;62(2):567-74. PubMed PMID: 11809711.
82. Granelli P, Cattaneo M, Ferrero S, Bottiglieri L, Bosari S, Fichera G, Biunno I. Sel1L and squamous cell carcinoma of the esophagus. Clinical cancer research : an official journal of the American Association for Cancer Research. 2004;10(17):5857-61. doi: 10.1158/1078-0432.CCR-04-0075. PubMed PMID: 15355917.
83. Christianson JC, Shaler TA, Tyler RE, Kopito RR. OS-9 and GRP94 deliver mutant alpha1-antitrypsin to the Hrd1-Sel1L ubiquitin ligase complex for ERAD. Nature cell biology. 2008;10(3):272-82. doi: 10.1038/ncb1689. PubMed PMID: 18264092; PMCID: 2757077.
84. Hosokawa N, Kamiya Y, Kamiya D, Kato K, Nagata K. Human OS-9, a lectin required for glycoprotein endoplasmic reticulum-associated degradation, recognizes mannose-trimmed N-glycans. J Biol Chem. 2009;284(25):17061-8. doi: 10.1074/jbc.M809725200. PubMed PMID: 19346256; PMCID: 2719344.
85. Baek JH, Mahon PC, Oh J, Kelly B, Krishnamachary B, Pearson M, Chan DA, Giaccia AJ, Semenza GL. OS-9 interacts with hypoxia-inducible factor 1alpha and prolyl hydroxylases to promote oxygen-dependent degradation of Hif-1alpha. Molecular cell. 2005;17(4):503-12. doi: 10.1016/j.molcel.2005.01.011. PubMed PMID: 15721254.
86. Ivan M, Kondo K, Yang H, Kim W, Valiando J, Ohh M, Salic A, Asara JM, Lane WS, Kaelin WG, Jr. Hifalpha targeted for VHL-mediated destruction by proline hydroxylation: implications for O2 sensing. Science (New York, NY). 2001;292(5516):464-8. doi: 10.1126/science.1059817. PubMed PMID: 11292862.

87. Yanagisawa K, Konishi H, Arima C, Tomida S, Takeuchi T, Shimada Y, Yatabe Y, Mitsudomi T, Osada H, Takahashi T. Novel metastasis-related gene CIM functions in the regulation of multiple cellular stress-response pathways. Cancer research. 2010;70(23):9949-58. doi: 10.1158/0008-5472.CAN-10-1055. PubMed PMID: 21118962.
88. Chien W, Ding LW, Sun QY, Torres-Fernandez LA, Tan SZ, Xiao J, Lim SL, Garg M, Lee KL, Kitajima S, Takao S, Leong WZ, Sun H, Tokatly I, Poellinger L, Gery S, Koeffler PH. Selective inhibition of unfolded protein response induces apoptosis in pancreatic cancer cells. Oncotarget. 2014;5(13):4881-94. PubMed PMID: 24952679; PMCID: 4148107.
89. Li X, Zhang K, Li Z. Unfolded protein response in cancer: the physician's perspective. Journal of hematology & oncology. 2011;4:8. doi: 10.1186/1756-8722-4-8. PubMed PMID: 21345215; PMCID: 3060154.
90. Mahoney DJ, Lefebvre C, Allan K, Brun J, Sanaei CA, Baird S, Pearce N, Gronberg S, Wilson B, Prakesh M, Aman A, Isaac M, Mamai A, Uehling D, Al-Awar R, Falls T, Alain T, Stojdl DF. Virus-tumor interactome screen reveals ER stress response can reprogram resistant cancers for oncolytic virus-triggered caspase-2 cell death. Cancer cell. 2011;20(4):443-56. doi: 10.1016/j.ccr.2011.09.005. PubMed PMID: 22014571.
91. Schonthal AH. Endoplasmic reticulum stress: its role in disease and novel prospects for therapy. Scientifica. 2012;2012:857516. doi: 10.6064/2012/857516. PubMed PMID: 24278747; PMCID: 3820435.
92. Wang Q, Shinkre BA, Lee JG, Weniger MA, Liu Y, Chen W, Wiestner A, Trenkle WC, Ye Y. The ERAD inhibitor Eeyarestatin I is a bifunctional compound with a membrane-binding domain and a p97/VCP inhibitory group. PLoS One. 2010;5(11):e15479. doi: 10.1371/journal.pone.0015479. PubMed PMID: 21124757; PMCID: 2993181.
93. Alexanian R, Delasalle K, Wang M, Thomas S, Weber D. Curability of multiple myeloma. Bone marrow research. 2012;2012:916479. doi: 10.1155/2012/916479. PubMed PMID: 22675638; PMCID: 3366198.
94. Leung-Hagesteijn C, Erdmann N, Cheung G, Keats JJ, Stewart AK, Reece DE, Chung KC, Tiedemann RE. Xbp1s-negative tumor B cells and pre-plasmablasts mediate therapeutic proteasome inhibitor resistance in multiple myeloma. Cancer cell. 2013;24(3):289-304. doi: 10.1016/j.ccr.2013.08.009. PubMed PMID: 24029229; PMCID: 4118579.
95. He Y, Beatty A, Han X, Ji Y, Ma X, Adelstein RS, Yates JR, 3rd, Kemphues K, Qi L. Nonmuscle myosin IIB links cytoskeleton to Ire1alpha signaling during ER stress. Developmental cell. 2012;23(6):1141-52. doi: 10.1016/j.devcel.2012.11.006. PubMed PMID: 23237951; PMCID: 3547290.
96. Sha H, He Y, Chen H, Wang C, Zenno A, Shi H, Yang X, Zhang X, Qi L. The Ire1alpha-Xbp1 pathway of the unfolded protein response is required for adipogenesis. Cell metabolism. 2009;9(6):556-64. doi: 10.1016/j.cmet.2009.04.009. PubMed PMID: 19490910; PMCID: 2963107.
97. Yang L, Xue Z, He Y, Sun S, Chen H, Qi L. A Phos-tag-based approach reveals the extent of physiological endoplasmic reticulum stress. PloS one. 2010;5(7):e11621. doi: 10.1371/journal.pone.0011621. PubMed PMID: 20661282; PMCID: 2905412.

4.13 FIGURES

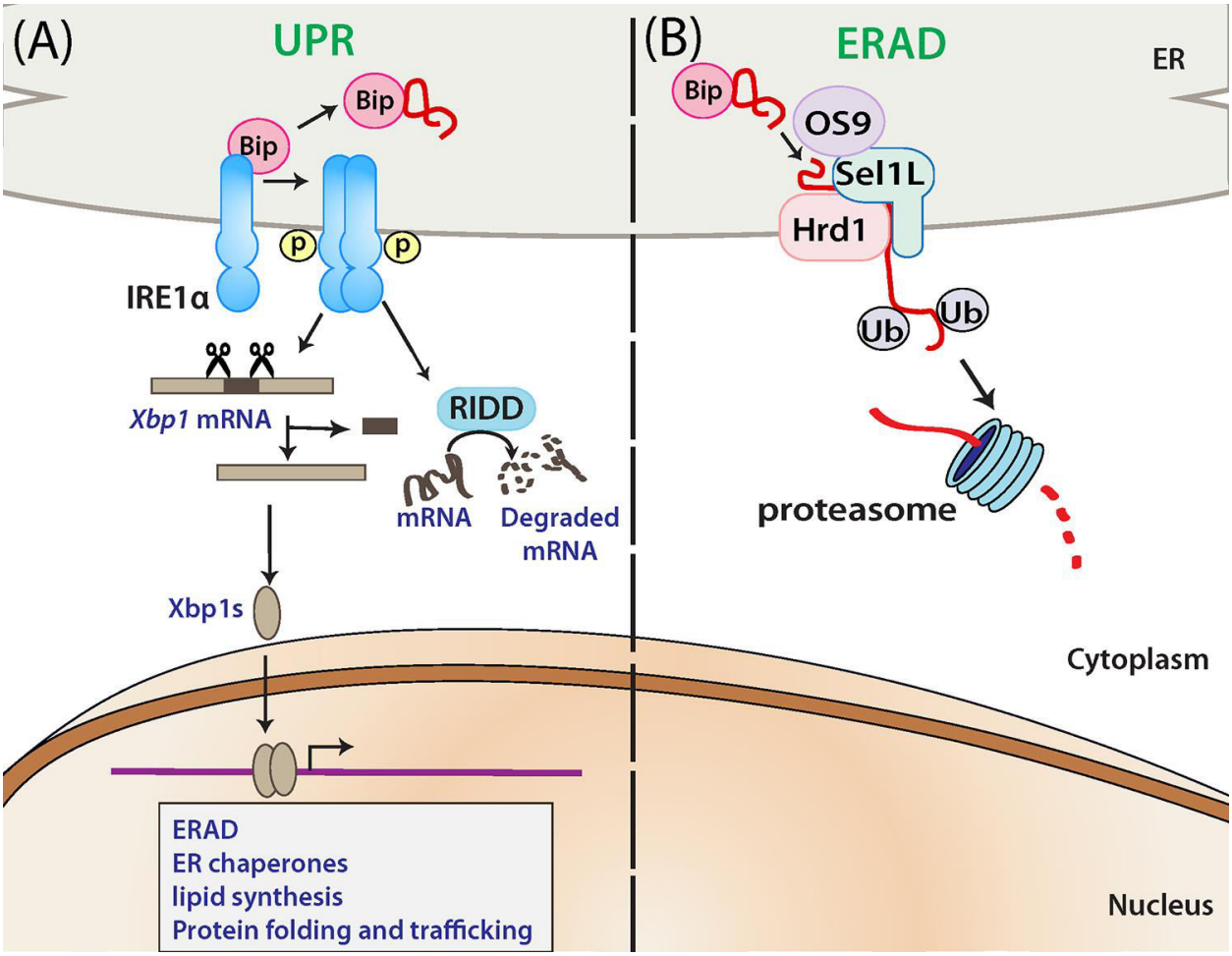

Figure 1. Schematic diagrams depicting the roles of Ire1α in UPR and Sel1L-Hrd1 in ERAD.

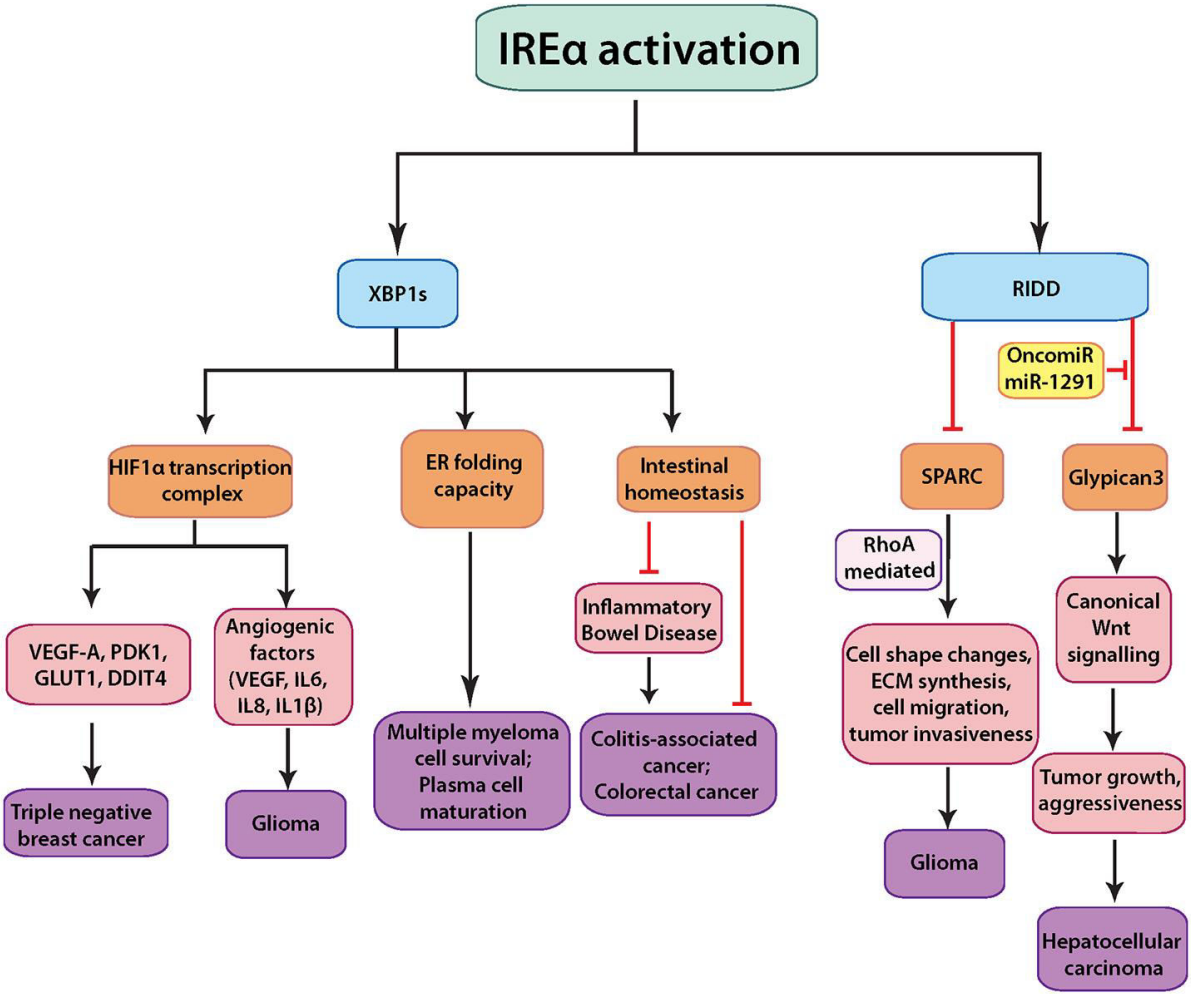

Figure 2. The role of Ire1α-mediated signaling pathways in cancer pathogenesis.

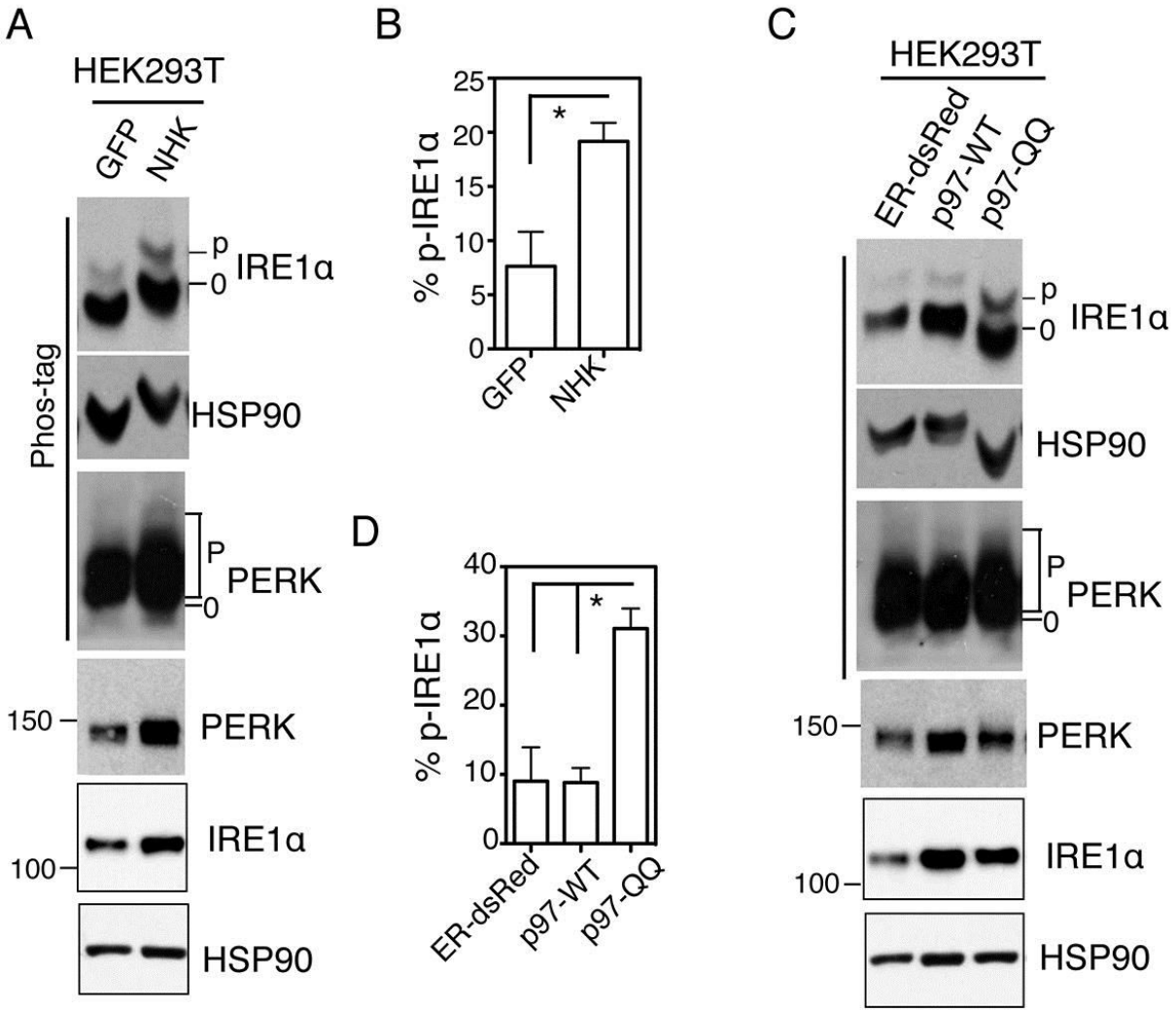

Figure 3. Methods for quantitation of Ire1α activation and stress levels in the ER.

4.14 TABLES

Table 1. The role of Ire1α in various types of cancer.

Type of cancer	System	Mechanism	Reference
Multiple myeloma	B cell specific *Xbp1s* transgenic mice and patient samples	Aiding in secretory maturation of plasma cells and resistance to anti-cancer drugs	(38, 43, 93, 94)
Triple negative breast cancer	Breast cancer lines and mice with mammary glands injected with tumor cells	High Xbp1s levels aid in sustaining hypoxia (co-localizing with hypoxia markers), promoting angiogenesis and invasion in collaboration with Hif1α via transcriptional regulation of various genes including *Vegfa, Pdk1, Glut1, Ddit4*	(46)
Colon cancer	Eleven patient primary tumor samples	High levels of Xbp1 expression in colorectal carcinoma and adenoma	(44)
Glioma	Human U87 glioma cell line; mouse orthotopic brain model; chick chorio-allantoic membrane	Supports tumor vascularity, blood vessel cooption and invasiveness by promoting pro-angiogenic Vegfa, IL-6, IL-8, IL-1β, and by inhibiting anti-angiogenic thrombospondin1, decorin.	(48)
Several cancers	Cell lines	Ire1α mutations identified in tumor cells are defective in signaling	(56, 57)
Liver cancer	Hepatoma HuH7 cell line	Downregulates Gpc3 (mediator of tumor growth via canonical Wnt signaling) by RIDD; itself silenced in cancer cells by oncomiR miR-1291	(52)
Colon cancer	In vivo Xbp1 intestine-specific-null mouse model	Protects against colitis-associated-cancer and Apc-mediated colorectal cancer; depletion of Xbp1 predisposes intestinal epithelium to inflammatory diseases and tumorigenesis	(45)
Glioma	Human U87 glioma cell line	Suppresses attachment and migration properties by downregulating RhoA and Sparc (a matrix protein that retards cell cycle, induces cell shape change and promotes invasiveness)	(51)

Abbreviations – Apc: Adenomatous polyposis coli; Ddit4: DNA-damage-inducible transcript 4; Glut1: Glucose transporter 1; Gpc3: Glypican 3; Hif1α: Hypoxia inducible factor 1 alpha; IL-6, -8, -1β: Interleukin 6, 8, 1beta; Ire1α: Inositol requiring enzyme 1 alpha; miR: microRNA; Pdk1: Phosphoinositide-dependent kinase 1; RIDD: Regulated Ire1-dependent decay; RhoA: Ras homolog gene family member A; Sparc: Secreted protein acidic and rich in cysteine; Vegfa: Vascular endothelial growth factor A; Xbp1s: Xbox binding protein 1 spliced.

Table 2. Therapeutic interventions in cancer targeting Ire1α and ERAD.

Agent	Mechanism	Effect	Functional partners	Reference
STF-083010, 3-Ethoxy-5,6-dibromosalicylaldehyde, 2-Hydroxy-1-naphthaldehyde, toyocamycin	Ire1α inhibition	Growth retardation owing to cell cycle arrest or induced apoptosis; reduction in invasiveness	Synergistic effects seen when used in combination or with gemcitabine/bortezomib	(88)
Rhabdovirus	Oncolytic virus therapy plus Ire1α inhibition	Ire1α inhibition preconditions cancer cells specifically and sensitizes them to apoptosis following rhabdovirus infection – called “one-two punch”	shRNA or small molecule inhibitors targeting Ire1a	(90)
Bortezomib	Blocks proteasome activity	Leads to abrogation of NF-κB function, increased sensitivity to apoptosis, thereby pushing tumor cells towards proteotoxicity	Tnfα and caspase (mediating apoptosis)	(89)
Nelfinavir	Blocks proteasome activity	Exercises protease property in blocking cellular proteasome activity and inducing pro-apoptotic effects via amassing polyubiquitinated proteins	BiP/Grp78, Chop and caspase activation induced	
Eeyarestatin I	Targeting p97 ATPase	Blocks ERAD by preventing de-ubiquitination of ERAD substrates and preferentially pushing cancer cells towards cytotoxicity		
Irestatin	Ire1α RNase inhibitor	Blocks UPR by abrogating Xbp1s transcription, thereby impairing proliferation or inhibiting tumor cell survival in oxygen-starvation conditions		

Abbreviations – BiP: Binding immunoglobulin protein; Chop: C/EBP homologous protein; ERAD: Endoplasmic reticulum associated degradation; Ire1α: Inositol requiring enzyme 1 alpha; Grp78: 78 kDa glucose-regulated protein; NF-κB: Nuclear factor kappa-light-chain-enhancer of activated B cells; shRNA: short hairpin ribonucleic acid; Tnfα: Tumor necrosis factor alpha; UPR: Unfolded protein response; Xbp1s: Xbox binding protein 1 spliced.

CHAPTER 5

Sel1L-Hrd1 ERAD suppresses liver cancer via the Wnt signaling pathway

Asmita Bhattacharya[1,2], Dafydd Thomas[3], Ligong Chen[4], Ling Qi[1,5] *

[1] Department of Molecular and Integrative Physiology, University of Michigan Medical School, Ann Arbor, MI 48105, USA;
[2] Graduate Program of Genetics, Genomics and Development, Cornell University, Ithaca, NY 14853, USA;
[3] Department of Pathology, University of Michigan Medical School, Ann Arbor, MI 48105, USA;
[4] Tsinghua University, Beijing 100084, China;
[5] Division of Metabolism, Endocrinology & Diabetes, Department of Internal Medicine, University of Michigan Medical School, Ann Arbor, MI 48105, USA;

*** Correspondence:**
Ling Qi: lingq@med.umich.edu

This project is in preparation for submission.

5.1 ABSTRACT

Hepatocellular carcinoma is a malignant disease characterized with rapid growth and difficulty of diagnosis, resulting in poor prognosis coupled with limited availability of systemic therapies. Here, we show that hepatic endoplasmic reticulum (ER)-associated degradation (ERAD) guards against tumorigenesis and correlates positively with good prognosis in human liver cancer patients. Mice lacking a key ERAD cofactor Sel1L in hepatocytes develop spontaneous liver tumors with age, and are greatly predisposed to chemically induced liver cancer models, marked with increased Ki67 and CyclinD1 levels. Mechanistically, we find that these livers show an unrestrained proliferation program with significant alterations in the Wnt pathway. Strikingly, a proteomics screen revealed Wnt5A protein to be markedly accumulated, non-transcriptionally, in the *Sel1L*-deficient hepatic ER. Further biochemical analysis revealed that Sel1L-Hrd1 ERAD is responsible for the degradation of Wnt5A, the absence of which leads to stabilization of Wnt5A in the hepatic ER, leading to excess proliferation and propensity towards tumor development.

5.2 INTRODUCTION

Hepatocellular carcinoma (HCC) is an aggressive malignancy of the liver, ranking as the sixth most common forms of cancer worldwide (1), and the second leading cause of cancer mortality all over the world. In the United States of America, over the past thirty years, liver cancer rates have tripled, now making it the fastest-growing cause of cancer-related deaths (2). Therapeutic management of HCC includes liver transplantation, surgical resection and/or sorafenib treatment, chemotherapy and radiotherapy being mostly ineffective, although the asymptomatic early stage and delay in diagnosis usually result in poor prognosis (3). Risk factors for liver cancer include liver cirrhosis, hepatitis B or C virus infection, fatty liver disease, obesity, smoking, and genetic factors (4-8). At a molecular level, of all the signalling cascades implicated in HCC pathogenesis, the *wingless* or Wnt pathway is one of the most frequently activated, making it a popular therapeutic target and warranting further investigation into its relationship with liver cancer (9-12).

Wnt5A, a non-canonical ligand belonging to the Wnt family, has widespread functions in cancer or normal stem cell self-renewal, proliferation and metastasis, often specifically targeting oncogene expression (13-15). Wnt family ligands bind to Frizzled (Fzd) and Low-density-lipoprotein receptor-related protein (Lrp) receptors, thereby activating either canonical signalling

that involves stabilization of beta-catenin and its transcriptional activity, or non-canonical signalling that is independent of beta-catenin and largely uncharacterized, although believed to antagonize the canonical Wnt signalling pathway (13). Wnt5A operates in the enigmatic area between these two pathways, with studies reporting its activity in both canonical and non-canonical roles, in the context of maintaining the balance between proliferation and differentiation during embryonic morphogenesis and adult tissue homeostasis (14). One among the nineteen secreted, cysteine-rich Wnt family members identified to date in humans and mice, Wnt5A remains a robust, yet poorly understood molecular playmaker, especially with regards to its complex maturation process.

Endoplasmic Reticulum Associated Degradation (ERAD) functions as a major protein folding quality control system within the cell, whereby it recognizes and retro-translocates substrate proteins to the cytosol for degradation by the proteasome, as a means of post-translational quality or quantity control (16, 17). Sel1L is a key adaptor protein that, together with its partner E3 ligase Hrd1, nucleates the most highly conserved ERAD complex in mammalian cells (18-21). Global deletions of either of these two genes causes embryonic lethality (22, 23). Previous work from our laboratory and others have shown, using tissue-specific knockout mouse models, that Sel1L-Hrd1 ERAD functions to triage excess or misfolded proteins, in a substrate-specific manner, thereby directly regulating debilitating patho-physiological syndromes associated with them (17). These include, but are not limited to, diabetes insipidus due to pro-arginine-vasopressin (Avp) misfolding in proAvp-neurons (24), hyperphagia associated obesity due to defective pro-opiomelanocortin (Pomc) maturation in Pomc-neurons (25), ileitis caused by excess signaling by inositol-requiring enzyme-1a (Ire1α) in enterocytes (26), and most recently, altered growth and systemic metabolic profiles owing to exorbitant Fgf21 hormone production from accumulation and over-activation of cAMP-responsive element-binding protein, hepatocyte specific (Crebh) in the liver (27, 28).

More intriguingly, Sel1L and ERAD have extensively been linked to cancer pathogenesis in various publications, both independently and together, although no clear mechanism or mouse model has been characterized to date that can elicit the relationship among them (29-35). Here we describe using different liver cancer models (spontaneous, chemically induced) that the loss of hepatic Sel1L predisposes mice to increased proliferative response and tumorigenesis. At a molecular level, we show that Wnt5A is an ERAD substrate and that Wnt5A accumulates in the absence of Sel1L-Hrd1 mediated ERAD, leading to significant aberrations in the Wnt signaling

pathway and cellular proliferation. Last, we also show a strong co-relationship between Sel1L-Hrd1 levels and human liver cancers, further underscoring the momentous role played by this complex in liver cancer prevention and consequently their value as potential therapeutic agents.

5.3 RESULTS

Expression of *SEL1L* in human liver cancers

We first examined the relationship between SEL1L-HRD1 ERAD and liver cancer in human patients. Interestingly, higher levels of hepatic SEL1L and HRD1 proteins correlated with good prognosis for liver cancer patients, both individually and combined (Figures 1A-C). In addition to this, analysis of tumor and adjacent normal tissue excised from human liver cancer patients revealed that SEL1L levels were consistently and significantly elevated in tumor tissues, whereas HRD1 levels were mildly yet significantly decreased (Figure 1D). As Sel1L and Hrd1 are known to function both independently and together, we next checked for the association between these two proteins in liver hepatocellular carcinoma (LIHC) samples. In tumor samples, SEL1L and HRD1 showed a stronger and positive correlation (Figure 1E) than in adjacent normal tissues (Figure 1F). Overall, these findings showed a significant involvement of this ERAD complex in human liver cancer pathogenesis.

Sel1L^{Alb} livers show exaggerated proliferation during regeneration following hepatectomy

Proliferation being an integral aspect of tumorigenesis, we aimed to examine the proliferation potential in *Sel1L*$^{f/f}$ and *Sel1L*^{Alb} hepatocytes. To this end, we subjected both *Sel1L*$^{f/f}$ and *Sel1L*^{Alb} mice to two-thirds partial hepatectomy surgery, where the left lateral lobe and the median lobe were tied off and resected out. Post-surgery, both groups of mice recovered equally well (Figure 2A). Interestingly, the remaining lobes of *Sel1L*^{Alb} livers showed faster kinetics in mass restoration than those of *Sel1L*$^{f/f}$ livers (Figures 2B-C). Histological examination showed larger hepatocyte and nuclear size in *Sel1L*^{Alb} livers 48 hours post-surgery (Figure 2D). Upon staining with proliferation marker CyclinD1, we observed it to be significantly increased in *Sel1L*^{Alb} livers 48 hours post hepatectomy (Figure 2E). These results indicated that *Sel1L*^{Alb} livers have a more aggressive proliferation paradigm than their *Sel1L*$^{f/f}$ counterparts.

Sel1L^{Alb} livers exhibit immense proliferation in response to CCL4 induced damage

The hepatotoxin carbon tetrachloride (CCL4) is classically used to simulate liver damage in mice owing to its free radical generating properties caused by reaction with hepatic Cyp450

enzymes and its ability to cause hepatocellular necrosis (upon acute dosage) and fibrosis (upon chronic dosage) (36-38). To assess the proliferation generated in response to chronic yet mild liver injury, we treated 8-week-old *Sel1L*$^{f/f}$ and *Sel1L*^{Alb} mice with a very low dose (0.2ml/kg intraperitoneally) of CCL4 three times a week for 3 months (Supplementary Figure 1A). In response to this treatment, *Sel1L*^{Alb} mice gained more body weight compared to *Sel1L*$^{f/f}$ mice (Supplementary Figure 1B), and had significantly enlarged livers compared to their *Sel1L*$^{f/f}$ littermates (Supplementary Figures 1C-D), signifying hepatomegaly. Upon measurement of serum levels of liver enzymes as classical parameters for liver injury, we found that alanine aminotransferase (ALT) and aspartate aminotransferase (AST) levels were similarly elevated in both cohorts of mice (Supplementary Figures 1E-F), whereas alkaline phosphatase (ALP) levels were higher in *Sel1L*^{Alb} mice (Supplementary Figure 1G), indicating mostly similar extents of liver dysfunction in both cohorts. Upon histological examination using hematoxylin-eosin stain to assess morphology and Trichrome Masson's stain to assess fibrosis/collagen deposition, we observed no striking difference between *Sel1L*$^{f/f}$ and *Sel1L*^{Alb} livers (Supplementary Figure 1H, left and middle panels). However, upon staining with Ki67, *Sel1L*^{Alb} livers showed significantly higher frequency of proliferating hepatocytes than *Sel1L*$^{f/f}$ livers (Supplementary Figure 1H, right panel), again showcasing the excess proliferative potential of *Sel1L*$^{f/f}$ hepatocytes.

Sel1L^{Alb} mice are prone to developing chemical and diet induced liver tumors

A classical model of studying liver cancer in mice involves a combination of high fat diet (HFD) feeding following an early administration of the diethylnitrosamine (DEN). DEN acts as a potent carcinogen upon modification by hepatic Cyp450 enzymes resulting in it becoming a DNA adduct, leading to mutations and genomic instability (39-41). To explore the propensity of *Sel1L*^{Alb} mice to liver cancer, we injected *Sel1L*$^{f/f}$ and *Sel1L*^{Alb} mice with DEN (25mg/kg intraperitoneally) at 2-weeks of age, followed by HFD feeding starting at 4-weeks of age (Figure 3A). At 6-months of age, these animals were analyzed for the presence of liver tumors. *Sel1L*^{Alb} mice developed significant and marked tumor growth in their livers, whereas *Sel1L*$^{f/f}$ livers showed no to very few tumors (Figures 3B-D). Among these tumors, we found evidences for less transformed adenomas (low CyclinD1, high E-cadherin) as well as more advanced carcinomas (high CyclinD1, low E-cadherin) in *Sel1L*^{Alb} livers (Figure 3E). Histological analysis showed normal HFD fed liver morphology for *Sel1L*$^{f/f}$ mice, and abnormal tumor growth in *Sel1L*^{Alb} mice with densely packed tumor cells, often surrounded by compressed normal adjacent parenchyma tissue (Figure 3F). Staining for CyclinD1 and Ki67 further confirmed the

profound proliferation in tumor areas (Figures 3G-H) of *Sel1L*^{Alb} livers, thereby illustrating that the loss of hepatic Sel1L led to tumorigenesis in chemically induced murine cancer models.

Loss of hepatic Sel1L predisposes mice to spontaneous liver tumors

Intrigued by the chemically induced liver cancer phenotypes exhibited by *Sel1L*^{Alb} mice, we wondered if these mice might be prone to developing spontaneous liver tumors with age. At 22-months of age, even in the absence of any chemical or dietary manipulation, male *Sel1L*^{Alb} mice were found to have enlarged and tumor-ridden livers, whereas *Sel1L*$^{f/f}$ livers were completely normal (Figures 4A-B). Histological examination showed these *Sel1L*^{Alb} livers to be of grossly abnormal morphology as compared to their *Sel1L*$^{f/f}$ littermates (Figure 4C). Proliferation marked by CyclinD1 levels was also hugely elevated in these livers (Figure 4D), further validating the spontaneous tumor development phenotype in these Sel1L-deficient livers.

Wnt5A pathway is significantly altered in *Sel1L*^{Alb} livers

To investigate the molecular mechanism behind the altered proliferation paradigm observed in *Sel1L*^{Alb} livers, we surveyed hepatic gene expression profiles of *Sel1L*$^{f/f}$ and *Sel1L*^{Alb} mice as procured in our previous microarray experiment, deposited as GSE118658. Interestingly, we found several cell cycle related genes to be significantly upregulated (Figure 5A, lower half) in *Sel1L*^{Alb} livers, which was validated via qPCR analysis (Supplementary Figure 2A). Indeed, proliferation marked by Ki67 and CyclinD1 levels was found to be slightly, yet significantly, higher in 12-weeks-old adult *Sel1L*^{Alb} livers (Figure 5B) compared to their *Sel1L*$^{f/f}$ littermates. In contrast, we found a large number of genes associated with the Wnt pathway to be significantly downregulated in these livers as compared to their *Sel1L*$^{f/f}$ counterparts (Figure 5A, upper half), which was also confirmed via qPCR analysis (Supplementary Figures 2B-C). As a deficiency in ERAD is highly likely to cause the accumulation of potential substrate proteins in the ER owing to defective clearance, a proteomics analysis of the *Sel1L*$^{f/f}$ and *Sel1L*^{Alb} hepatic ER proteins was performed, which revealed a huge upregulation of proteins in *Sel1L*^{Alb} livers (Figure 5C, top right quadrant). Strikingly, one of the top upregulated protein species in this pool was Wnt5A (Figures 5C-D). Indeed, Wnt5A protein was found to be greatly accumulated in the hepatic ER of *Sel1L*^{Alb} mice (Figure 5E). This upregulation was found to be non-transcriptional (Figure 5A), implying that this protein may be accumulating, trapped in the ER, due to faulty degradation by the Sel1L-Hrd1 complex. Furthermore, Wnt5A/B has previously been known to play a critical role in the transition from proliferation to differentiation in certain cellular contexts, making it even more relevant for the *Sel1L*^{Alb} liver phenotype (42, 43).

Wnt5A is an endogenous hepatic Sel1L-Hrd1 ERAD substrate

Wnt5A is a secreted protein spanning 380 amino acids, and containing 11 disulfide bonds, 4 glycosylation sites and 1 palmitoylation site (Figure 6A). Owing to the potential complexity in the maturation process of such a peptide, it is prone to folding errors which may be subjected to ERAD mediated quality control. Inspired by the non-transcriptional accumulation of Wnt5A in Sel1L-deficient hepatocytes, we tested the hypothesis that Wnt5a may be an endogenous substrate of Sel1L-Hrd1 ERAD in the liver. In order to examine if a protein is a bona fide ERAD substrate, it needs to be stabilized in the absence of ERAD, interact with core components of the ERAD complex, and get ubiquitinated by the E3 ligase. To explore our claim, we first performed a protein translation shut off assay in WNT5A-V5 transfected HEK293T cells, where we found that WNT5A was stabilized in the absence of HRD1 (Figure 6B) with its half-life increasing to 4 hours from approximately 1.5 hours in wildtype (WT) cells. Furthermore, with the help of co-immunoprecipitation studies, we demonstrated that WNT5A interacts with and is ubiquitinated by HRD1 (Figure 6C). This ubiquitination was reduced in the presence of the catalytically dead HRD1-C2A mutant, thus demonstrating HRD1 to indeed be the E3 ligase for WNT5A ubiquitination and subsequent degradation. These results confirmed WNT5A to indeed be a substrate for SEL1L-HRD1 mediated ERAD.

5.4 DISCUSSION

Hepatocellular carcinoma (HCC) constitutes about 90% of all primary liver cancers, with its incidence increasing, and over half a million cases currently being reported worldwide (9). Together with its unpredictability in activating different downstream signaling cascades via different receptors, and its relatively poor functional characterization, Wnt5A has long been associated with both suppression of oncogenic development and aggressiveness of specific malignancies, thereby showcasing seemingly opposing roles in overall cancer pathogenesis (13, 44). Akin to most other members of the Wnt family, the Wnt5A maturation process starts within the ER, and involves careful chaperoning (e.g. by BiP), numerous cysteine residues participating in the formation of disulfide bridges – both intramolecular (for a stable globular structure) and intermolecular (for dimerization and function), multiple glycosylations for secretion, and acylation (palmitoylation) for activity (45). These complexities intuitively present Wnt proteins as attractive candidates for folding errors, thereby making them potential substrates for ERAD mediated quality or quantity control.

In this study, we present intriguing data whereby we establish a compelling relationship existing between Sel1L-Hrd1 mediated ERAD and the pathogenesis of HCC, linked together by Wnt5A maturation. We describe here, using spontaneous and chemically-induced liver cancer models, how the ablation of hepatic Sel1L leads to increased proliferation programs and susceptibility to tumorigenesis. Further cementing this association, we show a strong correlation between Sel1L-Hrd1 levels and various human liver cancer patient samples. This is largely in keeping with various previous publications that allude to a crucial role played by Sel1L in the pathogenesis of different cancers (29-35). At a more mechanistic level, we have identified and characterized Wnt5A as a bona fide endogenous hepatic Sel1L-Hrd1 ERAD substrate, which may be responsible, at least in part, for the tumor burden carried by the liver-specific Sel1L-deficient mice.

As a continuation of this study, to conclusively establish Wnt5A as the link between hepatic Sel1L and tumorigenesis, we will check Wnt5A levels in the tumor samples obtained from the liver cancer models used in this study. Next, we will treat primary hepatocytes isolated from *Sel1L*$^{f/f}$ and *Sel1L*^{Alb} livers either with Wnt5A recombinant protein (gain of function) or with siRNA targeted against *Wnt5A* gene (loss of function), and asses the effect of Wnt5A gain/loss of function on hepatocyte proliferation and cell cycle gene expression. Furthermore, owing to the closeness shared by a large number of Wnt family members in structural complexity, we will examine other members of the Wnt family including, but not limited to, the canonical Wnt3A/B, in terms of their relationship with the Sel1L-Hrd1 ERAD complex. Here, stability, degradation and localization studies will be performed in the presence and absence of ERAD, along with an analysis of how these proteins may be dependent on the ER chaperone Grp78 during their maturation process. Overall, this study identifies a novel and unique relationship that exists between Sel1L-Hrd1 and hepatic proliferation via Wnt signaling pathway, and describes a vital role played by this hepatic ERAD complex in protecting against liver cancer pathogenesis.

5.5 METHODS

Mice. Liver-specific Sel1L-deficient mice (*Sel1L*^{Alb}) and their wildtype WT littermates (*Sel1L*$^{f/f}$) were generated after crossing *Sel1L*$^{f/f}$ mice with mice of C57BL/6J background that express Cre driven from the Albumin-promoter (JAX 003574, B6.Cg-Tg(Alb-Cre)21Mgn/J). Characterization of these mice has been described previously (27). Due to the impaired female fertility of

Sel1L^{Alb} mice, only *Sel1L*^{Alb} male mice were used for all breeding. Mice were fed normal chow diet (LabDiet 5LOD, 13% fat, 30% protein, 57% carbohydrate) or high-fat diet (60% fat, 20% protein, 20% carbohydrate) as indicated. All mice procedures were in compliance with IACUC at the University of Michigan (PRO00008989). Isoflurane anesthesia before major organ removal was the method used for euthanasia. All tissues were either fixed or frozen in liquid nitrogen right upon isolation.

Metabolite analysis. Serum levels of alanine aminotransferase (ALT), alkaline phosphatase (ALP), aspartate aminotransferase (AST), albumin (ALB), triglycerides (TG) and cholesterol (CHOL) were measured by the In Vivo Animal Core (IVAC) at University of Michigan, with affiliation to the National Mouse Metabolic Phenotyping Center (MMPC).

Partial hepatectomy. Two-third of the adult mouse liver was surgically resected to observe the regeneration of hepatocytes thereafter. During this procedure, 2-3 months old mice were anesthetized via isoflurane inhalation and placed on a heating pad. Abdominal hair was shaved, followed by the surgical area being wiped with betadine and 70% alcohol and draped. A transverse bilateral skin incision was made, followed by entry into the peritoneal cavity. A stitch was placed just above the xiphoid process and taped to the nosepiece to allow proper visualization of the liver. The body cavity was intermittently moistened with sterile saline during the procedure. The ligament connected to the median lobe was gently cut away and the left lobe mobilized with a cotton tip. A suture knot was tied just around the base of the lobe and tightened, darkening it. This lobe was then excised, leaving a small stump preventing knot slippage. This procedure was repeated to transect the median lobe next, taking care not to ligate too close to the vena cava. The peritoneal cavity was checked with cotton tip to ensure no bleeding and closed using interrupted sutures. The skin was then closed with 7mm would clips. Mice were kept solitary in a cage supplied with soft food, water and heating pad until fully recovered and ambulatory. All surgical animals were given i.p. injection of carprofen 10mg/kg preemptively and every 24 hours postoperatively for 48 hours, and monitored daily. All animals recovered steadily and fully after the surgery without any overt signs of pain or inflammation.

Liver injury/cancer models. In this study, we have used the following models of liver injury and/or tumorigenesis: (i) 2-weeks-old male mice were injected i.p. with a single dose of 25mg/kg diethylnitrosamine (DEN; Sigma N0258), then put on high fat diet at 4 weeks of age, and finally euthanized for analysis at 28 weeks of age. (ii) 8-weeks-old male mice were injected i.p. with

0.2ml/kg carbon tetrachloride (CCL4; Sigma 289116) dissolved in oil thrice a week for up to 12 weeks, and finally euthanized for analysis at 20 weeks of age.

Western blot analysis. Protein extraction from cells and tissues and analysis via SDS-PAGE and Western blotting were carried out as described previously (46, 47). Quantification of signals was done using BioRad ImageLab software. Total protein levels were normalized with the help of loading controls. The following primary antibodies were used: Ki67 (1:200 for staining, Abcam ab16667); CyclinD1 (1:100 for staining, 1:2000 for Western blot, Abcam ab16663); V5 (1:500 for staining, 1:5000 for Western blot; Invitrogen R960-25); HA (1:2,000; Sigma H9658); Myc (1:1000; Sigma); Wnt5A (1:1000, Proteintech 55184-1-AP); E-cadherin (1:100 for staining, 1:1000 for Western blot; BD 610181); α-Tubulin (1:2,000, Santa Cruz sc-5286); Hsp90 (1:1,000, Abcam ab13492); Sel1L (1:2,000; Abcam ab78298); Hrd1 (1:300) kindly gifted by Dr. Richard Wojcikiewicz (SUNY Upstate Medical University). The following secondary antibodies were used: for Western blot, donkey anti-goat IgG-HRP (1:5000; Jackson ImmunoResearch), and goat anti-mouse and goat anti-rabbit IgG-HRP (1:5,000; BioRad); for immunostaining, anti-mouse IgG FITC and Cy3; anti-rabbit IgG Alexa Fluor 488 and Alexa Fluor 647; anti-rat IgG Alexa Fluor 680, and anti-goat IgG Alexa Fluor 488 (all 1:500; Jackson ImmunoResearch).

Proteomics analysis. ER fraction was extracted after ultracentrifugation from freshly liver tissue as the microsomal pellet, which was purified by sucrose gradient fractionation. Protein concentration between samples was normalized via Bradford assay. Mass spectrometric analysis was carried out with 75 μg of protein per sample using the Tandem Mass Tag technique.

RNA extraction, RT and qPCR. Total RNA was isolated from tissues and cells with the help of Trizol and BCP reagent, followed by RNA quality measurement via OD. qPCR analysis was performed using SYBR-Green based master mix, oilgo-dT primer, Taq polymerase, and the Applied Biosystems machine. All qPCR data were normalized to expression levels of the ribosomal *L32* gene. The primer sequences are as follows: *Wnt5A* F: , R: ; *Wnt5B* F: , R: ; *Fzd4* F: GATATCCCGCACATTCTCGT, R: TGGCACATAAACCGAACAAA; *Fzd5* F: CACTCAAGACTCCGGAGAGG, R: GGTAGCGGCTTGTGGTAGTC; *Lgr4* F: CATTTTGGGGGTGTGACTCT, R: CGACCAGGAAAATGAACCAC; *Lgr5* F: CCTTCCCTGTGACTGGGTTA, R: CACTGTTGCCGTCGTCTTTA; *Ctnnb1* F: GACACCTCCCAAGTCCTTTATG, R: CTGAGCCCTAGTCATTGCATAC; *Ctnnbip1* F:

AGGAAGATGGGGTCAAACCTG, R: CATCACCACGTCCTCTGCAC; *Tcf7l1* F: CCCCCTACTTTCCCAGCTAC, R: CTTTGTGTTTCCCCCTTCCT; *Tcf7l2* F: ATAAAACCCAGATGCCACCA, R: CACACGGTCAGTCCATGTTC; *Cdh1* F: CCTGCCAATCCTGATGAAAT, R: GTCCTGATCCGACTCAGAGG; *Vegfa* F: CAGGCTGCTCTAACGATGAA, R: CAGGAATCCCAGAAACAACC; *CycD1* F: CACAACGCACTTTCTTTCCA, R: ACCAGCCTCTTCCTCCACTT; *CycD3* F: TAGGCGCCTGCTCTATGTCT, R: ATCTGTGGGAGTGCTGGTCT; *p21* F: ACAAGAGGCCCAGTACTTCC, R: GGGCACTTCAGGGTTTTCTC.

Immunostaining and histology. For staining and histology, tissues were directly immersed in 10% neutral buffered formalin after dissection and stored at 4°C. These were either paraffin embedded and sectioned (and also H&E stained) by the Michigan Histology Core for fee-for-service, or dehydrated in 15% sucrose, OCT embedded and cryo-sectioned at 5 µm thickness. For certain in vivo stains, livers were perfused with warm PBS followed by perfusion-fixation in 4% paraformaldehyde. The next day, these livers were sucrose-dehydrated, OCT embedded and sectioned on a cryotome for further staining. In case of immunocytochemistry, cells were grown on coverslips and fixed in 4% formalin at room temperature for 15 mins. For paraffin sections, antigen retrieval was done by boiling in sodium citrate buffer for 20 minutes. For cells and cryo-sections, permeabilization was done for 10 min at room temperature with 0.3% Triton X-100 and 0.3% Glycine. All sections/cells were incubated at room temperature in 1% donkey serum containing 0.03% TritonX-100 blocking solution for an hour, followed by primary antibody incubation at 4°C, overnight, in humidified chambers. In case of immunohistochemistry, peroxidase quenching was carried out before antigen retrieval, and avidin-biotin kit was used to amplify the signal obtained using the DAB substrate kit. The next day, sections were washed thrice in PBS-Tx (0.03% TritonX-100) and treated with secondary antibody at room temperature for 2 hours. Counterstaining and/or mounting were done using either Permount or hard-set DAPI-containing mounting medium (Vector H-1200). Trichrome staining was carried out using the TRM-1 kit from ScyTek. Fluorescent imaging was done using Nikon A1 Confocal Microscope at University of Michigan Imaging Core, keeping imaging parameters consistent within each experiment. H&E and DAB stained sections were scanned with the help of Aperio Scanscope (Leica Biosystems). All images were analyzed using ImageJ plugin (FIJI).

Cell lines and transfection. HEK293T cells from ATCC were cultured in DMEM (Corning, NY) with heat inactivated 10% FBS (GIBCO), 1% sodium pyruvate and 1% penicillin/streptomycin.

CRISPR technology was used to produce *HRD1-/-* HEK293T cells as described previously (26). Transfection of cells was carried out 16-24 hours after plating with Lipofectamine 2000 reagent and harvested in about another 24 hours for analysis.

Plasmids. Plasmid constructs for Active-WNT5A-V5 was purchased from Addgene. Myc-tagged WT and C2A mutant HRD1 constructs were gifted by Dr. Yihong Ye (NIDDK), and pcDNA3-HA-Ub was kindly provided by Dr. Hideki Nishitoh (University of Miyazaki, Japan).

Statistical Analysis. All results in this study have been expressed in the form of mean ± SEM unless otherwise depicted. Groups of data were compared via the paired two-tailed Student's t test or the 2-way ANOVA as necessary. All experiments were repeated at least twice, and executed using multiple independent biological samples out of which the most representative data have been shown here.

5.6 ACKNOWLEDGEMENTS

We sincerely thank Drs. Yihong Ye and Richard Wojcikiewicz for reagents; and Drs. Robert Weiss, Peter Arvan, Natasza Kurpios and Kenneth Simpson for discussion and insightful comments; the Histology, Pathology, Vision, Animal testing and Vector Cores at University of Michigan for assistance; and other members of the Qi laboratory for critique, discussion and support.

5.7 AUTHOR CONTRIBUTION

A.B. designed and performed most experiments; D.T. provided human tissues and associated reagents; L.C. performed statistical analyses of human liver cancer data; A.B. and L.Q. wrote the manuscript.

5.8 FIGURE LEGENDS

Figure 1. ***SEL1L* expression in human liver cancer**. (A-C) Km plots depicting probability of overall survival in liver cancer patients for varying hepatic levels of SEL1L protein (A), HRD1 protein (B), and SEL1L+HRD1 combined (C). (D) Western blot analysis and quantitation of SEL1L and HRD1 protein levels in tumor and adjacent normal tissue obtained from human liver cancer patients, with αTUBULIN as loading control (n=5 per group, 2 repeats). (E-F) Correlation analysis between SEL1L and HRD1 levels in tumor tissue (E) and adjacent normal

tissue (F) obtained from human liver cancer patients. Values mean ± SEM; *, p<0.05; **, p<0.01; ***, p<0.001 by Student's t test.

Figure 2. ***Sel1L^{Alb}*** **livers exhibit excessive proliferation during regeneration**. (A-B) Body weight gain (A), and liver weight gain (B) curves of 10-week-old mice post two-thirds partial hepatectomy surgery (n=4 per group). (C) Representative images of 10-week-old mice 7 days after two-thirds partial hepatectomy surgery (n=2 per group). (D-E) Representative images of hematoxylin-eosin stain (D) and CyclinD1 stain (E) on livers of 10-week-old mice 48 hours post two-thirds partial hepatectomy surgery (n=4 per group). Values mean ± SEM; *, p<0.05; **, p<0.01; ***, p<0.001 by Student's t test.

Figure 3. **Loss of hepatic Sel1L predisposes mice to chemical and diet induced tumors**. (A) Schematic timeline of experiment. (B-D) Representative images of liver (B), liver-to-body weight ratios (C), and tumor counts (D) of 6-months-old male mice at the end of experiment as outlined in A (n=5-7 per group). (E) Western blot analysis of tumor and adjacent normal liver tissue obtained from 6-months-old male mice at the end of experiment as outlined in A (n=2 per group, 2 independent repeats). (F-H) Representative images of hematoxylin-eosin stain (F), CyclinD1 stain (G), and Ki67 stain (H) on livers of 6-months-old male mice at the end of experiment as outlined in A (n=4 per group). Hsp90, loading control. Values, mean ± SEM; *, p<0.05; **, p<0.01; ***, p<0.001 by Student's t test.

Figure 4. ***Sel1L^{Alb}*** **mice develop spontaneous liver tumors**. (A-B) Representative images of liver (A), and liver-to-body weight ratios (B) of 23-months-old male mice (n=3 per group). (C-D) Representative images of hematoxylin-eosin stain (C) and CyclinD1 stain (D) on livers of 23-months-old male mice (n=3 per group). Values, mean ± SEM; *, p<0.05; **, p<0.01; ***, p<0.001 by Student's t test.

Figure 5. **Wnt5A pathway is altered in *Sel1L^{Alb}* livers**. (A) Heat map of genes associated with Wnt pathway (top half) and cell cycle (bottom half) in 9-week-old *Sel1L^{Alb}* livers, logarithm of fold change over *Sel1L$^{f/f}$* livers (n=3 per group). (B) Representative images of Ki67 and CyclinD1 stain on livers of 10-weeks-old mice (n=3 per group). (C-D) Volcano plot (C) and tabular depiction (D) of proteomics data obtained via TMT-LC/MS analysis of hepatic ER isolated from 3-months-old mice (n=3 per group). (E) Western blot analysis of Wnt5A protein in liver microsomal fractions obtained from 8-weeks-old mice (n=6 per group). Calnexin, loading control. Values, mean ± SEM; *, p<0.05; **, p<0.01; ***, p<0.001 by Student's t test.

Figure 6. **Hepatic Wnt5A is a Sel1L-Hrd1 ERAD substrate**. (A) Schematic diagram depicting WNT5A protein domains: signal peptide (sp), propeptide (pro), amino terminal (amino), hairpin1, hairpin2/thumb, cysteine knot (cys knot), hairpin3/index finger, 11 disulfide bonds (black lines), 1 putative disulfide bond (grey line), 4 glycosylation sites (red triangles), and 1 palmitoylation site (blue triangle). (B) Western blot analysis and quantitation of WNT5A protein half-life in V5-WNT5A-transfected WT and HRD1-/- HEK293T cells after treatment with cycloheximide (CHX) for indicated times (2 independent repeats). (C) Western blot analysis depicting WNT5A interaction with and ubiquitination by HRD1 in WT HEK293T cells pre-treated for 4 hours with proteasomal inhibitor bortezomib (BTZ). Hsp90, loading control. Values, mean ± SEM; *, p<0.05; **, p<0.01; ***, p<0.001 by Student's t test.

Supplementary Figure 1. ***Sel1L^{Alb}*** **livers exhibit massive proliferation upon CCL4 induced damage**. (A) Schematic timeline of experiment. (B) Body weight gain curves of 8-weeks-old male mice following CCL4 treatment thrice per week (n=4 per group). (C-D) Representative images (C), and liver-to-body weight ratios (D) of 5-months-old male mice following 3 months of

CCL4 treatment (n=4 per group). (E-G) Serum levels of alanine aminotransferase (ALT) (E), aspartate aminotransferase (AST) (F), and alkaline phosphatase (ALP) (G) of 5-months-old male mice following 3 months of CCL4 treatment (n=4 per group). (H) Representative images of hematoxylin-eosin stain (left), Trichrome Masson's (TCM) stain (middle), and Ki67 stain (right) on livers of 5-months-old male mice following 3 months of CCL4 treatment (n=3 per group). Values, mean ± SEM; *, p<0.05; **, p<0.01; ***, p<0.001 by Student's t test.

Supplementary Figure 2. **Wnt5A pathway is altered in *Sel1L*^{Alb} livers**. (A-C) qPCR mRNA analysis of cell cycle genes (A), Wnt5A receptors (B), and Wnt pathway downstream effectors (C) in 3-months-old mice livers (n=5 per group). *L32*, loading control. Values, mean ± SEM; *, p<0.05; **, p<0.01; ***, p<0.001 by Student's t test.

5.9 REFERENCES

1. Ferenci P, Fried M, Labrecque D, Bruix J, Sherman M, Omata M, Heathcote J, Piratsivuth T, Kew M, Otegbayo JA, Zheng SS, Sarin S, Hamid SS, Modawi SB, Fleig W, Fedail S, Thomson A, Khan A, Malfertheiner P, Lau G, Carillo FJ, Krabshuis J, Le Mair A, World Gastroenterology O. Hepatocellular carcinoma (HCC): a global perspective. J Clin Gastroenterol. 2010;44(4):239-45. doi: 10.1097/MCG.0b013e3181d46ef2. PubMed PMID: 20216082.
2. Altekruse SF, McGlynn KA, Reichman ME. Hepatocellular carcinoma incidence, mortality, and survival trends in the United States from 1975 to 2005. J Clin Oncol. 2009;27(9):1485-91. doi: 10.1200/JCO.2008.20.7753. PubMed PMID: 19224838; PMCID: PMC2668555.
3. Finn RS. Emerging targeted strategies in advanced hepatocellular carcinoma. Semin Liver Dis. 2013;33 Suppl 1:S11-9. doi: 10.1055/s-0033-1333632. PubMed PMID: 23457035.
4. Janevska D, Chaloska-Ivanova V, Janevski V. Hepatocellular Carcinoma: Risk Factors, Diagnosis and Treatment. Open Access Maced J Med Sci. 2015;3(4):732-6. doi: 10.3889/oamjms.2015.111. PubMed PMID: 27275318; PMCID: PMC4877918.
5. El-Serag HB, Rudolph KL. Hepatocellular carcinoma: epidemiology and molecular carcinogenesis. Gastroenterology. 2007;132(7):2557-76. doi: 10.1053/j.gastro.2007.04.061. PubMed PMID: 17570226.
6. Polesel J, Zucchetto A, Montella M, Dal Maso L, Crispo A, La Vecchia C, Serraino D, Franceschi S, Talamini R. The impact of obesity and diabetes mellitus on the risk of hepatocellular carcinoma. Ann Oncol. 2009;20(2):353-7. doi: 10.1093/annonc/mdn565. PubMed PMID: 18723550.
7. De Mattia E, Cecchin E, Polesel J, Bignucolo A, Roncato R, Lupo F, Crovatto M, Buonadonna A, Tiribelli C, Toffoli G. Genetic biomarkers for hepatocellular cancer risk in a caucasian population. World J Gastroenterol. 2017;23(36):6674-84. doi: 10.3748/wjg.v23.i36.6674. PubMed PMID: 29085212; PMCID: PMC5643288.
8. McGlynn KA, Petrick JL, London WT. Global epidemiology of hepatocellular carcinoma: an emphasis on demographic and regional variability. Clin Liver Dis. 2015;19(2):223-38. doi: 10.1016/j.cld.2015.01.001. PubMed PMID: 25921660; PMCID: PMC4712629.
9. Lee JM, Yang J, Newell P, Singh S, Parwani A, Friedman SL, Nejak-Bowen KN, Monga SP. beta-Catenin signaling in hepatocellular cancer: Implications in inflammation, fibrosis, and proliferation. Cancer Lett. 2014;343(1):90-7. doi: 10.1016/j.canlet.2013.09.020. PubMed PMID: 24071572; PMCID: PMC3874258.

10. Vilchez V, Turcios L, Marti F, Gedaly R. Targeting Wnt/beta-catenin pathway in hepatocellular carcinoma treatment. World J Gastroenterol. 2016;22(2):823-32. doi: 10.3748/wjg.v22.i2.823. PubMed PMID: 26811628; PMCID: PMC4716080.
11. Polakis P. Wnt signaling and cancer. Genes & development. 2000;14(15):1837-51. PubMed PMID: 10921899.
12. Gedaly R, Galuppo R, Daily MF, Shah M, Maynard E, Chen C, Zhang X, Esser KA, Cohen DA, Evers BM, Jiang J, Spear BT. Targeting the Wnt/beta-catenin signaling pathway in liver cancer stem cells and hepatocellular carcinoma cell lines with FH535. PLoS One. 2014;9(6):e99272. doi: 10.1371/journal.pone.0099272. PubMed PMID: 24940873; PMCID: PMC4062395.
13. Asem MS, Buechler S, Wates RB, Miller DL, Stack MS. Wnt5a Signaling in Cancer. Cancers (Basel). 2016;8(9). doi: 10.3390/cancers8090079. PubMed PMID: 27571105; PMCID: PMC5040981.
14. Zhou Y, Kipps TJ, Zhang S. Wnt5a Signaling in Normal and Cancer Stem Cells. Stem Cells Int. 2017;2017:5295286. doi: 10.1155/2017/5295286. PubMed PMID: 28491097; PMCID: PMC5405594.
15. Zhan T, Rindtorff N, Boutros M. Wnt signaling in cancer. Oncogene. 2017;36(11):1461-73. doi: 10.1038/onc.2016.304. PubMed PMID: 27617575; PMCID: PMC5357762.
16. Guerriero CJ, Brodsky JL. The delicate balance between secreted protein folding and endoplasmic reticulum-associated degradation in human physiology. Physiological reviews. 2012;92(2):537-76. doi: 10.1152/physrev.00027.2011. PubMed PMID: 22535891; PMCID: 4162396.
17. Qi L, Tsai B, Arvan P. New Insights into the Physiological Role of Endoplasmic Reticulum-Associated Degradation. Trends Cell Biol. 2017;27(6):430-40. doi: 10.1016/j.tcb.2016.12.002. PubMed PMID: 28131647; PMCID: PMC5440201.
18. Mueller B, Klemm EJ, Spooner E, Claessen JH, Ploegh HL. SEL1L nucleates a protein complex required for dislocation of misfolded glycoproteins. Proc Natl Acad Sci USA. 2008;105(34):12325-30. doi: 10.1073/pnas.0805371105. PubMed PMID: 18711132.
19. Sun S, Shi G, Han X, Francisco AB, Ji Y, Mendonca N, Liu X, Locasale JW, Simpson KW, Duhamel GE, Kersten S, Yates JR, 3rd, Long Q, Qi L. Sel1L is indispensable for mammalian endoplasmic reticulum-associated degradation, endoplasmic reticulum homeostasis, and survival. Proc Natl Acad Sci U S A. 2014;111:E582-91. Epub 2014/01/24. doi: 10.1073/pnas.1318114111.
20. Mehnert M, Sommermeyer F, Berger M, Kumar Lakshmipathy S, Gauss R, Aebi M, Jarosch E, Sommer T. The interplay of Hrd3 and the molecular chaperone system ensures efficient degradation of malfolded secretory proteins. Mol Biol Cell. 2015;26(2):185-94. doi: 10.1091/mbc.E14-07-1202. PubMed PMID: 25428985; PMCID: PMC4294667.
21. Vashistha N, Neal SE, Singh A, Carroll SM, Hampton RY. Direct and essential function for Hrd3 in ER-associated degradation. Proc Natl Acad Sci U S A. 2016;113(21):5934-9. doi: 10.1073/pnas.1603079113. PubMed PMID: 27170191; PMCID: PMC4889393.
22. Francisco AB, Singh R, Li S, Vani AK, Yang L, Munroe RJ, Diaferia G, Cardano M, Biunno I, Qi L, Schimenti JC, Long Q. Deficiency of suppressor enhancer Lin12 1 like (SEL1L) in mice leads to systemic endoplasmic reticulum stress and embryonic lethality. J Biol Chem. 2010;285(18):13694-703. doi: 10.1074/jbc.M109.085340. PubMed PMID: 20197277; PMCID: PMC2859532.
23. Yagishita N, Ohneda K, Amano T, Yamasaki S, Sugiura A, Tsuchimochi K, Shin H, Kawahara K, Ohneda O, Ohta T, Tanaka S, Yamamoto M, Maruyama I, Nishioka K, Fukamizu A, Nakajima T. Essential role of synoviolin in embryogenesis. J Biol Chem. 2005;280(9):7909-16. doi: 10.1074/jbc.M410863200. PubMed PMID: 15611074.

24. Shi G, Somlo D, Kim GH, Prescianotto-Baschong C, Sun S, Beuret N, Long Q, Rutishauser J, Arvan P, Spiess M, Qi L. ER-associated degradation is required for vasopressin prohormone processing and systemic water homeostasis. J Clin Invest. 2017;127(10):3897-912.
25. Kim GH, Shi G, Somlo D, Haataja L, Soon S, Long Q, Nillni EA, Low MJ, Arvan P, Myers MG, Qi L. Hypothalamic ER-associated degradation regulates POMC maturation, feeding and age-associated obesity. J Clin Invest. 2018;In press.
26. Sun S, Shi G, Sha H, Ji Y, Han X, Shu X, Ma H, Inoue T, Gao B, Kim H, Bu P, Guber RD, Shen X, Lee AH, Iwawaki T, Paton AW, Paton JC, Fang D, Tsai B, Yates Iii JR, Wu H, Kersten S, Long Q, Duhamel GE, Simpson KW, Qi L. IRE1alpha is an endogenous substrate of endoplasmic-reticulum-associated degradation. Nature cell biology. 2015;17(12):1546-55. doi: 10.1038/ncb3266. PubMed PMID: 26551274; PMCID: PMC4670240.
27. Bhattacharya A, Sun S, Wang H, Liu M, Long Q, Yin L, Kersten S, Zhang K, Qi L. Hepatic Sel1L-Hrd1 ER-associated degradation (ERAD) manages FGF21 levels and systemic metabolism via CREBH. The EMBO journal. 2018;37(22). doi: 10.15252/embj.201899277. PubMed PMID: 30389665; PMCID: PMC6236331.
28. Wei J, Chen L, Li F, Yuan Y, Wang Y, Xia W, Zhang Y, Xu Y, Yang Z, Gao B, Jin C, Melo-Cardenas J, Green RM, Pan H, Wang J, He F, Zhang K, Fang D. HRD1-ERAD controls production of the hepatokine FGF21 through CREBH polyubiquitination. The EMBO journal. 2018;37(22). doi: 10.15252/embj.201898942. PubMed PMID: 30389664; PMCID: PMC6236336.
29. Kim H, Bhattacharya A, Qi L. Endoplasmic reticulum quality control in cancer: Friend or foe. Seminars in cancer biology. 2015;33:25-33. doi: 10.1016/j.semcancer.2015.02.003. PubMed PMID: 25794824; PMCID: PMC4523434.
30. Liu Q, Chen J, Mai B, Amos C, Killary AM, Sen S, Wei C, Frazier ML. A single-nucleotide polymorphism in tumor suppressor gene SEL1L as a predictive and prognostic marker for pancreatic ductal adenocarcinoma in Caucasians. Molecular carcinogenesis. 2012;51(5):433-8. doi: 10.1002/mc.20808. PubMed PMID: 21656579; PMCID: PMC3780592.
31. Cattaneo M, Fontanella E, Canton C, Delia D, Biunno I. SEL1L affects human pancreatic cancer cell cycle and invasiveness through modulation of PTEN and genes related to cell-matrix interactions. Neoplasia. 2005;7(11):1030-8. PubMed PMID: 16331889; PMCID: PMC1502024.
32. Ashktorab H, Green W, Finzi G, Sessa F, Nouraie M, Lee EL, Morgano A, Moschetta A, Cattaneo M, Mariani-Costantini R, Brim H, Biunno I. SEL1L, an UPR response protein, a potential marker of colonic cell transformation. Digestive diseases and sciences. 2012;57(4):905-12. doi: 10.1007/s10620-011-2026-y. PubMed PMID: 22350780; PMCID: PMC3345950.
33. Cardano M, Diaferia GR, Cattaneo M, Dessi SS, Long Q, Conti L, Deblasio P, Cattaneo E, Biunno I. mSEL-1L (Suppressor/enhancer Lin12-like) protein levels influence murine neural stem cell self-renewal and lineage commitment. J Biol Chem. 2011;286(21):18708-19. doi: 10.1074/jbc.M110.210740. PubMed PMID: 21454627; PMCID: PMC3099688.
34. Orlandi R, Cattaneo M, Troglio F, Casalini P, Ronchini C, Menard S, Biunno I. SEL1L expression decreases breast tumor cell aggressiveness in vivo and in vitro. Cancer research. 2002;62(2):567-74. PubMed PMID: 11809711.
35. Granelli P, Cattaneo M, Ferrero S, Bottiglieri L, Bosari S, Fichera G, Biunno I. SEL1L and squamous cell carcinoma of the esophagus. Clinical cancer research : an official journal of the American Association for Cancer Research. 2004;10(17):5857-61. doi: 10.1158/1078-0432.CCR-04-0075. PubMed PMID: 15355917.
36. Fujii T, Fuchs BC, Yamada S, Lauwers GY, Kulu Y, Goodwin JM, Lanuti M, Tanabe KK. Mouse model of carbon tetrachloride induced liver fibrosis: Histopathological changes and expression of CD133 and epidermal growth factor. BMC Gastroenterol. 2010;10:79. doi: 10.1186/1471-230X-10-79. PubMed PMID: 20618941; PMCID: PMC2912240.

37. Scholten D, Trebicka J, Liedtke C, Weiskirchen R. The carbon tetrachloride model in mice. Lab Anim. 2015;49(1 Suppl):4-11. doi: 10.1177/0023677215571192. PubMed PMID: 25835733.
38. Uehara T, Pogribny IP, Rusyn I. The DEN and CCl4 -Induced Mouse Model of Fibrosis and Inflammation-Associated Hepatocellular Carcinoma. Curr Protoc Pharmacol. 2014;66:14 30 1-10. doi: 10.1002/0471141755.ph1430s66. PubMed PMID: 25181010; PMCID: PMC4214366.
39. Heindryckx F, Colle I, Van Vlierberghe H. Experimental mouse models for hepatocellular carcinoma research. Int J Exp Pathol. 2009;90(4):367-86. doi: 10.1111/j.1365-2613.2009.00656.x. PubMed PMID: 19659896; PMCID: PMC2741148.
40. Tolba R, Kraus T, Liedtke C, Schwarz M, Weiskirchen R. Diethylnitrosamine (DEN)-induced carcinogenic liver injury in mice. Lab Anim. 2015;49(1 Suppl):59-69. doi: 10.1177/0023677215570086. PubMed PMID: 25835739.
41. Bakiri L, Wagner EF. Mouse models for liver cancer. Mol Oncol. 2013;7(2):206-23. doi: 10.1016/j.molonc.2013.01.005. PubMed PMID: 23428636; PMCID: PMC5528415.
42. Fan J, Wei Q, Liao J, Zou Y, Song D, Xiong D, Ma C, Hu X, Qu X, Chen L, Li L, Yu Y, Yu X, Zhang Z, Zhao C, Zeng Z, Zhang R, Yan S, Wu T, Wu X, Shu Y, Lei J, Li Y, Zhang W, Haydon RC, Luu HH, Huang A, He TC, Tang H. Noncanonical Wnt signaling plays an important role in modulating canonical Wnt-regulated stemness, proliferation and terminal differentiation of hepatic progenitors. Oncotarget. 2017;8(16):27105-19. doi: 10.18632/oncotarget.15637. PubMed PMID: 28404920; PMCID: PMC5432321.
43. Prestwich TC, Macdougald OA. Wnt/beta-catenin signaling in adipogenesis and metabolism. Curr Opin Cell Biol. 2007;19(6):612-7. doi: 10.1016/j.ceb.2007.09.014. PubMed PMID: 17997088; PMCID: PMC2709272.
44. McDonald SL, Silver A. The opposing roles of Wnt-5a in cancer. Br J Cancer. 2009;101(2):209-14. doi: 10.1038/sj.bjc.6605174. PubMed PMID: 19603030; PMCID: PMC2720208.
45. Willert K, Nusse R. Wnt proteins. Cold Spring Harbor perspectives in biology. 2012;4(9):a007864. doi: 10.1101/cshperspect.a007864. PubMed PMID: 22952392; PMCID: PMC3428774.
46. Yang L, Xue Z, He Y, Sun S, Chen H, Qi L. A Phos-tag-based approach reveals the extent of physiological endoplasmic reticulum stress. PLoS One. 2010;5(7):e11621. doi: 10.1371/journal.pone.0011621. PubMed PMID: 20661282; PMCID: 2905412.
47. Sha H, He Y, Chen H, Wang C, Zenno A, Shi H, Yang X, Zhang X, Qi L. The IRE1alpha-XBP1 pathway of the unfolded protein response is required for adipogenesis. Cell metabolism. 2009;9(6):556-64. doi: 10.1016/j.cmet.2009.04.009. PubMed PMID: 19490910; PMCID: 2963107.

5.10 FIGURES

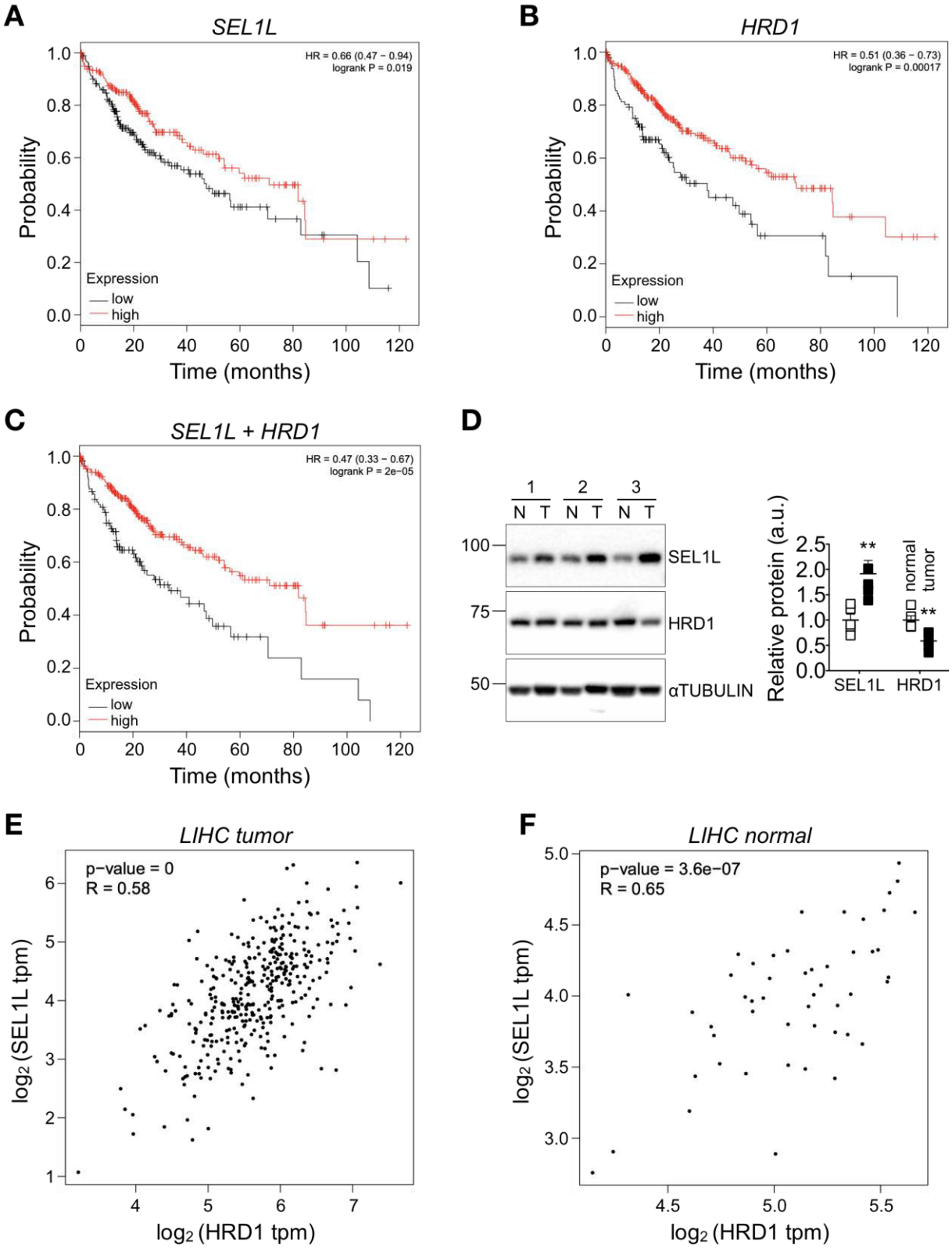

Figure 1. ***SEL1L*** **expression in human liver cancer**.

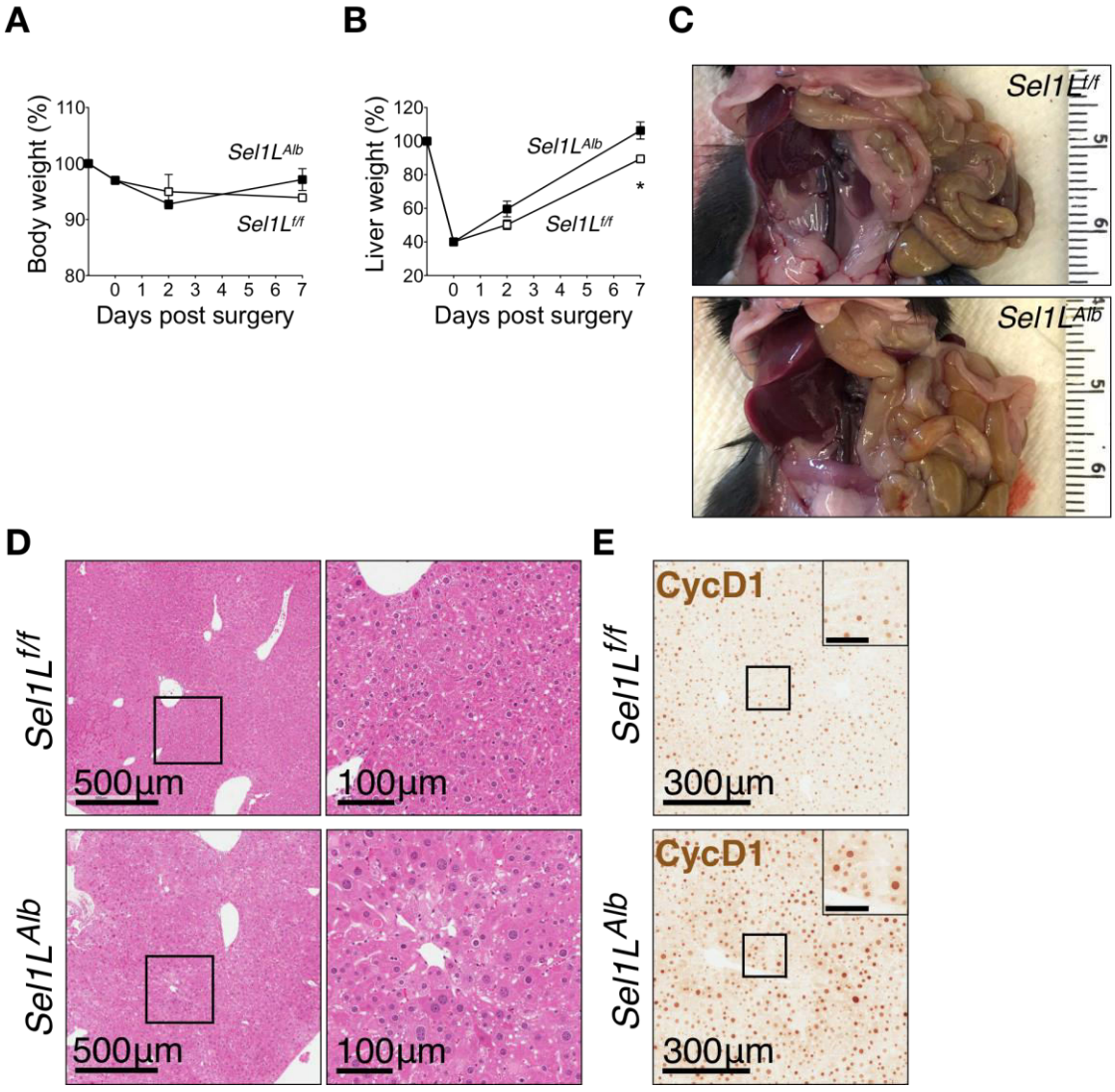

Figure 2. ***Sel1L^{Alb}*** **livers exhibit excessive proliferation during regeneration**.

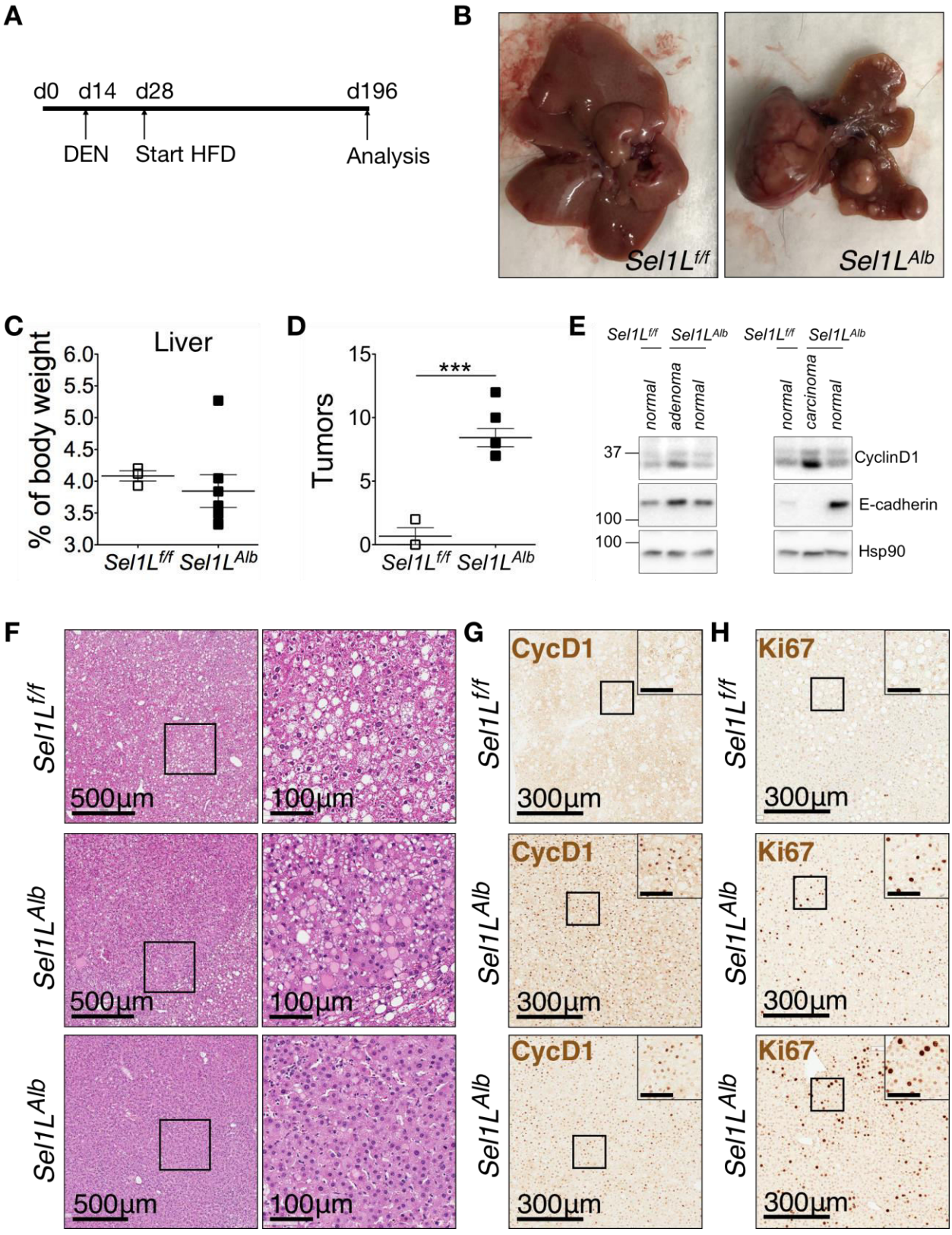

Figure 3. Loss of hepatic Sel1L predisposes mice to chemical and diet induced tumors.

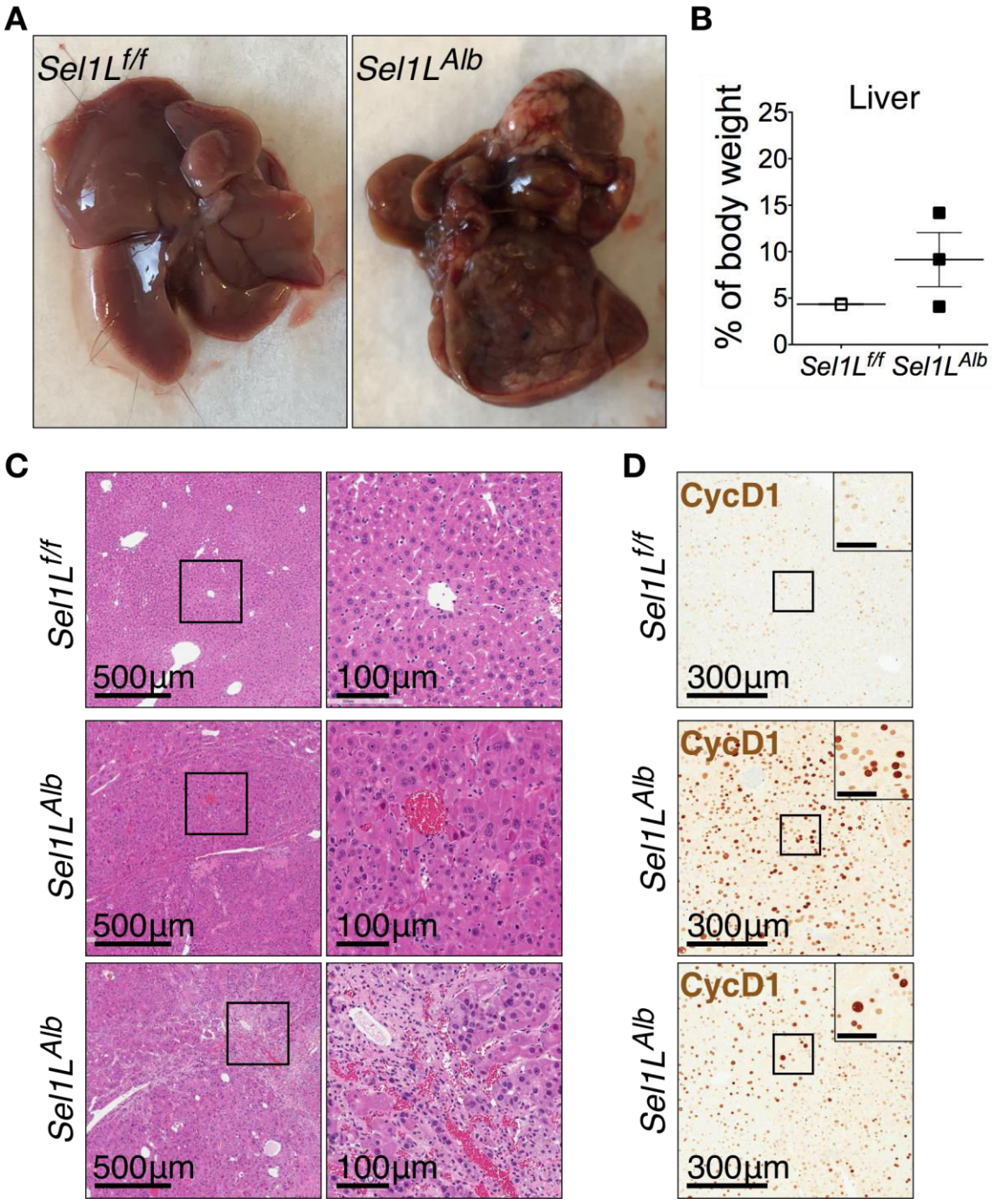

Figure 4. ***Sel1L*^{Alb} mice develop spontaneous liver tumors**.

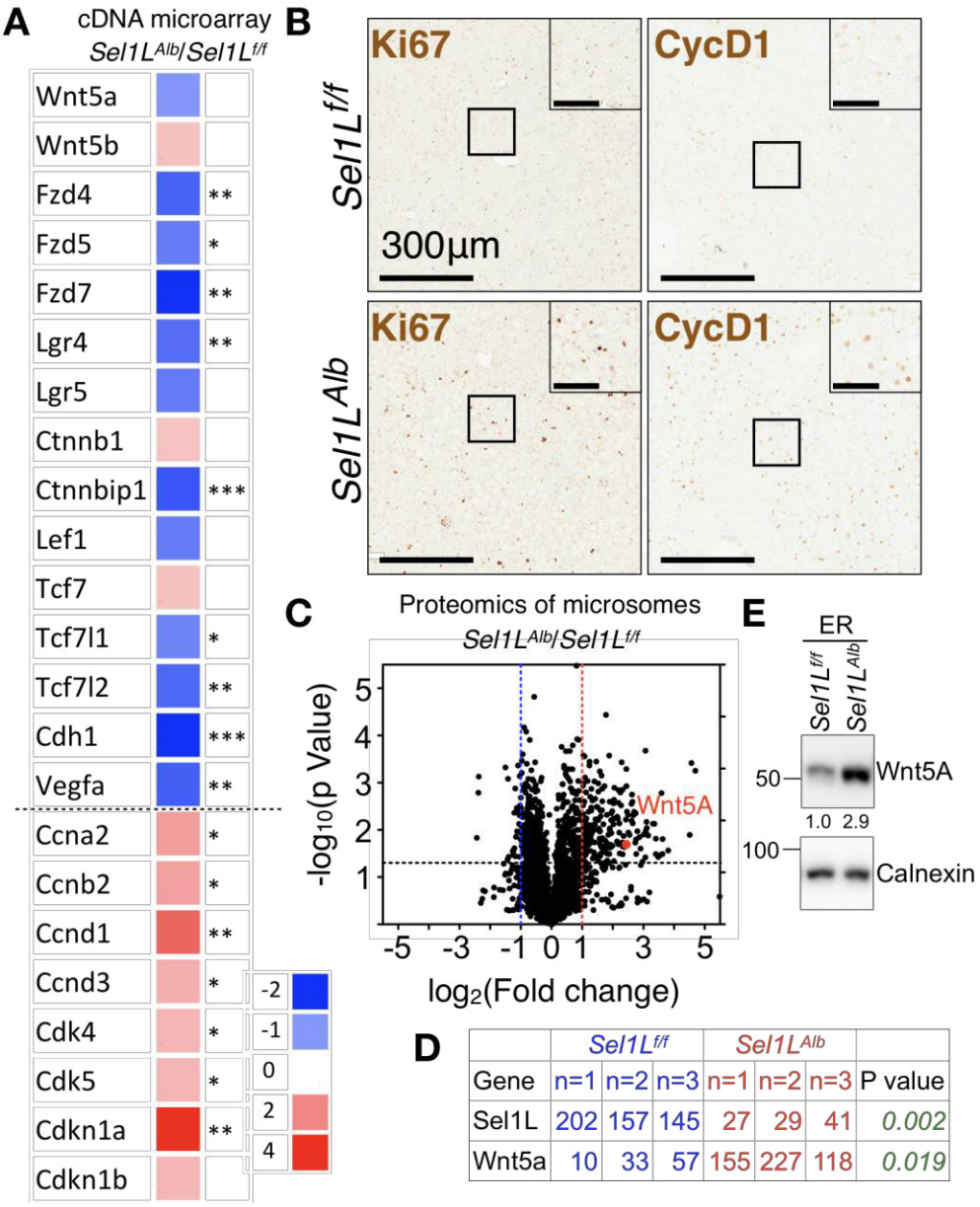

Figure 5. **Wnt5A pathway is altered in *Sel1L*^{Alb} livers**.

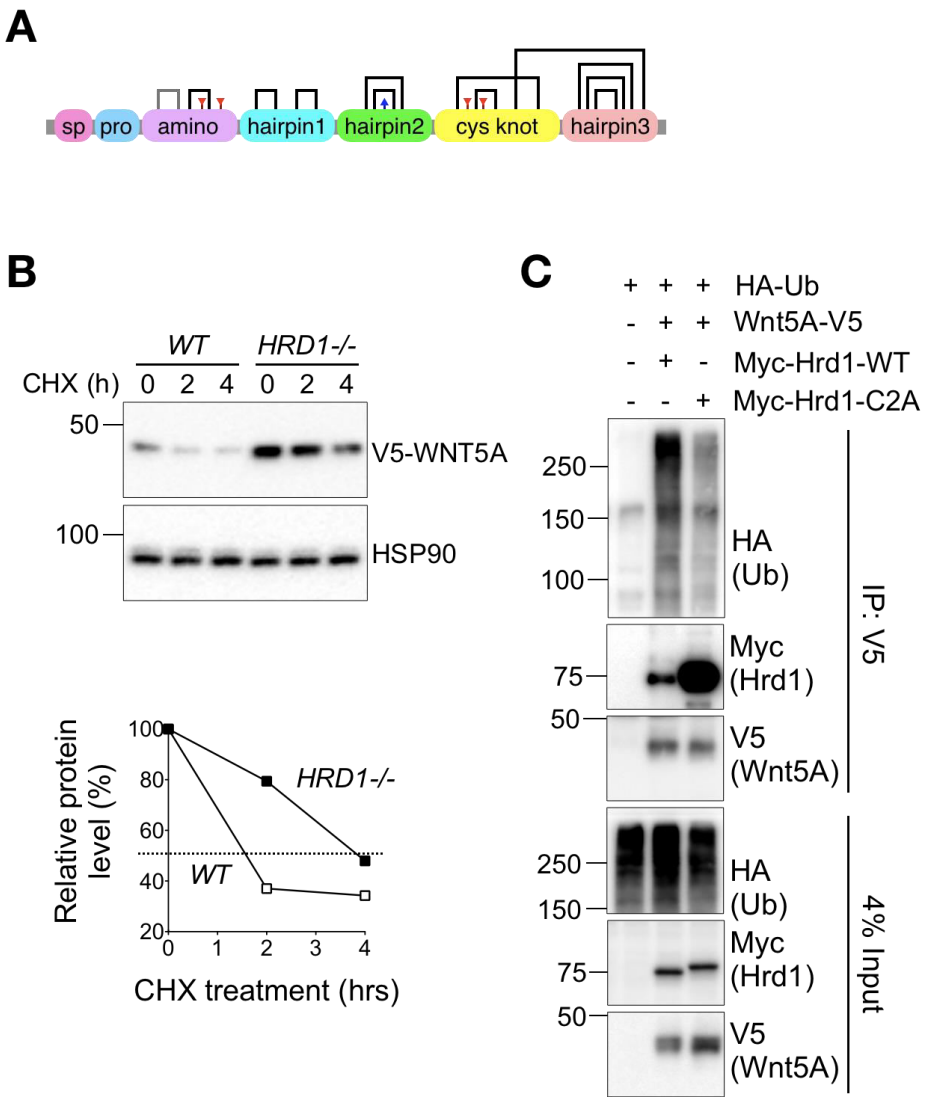

Figure 6. Hepatic Wnt5A is a Sel1L-Hrd1 ERAD substrate.

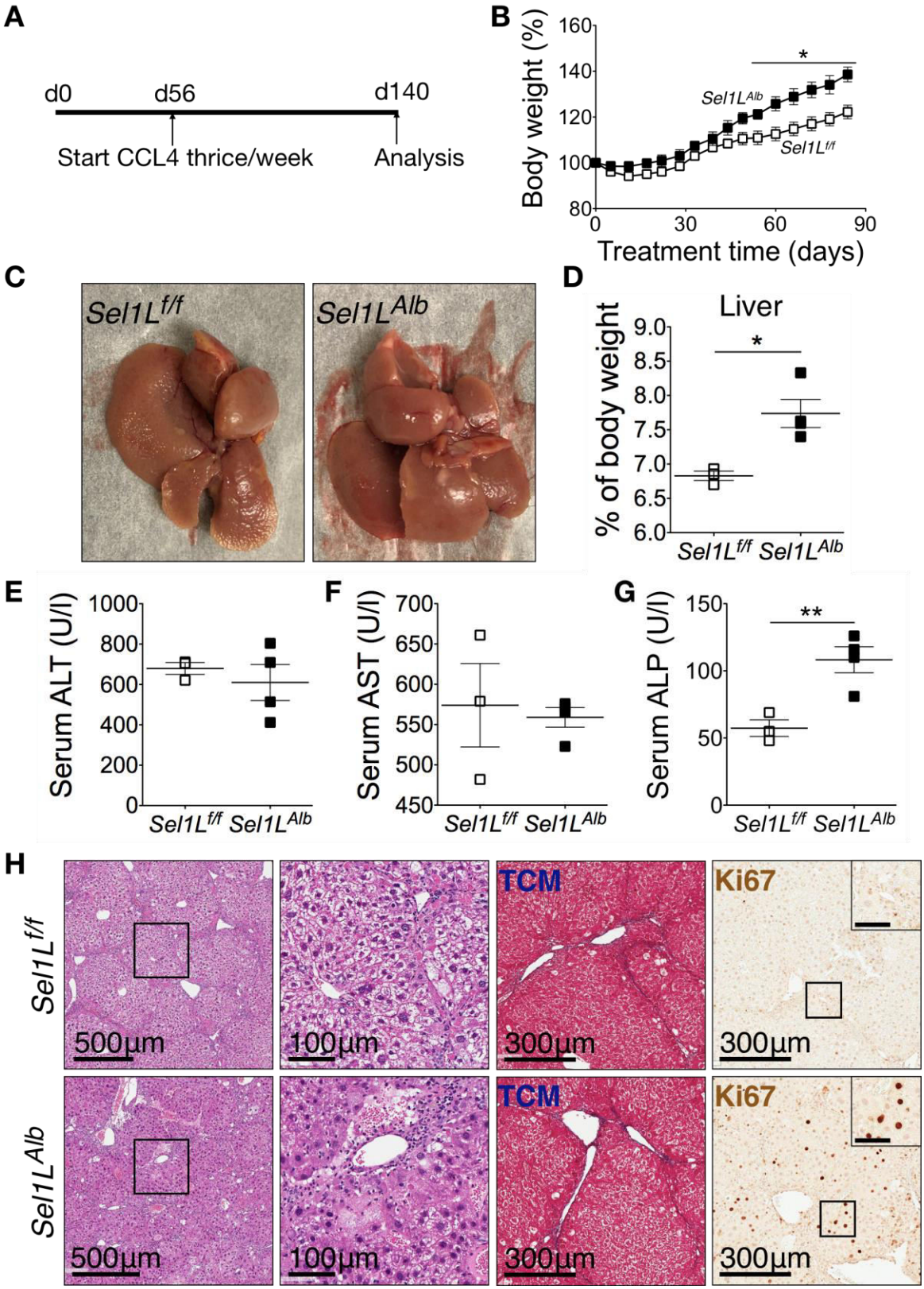

Supplementary Figure 1. ***Sel1L^{Alb}*** **livers exhibit massive proliferation upon CCL4 induced damage**.

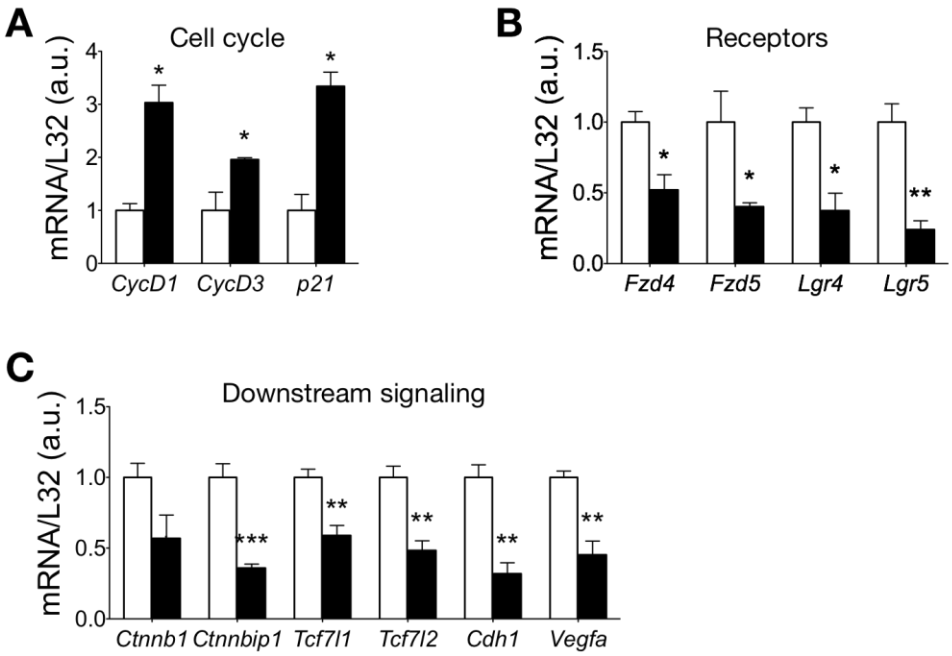

Supplementary Figure 2. **Wnt5A pathway is altered in *Sel1L*^{Alb} livers**.

CHAPTER 6

Sel1L-Hrd1 ERAD in the Liver: A Perspective

Protein misfolding and aggregation can lead to the disruption of multiple cellular pathways, thereby forming the basis for a myriad of disease conditions in humans. The endoplasmic reticulum (ER) being the designated organelle for the maturation of one-third of the total cellular proteome, Endoplasmic Reticulum Associated Degradation (ERAD) constitutes a critical system dedicated to the triage of aberrant proteins within the cell. The Sel1L-Hrd1 complex is the most highly conserved, well characterized and major ERAD machinery in mammalian cells. The liver, being a central regulator of metabolic processes in the body, deals with a heavy load of protein turnover on a daily basis. My thesis work has shown that the hepatic Sel1L-Hrd1 ERAD complex plays a vital role in ensuring optimal liver function and maintaining systemic energy homeostasis in the body.

Using ERAD-deficient animal and cell culture models, we first show that hepatic ERAD regulates the production of Fibroblast growth factor 21 (Fgf21), a fasting-induced hormone with broad effects on growth, nutrient metabolism and insulin sensitivity in the body. Mechanistically, we show that the Sel1L-Hrd1 ERAD complex controls *Fgf21* transcription by regulating the ubiquitination and turnover (and thus activity) of ER-resident transcription factor Crebh, while having no effect on the other well-known Fgf21 transcription factor Pparα. This study identifies reveals a novel hepatic "ERAD-Crebh-Fgf21" axis, and establishes the importance of Sel1L-Hrd1 ERAD in the liver in the regulation of gene transcription and systemic energy metabolism.

Next, we describe how ERAD also plays a critical role in regulating bile homeostasis in the body by triaging bile associated exporter proteins in the liver. In the absence of hepatic ERAD, bile acid, cholesterol and phosphatidylcholine secretion into bile is significantly impaired, resulting in hypercholanemia and severe sensitivity to dietary bile acid challenge. Finally, we demonstrate that Sel1L-Hrd1 ERAD guards against tumorigenesis in the liver via the Wnt signaling pathway. A deficiency in hepatic ERAD predisposes mice to spontaneous and chemically induced liver tumors, marked with increased Ki67 and CyclinD1 levels. Mechanistically, we find that Sel1L-Hrd1 ERAD is responsible for the maturation and quality control of the secreted signaling ligand Wnt5A. An absence of ERAD function leads to Wnt5A aggregation and aberrant Wnt signaling in the liver, leading to unrestrained hepatocyte proliferation and an increased susceptibility towards liver cancer development.

Taken together, we establish a novel paradigm where Sel1L-Hrd1 ERAD in the liver constitutively functions to critically modulate cellular and organismal function, and plays a vital role in guarding against disease pathogenesis. These findings pave the way for future investigations that can further delineate the undeniable significance of ERAD function at a

physiological capacity in regulating metabolic processes the body, and answer several outstanding questions that have now risen from recent studies depicting ERAD as a vital mediator of systemic energy homeostasis. A burning question arising now is how to predict if a protein may be a substrate of ERAD. Are there signature motifs in its structure (e.g. disulphide bonds, transmembrane domains, glycosylations), function (e.g. hormones, ligands, receptors), and/or subcellular localization (e.g. secreted, ER-resident, nuclear) which dictate its susceptibility to ERAD? Is recognition by ERAD a stoichiometry-driven, relatively stochastic event, or is this a deterministic process mediated by specific chaperone proteins (e.g. Os9, Grp78)? Furthermore, while it has been demonstrated that changes in the physiological states of the body (e.g. feeding, thirst, growth) leads to ERAD induction in specific organs, the search is still ongoing for undiscovered transcription factors and/or post-translational modifications mediating this. Is it possible to apply small molecule drugs targeted to these pathways that in order to tune ERAD levels/function within the cell?

Classical liver syndromes such as non-alcoholic fatty liver disease (NAFLD), cholestasis and chronic viral hepatitis (caused by HBV or HCV) have long been associated with alterations in ER stress prolife and unfolded protein response (UPR) activation. Indeed, specific liver diseases have been known to be caused primarily due to protein misfolding and aggregation in the ER such as hyperhomocysteinemia (mutations in homocysteine metabolism enzymes) and hemochromatosis (mutant *Hfe* gene). A natural question arises as to the role of hepatic ERAD in mediating these disorders in a substrate specific manner – are these disease mutants resistant to ERAD mediated clearance (or ERAD insufficiency)? These studies also bring forth a complex concept of three primary machineries of cellular quality control – ERAD, UPR and autophagy – working together to safeguard against proteotoxic events. Now, it is imperative for future research to attempt to tease apart the relative contribution, at both pathological and physiological levels, of these three systems. Upon cursory analysis, it is conceivable that ERAD works as the cell's first line of defense upon proteotoxic insult (misfolding) to degrade aberrant proteins, thereby preventing their aggregation. If ERAD function is insufficient, then the accumulation of misfolded proteins may trigger the activation of UPR, which reduces translation and induces ER chaperone and ERAD gene expression, in an effort to the lessen the proteomic burden in the cell. When these measures still do not suffice, causing large protein aggregates to build up within the cell, autophagy functions to degrade these accumulations *en masse*, thereby attempting to resolve the proteotoxic stress at a macroscale and restore cellular proteostasis. Tissue and cell-specific knockouts of ERAD, UPR and autophagy, singly and in combination, will be instrumental in delineating the exact timeline and crosstalk between these three processes, thereby allowing us to map out the relative significance of these pathways in normal physiology and disease pathogenesis.